



## City Research Online

### City, University of London Institutional Repository

---

**Citation:** Yan, Y. (1996). The effects of electric fields on phase change processes in industry. (Unpublished Doctoral thesis, City, University of London)

This is the accepted version of the paper.

This version of the publication may differ from the final published version.

---

**Permanent repository link:** <https://openaccess.city.ac.uk/id/eprint/30985/>

**Link to published version:**

**Copyright:** City Research Online aims to make research outputs of City, University of London available to a wider audience. Copyright and Moral Rights remain with the author(s) and/or copyright holders. URLs from City Research Online may be freely distributed and linked to.

**Reuse:** Copies of full items can be used for personal research or study, educational, or not-for-profit purposes without prior permission or charge. Provided that the authors, title and full bibliographic details are credited, a hyperlink and/or URL is given for the original metadata page and the content is not changed in any way.

**The Effects of Electric Fields on  
Phase Change Processes  
in Industry**

by  
**YUYING YAN**

**A thesis submitted for the degree  
of Doctor of Philosophy of the  
City University**

**January 1996**

**Department of Mechanical Engineering and Aeronautics  
City University  
LONDON, U.K.**

**To my wife and my daughter**

# Contents

0.1	ACKNOWLEDGEMENTS . . . . .	17
0.2	DECLARATION . . . . .	18
0.3	ABSTRACT . . . . .	19
0.4	NOMENCLATURE . . . . .	20
<b>1</b>	<b>General Introduction</b>	<b>24</b>
1.1	Introduction . . . . .	24
1.2	Enhancement of Heat Transfer . . . . .	25
1.3	Enhancement of Crystallization . . . . .	26
1.4	A Summary of the Thesis . . . . .	27
<b>I</b>	<b>Effects of Electric Fields on Nucleate Boiling at Low Superheat Surfaces in Heat Exchangers</b>	<b>29</b>
<b>2</b>	<b>Part One Introduction</b>	<b>30</b>
<b>3</b>	<b>Part One Literature Review</b>	<b>34</b>
3.1	Introduction . . . . .	34
3.2	Nucleate Boiling with Zero Field . . . . .	34
3.2.1	The boiling regimes . . . . .	35
3.2.2	Nucleation at a pure liquid . . . . .	36
3.2.3	Nucleation at surfaces . . . . .	37
3.2.4	Bubble behaviour . . . . .	39
3.2.5	Bubble departure from a heated surface . . . . .	40
3.2.6	Correlation of nucleate boiling . . . . .	41
3.3	Dielectric Liquids in an Electric Field . . . . .	42

3.3.1	Polar and non-polar . . . . .	43
3.3.2	Polarization . . . . .	45
3.3.3	The motion behaviour . . . . .	47
3.4	Research on EHD Nucleate Boiling . . . . .	48
3.4.1	Experimental (before the 1980's) . . . . .	48
3.4.2	Experimental (after the 1980's) . . . . .	53
3.4.3	The correlations . . . . .	56
3.4.4	EHD enhancement mechanism . . . . .	59
3.4.5	Computational prediction of EHD effects . . . . .	63
3.5	Summary of the Review . . . . .	64
<b>4</b>	<b>Theoretical Study</b>	<b>67</b>
4.1	Introduction . . . . .	67
4.2	Potential Distribution for Different Surfaces . . . . .	68
4.2.1	Physical description . . . . .	68
4.2.2	Numerical method . . . . .	69
4.2.3	Results and discussion . . . . .	73
4.3	EHD Nucleation . . . . .	81
4.3.1	Nucleation without EHD . . . . .	81
4.3.2	Mathematical description . . . . .	82
4.3.3	Case calculation . . . . .	86
4.4	Bubbles Movement . . . . .	88
4.5	Summary . . . . .	93
<b>5</b>	<b>Experimental Study</b>	<b>95</b>
5.1	Introduction . . . . .	95
5.2	Experimental Details . . . . .	96
5.2.1	Passive surfaces . . . . .	96
5.2.2	The working fluid . . . . .	97
5.2.3	Equipment and system . . . . .	97
5.2.4	Method and procedures . . . . .	102
5.2.5	Experimental accuracy . . . . .	104

5.3	Results and Discussion . . . . .	106
5.3.1	Boiling hysteresis at zero field . . . . .	106
5.3.2	Elimination of boiling hysteresis . . . . .	107
5.3.3	Enhancement of heat transfer at low superheat . . . . .	107
5.3.4	EHD as a control mechanism . . . . .	110
5.3.5	The effect of surface geometry . . . . .	112
5.3.6	The compound effects . . . . .	116
5.3.7	Electric power consumption . . . . .	118
5.4	Conclusions . . . . .	118

## **II Effects of an Electric Field on Crystallization Processes from Industry Melts 120**

### **6 Part Two Introduction 121**

### **7 Research History and Progress 124**

7.1	Historical Review . . . . .	124
7.2	The Mechanism Study . . . . .	130
7.3	Critical Nucleus Size . . . . .	132
7.4	Kinetics of the Crystallization Process . . . . .	133
7.4.1	Activation energy and diffusion coefficient . . . . .	134
7.4.2	The rate of nucleation . . . . .	135
7.4.3	Linear crystallization rate . . . . .	140
7.4.4	Kinetics of massive crystallization . . . . .	142
7.5	The Assessment of Experimental Results . . . . .	145
7.6	Summary . . . . .	147

### **8 Experimental Samples 149**

8.1	Introduction . . . . .	149
8.2	Composition of Cocoa butter . . . . .	152
8.3	Polymorphic Property of Cocoa Butter . . . . .	154
8.3.1	The polymorphism of POP, POS and SOS . . . . .	154
8.3.2	Classification for cocoa butter crystal . . . . .	154

8.3.3	Cocoa butter and POP, POS, SOS molecules . . . . .	156
8.4	Physical Properties of Cocoa Butter . . . . .	156
8.4.1	Properties of cocoa butter . . . . .	157
8.4.2	Cooling curves . . . . .	157
8.4.3	The speed of crystallization . . . . .	159
8.4.4	Contraction . . . . .	159
8.5	Dielectric Property . . . . .	160
8.5.1	Relative permittivity . . . . .	161
8.5.2	Complex permittivity . . . . .	162
8.5.3	Dielectric Susceptibility . . . . .	162
8.5.4	Experimental arrangement . . . . .	162
8.5.5	Results and discussion . . . . .	164
8.6	Chocolate Production . . . . .	166
8.6.1	Tempering . . . . .	166
8.6.2	Fat bloom . . . . .	169
8.7	Summary . . . . .	170
<b>9</b>	<b>Experimental Study on Crystallization</b>	<b>173</b>
9.1	Introduction . . . . .	173
9.2	Experimental Method and the System . . . . .	174
9.2.1	Experimental system and equipment . . . . .	174
9.2.2	Electrodes . . . . .	176
9.2.3	Experimental method and procedures . . . . .	178
9.3	The Behaviour of Olive Oil . . . . .	180
9.4	Cocoa Butter Crystallization . . . . .	183
9.4.1	The cooling curves . . . . .	183
9.4.2	DSC analysis . . . . .	190
9.4.3	The cutting off effects . . . . .	192
9.4.4	The electrode effect . . . . .	195
9.5	Crystallization of Cocoa Butter Mixture . . . . .	198
9.6	Conclusions . . . . .	206

<b>10 Experiments on Untempered Chocolate for Different Conditions</b>	<b>207</b>
10.1 Introduction . . . . .	207
10.2 Experimental Design Using the Taguchi Method . . . . .	209
10.2.1 Taguchi method and orthogonal arrays . . . . .	209
10.2.2 Orthogonal array selection . . . . .	210
10.2.3 The experimental arrangement . . . . .	211
10.3 Experimental Detail . . . . .	212
10.3.1 The test rig system and equipment . . . . .	213
10.3.2 Sample preparation . . . . .	216
10.3.3 Differential scanning calorimetry (DSC) . . . . .	217
10.4 DSC Results and Comparisons . . . . .	218
10.4.1 Normalization . . . . .	218
10.4.2 The definition of a baseline . . . . .	219
10.4.3 The criterion for comparisons . . . . .	228
10.4.4 Numerical Integration . . . . .	229
10.5 Analysis Method and Results . . . . .	231
10.5.1 The method . . . . .	231
10.5.2 The results . . . . .	233
10.5.3 Discussions . . . . .	234
10.6 Summary . . . . .	238
<b>11 Theoretical Approach</b>	<b>240</b>
11.1 Introduction . . . . .	240
11.2 Derivation of Basic Relations . . . . .	240
11.2.1 The changes of chemical potential . . . . .	241
11.2.2 The change of temperature with field strength . . . . .	243
11.2.3 The change of pressure with field strength . . . . .	244
11.3 The Rate of Nucleation . . . . .	245
11.4 Heat and Mass Transfer Analysis for Crystal Growth . . . . .	247
<b>12 Conclusions of the Thesis</b>	<b>252</b>

12.1	Conclusions for EHD Effect on Nucleate Boiling at Low Superheat Surfaces . . . . .	252
12.1.1	General conclusions for experimental study . . . . .	252
12.1.2	The effect of surface geometries on EHD application . . . . .	253
12.1.3	EHD enhancement on bubble nucleation . . . . .	254
12.2	Conclusions for Effects of an Electric Field on Crystallization . . . . .	254
12.2.1	The effect on no-crystallization dielectric oil . . . . .	254
12.2.2	The effect on polymorphism crystallization of dielectric melt . . . . .	255
12.2.3	The effect on dielectric melt mixture . . . . .	255
12.2.4	The method for DSC assessment using the Taguchi method . . . . .	255
12.2.5	Theoretical approach . . . . .	256
<b>13</b>	<b>References</b>	<b>257</b>
<b>14</b>	<b>Appendix</b>	<b>272</b>

# List of Figures

3.1	Pool boiling regimes. A-B, natural convection; B-C, nucleate boiling; C-D, partial film boiling; D-E, stable film boiling. . . . .	35
3.2	Nucleation from cavities . . . . .	38
3.3	A molecule becomes polarized in an electric field. The positive nucleus moves one way and electron orbital the other. . . . .	43
3.4	A dipole experiences a couple in an electric field. The dotted lines represent the forces felt by each charge. . . . .	44
3.5	Schematic representation of dielectric polarization . . . . .	46
3.6	A classical fine wire apparatus . . . . .	49
3.7	Interactions among electric, flow and temperature fields . . . . .	60
4.1	Six surface geometries of boiling tubes (a) smooth; (b) Gewa-T; (c) U-shape; (d) low-fin(1); (e) low-fin(2); (f) Thermoexcel-C. . . . .	69
4.2	surface shapes to be analyzed in the 2-D control volumes with the coordinates . . . . .	71
4.3	Grids for computation (a) smooth; (b) Gewa-T; (c) U-shape; (d) low-fin(1); (e) low-fin(2); (f) Thermoexcel-C. . . . .	72
4.4	Equi-potential contours for Case (a) to Case (f) (Numbers shown are percentages of full/electrode applied voltage) . . . . .	74
4.5	Magnified view of Case (b) contours (Number shown are in volts, for electrode potential $\phi_e = 30$ kV) . . . . .	75
4.6	Localised field strength versus local voltage for Case (b) for electrode potential $\phi_e = 30$ kV. ( $E'$ for localised field strength; $E_{10}$ for 10% of the electrode strength; $\phi'$ for local voltage) . . . . .	75

4.7	Magnified view of Case (f) contours (Numbers shown are in volts, for electrode potential $\phi_e = 30$ kV) . . . . .	76
4.8	Localised field strength versus local voltage for Case (f) for electrode potential $\phi_e = 30$ kV. ( $E'$ for localised field strength; $E_{10}$ for 10% of the electrode strength; $\phi'$ for local voltage) . . . . .	77
4.9	Localised field strength versus local voltage for Case (a) to Case (f) for electrode potential $\phi_e = 30$ kV. ( $E'$ for localised field strength; $E_{10}$ for 10% of the electrode strength; $\phi'$ for local voltage) . . . . .	78
4.10	The ratio of field strength versus local voltage for Case (b) for different local area and electrode potentials. ( $E'$ for localised field strength; $E_{10}$ for 10% of the electrode strength; $\phi'$ for local voltage) . . . . .	79
4.11	The ratio of field strength versus local voltage for Case (F) for different local area and electrode potentials. ( $E'$ for localised field strength; $E_{10}$ for 10% of the electrode strength; $\phi'$ for local voltage) . . . . .	80
4.12	Surface tension forces acting at point of bubble contact . . . . .	84
4.13	Critical radius of a bubble nucleus versus superheat for different field strengths . . . . .	87
4.14	Relative nucleation rates versus superheat for different field strengths . . . . .	87
4.15	Relative nucleation rates versus field strengths at a given superheat . . . . .	88
4.16	Force analysis on a generated bubble . . . . .	89
4.17	Coordinates for the analysis of potential distribution around a bubble at a smooth surface . . . . .	89
4.18	Coordinates for the analysis of potential distribution around a bubble at a Gewa-T surface . . . . .	90
4.19	Equi-potential contours around a bubble for a smooth surface (Numbers shown are percentages of full/electrode applied voltage) . . . . .	91
4.20	Equi-potential contours around a bubble for a Gewa-T surface (Numbers shown are percentages of full/electrode applied voltage) . . . . .	92
5.1	Profile of passive enhanced surfaces (a) Thermoexcel-HE; (b) Gewa-T. . . . .	96
5.2	The single tube test rig . . . . .	98
5.3	The mesh electrode assemblies . . . . .	99

5.4	Thermocouple arrangement on the test tube . . . . .	100
5.5	Illustration of wall thermocouple installation . . . . .	100
5.6	Electrical circuitry (1) high voltage supply; (2) potential divider; (3) voltmeter; (4) ammeter; (5) single tube test rig . . . . .	102
5.7	Boiling hysteresis for the T-HE tube at zero field. (+): increasing $\Delta T$ and (-): decreasing $\Delta T$ . . . . .	106
5.8	Boiling hysteresis for the G-T tube at zero field. (+): increasing $\Delta T$ and (-): decreasing $\Delta T$ . . . . .	107
5.9	Elimination of boiling hysteresis and enhancement of heat transfer for the T-HE tube. (+): increasing $\Delta T$ and (-): decreasing $\Delta T$ . . .	108
5.10	Elimination of boiling hysteresis and enhancement of heat transfer for the G-T tube. (+): increasing $\Delta T$ and (-): decreasing $\Delta T$ . . .	109
5.11	Effect of electric field on superheat for bubble initiation . . . . .	110
5.12	Ratio of heat transfer coefficients versus field strengths for the T-HE tube . . . . .	111
5.13	Ratio of heat transfer coefficients versus field strengths for the G-T tube . . . . .	111
5.14	Results for the T-HE compared with that for the smooth tube . . .	112
5.15	Results for the G-T compared with that for the smooth tube . . . .	113
5.16	Results for the T-HE compared with that for the G-T . . . . .	114
5.17	Results for the T-HE compared with that for the T-C . . . . .	115
5.18	Results for the G-T compared with that for the l-F . . . . .	115
5.19	Tube rating versus superheat for different surfaces at zero field . . .	116
5.20	Tube rating versus superheat for different surfaces, $E=3.0$ MV/m . .	118
7.1	The routes for a homogeneous medium in zero field to a nucleated medium in a field $E$ . . . . .	138
7.2	Effect of electric field strength on nucleation rates ratio $I_e$ for various undercoolings. (a) nonpolar $\alpha$ phase; (b) polar $\gamma$ phase. . . . .	140
7.3	The time dependence of the total crystallization. (1) with an electric field; (2) without a field. . . . .	143

7.4	Time dependence of the degree of total crystallization with non-steady state thermal nucleation. (1) with an electric field; (2) without the field. . . . .	145
8.1	Graph of percent solid phase versus temperature of cocoa butters (Kattenberg, 1981) . . . . .	153
8.2	Shukoff cooling curve (phase transitions during cooling, Diffraction Pattern Temperature (DPT) x-ray studies) . . . . .	158
8.3	Experimental arrangement for measuring dielectric properties . . .	163
8.4	Dielectric constant of liquid samples . . . . .	165
8.5	Crystallization during tempering in a scarped cooler . . . . .	168
8.6	A model of fat bloom formation . . . . .	170
9.1	The experimental system for crystallization with or without an electric field . . . . .	175
9.2	The test rig for crystallization in the presence of an electric field . .	176
9.3	Electrodes used in experiments. (1) brass rod electrode; (2) stainless steel bucket structure electrode; (3) brass plate electrode; (4) stainless steel plate electrode; (5) stainless steel cylindrical structure electrode and (6) ball electrode. . . . .	177
9.4	An electrode system for DSC sample preparation . . . . .	178
9.5	Positions of electrode and thermocouple junction . . . . .	180
9.6	Cooling curves for olive oil at different field potentials ( $x=18\text{mm}$ , $x_1 = 10\text{mm}$ and $x_2 = 18\text{mm}$ ) . . . . .	181
9.7	Cooling time versus field strength for olive oil at different cooling levels . . . . .	182
9.8	Cooling curves for olive oil with an electric field and cutting off the field supply at different times . . . . .	182
9.9	Cooling curves for cocoa butter with 0 kV field . . . . .	184
9.10	Comparison between the 0 kV curve and "Shukoff cooling curve" . .	184
9.11	Cooling curves for cocoa butter with 10 kV field . . . . .	185
9.12	Cooling curves for cocoa butter with 15 kV field . . . . .	186
9.13	Cooling curves for Ghanaian cocoa butter at different voltages . . .	186

9.14	Cooling curves for Nederland cocoa butter at different voltages . . .	187
9.15	Comparison of cooling curves between Ghanaian and Nederland cocoa butter at 10 kV . . . . .	188
9.16	Comparison of cooling curves between Ghanaian and Nederland cocoa butter at 15 kV . . . . .	188
9.17	Cooling rate for cocoa butter using different electrodes at 15 kV . .	189
9.18	Cooling time versus the field strengths for different crystal forms . .	189
9.19	Results of DSC analysis . . . . .	191
9.20	Comparison of DSC results for different samples . . . . .	192
9.21	Cooling curves for cocoa butter when the field was cut off at different times . . . . .	193
9.22	Comparison between 0 kV curve and the curve for which the field was cut off at the beginning of the crystallization . . . . .	193
9.23	Field was cut off at the point with the highest temperature . . . . .	195
9.24	Cooling curves for cocoa butter crystallization using a “⊥” shape electrode at different field strengths . . . . .	196
9.25	Cooling curves for cocoa butter crystallization using stainless steel electrodes . . . . .	196
9.26	Cooling curves for cocoa butter crystallization using the electrode with same material but different geometries . . . . .	197
9.27	Cooling curves for cocoa butter crystallization using the electrode with same geometry but different material . . . . .	197
9.28	Cooling curves for cocoa butter with different percentages of chocolate using a rod electrode at 15 kV . . . . .	199
9.29	Cooling curves for cocoa butter with different percentages of chocolate using a “bucket” shape electrode at 15 kV . . . . .	200
9.30	The time for $\beta_{III}$ crystals appearing versus percentages of chocolate in samples . . . . .	200
9.31	The time for $\beta_{III}$ crystals appearing versus percentages of chocolate in samples . . . . .	201
9.32	Cooling curves for cocoa butter mixture with 25% of chocolate using different electrodes at 15 kV . . . . .	201

9.33	Cooling curves for cocoa butter mixture with 50% of chocolate using different electrodes at 15 kV . . . . .	202
9.34	The cutting off effect for cocoa butter mixture with 50% of chocolate in the presence of an electric field . . . . .	203
9.35	Cooling curves for cocoa butter mixture with different codes of chocolate . . . . .	203
9.36	Cooling curves for cocoa butter mixture with chocolate Code 2 in the presence of an electric field . . . . .	204
9.37	Comparison for the crystallization of cocoa butter mixture with different codes of chocolate using the same electrode . . . . .	205
9.38	Cooling curves for cocoa butter mixture using a “ball” shaped electrode	205
10.1	The water bath system used in experiments . . . . .	213
10.2	The high voltage cabinet used in experiments . . . . .	214
10.3	The electrode system for DSC sample treatment . . . . .	215
10.4	The electrode assembly and the paralleled radiator inside the cabinet	215
10.5	The flow chart of the sample preparation process . . . . .	216
10.6	The DSC7 testing system . . . . .	217
10.7	The microweigh meter used for DSC sample weighing . . . . .	218
10.8	The definition of $Q(T_i)$ and $Q_B$ . . . . .	219
10.9	The thermogram for the sample of trial No. 1 . . . . .	220
10.10	The thermogram for the sample of trial No. 2 . . . . .	220
10.11	The thermogram for the sample of trial No. 3 . . . . .	221
10.12	The thermogram for the sample of trial No. 4 . . . . .	221
10.13	The thermogram for the sample of trial No. 5 . . . . .	222
10.14	The thermogram for the sample of trial No. 6 . . . . .	222
10.15	The thermogram for the sample of trial No. 7 . . . . .	223
10.16	The thermogram for the sample of trial No. 8 . . . . .	223
10.17	The thermogram for the sample of trial No. 9 . . . . .	224
10.18	The thermogram for the sample of trial No. 10 . . . . .	224
10.19	The thermogram for the sample of trial No. 11 . . . . .	225
10.20	The thermogram for the sample of trial No. 12 . . . . .	225

10.21	The thermogram for the sample of trial No. 13 . . . . .	226
10.22	The thermogram for the sample of trial No. 14 . . . . .	226
10.23	The thermogram for the sample of trial No. 15 . . . . .	227
10.24	The thermogram for the sample of trial No. 16 . . . . .	227
10.25	An example of the DSC result for the 24-hour-sample and the comparison . . . . .	228
10.26	Analysis result $\eta_A$ versus experimental levels for voltages of the applied field (factor A); (1: 0kV, 2: 10kV, 3: 15kV, 4: 25kV) . . . . .	234
10.27	Analysis result $\eta_B$ versus experimental levels for the coolant temperature (factor B); (1: 0°C, 2: 5°C, 3: 10°C, 4: 15°C) . . . . .	235
10.28	Analysis result $\eta_C$ versus experimental levels for the original temperature of samples (factor C); (1: 28°C, 2: 30°C, 3: 35°C, 4: 42°C) . . . . .	235
10.29	Analysis result $\eta_D$ versus experimental levels for the time of applying field (factor D); (1: 2min, 2: 5min, 3: 10min, 4: 20min) . . . . .	236
10.30	Analysis result $\eta_E$ versus experimental levels for the thickness of samples (factor E); (1: 4mm, 2: 6mm, 3: 10mm, 4: 13mm) . . . . .	237
10.31	Analysis result $w'_\beta$ versus experimental levels for different factors . . . . .	238
11.1	Conditions of heat transfer . . . . .	248

# List of Tables

1.1	The general phase change processes . . . . .	24
4.1	Physical properties of Refrigerant R114 . . . . .	86
5.1	Dimensions of tubes for test and comparison . . . . .	97
8.1	The percentages of the continuent glycerides . . . . .	152
8.2	Triglyceride composition of cocoa butter . . . . .	153
8.3	Classification of cocoa butter crystallization forms . . . . .	155
8.4	Davis and Dimick's classffication on crystal forms of cocoa butter .	155
8.5	Solid fat of cocoa butter . . . . .	157
8.6	Some properties of commercial cocoa butter . . . . .	157
8.7	Percentage of contraction volume . . . . .	160
8.8	Pcentage of liquid phase cocoa butter with temperature . . . . .	160
8.9	Standard capacitor and mica permittivity . . . . .	164
8.10	Real part of dielectric constant $\epsilon'$ , loss $\epsilon''$ and loss tangent $\tan(\delta)$ . .	164
10.1	The experimental conditions . . . . .	208
10.2	The orthogonal array L16 ( $4^5$ ) . . . . .	211
10.3	The experimental arrangement . . . . .	212
10.4	Results of the numerical integration . . . . .	230
10.5	Results of the numerical integration for 24-hours thermograms . . .	231
10.6	Response Table – Mean (I) . . . . .	233
10.7	Response Table – Mean (II) . . . . .	233

## 0.1 ACKNOWLEDGEMENTS

The author would like to sincerely thank his supervisor Dr. R.S. Neve for his advice and encouragement during every stage of his work. It is by Dr. Neve's support and recommendation that an Overseas Research Student Award was issued by the C.V.C.P.

The author is also grateful to Prof. M.W. Collins for suggesting the projects and arranging the financial support from industry. In the research project on EHD enhancement of nucleate boiling, the author has benefitted greatly from discussions with Prof. P.H.G. Allen and Dr. T.G. Karayiannis. Their help and encouragement is greatly appreciated. The author has also benefitted from the help and suggestions of Dr. J. Meyer and his colleagues.

Thanks are also due to the following:

Prof. A.R.D. Thorley, the head of Department for supporting to apply the ORS award;

Prof. R.N. Franklin, the Vice Chancellor for his financial help which enabled to complete the Thesis;

Mr. I. Wright, Mr. J. Spencer and his technicians for help in the construction of the apparatus;

Dr. F. Henry and Dr. X.Y. Xu for allowing to use the printer in their office;

The secretaries of the Dept. of Mechanical Engineering and Aeronautics for help during the whole course of the research.

Grateful acknowledgement is made for the Overseas Research Student Award from the C.V.C.P., the British Council's Award for Technique Cooperation, the Grant Award and C.A.S.E. Award from industry.

## 0.2 DECLARATION

This is a declaration to grant powers of discretion to the University Librarian to allow the thesis to be copied whole or in part without further reference to the author. This permission covers only single copies made for study purposes, subject to normal conditions of acknowledgement.

However, for reasons of commercial confidentiality, chapters 8, 9 and 10 in part 2 are temporarily denied to the public for five years.

### 0.3 ABSTRACT

This thesis describes an experimental and theoretical investigation of the effects of an electric field on two kinds of phase change process in industry: nucleate boiling in heat exchangers and crystallization from industrial melts.

The first is called electrohydrodynamic (EHD) enhancement of nucleate boiling heat transfer at low superheat surfaces in heat exchangers. The major emphasis of the work has been to probe the compound effect of EHD and passive enhanced surfaces on nucleate boiling. Field potential distribution for six different surfaces has been predicted and analyzed using a computational fluid dynamics (CFD) method. The analysis has shown that the shapes of passive enhanced surfaces potentially create considerable increases in local field gradient to produce such favourable conditions. The critical bubble radius, bubble nucleation rate and bubble movement in the presence of an electric field have been also studied and discussed. Equations are derived showing that a local electric field gradient will enhance nucleation rate and decrease critical bubble radius, both leading to improved heat transfer rate. In the mean time, experimental work for two typical low superheat surfaces, Hitachi Thermoexcel-HE and Wieland Gewa-T tubes was carried out using a single tube test rig. Furthermore, comparisons for current experimental results and those for other surfaces are made. Major improvements are shown in the performance of heat exchangers fitted with enhanced tube surfaces by applying up to 30 kV between those surfaces and a surrounding electrode.

In parallel with this, the effect of an electric field on melt crystallization has been studied. The experimental samples were selected from industry; the simplicity of laboratory preparation, the dielectric properties and the polymorphic behaviour were typical and attractive for the research purpose. A large number of experiments under different conditions for the effects of an electric field on the crystallization of a dielectric with polymorphic behaviour and lower molten temperature has been carried out for the first time. The experiments are assessed by time-temperature measurement and differential scanning calorimetry (DSC), respectively. The results have shown that the crystallization of the melt on cooling is enhanced under the action of an electric field. For the effect of an electric field on the melt mixture, a novel approach of applying the Taguchi method to the experimental DSC results has been used. Also, a theoretical analysis for dielectric crystallization in the presence of an electric field has been carried out.

## 0.4 NOMENCLATURE

$A$	surface area based on overall diameter ( $\text{m}^2$ ) (in chapter 5)
$A$	experimental factor (in chapter 10)
$A$	parameter (in chapter 4 and 7)
$a$	total crystallization rate (chapter 7)
$B$	a function of the pressure ratio $(p_v - p_l)/p_l$
$B$	experimental factor (in chapter 10)
$c_p$	specific heat ( $\text{kJ/kg K}$ )
$C$	constant (in chapter 4)
$C$	experimental factor (in chapter 10)
$d$	the distance between the positive and negative charges
$d$	parameter $(\chi_1 V_1 - x_3 V_3)$
$D$	bubble diameter (m)
$D$	dielectric displacement or electric induction
$D$	experimental factor (in chapter 10)
$D$	diffusion coefficient
$D_e$	electrode diameter (m)
$D_t$	nominal outside diameter of tubes (m)
$E$	electric field strength ( $\text{MV/m}$ )
$E$	experimental factor (in Chapter 10)
$F$	free energy
$F$	force ( $\text{N/m}^3$ )
$F_e$	EHD body force ( $\text{N/m}^3$ )
$f$	the frequency of bubble departure
$g$	specific Gibbs function
$G$	Gibbs free energy
$G$	ratio of electric forces to surface tension forces (in chapter 3)
$\Delta g$	the change of Gibbs free energy ( $\text{kJ/m}^3$ )
$h$	heat transfer coefficient ( $\text{W/m}^2\text{K}$ )
$h$	interval of DSC experimental temperature ( $T_{i+1} - T_i$ )
$\Delta H$	latent heat ( $\text{kJ/kg}$ )
$H_{fg}$	heat of evaporation per molecule

$I$	electric current
$I$	nucleation rate
$J$	nucleation rate
$K_G$	overall mass transfer coefficient
$k$	coefficient
$L$	tube length (m)
$M$	relative molecular mass (kg/mol)
$m$	coefficient
$m$	mass
$\dot{m}$	mass flow rate of water (kg/s)
$N$	the total number of molecules in a system
$N$	the number of dipoles per unit volume of melt
$n$	the number of nuclei
$n$	coefficient
$P$	polarization
$\overline{P}$	dielectric polarization
$p$	pressure (Pa)
$Q$	heat transfer rate (W)
$Q_o$	DSC data for heat flow per sample
$Q$	DSC data for heat flow per unit weight of the sample
$QB$	baseline data of DSC thermogram
$\Delta Q_{sol}$	latent heat for crystallization
$q$	heat flux (W/m <sup>2</sup> )
$q$	DSC data (Q-QB)
$q_e$	electric charge density (C/m <sup>3</sup> )
$R$	gas constant
$r$	radius of bubble nuclei (m)
$r_m$	tube rating (W/m)
$T$	dielectric temperature (°C)
$T_{in}$	temperature of water in (°C)
$T_{out}$	temperature of water out (°C)
$T_{wm}$	mean surface temperature (°C)
$t$	time

$\Delta T$	superheat temperature (K)
$\bar{u}$	electric dipole moment
$U$	velocity of bubble rise
$U$	internal energy
$U$	activity energy
$V$	volume of the system
$v$	linear crystallization rate
$\Delta w$	additional energy (kJ/m <sup>3</sup> )
$W$	additional energy for phase change
$W$	torque (N m)
$W$	integration data for heat flow during crystal melting

**Greek symbols:**

$\alpha$	crystal form
$\alpha$	polarizability
$\epsilon$	relative permittivity
$\epsilon_0$	permittivity of free space (F/m)
$\theta$	contact angle (°)
$\lambda$	electric conductivity
$\beta$	crystal form
$\beta$	parameter (in chapter 7)
$\sigma$	surface tension (N/m)
$\sigma$	electric stress
$\phi$	electric field potential (V)
$\gamma$	crystal form
$\gamma$	parameter
$\mu$	chemical potential
$\delta$	Kronecker number
$\delta$	thickness of effective film
$\eta$	the criterion for comparison (in chapter 10)
$\eta$	specific heat of evaporation (in chapter 7)
$\kappa$	thermal conductivity
$\kappa$	Boltzmann constant

$\kappa_v$	constant (in chapter 11)
$\xi_v$	ratio of the volume contraction ( $V_2/V_1$ )
$\rho$	density ( $\text{kg/m}^3$ )
$\tau$	time of complete crystallization
$\chi$	dielectric susceptibility

**Subscript:**

<i>1 or l</i>	liquid phase
<i>2 or v</i>	vapour phase (in chapter 3, 4 and 5)
<i>2</i>	solid phase (in chapter 7, 8, 9, 10 and 11)
<i>3</i>	vapour phase (in chapter 7)
<i>b</i>	bubble
<i>cr</i>	critical
<i>e</i>	with electric field
<i>o</i>	without electric field
<i>sat</i>	saturation
<i>lv</i>	liquid-vapour
<i>sl</i>	solid-liquid
<i>sv</i>	solid-vapour

**Superscript:**

<i>o</i>	without electric field
<i>e</i>	with electric field
<i>*</i>	optimum value
<i>'</i>	local field parameter

**Nondimensional Groups:**

<b>B</b>	Bond number (in chapter 3)
<b>Ja</b>	Jakob number (in chapter 3)
<b>Nu</b>	Nusselt number (in chapter 3)
<b>Pr</b>	Prandtl number (in chapter 3)
<b>Re</b>	Reynolds number (in chapter 3)

# Chapter 1

## General Introduction

### 1.1 Introduction

In the natural world, all matter exists in three general states, namely gaseous (or vapour), liquid and solid phases, which represent very different degrees of atomic or molecular mobility. The phase is normally defined as a portion of matter which is homogeneous, so both a single substance and the homogeneous mixture can exist in a single phase. As an important physical property, the state of matter can change from one phase to another under certain conditions. Problems involving the phase change processes occur in many branches of science and technology, in astrophysics, meteorology, chemistry, physics, geochemistry, biology, medicine, metallurgy, engineering, aerodynamics and the food industry. There remain a lot of interesting and challenging subjects which are on both theoretical and practical grounds worthy of investigation.

Phase changes likely to be encountered in industrial processes are listed in Table 1.1.

Table 1.1: The general phase change processes

liquid $\rightarrow$ vapour:	boiling	vapour $\rightarrow$ liquid:	condensation
liquid $\rightarrow$ solid:	crystallization	solid $\rightarrow$ liquid:	melting/dissolution
solid $\rightarrow$ vapour:	sublimation		

There is no doubt that the most common phase changes in industry are liquid  $\rightleftharpoons$  vapour and liquid  $\rightleftharpoons$  solid processes. For example, boiling and condensing, which are not only phase change conversions but also important heat transfer modes, have been extensively applied in power, nuclear power, aerospace, chemical industries, etc.; in particular, in the various types of heat exchangers which are largely used in refrigeration systems, air conditioners and various renewable sources applications. Crystallization is another common phenomenon in chemical, medical, food and many other industries, because large amounts of food, medicine, industrial raw material and products are obtained from liquid  $\rightarrow$  solid crystallization. Similarly, melting or dissolution is also often encountered in industrial processes. Therefore, it should be essential that the phase change processes can be enhanced and controlled in order to increase the efficiency and quality of the products. It is just for this reason that the enhancement and the control mechanism for different phase change processes have been pursued by scientists and engineers for many years.

## 1.2 Enhancement of Heat Transfer

Many techniques have been developed to enhance phase change heat transfer. These can be generally divided into passive (extended or treated surfaces, surface tension devices, etc.) and active (surface or fluid vibration, suction or injection, electric fields, etc.) methods respectively (Bergles, 1985). In the past, the enhancement of phase change heat transfer was mostly effected by using passive techniques. Even at present, passive enhancement methods, in particular some mechanically prepared (passive enhanced) surfaces called low superheat surfaces, are still extensively employed to enhance the processes in practical applications. However, the active heat transfer enhancement technique and the heat transfer control method of applying a strong electric field (termed electrohydrodynamic and abbreviated EHD) to heat transfer liquids/fluids is becoming more and more attractive for the applications in which heat transfer should be enhanced at small temperature differences or be controlled accurately and easily. This makes the EHD technique one of the most interesting and challenging subjects for enhancing and controlling phase change heat transfer.

Much work has been done for EHD enhancement of boiling and condensation since the 1960s, as reviewed in chapter 3, this has indeed pushed forward the development of phase-change heat transfer. However, the earlier work was mostly reported the EHD effects only, the compound effect of both EHD and passive enhanced surface is less emphasized.

### 1.3 Enhancement of Crystallization

Crystallization consists of two separate processes, namely, nucleation and crystal growth. The mechanism of the latter process is explained by several theories, such as surface energy, adsorption layer, kinematic and diffusion–reaction theories. However, stable crystals formed during nucleation are the required ones. Nucleation may occur spontaneously or be induced artificially. Traditionally, nucleation can often be induced by agitation, mechanical shock, friction and extreme pressures within solutions and melts. These methods can be traced back to the early experiments of Young (1911) and Berkeley (1912), and are still employed by manufacturers. In the meantime, some new methods have been developed, such as employing electric and magnetic fields, spark discharges, ultra-violet light, X-rays,  $\gamma$ -rays, sonic and ultrasonic irradiation, which used to be classified as external influences and be thought to have erratic effects on the nucleation (Khamskii, 1969). Nevertheless, in the expectation that the processes should be enhanced and controlled, the effects of strong electric fields on crystallization, as a new technology, appear very attractive for manufacturers.

Some works have been done for the effect of an electric field on crystallization. This will be reviewed in chapter 7. The early work was done for a single crystalline form in laboratories. In later of the 1980s, the work was studied towards to the industrial applications, but the temperature ranges for crystallization was normally higher than 150°C. In fact, the more challenging temperature range for practical applications should be less than 100°C and the crystallization behaviour should not only be a single form but with polymorphism. Thus the applications could be

attractive for the medical and the food industries. Unfortunately, this work has not yet been reported up to now.

## 1.4 A Summary of the Thesis

This thesis is concerned with the effects of electric fields on two kinds of phase change process in industry. The first is nucleate boiling at low superheat surfaces in heat exchangers. In parallel with this, a second system is also studied, namely crystallization from industrial melts. Because of the large differences between the two processes, the thesis has been divided into two independent parts:

- Part One: Effects of Electric Fields on Nucleate Boiling at Low Superheat Surfaces in Heat Exchangers.
- Part Two: Effects of Electric Fields on Crystallization Processes from Industrial Melts.

In **Part one**, the effects of electric fields on nucleate boiling at low superheat surfaces are investigated theoretically and experimentally. The major emphasis of the work has been to probe the compound effect of EHD and passive enhanced surfaces on nucleate boiling. In the theoretical studies, the field potential distribution for six different surfaces which have a gradual evolution from a smooth to a typical passive enhanced Thermoexcel-C has, for the first time, been predicted and analyzed. This is done by employing a computational fluid dynamics (CFD) method. The analysis has shown that the shapes of passive enhanced surfaces potentially create considerable increases in local field gradient (in particular the shoulder area). A model to predict the critical bubble radius and nucleation rate in the presence of an electric field is also for the first time developed on the basis of the traditional theories. Equations derived have shown that a local electric field strength will enhance nucleation rate and decrease critical bubble radius, both leading to improved heat transfer rate. The bubble movement under the action of an electric field is also discussed and analyzed in this part. In parallel with the theoretical work, experimental work for two typical low superheat surfaces, such as Hitachi

Thermoexcel-HE and Wieland Gewa-T tubes are carried out. As a result, the EHD enhancement performance of these kinds of surface is reported for the first time. In particular, the compound effect of EHD and passive enhancement on nucleate boiling is proposed and the use of EHD as a control mechanism is addressed. Also, comparisons are made between the current experimental results and those for other surfaces.

**Part two** is concerned with the effects of electric fields on another kind of phase change process – crystallization. The samples which have typical polymorphic and complex physical properties are selected from the industrial application. To undertake the experimental studies, the dielectric properties are first proved by experiments. Then a large number of experiments under different conditions have been carried out, for the first time, to investigate the effects of an electric field on the polymorphic crystallization of the samples (the molten point is at 35-50°C). The assessment for experimental results is carried out using different methods, such as the time-temperature measurement and differential scanning calorimetry (DSC) analysis. Indeed, the work described in this part are very impressive and the results are reported for the first time in this field. The Taguchi method for the design of orthogonal experiments is also employed in the experiments and for the first time applied to the DSC results. Accordingly, a relative method to treat and analyse the Taguchi-DSC results is developed and successfully applied. Parallel with the experimental work, a theoretical approach has also been carried out. In this analysis, the electric field effect on crystallization is further discussed on the basis of heat and mass transfer theory for crystallization.

## **Part I**

# **Effects of Electric Fields on Nucleate Boiling at Low Superheat Surfaces in Heat Exchangers**

# Chapter 2

## Part One Introduction

The phase change that occurs during a heat transfer process, such as boiling or condensation, is generally a very effective mode of heat transfer. However, there is further need to develop methods of enhancing the heat transfer rates in heat exchangers. A refrigeration or heat pump system usually operates with heat sink and heat source at predetermined or not controllable (e.g. atmospheric) temperature. The working fluid operating temperature must be significantly lower than the source and higher than the sink in order for the heat exchanger to be of reasonable efficiency and economic size. In a refrigeration/heat pump system these temperature differences, which constitute external thermal irreversibility, reduce the coefficient of performance (COP) of the refrigerator or heat pump. Similar arguments hold for the power producing cycles where the efficiency of the cycle is reduced as the greatest possible temperature difference is reduced by the external thermal irreversibility mentioned above. The beneficial result of heat transfer enhancement would be:

- the reduction in the size of heat exchanger (evaporator/condenser) for given rating.
- the reduction in the temperature difference between evaporator and heat source and condenser and heat sink and thus greater COP or cycle efficiency. (alternatively, the removal of greater rates of energy through a given size of heat exchanger (evaporator/condenser) while maintaining moderate temperature difference.)

Reducing the temperature differentials in heat exchangers becomes particularly important in the recent development of power production using new energy sources, such as solar, geothermal, Organic Rankine Cycle(ORC) engines and thermal energy conversion(OTEC) plants, which will have a significant application potential for mankind in the next century. In these plants, thermal energy is handled by means of heat exchangers. However, currently a major problem with the applications, apart from the relatively low thermodynamic quality, is their correspondingly low heat transfer rate at low temperature differences. For example, the heat sink is normally atmospheric air, or a river, lake or sea water. In the case of geothermal or solar energy applications, the working fluid is at 40 - 90°C. In OTECs the maximum source - sink temperature difference is as small as 20°C; that is between sea surface (20- 30°C) and deep water (4-7°C). Plants operating between such small temperature differences must be larger than high temperature plants, such as nuclear or fossil fuel plants, in order to produce similar outputs. In addition, their performance is more sensitive to the temperature differential at the evaporator-source and the condenser-sink. A certain degree of superheat must be exceeded in the evaporator for nucleate boiling to commence. Such plants may, therefore, face additional “start-up” problems if this degree of superheat is not available. This places an additional limitation on the maximum possible operating fluid temperature difference and thus reduces the plant efficiency. Therefore, actively increasing the heat transfer rates at a small temperature difference (low superheat) are thought to be the key and the most difficult problem in heat transfer applications.

Nucleate boiling has long been recognized as a very efficient mode of heat transfer and is used on the shell side of tubular heat exchangers in refrigeration and process industries. In the past, smooth tubes were mainly used in heat exchangers. As these are made by simple manufacturing processes their costs are low, but their heat transfer performance is not very high, resulting in large size. In the last couple of decades, passive enhanced surfaces have been developed to improve the nucleate boiling characteristics by a fundamental change in the boiling process (Webb, 1981). Firstly, low finned tubes are widely used in shell-and-tube evaporators for organic liquids to enhance the heat transfer in nucleate boiling. For further en-

hancement, the fins are partly flattened and a T-shaped cross section of the fins is achieved (Gewa-T tubes, such as shown in Figure 5.1 (b)), forming channels with comparatively narrow gaps for the release of the bubbles at the top of the fins. Several experimental results have been reported (Yilmaz, et al., 1980 and Webb and Pais, 1992). Also, further modification of these tubes includes the milling of small cavities into the tube surface at the bottom of each channel between the fins (Gorenflo, et al., 1990). This provides additional nucleation centres. Similarly, experimental results for other structure surfaces, such as high flux and Thermoexcel(s), have also been published (Nakayama, et al., 1980 and Bergles, 1989) The advantages of these passive enhanced surfaces are seen to be not only in a higher nucleate boiling heat transfer coefficient but also in the fact that the required superheat for incipient boiling with highly wetting liquids is generally lower than for smooth surfaces due to the greater probability of finding active sites over the larger surface areas. However, these structure surfaces are not exempt from temperature overshoots and resultant boiling curve hysteresis. An example of such hysteresis for a high flux surface was given by Bergles (1989).

The employment of high intensity electric fields (EHD) to enhance nucleate boiling is an active method which has become increasingly attractive in recent years. Initially, the effect of an electric field on heat transfer was studied nearly eighty years ago. Early work before 1960's was mostly concentrated on the enhancement of single phase convective heat transfer. It was only in the last thirty years that the greater potential of EHD in enhancing two-phase heat transfer rates has been realised by more industrial and academic researchers and much work has been done in Japan, the U.S.A., the U.K. and other countries. This will be reviewed in Chapter 3. In recent years, quite a lot of interesting results have been reported. For plain or smooth surfaces, EHD enhancement of heat transfer or elimination of boiling hysteresis have been demonstrated (Yokoyama, et al. 1987; Karayianis, et al. 1989; Ogata and Yabe, 1993a, 1993b). For passive enhanced surfaces, the experimental data for low-fin tubes with EHD have offered more significant enhancement than for smooth ones (Allen and Cooper, 1987; Cooper, 1990; etc.). Similarly, even more attractive results have been reported on EHD enhancement

for low superheat surfaces, such as Gewa-T, Thermoexcel-HE and Thermoexcel-C (Damianidis et al., 1992; Yan et al., 1994 and 1995a). Furthermore, the compound effect of both EHD and passive surface enhancement on nucleate boiling are also addressed (Yan et al., 1995b and Cheung, et al., 1995). As for practical applications, EHD heat exchangers have been designed using smooth tubes or low-fin tubes and experimental results for different tube bundles have been described in publications (Yamashita, et al., 1991; Ohadi, et al., 1992; Ogato et al, 1992; Damianidis, et al., 1991; Karayiannis et al., 1993; Yan et al. 1995b and Cheung et al., 1995). Nevertheless, the EHD effects on nucleate boiling, in particular, at passive enhanced surfaces have not been quite understood yet.

In this Part, literature on EHD effects on nucleate boiling is reviewed in detail. The author's work on EHD nucleate boiling is addressed. This includes the basic theoretical work on EHD nucleation and potential distribution at different surfaces and around a bubble; and experimental work on nucleate pool boiling for passive enhanced surfaces, such as Gewa-T and Thermoexcel-HE. The compound effect of both EHD and passive enhanced surfaces on nucleate boiling is particularly significant and EHD as a control mechanism is also discussed and reported.

# Chapter 3

## Part One Literature Review

### 3.1 Introduction

Electrohydrodynamic (EHD) effects on nucleate boiling are linked with many interacting subjects, such as the classical boiling heat transfer theory, electrodynamic theory, the fluid dielectric and the properties, the EHD effects and its applications, etc. Electrohydrodynamic (EHD) here refers to a coupling of the fluid flow field with a high voltage, low current electric field in a low electrical conductivity fluid (fluid dielectric) medium. The interesting phenomena which appeared when a fluid dielectric was in the presence of an electric field have encouraged researchers to probe into the mechanism and to study the applications. Clearly, it is essential to understand the whole background and the research history. In this chapter, the traditional nucleate boiling results, dielectric properties in the field and EHD research on nucleate boiling are reviewed, respectively.

### 3.2 Nucleate Boiling with Zero Field

Heat transfer associated with boiling had as its primary purpose, until recently, the conversion of liquid into vapour. With the development of the nuclear reactor, the rocket nozzle, and spacecraft, a great interest has developed in the boiling process as a method of increasing heat transfer rates at modest temperature differences. This had drawn great attention from many researchers to study this subject since the 1930's. Research results have been extensively applied in refrigeration processes

accordingly. The recent progress of this traditional technique depends to a great extent on the development of new heat transfer surfaces which can offer enhanced boiling performance and namely enhanced surfaces.

### 3.2.1 The boiling regimes

There are several regimes of boiling; this was first clearly discussed by Nukiyama (1934). Later, the experiments in pool boiling with an electrically heated horizontal wire submerged in a tank of saturated water were reported by McAdams et al. (1941) and Farber and Scoriah (1948) to verify the boiling regimes. Figure 3.1 shows the typical pool boiling regimes in terms of heat flux,  $q$ , versus wall superheat,  $\Delta T$ .

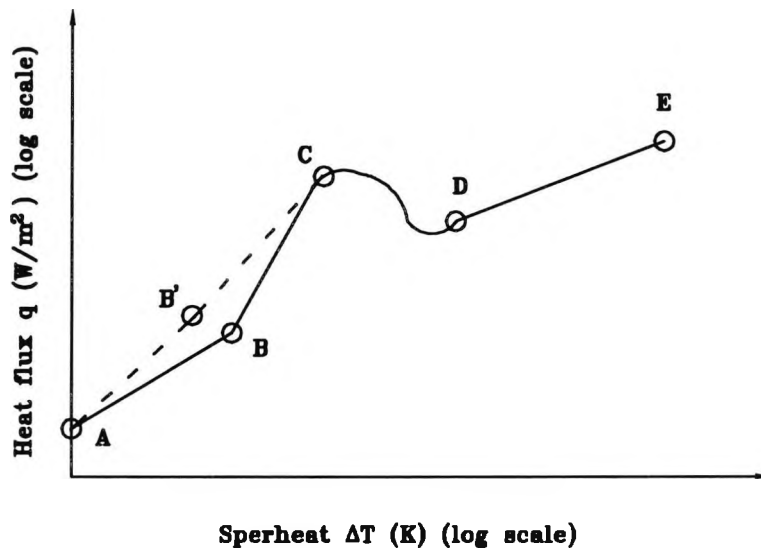


Figure 3.1: Pool boiling regimes. A-B, natural convection; B-C, nucleate boiling; C-D, partial film boiling; D-E, stable film boiling.

In the range of A-B, the water is heated by natural convection. In the range B-C, the liquid near the wall is superheated and tends to evaporate, forming bubbles wherever there are nucleation sites such as tiny pits or scratches on the surface.

The mechanism in this range is called nucleate boiling. When the population of bubbles becomes too high at some high heat flux point  $C$ , the outgoing bubbles may obstruct the path of the incoming liquid. The vapour thus forms an insulating blanket covering the heating surface and thereby raises the surface temperature. This is called the boiling crisis or DNB (Departure from Nucleate Boiling). In the range  $C-D$ , the boiling becomes unstable and then the mechanism is called partial film boiling or transition boiling. Finally, the range  $D-E$  is called stable film boiling and the heat transfer rate reaches minimum.

If from beyond  $C$ ,  $\Delta T$  is decreased, nucleate boiling continues along  $CB'$  towards  $A$ , giving *boiling hysteresis*. This is a product of the situation where only natural convection with poor heat transfer can occur until nucleation is activated, after which superheat can be reduced while ebullition and high rates of heat transfer are maintained. Corty and Foust (1955) have reported the hysteresis effect in nucleate boiling. They found by photographic inspection that the hysteresis effect is much concerned with the nucleation at heat transfer surfaces. For practical surfaces in heat exchangers, the boiling hysteresis has been demonstrated and reported by Allen and Cooper (1987) for a low-fin tube, Karayiannis et al (1989) for a smooth tube and Bergles (1989) for a high flux surface, respectively.

### 3.2.2 Nucleation at a pure liquid

Nucleate boiling involves two separate processes, namely the formation of bubbles or nucleation and the subsequent growth and motion of these bubbles. The primary requirement for nucleation to occur or for a nucleus to subsist in a liquid is that the liquid be superheated. There are two types of nuclei. One is formed in a pure liquid. Another is formed on a foreign object which can be either a cavity on the heating wall or suspended foreign material with a nonwetted surface.

For the first type of nuclei, Volmer (1939) established an expression for the rate of nucleation in a superheated liquid:

$$\frac{dn}{dt} = NB \exp [-(H_{fg}/RT + w_0/RT)] \quad (3.1)$$

where  $n$  is the number of nuclei;  $N$  the total number of molecules in a system;  $B$  a function of the pressure ratio  $(p_v - p_l)/p_l$ ;  $H_{fg}$  is the heat of evaporation per molecule;  $R$  the gas constant per molecule;  $T$  the temperature and  $w_0$  is the work of creating the free surface of nucleus, which was given by Volmer (1939) as

$$w_0 = (4\pi r^2 \sigma - v \Delta p) = \frac{16\pi \sigma^3}{3(p_v - p_l)} \quad (3.2)$$

For a nucleus to become useful as a seed for subsequent bubble growth, the size of the nucleus must exceed that of thermodynamic equilibrium corresponding to the state of the liquid. On the basis of the famous Clausius-Clapeyron equation, this equilibrium bubble size was derived as

$$r_{cr} = \frac{2\sigma}{H_{fg}\rho_v} \frac{T_{sat}}{(T_v - T_{sat})} \quad (3.3)$$

Hence, for increasing superheat, the nucleation size can be smaller, and by equation (3.1) the number of nuclei formed per unit time increases. Another implication of equation (3.3) is that only a nucleus of the equilibrium size is stable. A smaller nucleus will collapse, and a larger nucleus will grow. The above Volmer's equations were reported to agree well with Winsmer's experimental data (1922) obtained under very carefully controlled conditions of cleanliness.

### 3.2.3 Nucleation at surfaces

Nucleation at surfaces occurs from the cavities which already have some gas or vapour present – so called active cavities or nucleate sites. Typical nucleation sites at the cavities of a heating surface are shown in Figure 3.2. The angle  $\theta$  is called the contact angle between the surface and liquid/vapour interface. It has been suggested that it is possible for vapour to continue to exist in cavities in contact with subcooled liquids provided the contact angle  $\theta$  is greater than  $90^\circ$ . This is because a large  $\theta$  may give a better chance to trap gas inside the cavity by a capillary effect. Rohsenow (1952) suggested that the contact angle should be determined by the values of various surface tensions and the relation was given as

$$\cos(\theta) = \frac{\sigma_{sl} - \sigma_{vs}}{\sigma_{lv}} \quad (3.4)$$

where  $\sigma_{sl}$ ,  $\sigma_{lv}$  and  $\sigma_{vs}$  represent the surface tension of solid-liquid interface, liquid-vapour interface and vapour-solid interface, respectively. Hence the contact angle should be determined both by the kind of fluid and the kind of heating surface.

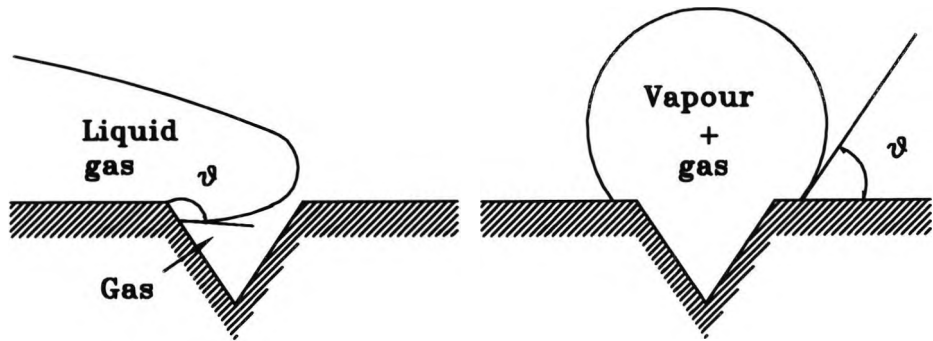


Figure 3.2: Nucleation from cavities

To calculate the wall superheat required for bubble growth occurring from a nucleation site of a solid surface, Hsu (1962) suggested a formula to evaluate the wall temperature for incipience of boiling as

$$T_w - T_{sat} = \frac{8\sigma T_{sat} C}{H_{fg} \rho_v \delta} \quad (3.5)$$

where  $C = 1.6$  and  $\delta$  is the thickness of superheated liquid layer. For applying equation (3.3), Tong (1965) suggested that the critical radius could be supposed to be equal to the cavity radius; but the reported prediction did not agree with observed data well. This probably was because of the supposition of the critical radius.

From a cursory examination of published data for five liquids boiling from three different surfaces, Gaertner (1962) has reported that the population of active sites

was found to be

$$\bar{N} = N_0 \exp\left(-\frac{K}{T_{wall}^3}\right) \quad (3.6)$$

where  $N_0$  and  $K$  represent the liquid and surface conditions.

### 3.2.4 Bubble behaviour

A bubble behaviour was described by the so called bubble dynamics. When the size of a bubble nucleus formed in a liquid exceeds that of thermodynamic equilibrium given by the equation

$$p_v - p_l = \frac{2\sigma}{r_{cr}} \quad (3.7)$$

the bubble will grow because of the excess vapour pressure that is no longer balanced by the surface tension forces. During the initial stage of the growth, the process is controlled by the inertia of the surrounding liquid and the surface forces. Rayleigh (1917), considering a single spherical bubble in an incompressible inviscid liquid of infinite extent, has derived an equation, called the Rayleigh equation, for *isothermal bubble dynamics* as

$$\frac{\rho_l}{g_c} \left[ r_{cr} \frac{d^2 r_{cr}}{dt^2} + \frac{3}{2} \left( \frac{dr_{cr}}{dt} \right)^2 \right] = \Delta p - \frac{2\sigma}{r_{cr}} \quad (3.8)$$

For many years, this equation has been solved by investigators for different models postulated to describe the actual bubble behaviour. As a result, an expression related to the bubble collapse time and the initial bubble size was normally obtained. However, the surface tension effects were not considered.

In the later part of bubble life, i.e., a few milliseconds after growth has begun, the inertia of surrounding liquid and the surface tension forces could be neglected. The pressure could be considered to be uniform throughout the bubble and the liquid. At this stage, bubble growth is governed by the rate at which heat can be supplied from the superheated liquid to the bubble interface to facilitate the vapour formation associated with growth. Accordingly the bubble behaviour was defined as *isobaric bubble dynamics* and described by the equation

$$\frac{\partial T}{\partial t} + u \frac{\partial T}{\partial r} = \alpha_l \frac{1}{r^2} \frac{\partial}{\partial r} \left( r^2 \frac{\partial T}{\partial r} \right) \quad (3.9)$$

$$\begin{aligned}
T(r, 0) &= T_{sup} \\
T(R, t) &= T_{sat} \\
T(\infty, t) &= T_{sup}
\end{aligned} \tag{3.10}$$

where  $T_{sup}$  denotes the superheated temperature of liquid and where the radial liquid velocity  $u$  for an incompressible liquid is subject to the continuity equation as

$$u = \left( \frac{\rho_l - \rho_v}{\rho_l} \right) \frac{dr_{cr}}{dt} \left( \frac{r_{cr}}{r} \right)^2 \tag{3.11}$$

The exact solution was obtained by Scriven (1959). The form of the solution was given as

$$r_{cr}(t) = 2C_1 \sqrt{\alpha_l t} \tag{3.12}$$

where the growth constant  $C_1$  is an implicit function of the Jakob number and the density ratio ( $\rho_l/\rho_v$ ) given by

$$\begin{aligned}
\mathbf{Ja} = \frac{\rho_l c_l}{\rho_v H_{fg}} (T_{sup} - T_{sat}) &= 2C_1^2 \exp \left[ C_1^2 \left( 3 + \frac{\rho_v}{\rho_l} \right) \right] \\
&\times \int_{C_1}^{\infty} \frac{1}{x} \exp \left[ \frac{-x^3 - 2(1 - \rho_v/\rho_l)C_1^3}{x} \right] dx \tag{3.13}
\end{aligned}$$

### 3.2.5 Bubble departure from a heated surface

At departure from a heated surface, the bubble size theoretically may be obtained from a dynamic force balance on the bubble. This should include allowance for surface forces, buoyancy, liquid inertia due to bubble growth, viscous forces and forces due to the liquid convection around the bubble. Such analysis was believed to be very difficult. However, for a horizontal surface, the maximum static bubble size was determined analytically as a function of contact angle, surface tension, and the liquid-vapour density difference. From such analyses, Fritz (1935) and Wark (1933) found the bubble diameter  $D_b$  just breaking off from a surface to be

$$D_b = C_d \theta \left[ \frac{2\sigma}{g(\rho_l - \rho_v)} \right]^{1/2} \tag{3.14}$$

where  $C_d$  is a constant (0.00148 for water) and  $\theta$  is the contact angle in degrees.

When a bubble starts to grow on a heating surface, a time interval  $\tau_d$  is required for it to depart from the surface. Griffith (1956) suggested that the inertia of the liquid could help detach the bubble from the surface and carry it away. Cold liquid then could rush in behind the departing bubble and touch the heating surface. A time interval  $\tau_c$  is required to heat the new liquid layer. Therefore, the frequency of bubble departure was defined as

$$f_b = \frac{1}{\tau_c + \tau_d} \quad (3.15)$$

A correlation between departure size and departure frequency was given by Peebles and Garber (1953) who observed the velocity of bubble rise in a gravitational field as

$$U_b = 1.18 \left[ \frac{\sigma g (\rho_l - \rho_v)}{\rho_l^2} \right]^{1/4} \quad (3.16)$$

Jakob and Linke (1933) observed that

$$U_b = D_b f_b = \frac{\tau_d}{\tau_d + \tau_c} 1.18 \left[ \frac{\sigma g (\rho_l - \rho_v)}{\rho_l^2} \right]^{1/4} \quad (3.17)$$

### 3.2.6 Correlation of nucleate boiling

For the nucleate boiling in water and organic coolant, Rohsenow (1951) assumed that the movement of bubbles at the instant of breaking away from the heating surface is of prime importance. The agitation caused by bubble release breaks the stagnant liquid film and thus provides an excellent convective heat transfer. From this convection concept, Rohsenow has developed a correlation for the nucleate pool boiling heat transfer coefficient by using nondimensional groups as follows:

$$\mathbf{Nu}_b = f(\mathbf{Re}_b, \mathbf{Pr}_l) \quad (3.18)$$

Empirically he found that

$$\frac{\mathbf{Re}_b \mathbf{Pr}_l}{\mathbf{Nu}_b} = C \mathbf{Re}_b^n \mathbf{Pr}_l^m = \mathbf{Sr} \quad (3.19)$$

where  $\mathbf{Sr}$ , the superheat ratio was defined as the ratio of liquid superheat at the heating surface to the heat of evaporation:

$$\mathbf{Sr} = \frac{C_l (T_w - T_{sat})}{H_{fg}} \quad (3.20)$$

and the correlation equation was in the form

$$\frac{C_l(T_w - T_{sat})}{H_{fg}} = C_{sf} \left( \frac{q/A}{\mu_l H_{fg}} \sqrt{\frac{g_0 \sigma}{g(\rho_l - \rho_v)}} \right)^{0.33} \left( \frac{C_l \mu_l}{k_l} \right)^{1.7} \quad (3.21)$$

where  $C_{sf}$  is a constant of surface-fluid combination for different fluids. It was reported that the Rohsenow correlation agreed remarkably well with the experimental data for different fluids.

Forster and Zuber (1955) assumed that the movement of the bubble boundary, while bubbles are still attached to the heating surface, is of prime importance. They considered isobaric bubble growth and obtained a relative solution. Their correlation was expressed as

$$\text{Nu} = 0.0015 \text{Re}_b^{0.62} \text{Pr}_l^{1/3} \quad (3.22)$$

where the Reynolds number was given as

$$\text{Re}_b = \frac{\rho_l \bar{r}}{\mu_l} \frac{d\bar{r}}{dt} = \frac{\rho_l}{\mu_l} \left( \frac{C_l \rho_l \Delta T \sqrt{\pi \alpha_l}}{H_{fg} \rho_v} \right)^2 \quad (3.23)$$

$\bar{r}$  is the characteristic radius and was expressed as

$$\bar{r} = \left( \frac{C_l \rho_l \Delta T \sqrt{\pi \alpha_l}}{H_{fg} \rho_v} \right) \left( \frac{2\sigma}{p_v - p_\infty} \right)^{1/2} \left( \frac{\rho_l}{p_v - p_\infty} \right)^{1/4} \quad (3.24)$$

Another different approach was given by Forster and Greif (1959), who suggested that the mechanism of the high heat transfer rate of nucleate boiling is mainly due to the liquid-vapour exchange. They also obtained a correlation for the pool boiling flux in water. However, the correlation was not as widely verified as the Rohsenow correlation.

### 3.3 Dielectric Liquids in an Electric Field

EHD techniques are thought to be best applied in dielectric or electrically insulated liquids. A dielectric is a material which is not an intrinsic conductor; in its purest form, it will contain no charge carriers. For example, hydrocarbon and other organic liquids, which have co-valent (shared electron) molecular bonds and have no free electrons, are classified as dielectric liquids. They do not conduct electricity to

any significant extent; what conductivity there is usually due to impurities. Metals contain large numbers of free electrons, and electrolytic solutions contain slightly smaller concentrations of ions, so they are good conductors of electricity.

Recent research in choosing dielectrics for EHD application suggests that slightly conducting fluids are better than insulators because the relaxation time should be much shorter than the bubble detachment period (Ogata & Yabe, 1993).

### 3.3.1 Polar and non-polar

Dielectric materials can normally be divided into polar and non-polar. A non-polar dielectric is one whose molecules possess no permanent dipole moment unless they are in the presence of an electric field. In this case the field induces molecular dipole moments by perturbing the electron cloud around the nucleus so as to produce a separation of the centre of negative charge and the centre of positive charge (Grant et al., 1978). This is shown in Figure 3.3.

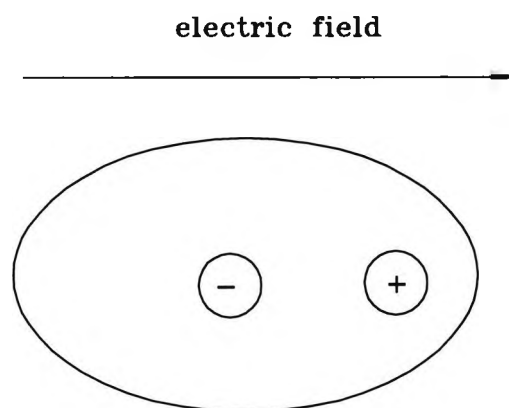


Figure 3.3: A molecule becomes polarized in an electric field. The positive nucleus moves one way and electron orbital the other.

A polar dielectric is one in which the individual molecules possess a dipole moment even in the absence of any applied electric field, i.e. the centre of positive charge is

displaced from the centre of negative charge. When a molecule having a permanent dipole moment is placed in an electric field, the positive end will tend to move in the direction of the field and negative end in the opposite direction; the molecule will therefore tend to rotate as shown in Figure 3.4. If there is no net charge on the molecule then it will experience no translational force. The molecule will not completely align itself in the field since it is also subject to the forces of Brownian motion transmitted by the random bombardment of its neighbours. In fact for the fields applied in typical dielectric work, the average angle of rotation caused by the field is only a small fraction of a degree, but for a system containing many such molecules the total effect is quite measurable and does give rise to high values of the relative permittivity.

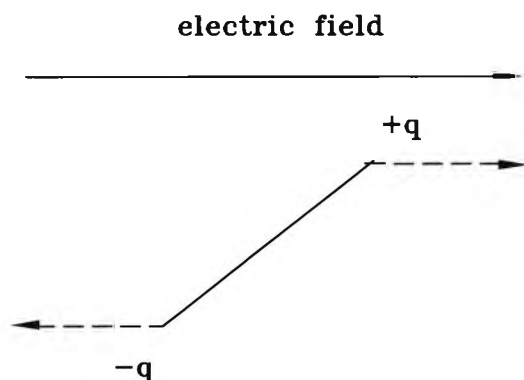


Figure 3.4: A dipole experiences a couple in an electric field. The dotted lines represent the forces felt by each charge.

The class of polar or non-polar can be easily recognized. A non-polar molecule must have a point of symmetry defined in such a way that the distribution of charges along (or near) any straight line passing through it must be symmetrical with respect to this point (Smyth, 1955 and Chelkowski, 1980). Thus a diatomic molecule is polar unless its two atoms are equal (e.g. the polar molecules *HCl*, *CO*

and the non-polar molecules  $H_2$ ,  $O_2$ ). Triatomic molecules of type  $AB_2$ , where  $A$  and  $B$  represent different atoms, are polar unless their nuclei lie on a straight line with  $A$  half-way between the two  $B$  atoms. Examples are the triatomic polar  $H_2O$  and the straight non-polar  $CO_2$  molecules.

The polar or non-polar can also be recognised from examining the properties of dielectric liquid (Grant, 1978). Owing to the interaction of the dipole moment with the electric field, a polar substance has a dielectric constant which is larger than that of a non-polar material. Another important difference between a non-polar and polar substance is that the dielectric constant of polar material is strongly dependent upon various physical parameters such as temperature, pressure, and frequency of applied field, whereas the electrical properties of a non-polar material are largely independent of them. Of particular importance is the variation of relative permittivity ( $\epsilon$ ) with frequency. For a polar substance,  $\epsilon$  decreases with increasing frequency as the motion of the molecular dipoles becomes progressively unable to keep up with the changes in direction of the electric field. Accompanying this fall in permittivity is an absorption of energy by the medium from the field.

### 3.3.2 Polarization

Polarization normally means the separation of negative and positive ions. Consider a condenser containing a dielectric material, with an external electric field. The dielectric increases the energy storage capacity of the condenser by neutralizing charges at the electrode surface. This phenomenon, called dielectric polarization and first identified by Faraday in 1837, might be visualized as the action of dipole chains which form in the material under the influence of the applied voltage and bind counter-charges on the conducting surfaces with their free ends, as illustrated in Figure 3.5.

This phenomenon involves the appearance of electric charges on the surface of the dielectric. These charges, known as induced charges, are not free and they generate a field known as the polarization field in the dielectric, whose direction is opposite

to that of the field that gives rise to polarization (Chelkowski, 1980).

The dielectric polarization is expressed as

$$\bar{P} = D - \epsilon_0 E = (\epsilon - 1)\epsilon_0 E = \chi\epsilon_0 E \quad (3.25)$$

where  $D$  is the dielectric displacement;  $E$  is the field intensity;  $\epsilon$  and  $\chi$  are relative permittivity and susceptibility, respectively.

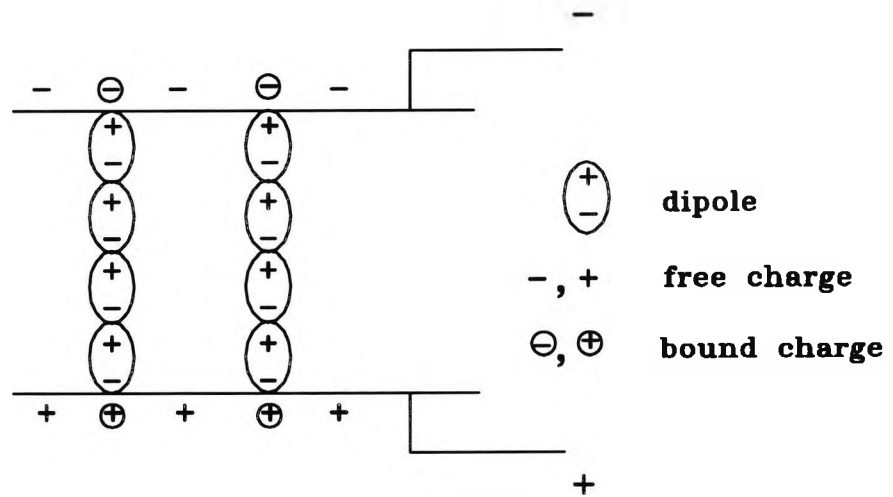


Figure 3.5: Schematic representation of dielectric polarization

There are four kinds of polarization, which can be characterised by appropriate polarizabilities, namely, electronic polarizability,  $\alpha_e$ , atomic polarizability,  $\alpha_a$ , orientation or dipole polarizability,  $\alpha_o$ , and space or surface-charge polarizability,  $\alpha_s$ , respectively. The resultant polarizability  $\alpha$  of a dielectric is the sum of these four kinds (Gemant, 1933 and Anderson, 1964):

$$\alpha = \alpha_e + \alpha_a + \alpha_o + \alpha_s \quad (3.26)$$

Accordingly, the four polarizations are called (1) electron polarization; (2) atomic polarization; (3) dipole polarization; (4) space or surface-charge polarization.

### 3.3.3 The motion behaviour

Motion is a basic behaviour of dielectric fluid/liquid in a strong electric field. The motions caused by an electric field may be subdivided into two groups, namely direct or electrical motions and indirect or mechanical motions.

By a direct motion is meant one where an electric force is applied directly to the liquid which is being displaced; thus the driving force here is of electrical nature. With an indirect motion the electrical force is first converted into mechanical, so that the dielectric which is being displaced is acted upon by a mechanical force.

In all, there are four possibilities of motion within a dielectric fluid/liquid under the influence of a high-voltage electric field:

1. *Dielectric displacement.* In this case dielectric liquid may be drawn to regions in which the electric field strength is higher because the polarization is greater there.
2. *The motion due to double-layers.* This may happen as cataphoresis of small particles in suspension, or as a motion of the liquid itself through a canal system (electro-endosmose).
3. *Space charge.* A dielectric liquid which contains a space charge may be directly accelerated by an electric field.
4. *Electric wind.* Ionized air acts mechanically as an electric wind upon an adjacent layer of the liquid and causes motions within it.

## 3.4 Research on EHD Nucleate Boiling

The use of electric fields to enhance heat transfer has been studied over nearly eighty years. The first research can be traced back to a UK patent reported by Chubb (1916) whose report on *Improvements relating to methods and apparatus for heating liquids* referred to the use of EHD in film boiling enhancement where a high voltage electrode placed in a liquid would destabilize the vapour film formed at the heat transfer surface at high rates of heat flux in the same way that a liquid condensate film can be electrically destabilized. Then, Senftleben and Braun (1936) are thought to be the first researchers to have reported results of EHD enhancement on single-phase heat transfer. After that, nearly all published work (Ahsmann and Kroning, 1950; Schmidt and Leidenfrost, 1953; Senftleben and Lange-Hahn, 1958; Allen, 1959) on EHD heat transfer was concerned with single-phase problems until the 1960s when the research on EHD phase change heat transfer began a relatively intense period.

### 3.4.1 Experimental (before the 1980's)

The first quantitative study on EHD pool boiling was published by Bochirol, et al (1960). After that quite a lot of experimental results which were relevant to EHD nucleate boiling were published. Some consistent conclusions, such as eliminating boiling hysteresis and promoting critical nucleate heat flux to higher values, have been reached. However, there is still some argument about whether nucleate boiling can be augmented by EHD action.

In the early experiments, many researchers employed a classical apparatus which was similar to the one originally developed by Senftleben and Braun (1936) to study EHD effects on single phase heat transfer, as shown in Figure 3.6. The apparatus was a relatively simple one which consisted of an electrically heated fine wire as a heat transfer surface and mounted along the horizontal central axis of a cylindrical tube which served as one electrode. These researchers include Bochirol (1960), Waston (1961), Bonjour (1962), Choi (1962) and Baboi (1968).

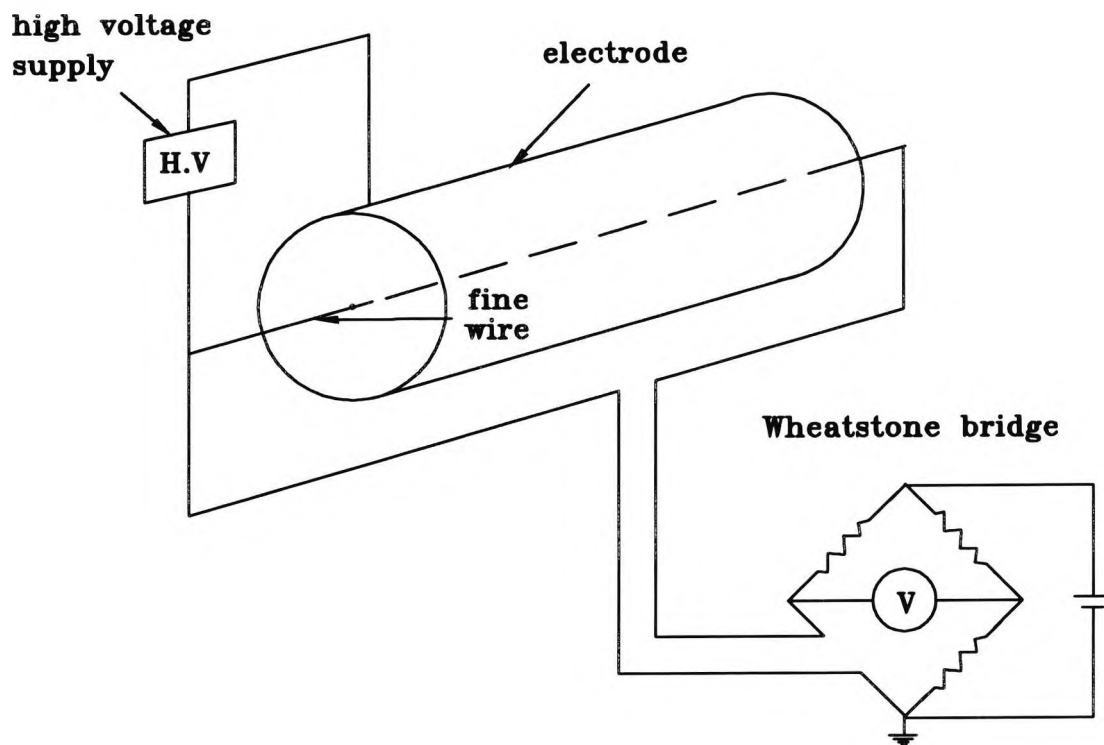


Figure 3.6: A classical fine wire apparatus

Bochirol, et al., (1960), applied 50-Hz a.c. potential to non-polar and polar insulating liquids as well as semi-conductors, respectively, in their experiments and reported the following results: (1) suppression of the number of active nucleation sites in the nucleate boiling regime. (2) destabilization of the vapour film in the film boiling. (3) absence of a distinct transition boiling regime between nucleate and film boiling for strong electric fields. This was probably due to the very high increases in heat transfer that could be achieved by EHD destabilization of film boiling and its reversion to nucleate boiling. Indeed, Bonjour, et al (1962), employing the same experimental method, observed that the bubble size in film boiling decreases with increasing field strength. He also suggested that the electric field

could be used to control boiling heat transfer by changing film boiling back to nucleate.

Similarly, Choi (1962), in an extensive study of EHD pool boiling of Refrigerant-113 using the fine wire apparatus and d.c. fields (48 – 168kV/cm at the wire surface), described EHD effects on nucleate boiling and on film boiling. He reported that, within nucleate boiling range, the electric field reduced the temperature difference ( $T_w - T_{sat}$ ) required for a given heat flux. He also noticed that the bubble diameter at departure decreases significantly with an increasing field, and the bubble frequency increases as well. The substantial increases in the peak nucleate and minimum heat flux values were also reported.

Waston (1961) is the first to report an EHD effect on the hysteretic nature of nucleation in an insulating liquid. This showed that EHD could eliminate nucleate boiling hysteresis.

Markels and Durfee (1964) have reported that pool boiling heat transfer to isopropanol from a steam-heated, chrome-plated copper tube was increased by as much as four times the normal peak heat flux by application of an electric field of up to 3.5 kV d.c. between the liquid and the tube. Film boiling and transition boiling with fields above 0.5 kV were completely eliminated, and the boiling was nucleate over the entire range of temperature difference covered (5-90°C).

Using two opposite facing circular plate electrodes, Asch (1966) investigated the effect of an electrostatic field on nucleate boiling of Refrigerant-113 and noted that bubbles are reduced in size and always move toward the positive electrode. Similar to Choi (1962), he also reported the significant increases in peak heat flux for both d.c. and a.c. potential, but only a slight effect on nucleate boiling.

Baboi, et al. (1968), using the fine wires apparatus, also reported some features of ebullition in an electric field, which are relevant to nucleate boiling problems. Both the boiling data and visual observation pictures were reported. These results can

be summarized as (1) In bubble boiling, the effectiveness of the field decreases as the thermal flux increases. (2) The boiling hysteresis (characteristic for fine wires in the absence of a field) was not observed under the action of an electric field. (3) The breakaway diameter of bubbles decreased with increasing field strength. (4) The electric field causes film boiling to revert to nucleate boiling, while the transitional region becomes smoother or disappears altogether, and at the intensities of about 500 kV/cm increase of the thermal load does not lead to the appearance of film boiling, even at the point when the heating elements burn out; this means that the transition regime is suppressed at high electric field.

Winer (1967) conducted an experimental study of the influence of nonuniform radial d.c. fields on Refrigerant-114. In his test rig a cylindrical resistance heater was used rather than a classical fine wire one. He found that the applied field could increase the heat transfer coefficient of the natural convection regime and both the peak and the minimum heat flux in the nucleate boiling regime. A great advantage he emphasized was that only a very small electrical power dissipation (less than  $2 \times 10^{-3}$  watts for the case of an applied voltage of 20 kV) for even a very high field strength was needed and this could make EHD control of fluid heat transfer so attractive. As a result, the great value of EHD in the design of actively controlled boilers was suggested.

Four years later, Lovenguth and Hanesian (1971), using d.c. potential and different types of dielectric liquids, corroborated other researchers' results concerning the EHD effect on the critical heat flux. As a result, a threefold increase was reported. The analytical model they developed for predicting the peak heat flux was also reported to be in good agreement with the experimental data.

At the same time, the effect of a uniform electric field on boiling heat transfer over the entire range of nucleate boiling and in the range of film boiling near the Leidenfrost point were studied by Olinger and Colver (1971). The study was made with pool boiling water from a 2×3 in. upward facing, flat, gold plated copper

surface with a parallel, flat, grid electrode. The results suggested that the polarity of the field (d.c.) and the amount of current passing through the boiling water could be the major factors for EHD nucleate boiling.

Zhorzholiani and Shekriladze (1972) obtained the transition data for several liquids by using cylindrical and planar electrode configurations. They examined the effects of both inhomogeneous and homogeneous fields on the boiling and found that the effect of an inhomogeneous field was not as significant as that of an homogeneous field.

Basu (1973), employing both d.c. and a.c. with carbon tetrachloride liquid, studied EHD effects on boiling hysteresis. He concluded that applying d.c. potential could produce more significant effects on the hysteresis than applying an a.c. potential.

In the late seventies, EHD effects on boiling cryogenic liquid were investigated by Rutkowski (1977 and 1980). In the experiments, liquid nitrogen was used and two types of electrode system, one consisting of two parallel cylinders and another of two coaxial cylinders, were employed. The experimental results indicated that the heat transfer in the natural convection zone and at the start of the nucleate boiling zone was greatly improved by electric field. By analysing the results, Rutkowski believed that the field could reduce the number and size of the bubbles; with an electric field influence, there is a smooth transition from convection zone to the nucleate boiling zone.

In order to study the effect of the field frequency on boiling, Zheltukhin (1978) examined the effects on both natural convection and boiling for three liquids using field frequencies from 15 to 1000 Hz. He found that the most significant effects on boiling were between 0 to 100 Hz and particularly at low heat flux densities.

In view of above results, the EHD effects on nucleate boiling seemed not very impressive.

### 3.4.2 Experimental (after the 1980's)

For EHD nucleate boiling, Allen and Cooper (1987) reported very interesting results in this area, which included that EHD eliminates boiling hysteresis and enhances nucleate boiling significantly. In their research, a single tube test rig, in which a cylindrical water-heated tube surrounded by a coaxial cylindrical copper mesh electrode was employed and a passive enhanced low-fin surface were tested. Refrigerant R-114 and Refrigerant-oil mixtures were used as the working fluids respectively. A video record was also provided by Allen and Cooper (Tenn.37996-2210) to prove the EHD effect on nucleate boiling. As a result, the potential applications of EHD boiling were suggested.

Almost at the same time, Yokoyama, et al. (1987) investigated the action of an electric field on boiling Refrigerant R-11 at smooth and porous plain surfaces. They found that the application of the field decreased the superheat required to initiate nucleation. The heat transfer coefficient for the smooth surface was increased to 3 to 6 times that of the zero field case. However, for the porous surface, the EHD augmentation was nearly zero.

The effect of an electric field on boiling heat transfer of Refrigerant-11 was also investigated experimentally by Kawahira, et al (1987). The test section consisted of a flat plate and a single tube with several rows of electrode wire. The following results were obtained. (1) As the applied voltage increased, the number of boiling bubbles decreased, but the heat transfer coefficient increased. (2) There was no deterioration of heat transfer by the oil contamination. (3) The polarity of the applied voltage affected the boiling heat transfer.

Yabe and Maki (1988) reported the augmentation effects of an EHD liquid jet on convection and nucleate boiling heat transfer of a mixture of Refrigerant R-113 (96% by weight) and ethanol (4%). The so called 'liquid jet', which was the jet flow ejected through the ring electrode in the direction away from the plate, was produced by applying a high voltage between the ring electrode and the plate elec-

trode. The results showed that the natural convection was enhanced by a maximum of over 100 times by the forced convection and turbulent effects of the EHD liquid jet. For nucleate boiling, the mean bubble detachment period was decreased and the critical flux was enhanced over times.

Karayiannis, et al. (1989), using the same test rig as Allen and Cooper (1987) and applying a radial d.c. electric field, studied the effects on nucleate boiling at a smooth tube with and without EHD. The results showed that applying EHD can eliminate boiling hysteresis for the smooth tube and reduce the superheat temperature requirement, but no further heat transfer enhancement was obtained.

Uemura, et al. (1990) reported their results for the boiling of Refrigerant R113 using d.c. potential. The enhancement of boiling heat transfer was addressed but this was especially emphasized for film boiling.

Damianidis, et al. (1991) examined the effect of EHD on nucleate boiling with a Thermoexcel-C surface, which is a commercial tube with a sharp sawtooth outer surface specially designed for condensation, in order to study the influence of the surface condition on EHD boiling. He found that this kind of condensing surface with EHD gave a better boiling result than for smooth or low-fin surfaces. An almost fivefold increase of EHD enhancement of boiling heat transfer coefficient was reported.

Results of an experimental study on EHD enhancement of nucleate pool boiling of R-123 and R-11 on a tube were reported by Ohadi, et al. (1992). It was demonstrated that the heat transfer performance can be significantly improved by utilizing EHD technique (In their experiments, a non-uniform circumferential field was applied). For the range of parameters investigated, they reported up to 450% enhancement for R-123 and corresponding 170% enhancement for R-11. However, they reported that the EHD enhancement was effective only on a smooth tube surface, there being no extra augmentation of boiling for porous or mechanical prepared surfaces.

To study EHD heat exchangers for the purpose of practical applications, experiments for the EHD effects on boiling augmentation in a tube bundle were carried out by Ogata, et al. (1992). Three types of apparatus had been made. One was a bundle element with five tubes, another was a short bundle with 50 tubes, and the third was a bench-scale model with a capacity of  $2.09 \times 10^5$  kJ/h. The experimental results clarified that the EHD augmentation of boiling heat transfer in the bundle was as effective as that in a single tube and the enhancement was reported of more than two and half times for the 50-smooth-tube bundle evaporator/boiler.

Similarly, the EHD enhancement of boiling for practical applications was also studied by Yabe, et al. (1992). A perforated coaxial cylindrical electrode inside the 3.75-m-long evaporator tube was employed in their experimental apparatus. The results of effective EHD boiling enhancement for an evaporator in heat pump systems using nonazeotropic mixtures of HCFC-123 and HFC-134a were reported. Some EHD phenomena observed, such as the bubble generation from the electrode, the EHD mixing of two-phase flow, the violent motion of bubbles along the heat transfer surface, and the flying of droplets generated by EHD surface instability, which would enhance heat transfer, were also addressed.

Also for practical applications, the performance of a 9-tube EHD heat exchanger developed in the U.K. was experimentally studied by Damianidis and Karayiannis, et al. (1992). The low-fin tubes were used in the tube bundle and Refrigerant R-114 was employed. Clear EHD enhancement for the tube bundle boiling was reported. The rate of enhancement was increased by increasing the electric field (from 0 – 30 kV).

Another 6-tube shell-and-tube evaporator (two-tube per pass and three-pass) designed in the U.K. was also studied by Karayiannis, et al. (1993). An R-12/oil mixture was used in their experiment. A significant increase in the heat transfer coefficient was obtained.

Ogata and Yabe (1993a and 1993b) published two papers concerned with EHD effect on nucleate boiling. Their experimental system consisted of a smooth copper tube and electrode wires with teflon insulators. The electrode wires ran along the length of the tube and were axially placed at equal distances along the tube. The positive d.c. potential was applied from the electrode. The test fluid was a mixture of Refrigerant R-11 and ethanol. They reported that the enhancement ratio of the boiling transfer with an electric field was about 8.5 times the maximum of that with no electric field. They observed that, under applied electric fields and temperature gradients, the number of boiling bubbles increased greatly, the generated bubbles were pushed against the injection plate and initially moved around on it violently, prior to migrating through the electric field. This could be one of the causes of heat transfer augmentation. It was also demonstrated that the heat transfer performance was augmented as the electric conductivity increased and became almost constant at electrical conductivities higher than  $7 \times 10^{-7} \text{ AV}^{-1}\text{m}^{-1}$ . The heat transfer augmentation reached a maximum of 50 times.

More recently, the compound effect of EHD and enhanced surfaces on boiling heat transfer enhancement was studied by Cheunh, et al. (1995) They have reported on the compound effect of EHD enhancement of boiling heat transfer of R-134a over an enhanced tube bundle using a straight wire electrode. Their results showed that the enhancement increased with applied electric field potential and the EHD effect was more pronounced at low heat flux levels. They also believed that the polarity of the electric field does not play any significant role in the nature and magnitude of the enhancement.

### **3.4.3 The correlations**

Correlation of heat transfer data in non-dimensional terms for specific geometries has long been proved a valuable tool for heat exchanger design. In the case of EHD assisted nucleate boiling, correlation has been attempted from the earlier work which was mainly concentrated on predicting the action of an electric field on critical nucleate boiling  $q_{cr}$ . The critical nucleate boiling is thought to be an important

factor since it could represent the maximum allowable heat transfer without leading to 'burn out'.

Choi (1962) tried to predict the effect of the electric field on the peak nucleate heat flux. He adopted Zuber's (1958) hydrodynamic approach and derived an equation as

$$\frac{(q)_{cr}}{\rho_v h_{fg}} \propto \left[ \frac{g_e \sigma (\rho_l - \rho_v)}{\rho_v^2} \right]^{\frac{1}{4}} \quad (3.27)$$

where  $g_e$  was the gravitational acceleration of a liquid-vapour system in the presence of the field and resulted from the polarization component of the electric force  $F_{e,p}$ . The  $g_e$  term was defined as

$$g_e \equiv \frac{F_{e,p}}{\rho} = \frac{\epsilon_o (\epsilon - 1) (\epsilon + 2) E_s^2}{3r_w \rho} \quad (3.28)$$

where  $\epsilon_o$  is vacuum permittivity,  $\epsilon$  the dielectric constant of the medium and  $r_w$  the radius of the heating wire.

Johnson (1968) considered the influence of the electric field on hydrodynamic stability. He amended the hydrodynamic theory of boiling heat transfer to include the effect of a perpendicular d.c. electric field across the vapour-liquid interfaces that exist at the maximum heat flux of nucleate boiling and correlated the ratio  $q_e/q_o$  as a function of fluid properties and electric field strength. The resulting equation for maximum heat flux condition was

$$\frac{(q_e)_{cr}}{(q_o)_{cr}} = \left\{ \frac{f \left[ 1 + \sqrt{1 + 3(\rho_l - \rho_v)g\sigma/f^2} \right]^{1/2}}{\sqrt{3(\rho_l - \rho_v)g\sigma}} \right\}^{1/2} \quad (3.29)$$

where

$$f = \frac{\epsilon_v (\epsilon_l - \epsilon_v)^2}{\epsilon_l \epsilon_l + \epsilon_v} E^2 \quad (3.30)$$

Baboi, et al (1968) analyzed the bubble departure diameter in the electric field. They assumed that the electric force acting on a bubble was purely dielectrophoretic, so the bubbles could not transport charges. The force was given as

$$F_e = \frac{3V_b \epsilon_l (\epsilon_v - \epsilon_l)}{2(\epsilon_v + 2\epsilon_l)} \nabla E^2 \quad (3.31)$$

where  $V_b$  is the volume of a bubble. By considering a steady-state balance between electric, buoyancy and surface tension forces and neglecting inertial or viscous forces, an expression for the breakaway diameter of a bubble was produced as

$$D_b^\epsilon = \omega(\theta) \sqrt{\frac{\sigma}{g(\rho_l - \rho_v)}} \left[ 1 + \frac{3\epsilon_l(\epsilon_v - \epsilon_l)\nabla E^2}{2(\epsilon_v + 2\epsilon_l)g(\rho_l - \rho_v)} \right]^{-1/2} \quad (3.32)$$

where  $\omega(\theta)$  is a given function of contact angle,  $\theta$ , which was assumed as

$$\omega(\theta) = 0.02\theta^\circ$$

Zhorzholiani and Shekrilardze (1972) found that the effect of application of both the homogeneous and inhomogeneous electric field was approximately the same. And the ratios  $q/q_{cr}$  were virtually identical for both homogeneous and inhomogeneous fields. On this basis, they have correlated their own data and those of Markels and Durfee (1964) on a log-log plot in the form

$$\frac{q}{q_{cr}} = f\left(\frac{F_D + g\rho}{g\rho}\right) \quad (3.33)$$

where  $F_D$  is the volume force density.

Berghmans (1976) considered a flat heater located in a conducting liquid and performed a stability analysis including the effect of a uniform d.c. field. This analysis resulted in

$$q_{cr} = \rho_v^{\frac{1}{2}} H_{fg} \frac{\pi}{2} \frac{1}{8} \left(\frac{1}{3}\right)^{\frac{1}{4}} (\sigma \rho_l g)^{\frac{1}{4}} \left[ \frac{G^2}{\sqrt{3}B} + \left(\frac{G^4}{3B^2} + 1\right)^{\frac{1}{2}} \right]^{\frac{1}{2}} \quad (3.34)$$

where

$$G^2 = \frac{\epsilon_v E^2 d}{\sigma} \quad (3.35)$$

is the ratio of electric forces to the surface tension forces. And the Bond number  $B$  is defined as

$$B^2 = \frac{\rho_l g d^2}{\sigma} \quad (3.36)$$

which is the ratio of inertia to surface tension forces.  $d$  is the vapour film thickness which can be obtained from experiments. This equation compared well with the data of Markels and Durfee (1964).

Cooper (1990) has proposed a model for EHD nucleate boiling that leads to the relationship

$$\left(\frac{h_e}{h_o}\right) Ne^{-n/2} = 0.3(Re_o)^{-0.16} \quad (3.37)$$

where  $h_e$  and  $h_o$  are the heat transfer coefficients with and without EHD respectively and  $n$  is found experimentally.  $Ne$  is an electrical influence number defined as

$$Ne = 1 + \left[ \frac{3\epsilon_l(\epsilon_l - \epsilon_v)}{2(\epsilon_v + 2\epsilon_l g(\rho_l - \rho_v))} \right] \nabla E^2 \quad (3.38)$$

The Reynolds number,  $Re_o$ , which took the bubble departure diameter under zero-field conditions as a characteristic dimension, was expressed as

$$Re_o = \frac{q}{H_{fg}\mu_l} \sqrt{\frac{\sigma}{g(\rho_l - \rho_v)}} \quad (3.39)$$

### 3.4.4 EHD enhancement mechanism

In parallel with the experimental studies of EHD effect on boiling heat transfer, the theoretical work for EHD enhancement mechanism has also drawn great attention from researchers for years. Indeed, EHD (electrohydrodynamic) is an interdisciplinary subject dealing with the interactions between electric fields and flow fields. Concerning the mechanism of EHD enhancement, any heat transfer phenomenon becomes more complicated when an electric field is applied.

The interactions among the electric field, flow field and temperature field have been analyzed and studied by many researchers. A quite detailed description for these interactions is shown in Figure 3.7 (Yabe, 1993). Actually, EHD enhancement mechanism studies are normally concerned with these interactions, either to describe the interactions mathematically or to predict the interaction results.

The interactions are thought to result from body forces (Coulomb force added to true electric charges and electrostriction force), interfacial stresses (Maxwell stress and the force due to the difference of dielectric constants across the surface), and the variation of physical properties due to temperature distribution (electrical conductivity, dielectric constant and mobility). In addition, there are some combined

body forces, such as the dielectrophoretic force due to the mutual effect of the temperature and electric fields. Therefore, the essential mechanism of enhancement phenomena is very complex.

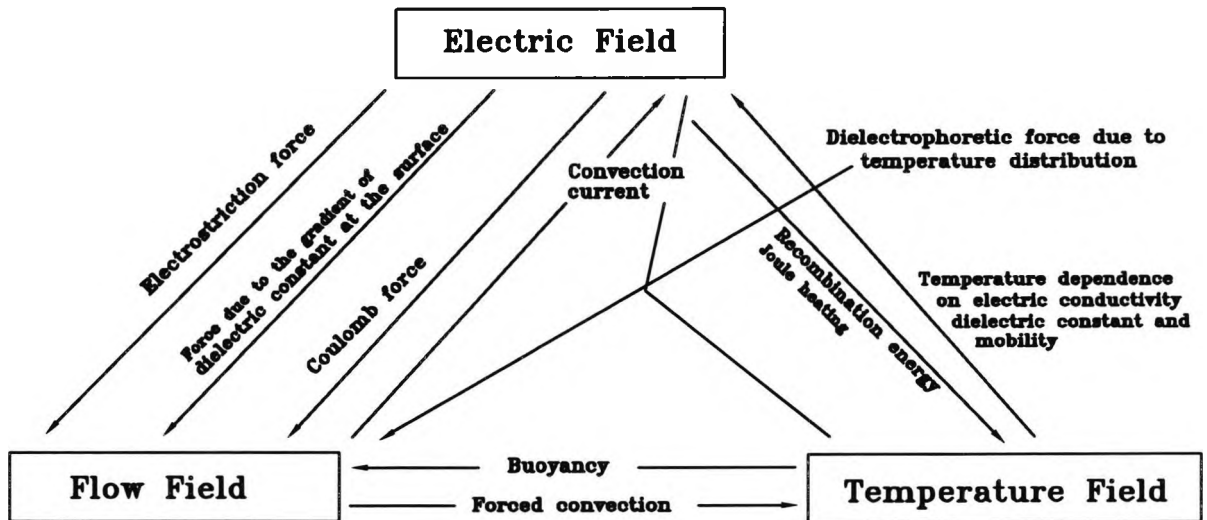


Figure 3.7: Interactions among electric, flow and temperature fields

### Electric body force

The electric body force which, in an electro-thermo-hydrodynamic system, is also called the EHD body force, has long been used to explain the enhancement mechanism. It can be derived by considering the changes of Helmholtz's free energy for virtual work with the energy  $[(1/2)\epsilon\epsilon_0 E^2]$  stored in the fluid under the electric field. The original expression for EHD force is from the branch of theoretical physics called *electrodynamics* and given by Stratton (1941) and Landau (1960)

$$F_e = q_e E - \frac{\epsilon_o}{2} E^2 \nabla \epsilon + \frac{\epsilon_o}{2} \nabla \left[ E^2 \left( \frac{\partial \epsilon}{\partial \rho} \right)_T \rho \right] \quad (3.40)$$

The first term of the right hand side of the equation, its electrophoretic component, is the Coulomb force exerted by an electric field upon a free charge in it. The electric charge density in the field,  $q_e$ , is the sum of charges of positive and negative ions and electrons within a unit volume. For single-phase convection where the permittivity of the fluid is more or less constant, the second and third terms on the right hand side of the equation become negligible. Therefore the Coulomb force (or the electrophoretic force) becomes the main driving force behind the EHD-induced secondary motions, known as the ionic wind or corona wind effect in a gas or a liquid. Miller (1981) suggested that the direction of this force is determined by the “sign” of charge and the field. By convection the “positive” force is in the direction of decreasing field strength.

The second term of the EHD force equation represents the force produced by spatial change of dielectric constant  $\epsilon$  and the magnitude of  $E^2$ . Physically, the sum of the second and third terms gives the force exerted on dielectric materials. Some researchers called these forces the dielectrophoretic and electrostrictive components of the force (Pohl, 1978).

The concept of forces exerted on dielectric materials was developed from the works of electrodynamics where dielectric polaribilities and dipole moment was considered. In particular, if the field were non-uniform, the driving force to cause dielectric displacement was suggested (Choi, 1962) as

$$F = \alpha E' \cdot \nabla E' \quad (3.41)$$

where  $E'$  represent the local electric field strength acting on the dipole and will be identical with the externally applied field strength  $E$  if the interaction between the molecules can be neglected (gases at low pressure);  $\alpha$  is the polarizability. On this basis, the dielectrophoretic and electrostrictive components of the EHD force could be obtained. If the fluid is non-polar, the electrostrictive force can be simplified by using the Clausius-Mossotti law and expressed as

$$\frac{\epsilon_o}{6}(\epsilon - 1)(\epsilon + 2)\nabla E^2$$

Although the net charge is zero in the case of polarization of dielectric materials, the polarized charges yielded at the stronger electric field are forced more strongly than the ones yielded at a weaker electric field. Therefore, the resultant force which is the sum of the forces exerted on each polarized charge, the fluid element is also forced to the stronger electric field region. These can be further explained by expressing the last two terms of the EHD force as  $[(\epsilon - \epsilon_o) \cdot \nabla] E_o$  (Yabe, 1993). This expression means that the polarized charge  $(\epsilon - \epsilon_o)$  is forced by the gradient of electric field strength.

Therefore, in phase change heat transfer (boiling and condensation), when the system is in the presence of an electric field, dielectrophoretic forces arise from the difference between vapour and liquid permittivities.

### Electric stress

The EHD force,  $F_e$ , can be transformed into the surface stress tensor form called Maxwell stress by the Gauss theorem as

$$\sigma_{ij}^M = -\frac{\epsilon_o}{2} \left[ \epsilon E^2 - E^2 \rho \left( \frac{\partial \epsilon}{\partial \rho} \right) \right] \delta_{ij} + \epsilon_o \epsilon E_i E_j \quad (3.42)$$

where  $i, j$  are the components of coordinate axes and  $\delta_{ij}$  is the Kronecker  $\delta$ . This stress is useful for examining EHD surface instabilities.

For two-phase heat transfer, Yabe (1993) suggested that the Maxwell stress should be effective at the vapour-liquid interface. For example, in the case of nucleate boiling, a vapour sphere with permittivity less than that of the host liquid will be driven towards regions of weaker electric field intensity. This means greater agitation of the adjacent liquid and disruption of the thermal boundary layer surrounding the heat transfer surface. Similarly in film boiling, destabilization of vapour interface and reduction in film thickness is the main driving mechanism behind enhancement.

Other expressions of stress tensor for a linear dielectric fluid in an electrostatic field

were also reported, for example, the Helmholtz tensor (Landau and Lifshitz, 1960)

$$\sigma_{ij}^H = \epsilon\epsilon_o E_i E_j - \frac{\epsilon_o E^2}{2} \left[ \epsilon - \rho \left( \frac{\partial \epsilon}{\partial \rho} \right)_T \right] \delta_{ij} - p_o(p, T) \delta_{ij} \quad (3.43)$$

and the Einstein-Laub tensor (Einstein and Laub, 1908 and Livens, 1916)

$$\sigma_{ij}^E = \epsilon\epsilon_o E_i E_j - \frac{\epsilon_o E^2}{2} \delta_{ij} \quad (3.44)$$

Clearly, these three stress tensors express the same physical phenomena subjected to different conditions. However recent research work on the stress tensor for a dielectric fluid in an electrostatic field conducted by Barletta and Zanchini (1993) has proved the limitations of the stress tensors proposed by Helmholtz and by Einstein-Laub.

### 3.4.5 Computational prediction of EHD effects

With the development of computational fluid dynamics (CFD), researchers attempted to predict the EHD effect on heat transfer by CFD methods. Wang, et al. (1989), using the Harwell code Flow3D release 2, predicted the effect of EHD forces on the flow and heat transfer in low Reynolds number laminar mixed convection in a vertical channel. The comparison between the predicted and experimental data was carried out and the theoretical results were reported to be in good agreement with the experimental results.

Dulikravich, et al. (1993) have reported the simulation results on EHD enhancement of laminar heat transfer. A mathematical model for laminar steady flow of an incompressible, viscous, neutrally-charged carrier fluid mixed with a fluid having electrically charged particles was developed and three cases, such as a closed container, a vertical channel and a U-shaped channel, were considered in the calculations. Numerical results have demonstrated the significant influence that an applied field and the consequent electric charge gradients can have on the flow pattern, temperature field and surface convection heat flux.

For phase change heat transfer, probably due to the complicated mechanism and

uncertain mathematical description, CFD simulations of EHD effects have not been reported yet. This future work would be challenging and attractive.

### **3.5 Summary of the Review**

In this Chapter, the literature concerning EHD effects on nucleate boiling, such as nucleate boiling at zero field, dielectric liquids in an electric field and research on EHD nucleate boiling, are reviewed. Conclusions from published literature can therefore be summarized.

Nucleate boiling with zero electric field as a traditional subject has given a basic description of the nucleate boiling behaviour and some background knowledge of the research.

There are two types of dielectric liquid, polar and non-polar, which can be identified by examining their properties. In particular, the non-polar one has molecules which possess no permanent dipole moment unless they are in the presence of an electric field. Polarization is a basic phenomenon for a dielectric fluid under the action of an electric field. Four kinds of polarization characterised by appropriate polarizabilities have been recognized. And motion is a basic behaviour of a dielectric fluid/liquid in a strong electric field.

The EHD effect on nucleate boiling has been studied for many years. This can be roughly classified as the experimental, the correlations and the mechanism studies.

The experimental work was reviewed according to the research progress before the 1980's and after the 1980's, respectively. In the first period, the EHD effects under different conditions, such as applying d.c or a.c potential, using polar or non-polar fluid and changing the polarities, were probed separately by different researchers. And major experimental work was done by employing the classic fine wire electrode system and a few by using a cylindrical electrode. The boiling surfaces investigated were normally plain or smooth ones. In that period, the research seems to

be much more concerned with EHD effects on the peak heat flux. Many consistent conclusions of EHD effects can be drawn from the published literature, such as: (1) increasing peak heat flux; (2) film boiling reverting to nucleate boiling or suppressing the transition regime; (3) the effect of a homogeneous field being more significant than that of an inhomogeneous field, (4) a d.c. potential producing more significant effects on boiling hysteresis elimination than an a.c. one. However, for nucleate boiling itself, there was no unanimous opinion as to whether it could be augmented by EHD action.

EHD nucleate boiling has become increasingly attractive since the 1980's and the research has been closer to the practical applications. To investigate EHD nucleate boiling at surfaces in heat exchangers, various coaxial (with the heating tube surface) cylindrical (mesh or rod) electrodes were employed and many kinds of refrigerant (pure or mixture) were tested. The test surfaces were not only smooth/plain but also mechanically prepared or passive enhanced ones. The consistent results may be summarized as: (1) nucleate boiling can be enhanced significantly by increasing electric field strength; (2) boiling hysteresis is eliminated by EHD effect; (3) nucleate bubbles are initiated at low superheat, which is thought to be attractive for applications with small temperature differences, such as the renewable source applications. (4) the number of boiling bubbles is increased greatly and bubble detachment period is decreased.

The correlation models were developed on the basis of hydrodynamic approach and have been used to predict the increase of the peak nucleate heat flux and the minimum film boiling heat flux under EHD actions. An expression for bubble breakaway diameter has been produced. Also, a correlation of nucleate boiling data has been presented with considerable success. This makes use of an electric field influence number and a modified Reynolds number based upon the bubble breakaway diameter.

The EHD enhancement mechanism has been extensively discussed by many researchers and was generally believed to lie in EHD body force. In the case of

nucleate boiling, dielectrophoretic forces arise from the difference between vapour and liquid permittivities and Maxwell stress is effective at the vapour-liquid interface.

# Chapter 4

## Theoretical Study

### 4.1 Introduction

The theoretical approach to EHD effects on nucleate boiling, as reviewed in the last chapter, has been attempted for many years. The major theoretical basis for EHD enhancement resulted from the EHD body force which was originally defined in electrodynamics. Much work has been carried out and discussed around the force. For EHD boiling heat transfer, the previous studies were mainly concerned with the critical nucleate boiling heat flux  $q_{cr}$  since it could represent the maximum allowable heat transfer without leading to 'burn out'. Some investigations have dealt with the bubble breakaway diameter, but the electric field effects on surface tension and contact angle were not considered. The basic research on EHD nucleation and nucleate boiling was less reported.

In the past years, many researchers have realized that different fields may have different effects on heat transfer; the electrode designs were therefore particularly emphasized. However, the surface (or the earthed electrode) geometry effect on EHD application was less noted. In fact, new developments in nucleate boiling, as reviewed in Chapter 2, are close connected with the employment of mechanically prepared or passively enhanced surfaces. These kinds of surface could offer a greater probability of finding active nucleation sites over the larger surface areas and in the meantime, they could also change the local electric field distribution and gradient on the surfaces, compared with smooth or plain surfaces. This re-

mains a very useful and interesting subject for EHD boiling research. This work is particularly worthwhile when the compound effect of using both EHD and passive enhanced methods on nucleate boiling is studied.

The present research focuses on the effects of an electric field on bubble generation in a refrigerant system of a heat exchanger and bubble movement. In particular, the enhancement of heat transfer using combined EHD and passive methods is discussed by predicting the surface geometry effect on EHD potential distribution.

## **4.2 Potential Distribution for Different Surfaces**

In order to investigate the effect of passive enhanced surface geometries on electric field strength, the computational analysis of the potential distribution near surfaces was undertaken using the PHOENICS CFD package, marketed by CHAM Ltd. of Wimbledon, U.K. In the present study, the smooth surface and five other types of passive enhanced surface are examined. The passive surfaces involved have a gradual shape change from the Gewa-T-like to the Thermoexcel-C-like surface.

### **4.2.1 Physical description**

Figure 4.1 gives six different outer surface geometries (Case (a) to Case (f)) for the boiling tubes. In practice, the Gewa-T surface is essentially a group of cavity slots on the tube surface causing the heating surface area to be increased and affecting the contact angles of the generated bubbles. The low fin surface is a passive enhanced surface which was initially introduced to enhance nucleate boiling and has had extensive application. The Thermoexcel-C surface was specifically designed for condensation and has sharp sawtooth fins. Finally, the smooth surface is a basis for comparison. In the practical system, the electric field is applied from the electrode which was co-axial with the boiling tube, and the boiling tube itself acted as another (earthed) electrode.

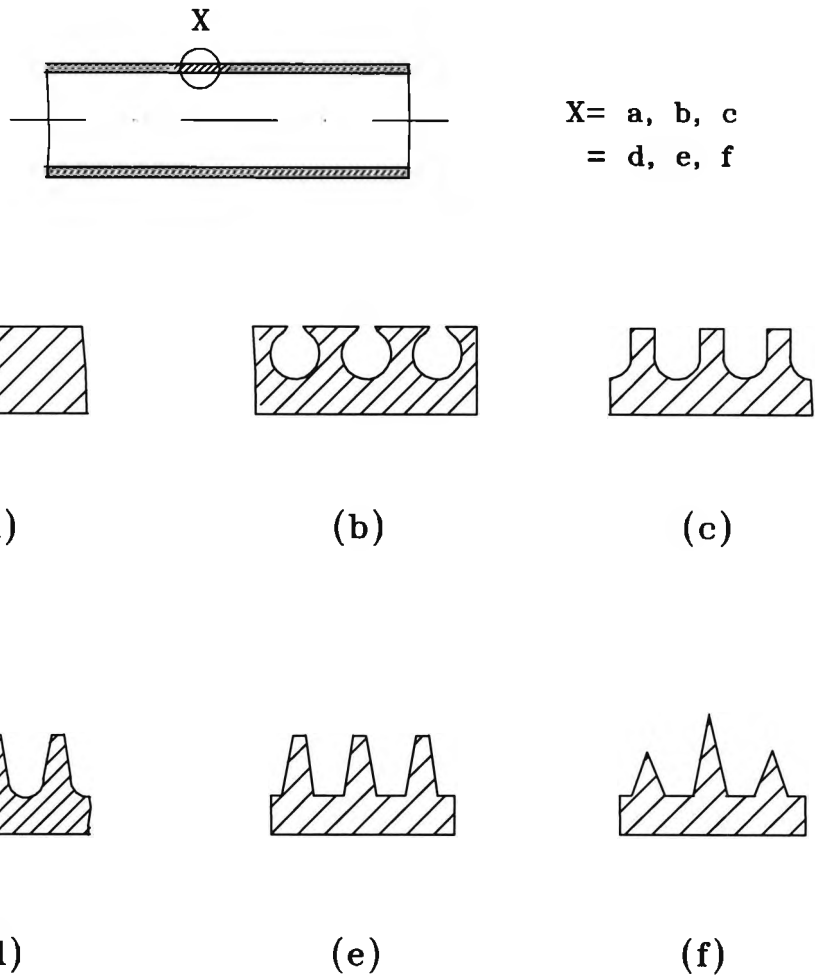


Figure 4.1: Six surface geometries of boiling tubes (a) smooth; (b) Gewa-T; (c) U-shape; (d) low-fin(1); (e) low-fin(2); (f) Thermoexcel-C.

## 4.2.2 Numerical method

### The basic equation

Since the relaxation time of electrical charge is much smaller than the boiling frequency, the liquid can be regarded as a conductive fluid (Jones, 1978). Also, due to the pool boiling being considered, the term for free charge is neglected. Therefore, the electric field potential distribution at surfaces can be described as

(1) continuity equation of electric current:

$$\nabla \cdot I = 0 \quad (4.1)$$

(2) by Ohm's law

$$I = \lambda_e E \quad (4.2)$$

(3) definition of electric field strength

$$E = -\nabla\phi \quad (4.3)$$

where  $\lambda_e$  is electric conductivity of the fluid between the electrode (upper electrode) and the surface (lower electrode). When  $\lambda_e$  is assumed to be constant, Laplace's equation can be obtained from the above equations as

$$\nabla^2\phi = 0 \quad (4.4)$$

This can be written in cylindrical coordinates as

$$\frac{1}{r} \frac{\partial}{\partial r} \left( r \frac{\partial \phi}{\partial r} \right) + \frac{1}{r^2} \frac{\partial^2 \phi}{\partial \theta^2} + \frac{\partial^2 \phi}{\partial z^2} = 0 \quad (4.5)$$

Neglecting the gravity field influence, circumferential axial symmetry can be assumed, that is :

$$\frac{\partial^2 \phi}{\partial \theta^2} = 0$$

then equation (4.5) becomes

$$\frac{1}{r} \frac{\partial}{\partial r} \left( r \frac{\partial \phi}{\partial r} \right) + \frac{\partial^2 \phi}{\partial z^2} = 0 \quad (4.6)$$

### Control volume and boundary conditions

Due to the periodic arrangement of these passive enhanced cavities on surfaces described in Figure 4.1 cases (b) to (f), the control domains were decided according to their symmetry. The domain for each kind of surface was chosen from the middle along the axial direction of the tube surface. The surface shapes to be analyzed in the 2-D control volumes with the coordinates are shown in Figure 4.2. Therefore, the boundary conditions can be expressed as

$$\begin{aligned} r = r_t = r_t(z), \quad 0 < z < z_b, \quad \phi = 0 \\ r = r_e(\%), \quad \phi = 10\% \text{ of applied field;} \\ z = 0, \quad \frac{\partial \phi}{\partial z} = 0; \\ z = z_b, \quad r \geq r_t, \quad \frac{\partial \phi}{\partial z} = 0; \end{aligned} \quad (4.7)$$

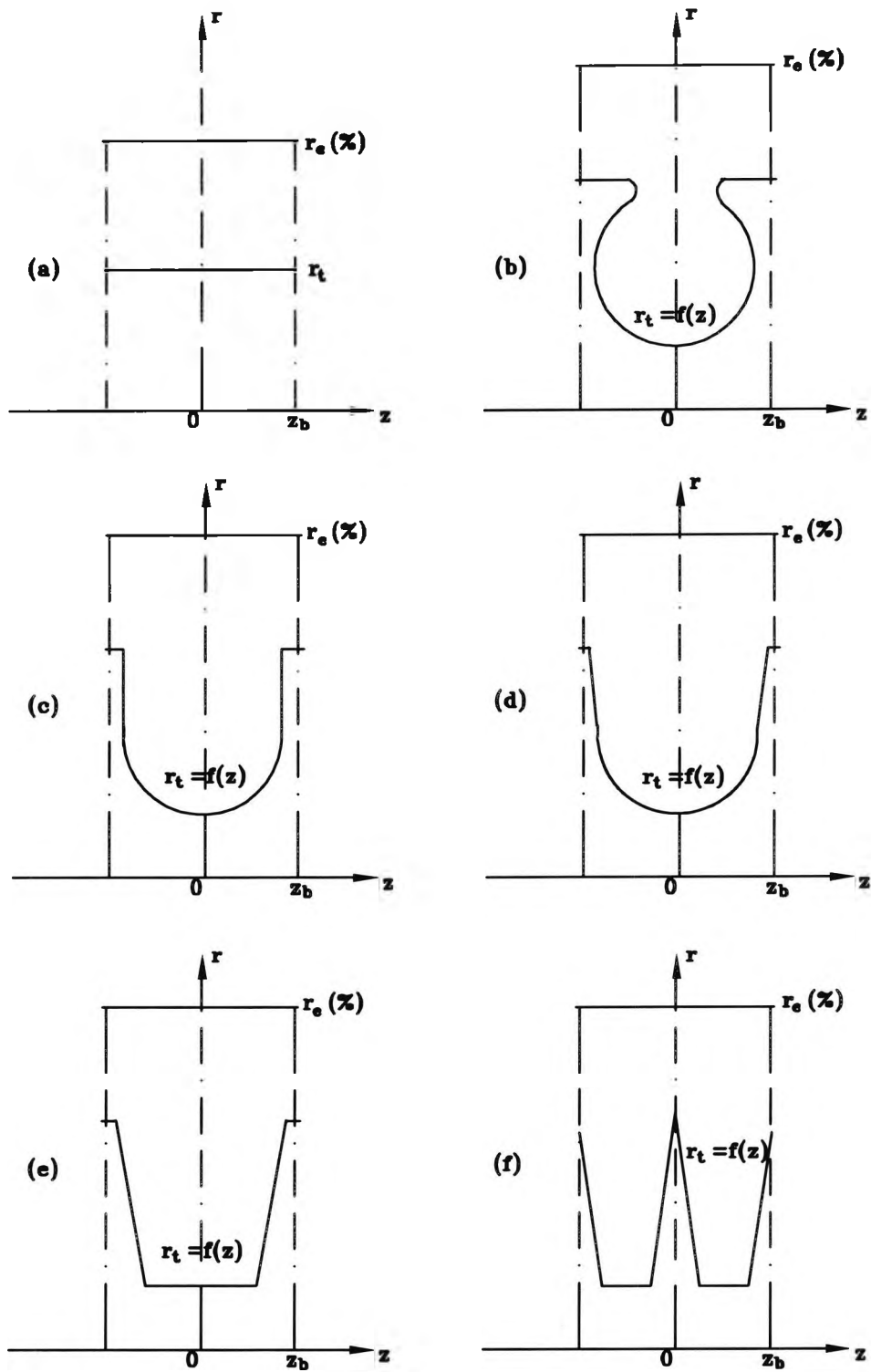


Figure 4.2: surface shapes to be analyzed in the 2-D control volumes with the coordinates

## Computational algorithm

To solve Laplace's equation described above, a PHOENICS CFD code was employed in which a finite volume technique is used. The body-fitted co-ordinates (BFC) method was applied to treat complex geometrical boundaries on different surface conditions and to generate the grids. The final generated grids for six different control volumes are shown in Figure 4.3. For each Case (b to f), they consist of 1440 cells and case (a) consists of 400 cells. Potential boundary conditions are specified for each case.

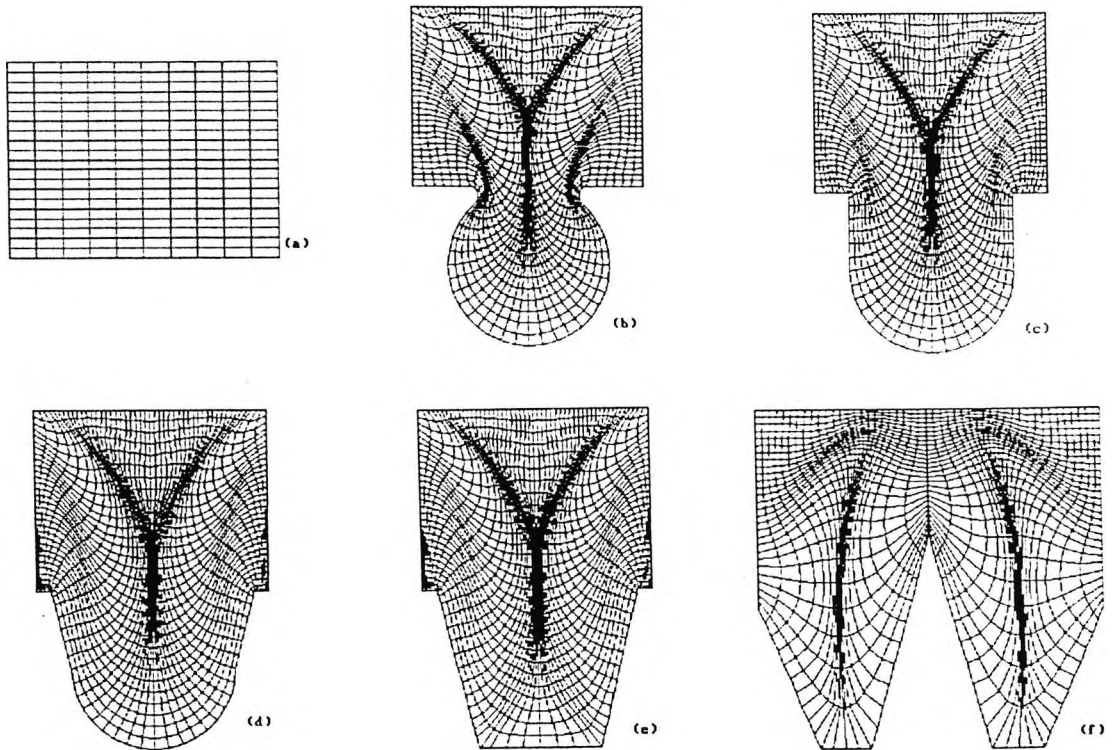


Figure 4.3: Grids for computation (a) smooth; (b) Gewa-T; (c) U-shape; (d) low-fin(1); (e) low-fin(2); (f) Thermoexcel-C.

### 4.2.3 Results and discussion

Solution of Laplace's equation for the electric field strength for all of the surface geometries shown in Figure 4.2 using the PHOENICS package gave equi-potential contours of voltage from which the field gradient could be measured to assess areas where the local value exceeded the far-field value by a marked amount. One would expect this to occur close to shoulders and points because these places were thought to become the first nucleate centres and as a result the higher local field gradient could stimulate the centres to be active and affect the contact angle of generated bubbles by influencing the surface tension at liquid-vapour interface and Figure 4.4 confirms this. Figure 4.4 shows the equi-potential contours applying an assumed 10% of the imposed (total) potential difference at the upper surface of the grid ( $r = r_{e(\%)}$ ) and zero voltage on the surface itself ( $r = r_t$ ). The numbers associated with each contour in the individual cases in Figures 4.4 are the percentages of the full voltage applied to the opposite plate (the surface). The field distortion and bunching of contours close to the corners and shoulders is quite clear.

Figure 4.5 shows a magnified version of the contours close to the shoulders marked "S" in Case (b). Although the contour smoothness has suffered slightly because of magnification, such plots enable the measurement of localised field gradients relative to the far-field value, given by the usual logarithmic relationship for cylindrical polar co-ordinates.

Figure 4.6 shows localised field gradients close to the shoulders marked "S" versus the relative voltages when the electrode potential was 30kV. This shows that in Case (b), the gradient close to the shoulders is much higher than the far-field value. Such a high potential gradient at the shoulders area should strongly affect the contact angles by decreasing the surface tensions at liquid-vapour interface. More analysis will be included in next section of this Chapter.

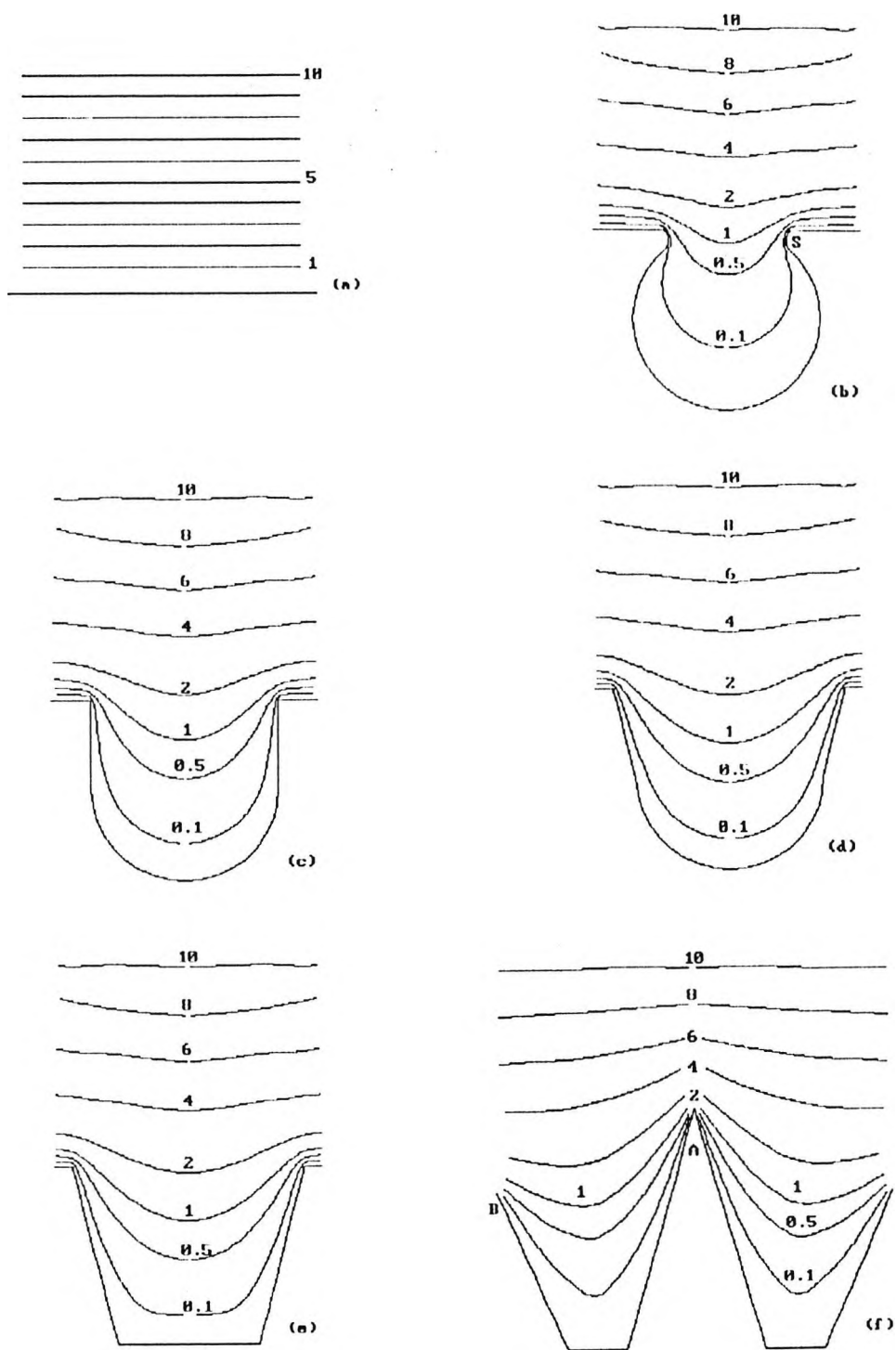


Figure 4.4: Equipotential contours for Case (a) to Case (f) (Numbers shown are percentages of full/electrode applied voltage)

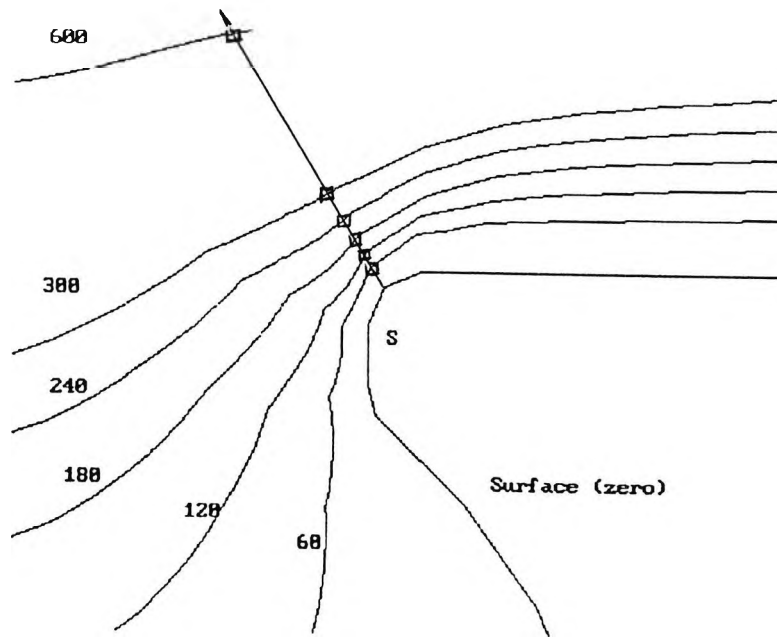


Figure 4.5: Magnified view of Case (b) contours (Number shown are in volts, for electrode potential  $\phi_e = 30$  kV)

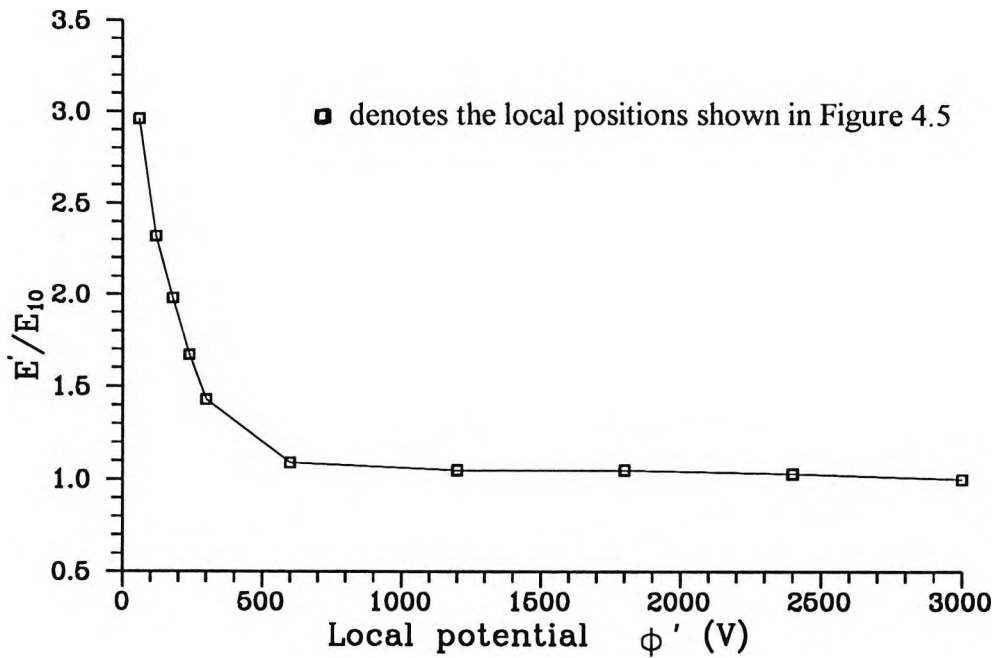


Figure 4.6: Localised field strength versus local voltage for Case (b) for electrode potential  $\phi_e = 30$  kV. ( $E'$  for localised field strength;  $E_{10}$  for 10% of the electrode strength;  $\phi'$  for local voltage)

Figure 4.7 shows a magnified view of the shoulders area marked "A" and "B", respectively, for Case (f) (the Thermoexcel-C) surface . Figure 4.8 gives the relative plot for the localised field gradients versus of the relative local voltages when the electrode potential was 30kV.

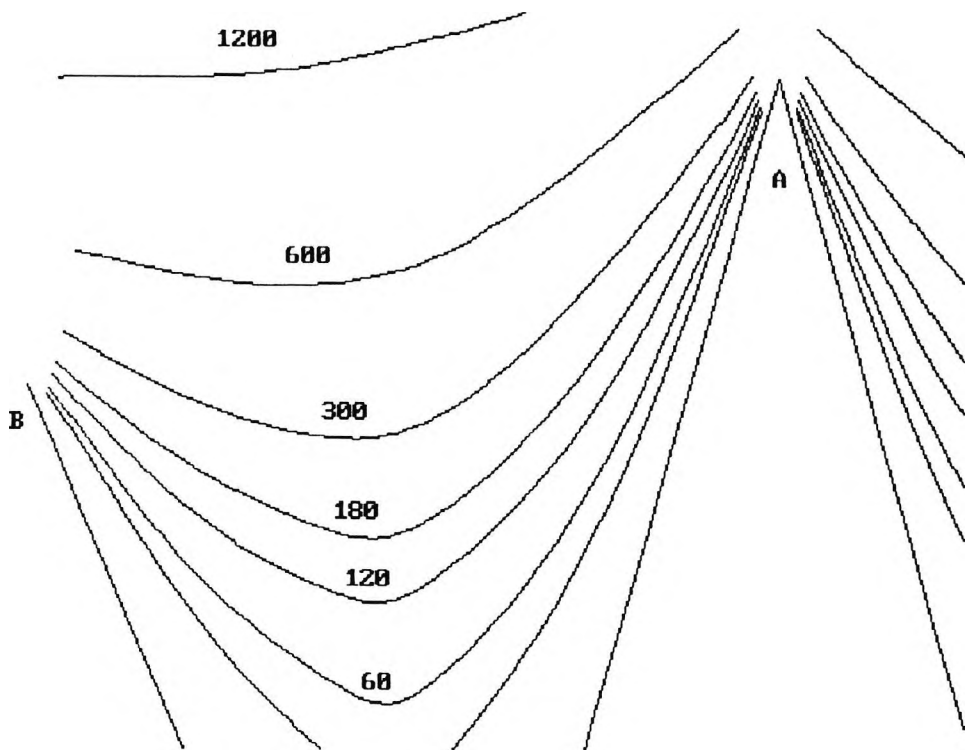


Figure 4.7: Magnified view of Case (f) contours (Numbers shown are in volts, for electrode potential  $\phi_e = 30$  kV)

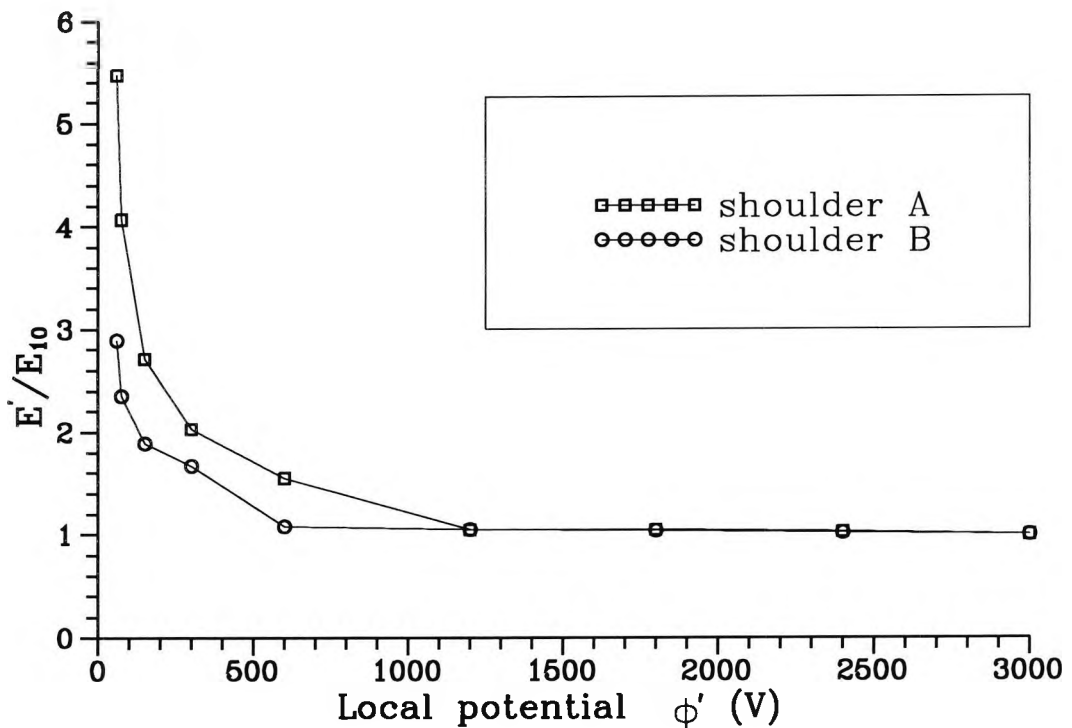


Figure 4.8: Localised field strength versus local voltage for Case (f) for electrode potential  $\phi_e = 30$  kV. ( $E'$  for localised field strength;  $E_{10}$  for 10% of the electrode strength;  $\phi'$  for local voltage)

Similarly, Figure 4.9 shows the localised field strength changes for all of the cases shown in Figure 4.2 when a 30kV electrode potential was applied. It can be seen from Figure 4.9 that in Case (a) an almost equi-field strength was obtained whereas the greatest localised increase in field gradient was found to be at the peaks in Case (f), where the relative increased values from a far-field gradient to the localised gradient close to the shoulders area was nearly twice as high as that in Case (b). However, Figure 4.7 should perhaps be regarded as optimistic, since the sharpness of surface points would be difficult to maintain in industrial use. Nevertheless, Case (f) closely resembles Thermoexcel-C and there is no doubting the very impressive performance of this surface under applied voltage, as reported in Chapter 5.

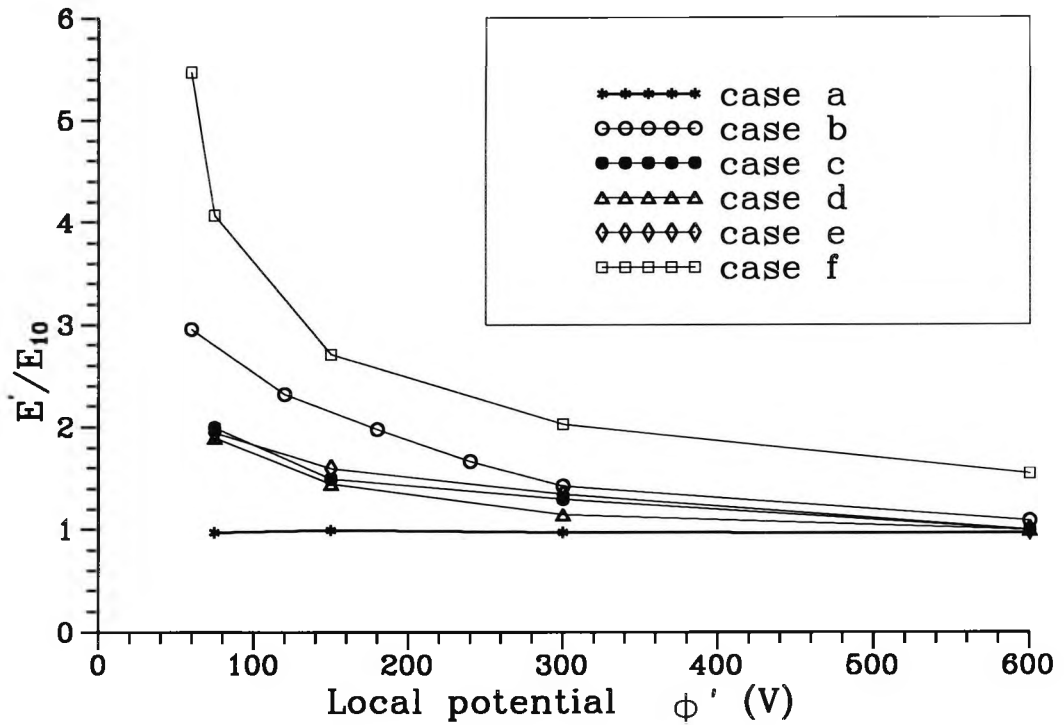


Figure 4.9: Localised field strength versus local voltage for Case (a) to Case (f) for electrode potential  $\phi_e = 30$  kV. ( $E'$  for localised field strength;  $E_{10}$  for 10% of the electrode strength;  $\phi'$  for local voltage)

From the localised field distribution on the passive surface cavities, it was interesting to note from the figures that high field gradients exist next to the shoulders area and that relatively low ones are inside surface cavities. These differences of field gradient in the surface cavities would help to drive the generated bubble sliding into the cavities to grow and move and result in heat transfer enhancement. Figures 4.10 and 4.11 give the localised field strengths changing with local voltages for different electrode potentials for Case (b) and Case (f), respectively.

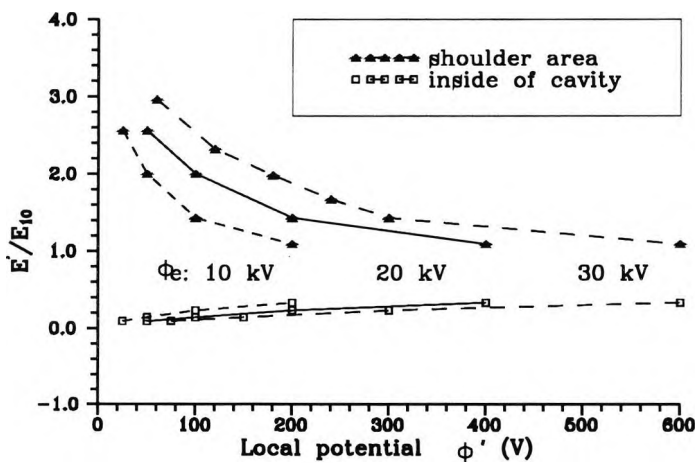
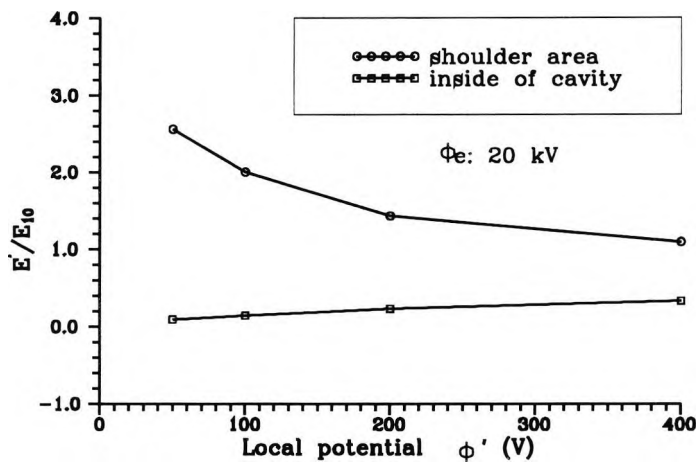
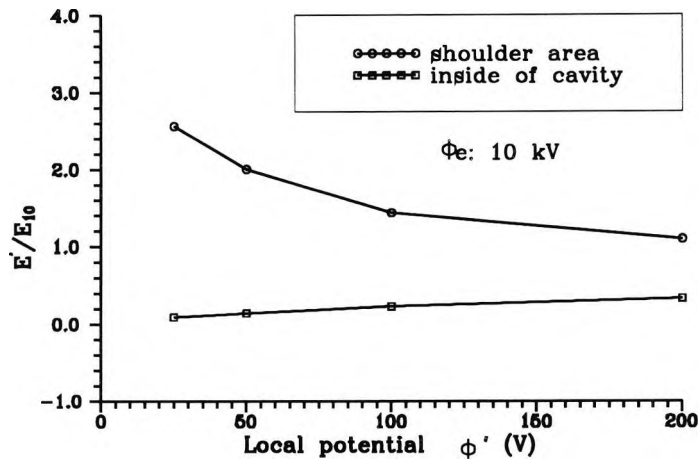


Figure 4.10: The ratio of field strength versus local voltage for Case (b) for different local area and electrode potentials. ( $E'$  for localised field strength;  $E_{10}$  for 10% of the electrode strength;  $\phi'$  for local voltage)

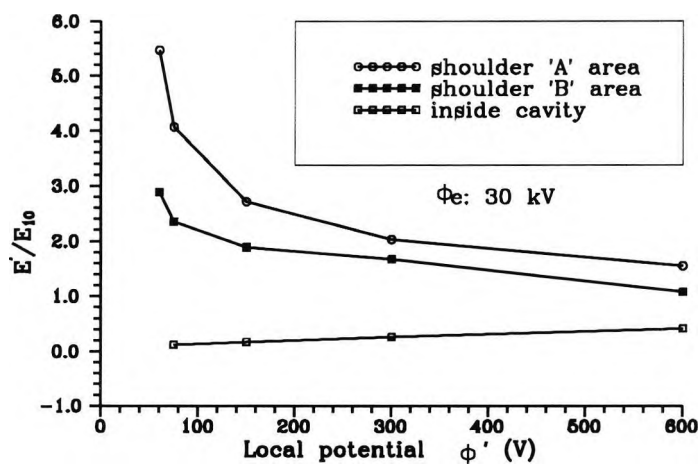
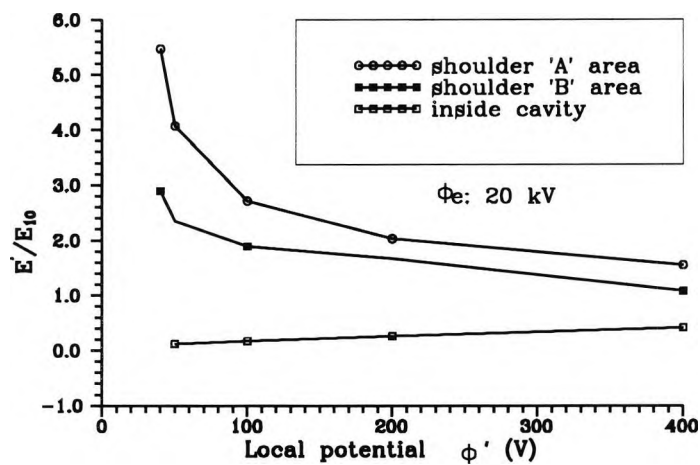
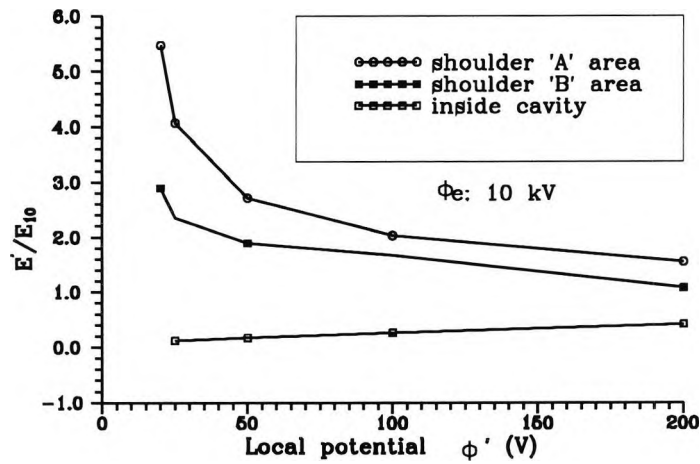


Figure 4.11: The ratio of field strength versus local voltage for Case (F) for different local area and electrode potentials. ( $E'$  for localised field strength;  $E_{10}$  for 10% of the electrode strength;  $\phi'$  for local voltage)

## 4.3 EHD Nucleation

Clearly, in a nucleate boiling process, nucleation itself is the basis. In this section, nucleation in the presence of an electric field is studied. This is based on the fact that the energy of the electric field in a dielectric fluid changes with bubble generation.

### 4.3.1 Nucleation without EHD

We first consider the nucleation in the *absence* of an electric field. For a refrigerant system in a heat exchanger, if the shape of a bubble nucleus is supposed to be spherical, the critical radius of the nucleus in the system can be derived from its equilibrium condition and be expressed by employing the Clausius-Clapeyron equation as

$$r_{cr}^o = \frac{2\sigma^o}{H_{fg}\Delta T} \frac{T_{sat}}{\rho_v} \quad (4.8)$$

where  $\sigma^o$  is the surface tension at the vapour-liquid boundary,  $H_{fg}$  the latent heat,  $\rho_v$  is the specific density of the vapour phase and  $\Delta T = T_w - T_{sat}$  is the wall superheat. The superheat used is different from the original definition for Clausius-Clapeyron equation, but similar treatment has been reported by Tong (1965).

From the fluctuational theory of fluid (Frenkel, 1946), the kinetic nucleation rate from liquid phase to vapour phase can be written as

$$J_o = C \exp \left[ -\frac{M}{R\rho_v T} \left( \Delta g^o + \frac{4\pi}{3} (r_{cr}^o)^2 \sigma^o \right) \right] \quad (4.9)$$

where C is a constant, M is relative molecular mass and R is the gas constant.

Obviously, in such a system, only the bubble nuclei whose radii are equal to or exceed the critical value are able to grow and move. Bubbles with a radius smaller than  $r_{cr}^o$  could not survive at all. There is no doubt that, on the basis of the heat transfer theory, a low superheat surface, such as the Gewa-T or the Thermoexcel versions, because of the greater probability of finding active sites over larger surface areas, can have a higher  $J_o$  than for plain or smooth surfaces.

### 4.3.2 Mathematical description

The additional energy  $\Delta w_{1-2}$

When the system with refrigerant fluid, which is a kind of dielectric liquid, is in the presence of an homogeneous electric field, an additional energy  $\Delta w_{1-2}$  must have been added to the system. This energy can be obtained by thermodynamic analysis. If the dielectric fluid is non-polar, like most refrigerants used in industry, such as R-114, etc., which has no permanent polarization, an infinitesimal change in the internal energy can be derived as (Guggenheim, 1967)

$$dU^e = TdS - pdV + V_c E dD \quad (4.10)$$

where  $V_c$  is the volume of the system that is subject to the electric field.  $D$  is the electric induction,  $D = \epsilon_o \epsilon E$ . Relatively, a new free energy can also be derived from the work of thermodynamics (Guggenheim, 1967)

$$F^e = U - TS - V_c E D$$

$$dF^e = -SdT - pdV - V_c D dE \quad (4.11)$$

and the free enthalpy was represented as

$$G^e = U - TS + pV - V_c E D$$

$$dG^e = V dp - SdT - V_c D dE \quad (4.12)$$

where  $V_c = V$  in a saturation state. Thus, an infinitesimal change in the Gibbs free energy per unit volume is

$$dg_i^e = dg_i^o - \epsilon_o \epsilon_i E dE \quad (4.13)$$

where  $g_i^o$  is the Gibbs free energy of the  $i$ -th phase in the absence of an electric field. The subscript  $i = 1$  is for liquid phase,  $i = 2$  is for vapour phase. By integration

$$g_i^e = g_i^o - \frac{1}{2} \epsilon_o \epsilon_i E^2 \quad (4.14)$$

Therefore, the change of Gibbs free energy during nucleation (from liquid-phase to vapour-phase) can now be obtained as

$$\Delta g^e = \Delta g^o + \frac{1}{2} \epsilon_o (\epsilon_2 - \epsilon_1) E^2 \quad (4.15)$$

and the additional energy is then obtained as

$$\Delta w_{1-2} = \Delta g^e - \Delta g^o = \frac{1}{2} \epsilon_o (\epsilon_2 - \epsilon_1) E^2 \quad (4.16)$$

### Surface tension $\sigma^e$

The surface tension at the liquid-vapour interface strongly depends on the strength of an external electric field. This was suggested by Frenkel (1946) who developed a formula as

$$\sigma^e = \sigma^o - \int_{-\infty}^{\infty} \epsilon_o \epsilon E^2 dx \quad (4.17)$$

where  $\sigma^o$  is the surface tension in the absence of the field. For the nucleate boiling system in a heat exchanger, if ignoring the changes of the permittivities in the same phase (the bulk liquid or the vapour state), the surface tension may be assumed as

$$\sigma^e = \sigma^o - \epsilon_o (\epsilon_1 - \epsilon_2) \int_{-\infty}^{\infty} E^2 dx \quad (4.18)$$

If the system is placed in a uniform electric field with two parallel plane plate electrodes, it can be expressed as

$$\sigma^e = \sigma^o - \Delta L \epsilon_o (\epsilon_1 - \epsilon_2) E^2 \quad (4.19)$$

where  $\Delta L$  is the vertical distance between the heat surface and the electrode.

For the case of heat exchangers with a coaxial cylindrical electrode system, the field strength is normally defined as

$$E = \frac{-\phi}{r \ln(r_e/r_t)} \quad (4.20)$$

where  $\phi$  is applied voltage from electrode;  $r$  is the distance from the heater surface to some point at which the magnitude of the field to be calculated;  $r_t$  and  $r_e$  respectively represent the heating tube radius and electrode radius. So the surface tension expression can be obtained as

$$\begin{aligned} \sigma^e &= \sigma^o - \epsilon_o (\epsilon_1 - \epsilon_2) \int_{r_t}^{r_e} E^2 dx \\ &= \sigma^o - \epsilon_o (\epsilon_1 - \epsilon_2) \int_{r_t}^{r_e} \left[ \frac{-\phi(r)}{r \ln(r_e/r_t)} \right]^2 dr \\ &= \sigma^o - \frac{\epsilon_o (\epsilon_1 - \epsilon_2)}{(\ln r_e - \ln r_t)^2} \int_{r_t}^{r_e} \left( \frac{\phi(r)}{r} \right)^2 dr \end{aligned} \quad (4.21)$$

Simply, if the electric field could be treated as uniform, then

$$\int_{r_t}^{r_e} \left( \frac{\phi(r)}{r} \right)^2 dr = \bar{E}^2 \cdot (r_e - r_t) \quad (4.22)$$

where  $\bar{E} = E = \phi(r)/r$  is a nominal uniform field strength at the radius  $r$ . For the area close to the shoulders of passive enhanced surfaces, based on the potential contours analysis mentioned before, the field strength may be represented as

$$E = \kappa \bar{E} \quad (4.23)$$

where  $\kappa$  is a coefficient for the enlargement. So the surface tension may then be generally expressed as

$$\sigma^e = \sigma^o - \Delta r \epsilon_o (\epsilon_1 - \epsilon_2) E^2 \quad (4.24)$$

where  $\Delta r = (r_e - r_t) / (\ln r_e - \ln r_t)^2$  is a nominal distance between the heater surface and the electrode.

#### Contact angle $\theta^e$

The bubble contact angle,  $\theta$ , is determined by the values of surface tension forces, namely  $\sigma_{sl}$ ,  $\sigma_{lv}$ ,  $\sigma_{vs}$ , and this is indicated in Figure 4.12.

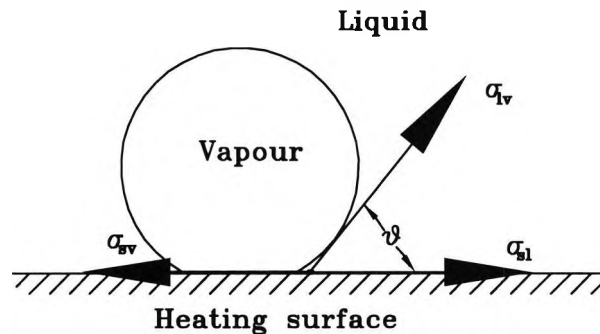


Figure 4.12: Surface tension forces acting at point of bubble contact

Taking account of the electric field effect on the surface tension at liquid-vapour interface, the contact angle is expressed as

$$\begin{aligned}\cos(\theta^e) &= \frac{\sigma_{sl} - \sigma_{vs}}{\sigma_{lv}^e} = \frac{\sigma_{sl} - \sigma_{vs}}{\sigma^e} \\ &= (\sigma_{sl} - \sigma_{vs}) / [\sigma^o - \Delta r \epsilon_o (\epsilon_1 - \epsilon_2) E^2]\end{aligned}\quad (4.25)$$

As the strength of electric field is increased, the value of  $\cos(\theta^e)$  ( $0 \leq \cos(\theta^e) \leq 1$ ) is enlarged. This means that the contact angle  $\theta^e$  ( $0^\circ \leq \theta \leq 90^\circ$ ) is decreased under the action of an electric field. According to the classic nucleate boiling theory, this may offer a better opportunity to initiate bubbles at reduced or lower superheat.

### Critical radius $r_{cr}^e$

From the theory of equilibrium thermodynamics, the Gibbs free energy can be expressed as (Zettlemoyer, 1969)

$$\Delta g^o = -\frac{\rho_2 H_{fg} \Delta T}{T_{sat}} \quad (4.26)$$

So the critical radius of a generated bubble nucleus can be written as

$$r_{cr}^e = \frac{2\sigma^e}{-\Delta g^e} = \frac{4T_{sat}\sigma^e}{2H_{fg}\Delta T\rho_2 + \epsilon_o T_{sat}(\epsilon_1 - \epsilon_2)E^2} \quad (4.27)$$

Considering the electric field influence on surface tension, then

$$r_{cr}^e = \frac{4T_{sat}[\sigma^o - \Delta r \epsilon_o (\epsilon_1 - \epsilon_2) E^2]}{2H_{fg}\Delta T\rho_2 + \epsilon_o T_{sat}(\epsilon_1 - \epsilon_2)E^2} \quad (4.28)$$

### Nucleation rate $J_e$

Similarly, if the effects of the electric field on critical radius and surface tension are considered in equation (4.9), the nucleation rate is obtained as

$$\begin{aligned}J_e &= C \exp \left[ -\frac{M}{R\rho_2 T} \left( \Delta g^e + \frac{4\pi}{3} (r_{cr}^e)^2 \sigma^e \right) \right] \\ &= C \exp \left\{ -\frac{M}{R\rho_2 T} \left[ \Delta g^o - \frac{1}{2} \gamma E^2 + \frac{A}{(2H_{fg}\Delta T\rho_2 + \gamma T_{sat} E^2)^2} \right] \right\}\end{aligned}\quad (4.29)$$

where  $C$  is constant;  $M$ , relative molecular mass (kg/mol);  $R$ , gas constant and

$$\gamma = \epsilon_o (\epsilon_1 - \epsilon_2) \quad (4.30)$$

$$A = \frac{64\pi}{3} T_{sat}^2 (\sigma^o - \Delta r \gamma E^2)^3 \quad (4.31)$$

### 4.3.3 Case calculation

Calculations have been carried out using the equations described above for Refrigerant R114, at different superheat temperatures and different electric field strengths. The physical properties of the refrigerant are given in Table 4.1.

Figure 4.13 shows the critical radii of bubble nuclei versus superheat for different field strengths. This indicates that the size of critical radii reduces with the increase of superheat significantly in the absence of an electric field; and as the applied field strength increases, this critical size becomes smaller and less dependent on the superheat. This suggests that increasing the field strength could help to initiate nucleate bubbles at lower superheat and as a result, more bubbles could be generated. Figure 4.14 shows the relative nucleation rate at different conditions. Nucleation rate increases with field strength but hardly at all with superheat. This may be used to explain why boiling hysteresis would still exist when wall superheat was increased, but could be eliminated under the action of an electric field. Figure 4.15 plots the relative nucleation rate versus applied electric field strengths at a given superheat.

Table 4.1: Physical properties of Refrigerant R114

name	Dichlorotetra-fluoroethane;
chemical formula	$\text{CClF}_2\text{CClF}_2$ ;
molecular weight $M$	$170.94 \times 10^{-3} \text{ kg/mol}$ ;
surface tension $\sigma^o$	0.014 N/m;
latent heat $H_{fg}$	130.459 kJ/kg;
saturation temperature $T_{sat}$	294.37 K;
density of saturated vapour $\rho_v$	13.958 kg/m <sup>3</sup>
relative permittivity, liquid $\epsilon_l$	1.83 (ambient temperature)
relative permittivity, vapour $\epsilon_v$	1.002 (ambient temperature)

There is no doubt that impressive performance, in terms of decreasing critical radii,

initiating bubbles at lower superheat and increasing nucleate rates, could be obtained at the shoulders area of passive enhanced surfaces under the action of an electric field because the very high localised field strengths exist there compared with the far-field or other area of the surfaces, as described in the last section.

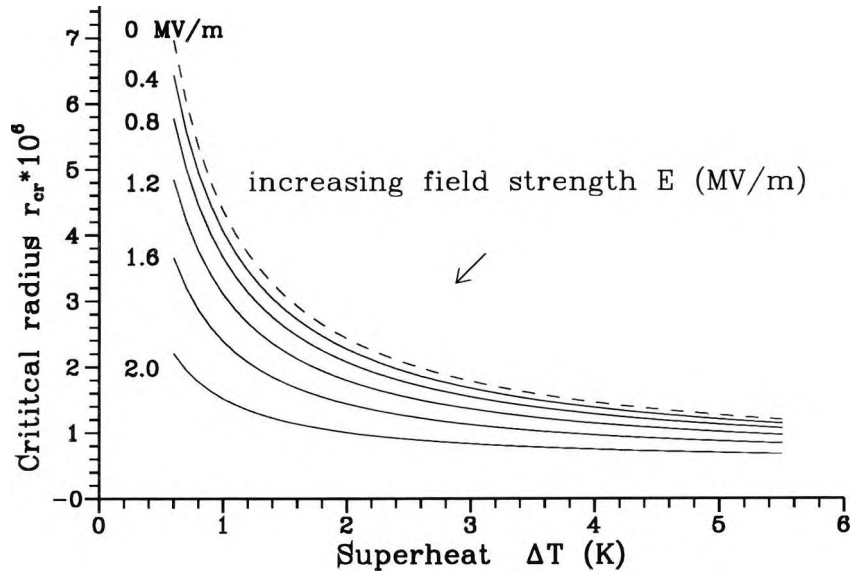


Figure 4.13: Critical radius of a bubble nucleus versus superheat for different field strengths

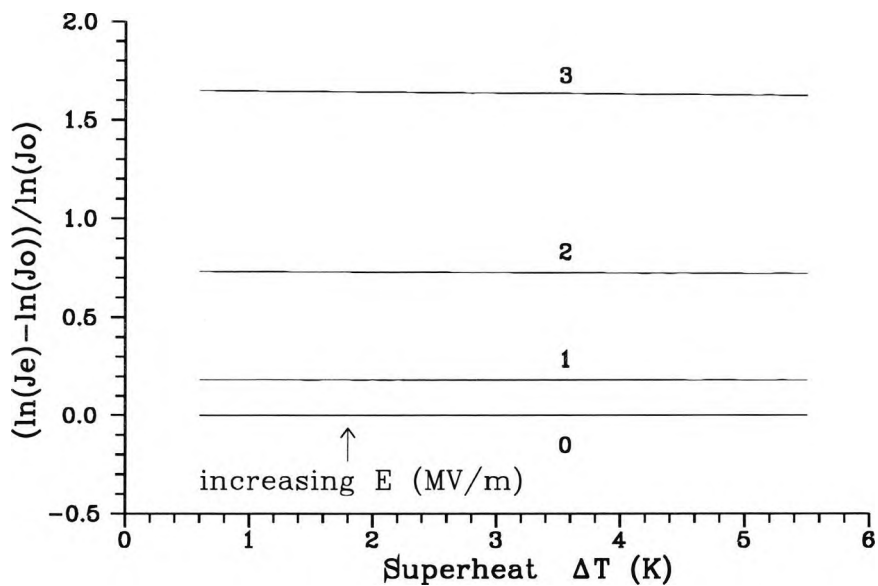


Figure 4.14: Relative nucleation rates versus superheat for different field strengths

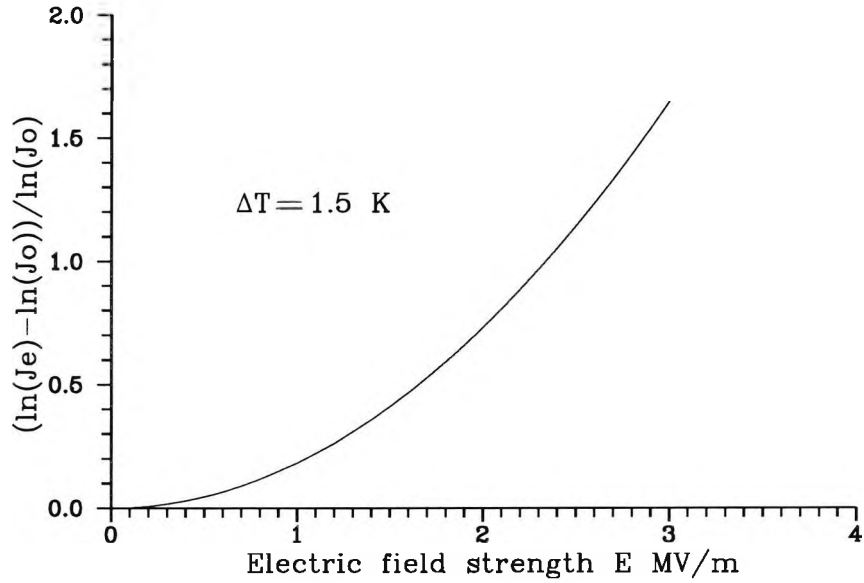


Figure 4.15: Relative nucleation rates versus field strengths at a given superheat

## 4.4 Bubbles Movement

In the nucleation process only small bubbles (nuclei), for which the size has exceeded critical radius, are formed. Initial growth from the nucleation size is controlled by inertia and surface tension effects. The growth rate is small at first but increases with bubble size as the surface tension effects become less significant.

When the system is in the presence of an electric field, the Maxwell stress is effective at the vapour-liquid interface of the generated bubbles. Since the gradient of the electric force should be normal to the boiling surface, the electric field in the lower part of the bubble should be weaker than in the upper part, so the bubbles are driven on to the heat surface by the dielectrophoretic force from EHD. At the same time, a vapour sphere with dielectric permittivity less than that of the host liquid will be driven towards regions of weaker electric field intensity. Figure 4.16

shows the EHD forces acting upon a generated bubble.

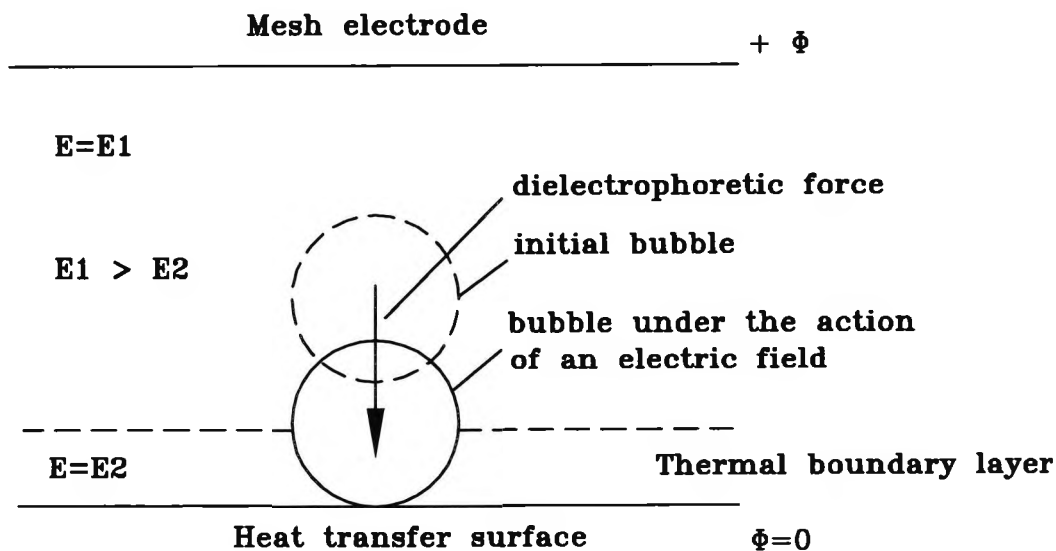


Figure 4.16: Force analysis on a generated bubble

Prediction and analysis for electric potential distribution around a spherical bubble at both a smooth and a Gewa-T surfaces were carried out. The co-ordinates are shown in Figure 4.17 and Figure 4.18, respectively.

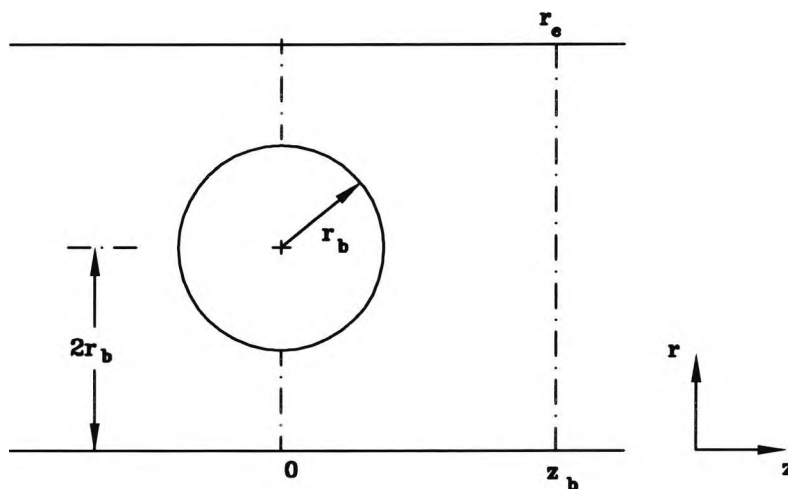


Figure 4.17: Coordinates for the analysis of potential distribution around a bubble at a smooth surface

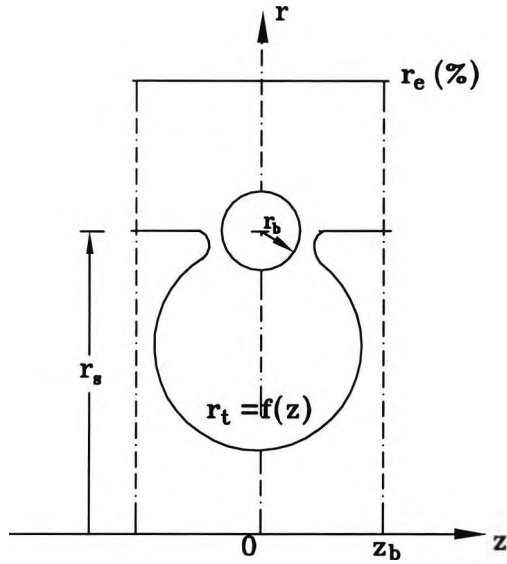


Figure 4.18: Coordinates for the analysis of potential distribution around a bubble at a Gewa-T surface

The analytical results are shown in Figure 4.19 and 4.20. These were done by using the PHOENICS CFD program. The mathematical model can be described as follows:

$$\nabla \cdot (\lambda_e \nabla \phi) = 0 \quad (4.32)$$

and

$$E = -\nabla \phi \quad (4.33)$$

If  $\lambda_e$  is assumed to be constant because the electric conductivity  $\lambda_e$  in the bulk liquid outside the bubble is nearly constant, then

$$\nabla^2 \phi = 0 \quad (4.34)$$

To simplify the problem, it has been treated two-dimensionally in order to assess the likely potential distribution near the cavity but a rigorous solution would need a three-dimensional approach.

For the smooth surface,

$$\begin{aligned}
 r = 0, & & \phi = 0; \\
 r = r_e, & & \phi = 10\% \text{ of applied field}; \\
 z = 0, \quad r > 3r_b, & & \\
 \text{and} \quad r < r_b, & & \frac{\partial \phi}{\partial z} = 0; \\
 z = z_b, & & \frac{\partial \phi}{\partial z} = 0; \\
 z^2 + (r - 2r_b)^2 = r_b^2, & & \frac{\partial \phi}{\partial n} = 0;
 \end{aligned} \tag{4.35}$$

normal to the liquid – vapour interface.

For the Gewa-T surface,

$$\begin{aligned}
 r = r_t = f(z), & & \phi = 0; \\
 r = r_e, & & \phi = 10\% \text{ of applied field}; \\
 z = 0, \quad r > r_s + r_b, & & \\
 \text{and} \quad r < r_s - r_b, & & \frac{\partial \phi}{\partial z} = 0; \\
 z = z_b, & & \frac{\partial \phi}{\partial z} = 0; \\
 z^2 + (r - r_s)^2 = r_b^2, & & \frac{\partial \phi}{\partial n} = 0;
 \end{aligned} \tag{4.36}$$

normal to the liquid – vapour interface.

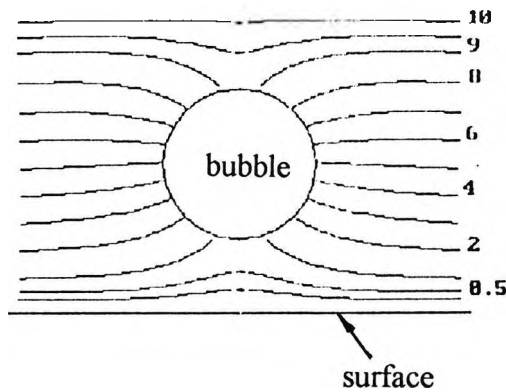


Figure 4.19: Equipotential contours around a bubble for a smooth surface (Numbers shown are percentages of full/electrode applied voltage)

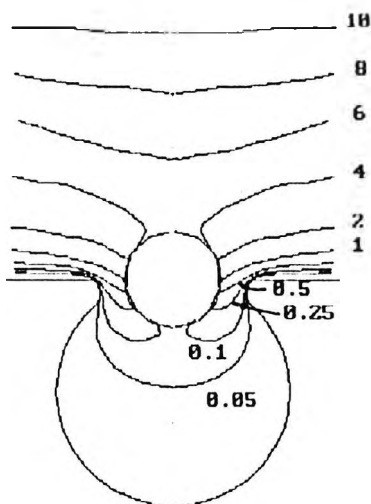


Figure 4.20: Equi-potential contours around a bubble for a Gewa-T surface (Numbers shown are percentages of full/electrode applied voltage)

These results indicated that a relatively lower localised field gradient exists in the area below the bubble and a relatively higher gradient in the area above the bubble when it was under the action of an electric field. And clearly, the field gradient difference above and below the bubbles for a passive enhanced surface like Gewa-T, as shown in Figure 4-20, is more significant than for a smooth surface, as shown in Figure 4-19. As a result the bubble would tend to move towards the heating surface by electric field effect. In other words, bubbles would be actively moved around the heat transfer surface by the radial component of the EHD force. Therefore, for boiling heat transfer, the EHD force could be *ordered* by designing the electrode system to make newly generated bubbles press onto the heat transfer surface, instead of breaking away from it.

In the meantime, bubbles moved around the heating surface would grow when the superheat was increased and tend to move up by the action of buoyancy. The compound effect of EHD force and buoyancy force would disintegrate bubbles into many smaller ones. As a result, the area of the thin liquid film under

the bubbles increases, and the heat transfer rate is enhanced. This is consistent with the enhancement mechanism explanation of nucleate boiling heat transfer, in which Cornwell (1990) suggested that, in the nucleate boiling region, the boiling heat transfer coefficient is dominated by sliding bubbles on the surface of heat transfer tubes and this sliding heat transfer is greatly influenced by the influx of liquid to the layer under the bubble as it slides along the surface.

For the case of EHD enhancement at passive enhanced surfaces, the compound effect of improvements in both nucleation rate and heat transfer enhancement should prove very attractive. There will be a greater probability of bubble nuclei generation over the increased surface areas and the surface geometry will affect the contact angle. Also, there will be marked differences in field gradient between the areas close to the shoulders and points, relative to the gradient in the cavities or the far field.

The above analysis is concerned with the EHD effect on a spherical bubble. In fact, deformations would happen when bubbles were under the action of an electric field. This has been proved by Ogata and Yabe (1993a) experimentally and the field distribution for a deformed bubble at a smooth surface was also reported (Ogata and Yabe, 1993a). However, for a passive enhanced surface, the type of bubble deformation has not been proved by experiment and the theoretical prediction for a deformed bubble would be a attractive.

## 4.5 Summary

The theoretical work reported in this chapter can be summarised as:

- The effect of applying an electric field on smooth and different passive enhanced surfaces has been analyzed by equi-potential contour calculation using a CFD method. The contour plots highlight the very high potential gradient existing near the shoulders area on these passive enhanced surfaces. The localised field gradients in the shoulders area are much higher than the far-

field gradients. Such a high potential gradient should strongly affect contact angles by decreasing surface tension at a liquid-vapour interface.

- For the localised field distribution on passive surface cavities, high field gradients exist next to the shoulders area and relatively lower ones inside the cavities. These differences of field gradient would help to drive the generated bubble sliding into the cavities to grow and move and result in heat transfer enhancement.
- Comparisons for the relative increase of localised field gradient close to the shoulders area and the far-field gradients for different surfaces as described in Case (a) to Case (f) have shown quite different results. This suggests that applying EHD techniques to a dielectric fluid at passive enhanced surfaces should lead to the development of an ideal surface shape for optimum performance. The enhancement would result in a compound effect on nucleation of both EHD enhancement and passive enhancement.
- The theoretical model for nucleation is based on equilibrium thermodynamics and fluid fluctuation theories. The calculated results from the model have indicated that, in the action of an electric field, the critical bubble radius becomes smaller and the nucleation rate is increased. This seems to be the basis for the EHD enhancement of nucleate boiling.
- The analysis of the bubble movement has indicated that the bubbles would be affected by the compound or cumulative factors of buoyancy and EHD forces. The resultant effect would enhance nucleate boiling heat transfer.

# Chapter 5

## Experimental Study

### 5.1 Introduction

Experimental studies of EHD effects on nucleate boiling, as reviewed before, have been carried out for many years. Concerning the EHD enhancement of nucleate boiling at practical surfaces in heat exchangers, much work has been done in the U.K., Japan and USA since 1980s.

In the U.K., the initial work was supported by the British Science and Engineering Research Council at Imperial College, London, between 1982 to 1984, when the EHD effect on nucleate boiling at a low-fin tube surface using Refrigerant 114 (also the condensation on a smooth surface using R-12) was examined by Allen and Cooper (1987). After that, the work was continued at City University, London, sponsored by British Technology Group, carried out by Karayannis et al. (1989) and Damianidis et al. (1992), and was concerned with EHD effects on nucleate boiling at smooth and Thermoexcel-C surfaces, as well as 9-tube EHD heat exchangers with low-fin tube surfaces using Refrigerant R114 as working fluid.

The present research, with the British Council's sponsorship, has been concentrating on the compound enhancement performance on nucleate boiling in heat exchangers using combined EHD and passive methods. EHD effects on nucleate boiling at passive enhanced surfaces, Thermoexcel-HE and Gewa-T, were particularly studied and results with those for other surfaces obtained under the same

experimental conditions were compared. The experimental work was carried out in the laboratories of City University.

## 5.2 Experimental Details

### 5.2.1 Passive surfaces

The tubes to be tested were selected from passive enhanced boiling tubes which were supplied by industry. One is Hitachi Thermoexcel-HE, another is Wieland Gewa-T. The surface geometries of these tubes are as shown in Figure 5.1 and the dimensions, together with those for comparison, are given in Table 5.1.

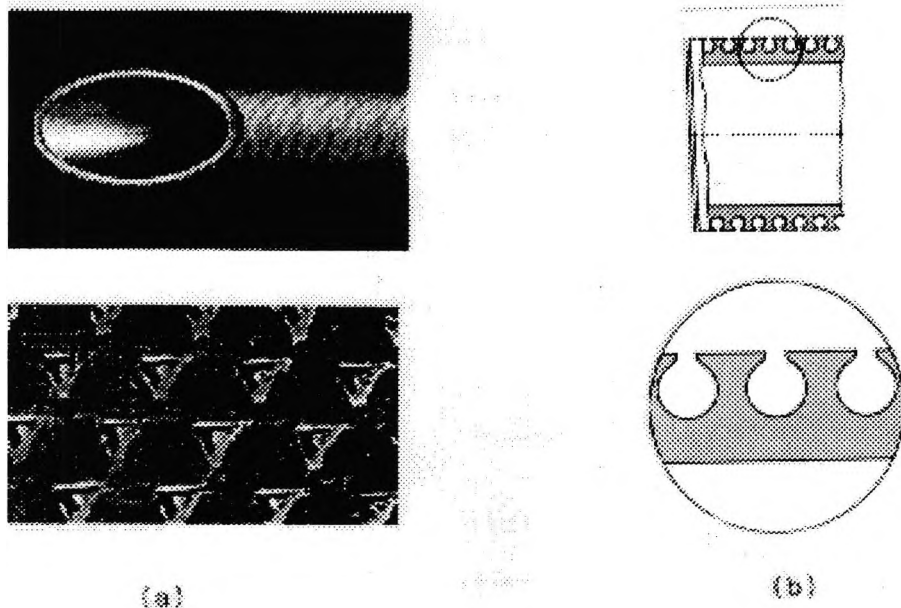


Figure 5.1: Profile of passive enhanced surfaces (a) Thermoexcel-HE; (b) Gewa-T.

Table 5.1: Dimensions of tubes for test and comparison

Tube type	$D_o$ (mm)	L (mm)	wall thickness (mm)	fin pitch (mm)	fin height (mm)
Thermoexcell-HE	19.0	506	1.1	0.5	1.1
Gewa-T(13515.5)	19.0	506	0.8	1.35	1.1
smooth	19.1	506	1.2	—	—
Low-fin	19.1	506	1.2	0.88	0.5
Thermoexcel-C	19.05	506	1.24	0.7	1.1

### 5.2.2 The working fluid

In order to compare experimental results with the earlier results for Thermoexcel-C, low-fin and smooth surfaces completed before, Refrigerant R114 ( $CClF_2CClF_2$ ) was used as working fluid in the experiments. The physical properties of this fluid has been given in Table 4-1.

### 5.2.3 Equipment and system

The experiments on EHD enhancement of nucleate boiling at passive enhanced surfaces were carried out using a single tube test rig shown in Figure 5.2. The shell consisted of a brass tube 0.0635 m inside diameter, and 0.506 m in length. A sight glass in the centre of the shell allowed visual observation of EHD boiling.

A cylindrical copper mesh electrode, 0.038 m in diameter, was aligned co-axially with the test tube, as shown in Figure 5.3. This dimension was chosen to give an inter-electrode-tube gap close the 'optimum' suggested by Didkovsky and Bologna (Cooper, 1986) while allowing sufficient clearance to accommodate the tolerance of manufacture. The electrode, which was supported and insulated from the shell by 'Tufnol' insulators, was at high voltage while the tubes and the heat exchanger shell were earthed. 0, 10, 20 and 30 kV were applied, which correspond to electric field strengths on the test tube surfaces of approximately 0, 1.5, 3.0 and 4.5 MV/m.

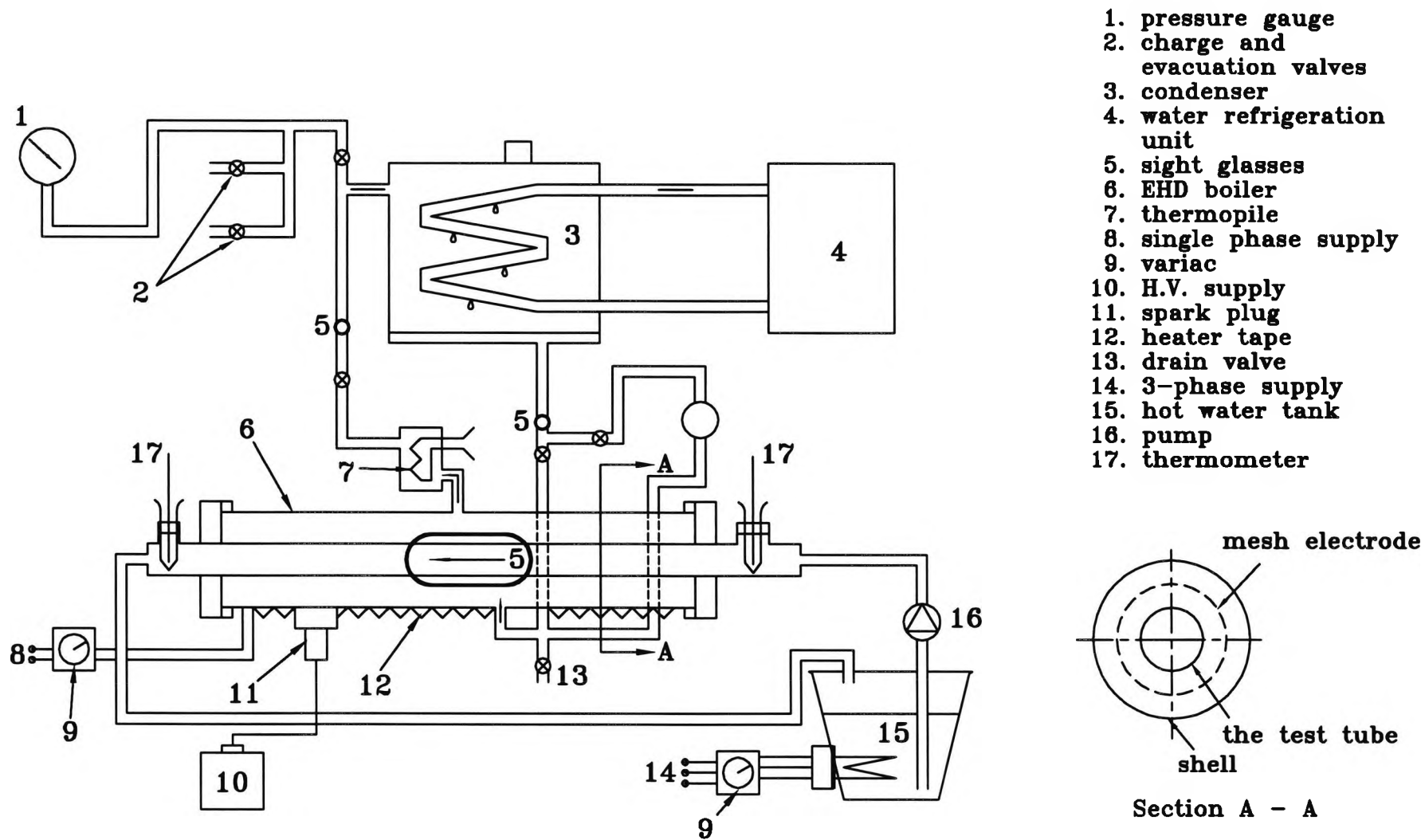


Figure 5.2: The single tube test rig

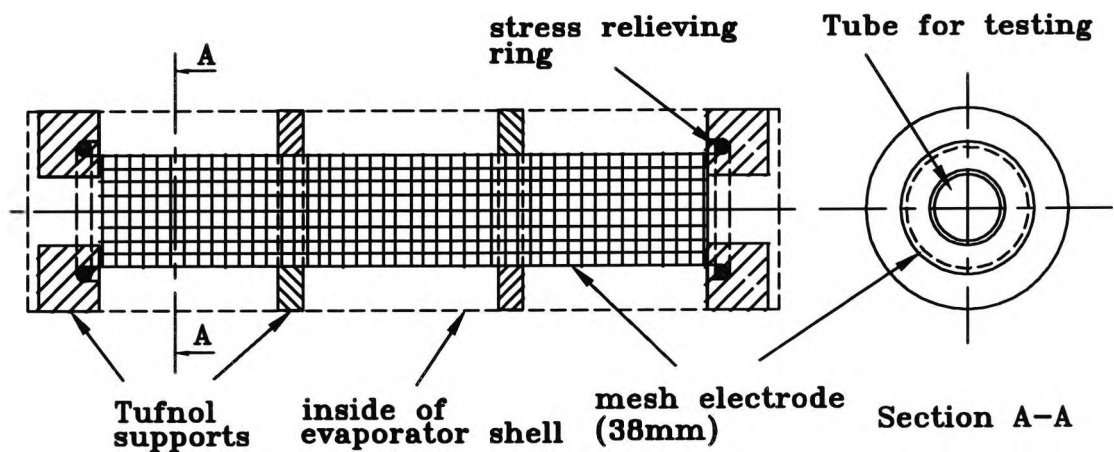


Figure 5.3: The mesh electrode assemblies

The test tubes were heated inside the tube by hot water and instrumented with copper-constantan thermocouples so that the surface temperature could be measured. The thermocouples were embedded in the tube wall at seven locations, as shown in Figure 5.4. Five of them (numbered as 3, 2, 1, 6, 7) were positioned equidistantly along the tube wall and two (numbered 4 and 5) in the middle of the tube at the top and bottom respectively. The thermocouple leads were isolated from the intense electric field by taking them out of the apparatus through the water side of the tube. Figure 5.5 shows the wall thermocouple installation.

Hot water to the test tube was provided by a pump from a water tank heated by a 3-phase 9 kW immersion heater which was controlled by a “Regavolt” variable three-phase auto-transformer (Variac) with a voltage output range 0 to 275V. The hot water flow rate was measured by a variable GAP flow meter with a range of 3 – 25 l/min for water at 20°C. The temperatures of the system were recorded by a PC computer by means of an SI3531F Data Acquisition system.



The working fluid, Refrigerant R114, was heated to boiling on the shell side and rose into the condenser where it was condensed and recirculated. Cooling at the condenser was accomplished by circulating water which was connected with a cooling/heating system, so that the cooling rate could be controlled by varying the flow rate and temperature of the cooling water. The saturation temperature was chosen to be constant at  $T_{sat} \simeq 21.5^\circ\text{C}$ . This was close to the ambient temperature and could be ensured by controlling the pressure inside condenser. Therefore the heat transfer to or from the surroundings was minimized. The temperature of the vapour existing in the evaporator was selected as the system saturation temperature. This is consistent with Hahne and Muller (1983) who suggested that saturation vapour temperature above the liquid surface should give the best correlation of results for boiling.

In addition, the single-tube heat exchanger was well insulated. The high voltage supply was obtained from a 'Sames' electrostatic generator for d.c. potential. This was capable of supplying positive d.c. up to 80kV with a maximum current of  $200\mu\text{A}$ . The high voltage was fed through a potential divider to the sparking plug in the wall of the single tube test equipment and was measured by a 'Pye' electrostatic voltmeter of 40kV maximum RMS indication. Electric current measurement was taken using a five-range d.c. microammeter calibrated to BS89 with a maximum reading of  $200\mu\text{A}$ . The electrical equipment and connections are shown schematically in Figure 5.6.

A Faraday cage was used to isolate the experimental rig and the high voltage equipment from the surroundings and allow safe operation. All parts of the high voltage circuit were earthed.

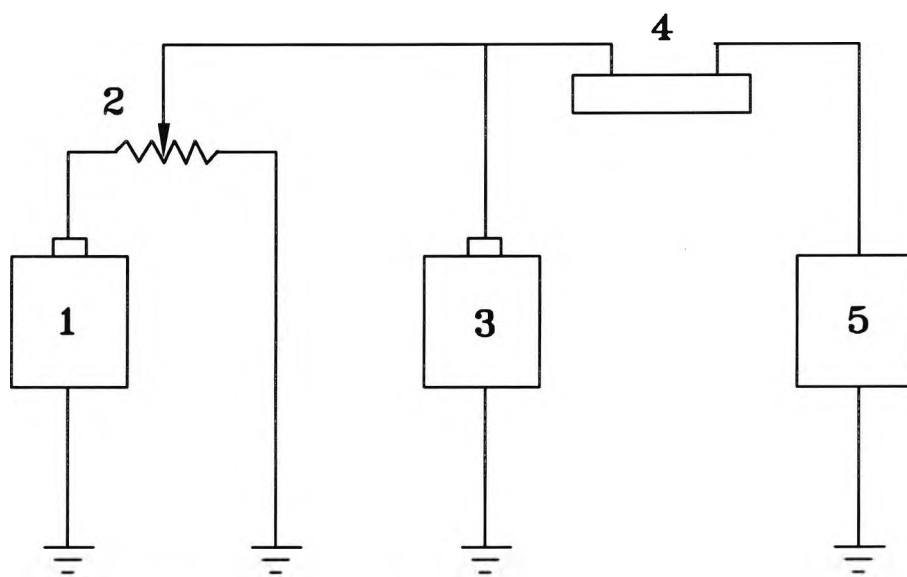


Figure 5.6: Electrical circuitry (1) high voltage supply; (2) potential divider; (3) voltmeter; (4) ammeter; (5) single tube test rig

#### 5.2.4 Method and procedures

During the experiments, an auxiliary heater tape attached to the underside of the boiler shell was first turned on for about 30 minutes to ensure degassing of the working fluid and initial isothermal conditions in the test rig. Then the hot and cooling water circuits were activated and the electric field was applied. After that, the system saturation temperature was normally maintained constant by adjusting the cooling water temperature and flow rate. Thus, the heat transferred to the

boiling refrigerant through the tube could be assumed equal to the rate of energy loss of the circulating water inside the tube, namely

$$Q = \dot{m}c_p(T_{in} - T_{out}) \quad (5.1)$$

where the physical properties were obtained from tables for mean water temperature  $T_m = (T_{in} + T_{out})/2$ . Finally, data were recorded when the system was at steady state. The mean wall temperature was calculated as

$$T_{wm} = \frac{1}{5} \sum_{i=1, i \neq 4, 5}^7 (T_i - \Delta T_c) \quad (5.2)$$

where  $T_i$ ,  $i = 1, \dots, 7$  are the measured wall temperatures as illustrated in Figure 5.4 and

$$\Delta T_c = \frac{T_1 + T_4 + T_5}{3} - T_1 \quad (5.3)$$

The heat flux  $q$  and the degree of superheat  $\Delta T$  were then calculated as:

$$q = \frac{Q}{A}; \quad \Delta T = T_{wm} - T_{sat} \quad (5.4)$$

where  $A$  is the surface area based on the overall diameter.

The mean heat transfer coefficient can then be obtained as follows

$$h = \frac{q}{\Delta T} \quad (5.5)$$

The actual outside surface area is different for each tube so in order to compare the heat transfer performance, the tube rating ( $r_m$ ) was used. This is defined as

$$r_m = \frac{Q}{L} = \frac{\dot{m}c_p(T_{in} - T_{out})}{L} \quad (5.6)$$

where  $L$  is the length of the tubes.

In the meantime, the field strength is defined as

$$E = \frac{\Delta\phi}{\frac{D_t}{2} \ln\left(\frac{D_e}{D_t}\right)} \quad (5.7)$$

where  $\Delta\phi$  is the applied electric potential;  $D_t$  the overall diameter of the test tube, and  $D_e$  the electrode diameter. This was obtained from solving

$$E = -\nabla\phi \quad (5.8)$$

Laplace's equation expressed in a cylindrical coordinate system

$$\frac{d^2\phi}{dr^2} + \frac{1}{r} \frac{d\phi}{dr} = 0$$

with boundary conditions:

$$\begin{aligned} r = \frac{D_e}{2}, \quad \phi = \phi_e \\ r = \frac{D_t}{2}, \quad \phi = 0 \text{ (being grounded)} \end{aligned} \quad (5.9)$$

### 5.2.5 Experimental accuracy

An error analysis was made, taking into account the uncertainty associated with the interpolation errors of the measuring devices, errors due to calibration, and fluctuations in thermocouple readings during boiling. In the calculations, the mass flow rate of hot water,  $\dot{m}$ , the physical properties of fluids, the temperature difference of water in and water out,  $(T_{in}-T_{out})$ , the saturation temperature,  $T_{sat}$ , and the mean wall temperature,  $T_{wm}$ , were taken as independent (directly measurement) variables. And the heat flux  $q$  and heat transfer coefficient  $h$ , based on the overall diameter, were taken as the first and the second dependent (indirectly measurement) variables, respectively. The error dissemination theory was employed to calculate the standard deviation of the variables and to estimate the experimental accuracy and uncertainties.

#### Mass flow rate

The accuracy of the GAP flow meter for hot water had been previously checked by the "bucket and stopwatch" method. The uncertainty depended on the flow rate and the error ranged from 2 – 3% for water temperature at 20°C (the average error for the experiments was estimated as 2.5 %).

#### Physical properties

Due to the very small changes of fluid temperatures during experiments, the changes in specific heat of water was considered small enough to be neglected. During the experiments, the maximum change of hot water temperature inside the test tube was 15°C and the maximum  $T_m = (T_{in}+T_{out})/2$  was less than 35°C.

## Saturation temperature

The system pressure was adjusted to remain at  $1.9^{-0.02}$  bar, so the relative saturation temperature at measured pressure typically agreed at  $21.5^{\pm(0.04\sim 0.05)}\text{ }^{\circ}\text{C}$ . The maximum error was less than 0.5%.

## Temperatures (see Appendix B)

The thermocouples were calibrated in a water bath against a British Standard calibrated mercury thermometer reading. The instantaneous temperature read is accurate to better than 0.1 K. The experimental accuracy was estimated to be 0.039 K. The major contribution to the uncertainty of heat flux was the fluctuations in thermocouple readings for water in and water out at a fixed mass flow rate. The magnitude of the fluctuation for  $(T_{in}-T_{out})$  over a 5 min time interval for data reading at a steady state was less than 0.05 K ( $\pm 0.025$  K). The accuracy for  $(T_{in}-T_{out})$  is therefore estimated as 0.046 K.

The uncertainty of heat transfer coefficient depended on the heat flux and the superheat temperature  $(T_{wm}-T_{sat})$ . The fluctuations of thermocouple readings for tube wall temperature,  $T_{wm}$ , varied and had a maximum of 0.08 K ( $\pm 0.04$  K) for the Thermoexcel-HE tube to 0.06 K ( $\pm 0.03$  K) for the Gewa-T tube over a 5 min time interval for data reading at a steady state. This was considered to result from nonuniform pool boiling outside the test tube. The accuracy of the superheat temperatures was therefore estimated as 0.0688 K for the Thermoexcel-HE and 0.0633 K for the Gewa-T.

## Heat flux and heat transfer coefficient (see Appendix B)

Taking account of deviations of the hot water flow rate, the temperature difference between water in and out and the system saturation temperature, the nominal uncertainty in heat fluxes (or the energy transferred to the boiling refrigerant) was estimated to be about 2.76 ~ 3.57 % (less than 3.5 %). Similarly, the nominal uncertainty in heat transfer coefficients was estimated to be about 3.19 ~ 5.0 % considering the errors in heat fluxes and superheats at 1.5 ~ 4.0 K.

## 5.3 Results and Discussion

### 5.3.1 Boiling hysteresis at zero field

Initially, experiments for the Thermoexcel-HE (T-HE) and Gewa-T (G-T) tubes with no electric field (zero field) were performed and the boiling hysteresis for both tubes was demonstrated for both increasing and decreasing the experimental superheat  $\Delta T$ . These are shown in Figures 5.7 and 5.8, respectively, which are plots of the heat flux  $q$ , calculated from equation (5.4), versus degree of superheat  $\Delta T$ .

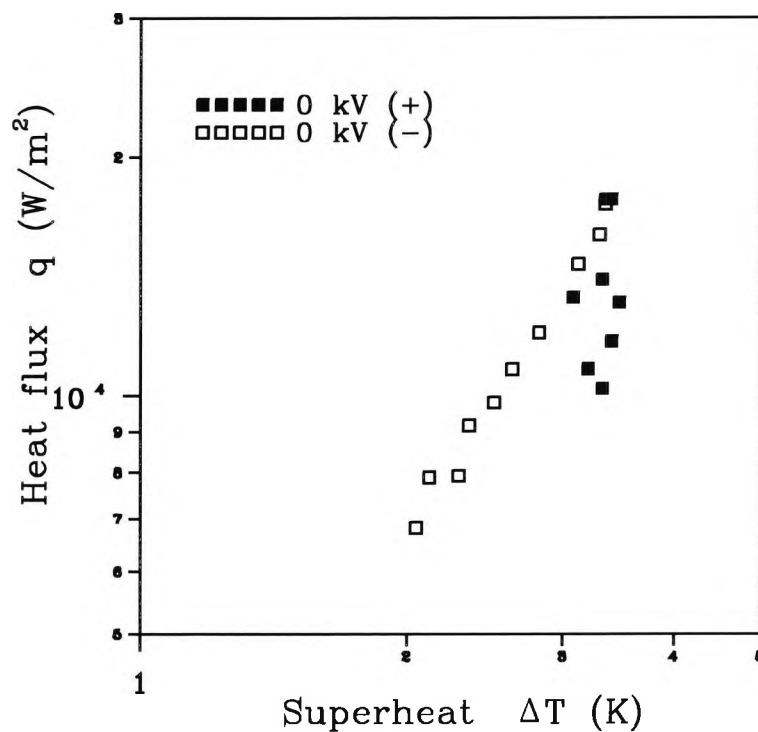


Figure 5.7: Boiling hysteresis for the T-HE tube at zero field. (+): increasing  $\Delta T$  and (-): decreasing  $\Delta T$

It can be seen clearly that under these conditions a considerable difference exists between the heat fluxes obtained for the increasing and decreasing superheat. This means that the boiling hysteresis for passive enhanced surfaces, such as the Thermoexcel-HE and the Gewa-T, at a zero-field strength is quite significant, even with the passive enhancement. A similar result was reported by Bergles (1989), in which the hysteresis for a high flux surface was described.

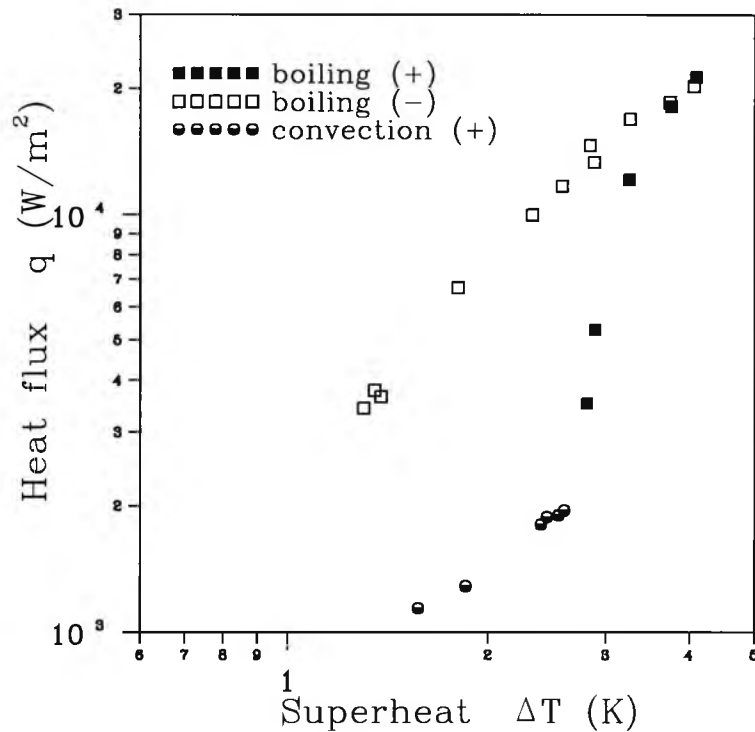


Figure 5.8: Boiling hysteresis for the G-T tube at zero field. (+): increasing  $\Delta T$  and (-): decreasing  $\Delta T$

### 5.3.2 Elimination of boiling hysteresis

The boiling hysteresis for both the Thermoexcel-HE (T-HE) and the Gewa-T (G-T) at zero field was demonstrated almost to disappear when the experimental system was subjected to an electric field strength of 1.5 MV/m (10kV). This can be seen in Figures 5.9 and 5.10. The results also indicate that the boiling hysteresis for both surfaces can be completely eliminated when the field strength is increased to 3 MV/m (20kV).

### 5.3.3 Enhancement of heat transfer at low superheat

Enhancement of nucleate boiling for the Thermoexcel-HE and the Gewa-T surfaces was very significant at low superheat. This has been shown in Figures 5.9 and 5.10. It can be seen from Figure 5.9 that the heat flux for the Thermoexcel-HE at 3 MV/m (20kV) is about 75% higher than that for zero field (decreasing  $\Delta T$ ) at

the same degree of superheat ( $\Delta T=2$  to  $3.5$  K). At the same levels of heat flux, the superheat required under the EHD conditions is much lower than that for the zero field condition. As the field strength increases, the differences become even bigger. In the case of  $q=1 \times 10^4$  kW/m<sup>2</sup>, the superheat at  $1.5$  MV/m ( $10$  kV) is about  $0.9$  K lower than for  $0$  MV/m and at  $3$  MV/m ( $20$  kV), about  $1.5$  K lower than for the zero field. Also, as the superheat increased, the EHD enhancement became smaller. Nevertheless, the peak flux with EHD was higher than without EHD. However, The heat fluxes for the Gewa-T at high superheat, with and without EHD, seems not to be very different as shown in Figure 5.10.

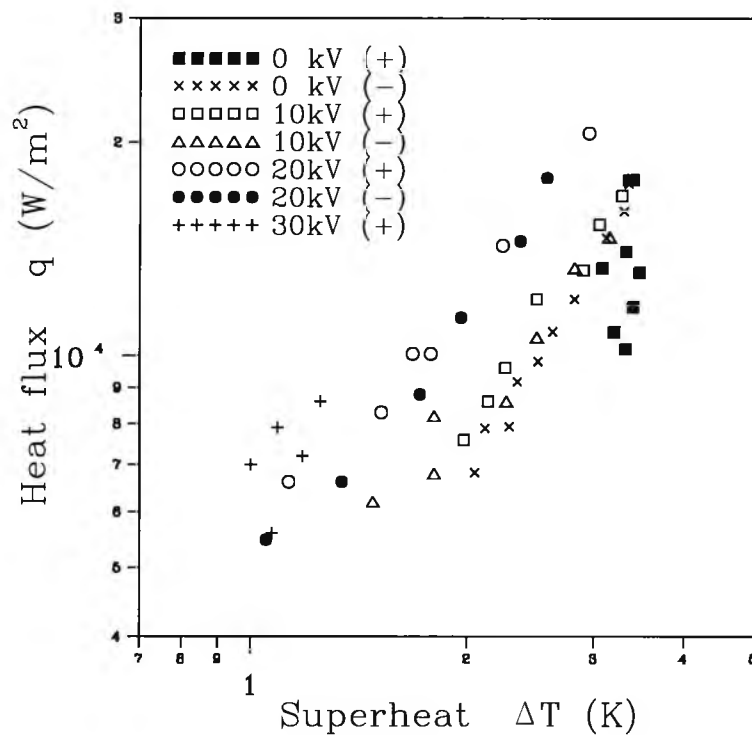


Figure 5.9: Elimination of boiling hysteresis and enhancement of heat transfer for the T-HE tube. (+): increasing  $\Delta T$  and (-): decreasing  $\Delta T$ )

The evidence of EHD enhancement can be also obtained from the observations during the experiments. It was observed through the sight glass in the test rig that, with EHD, boiling was initiated at much lower superheat than without EHD. This is shown in Figure 5.11. These results indicate that, for the case of the Gewa-T tube, boiling bubbles were initiated when the superheat was in the range  $2.8$  to  $3.2$  K at zero field strength; at  $1.5$  MV/m ( $10$  kV), it was initiated in the superheat

range 1.2 to 1.8 K; while at 3 MV/m (20kV), a superheat value of only about 0.8 to 1.0 K was sufficient for ebullition. Actually, the incipient bubbles could even be seen at 0.7 K when 20kV (the field strength was 3 MV/m) was applied. The typical data have been shown in Figure 5.11. Similar observations were also made for the Thermoexcel-HE, as also shown in Figure 5.11. Clearly, further work will be needed, employing a high speed video camera, to study the bubble behaviour and the impact of surface orientation on boiling under EHD conditions.

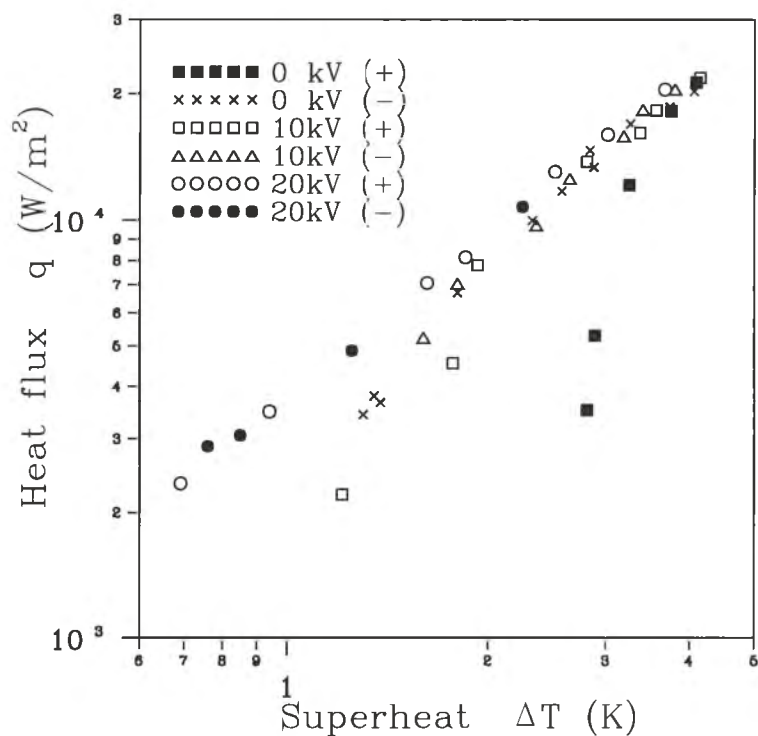


Figure 5.10: Elimination of boiling hysteresis and enhancement of heat transfer for the G-T tube. (+): increasing  $\Delta T$  and (-): decreasing  $\Delta T$

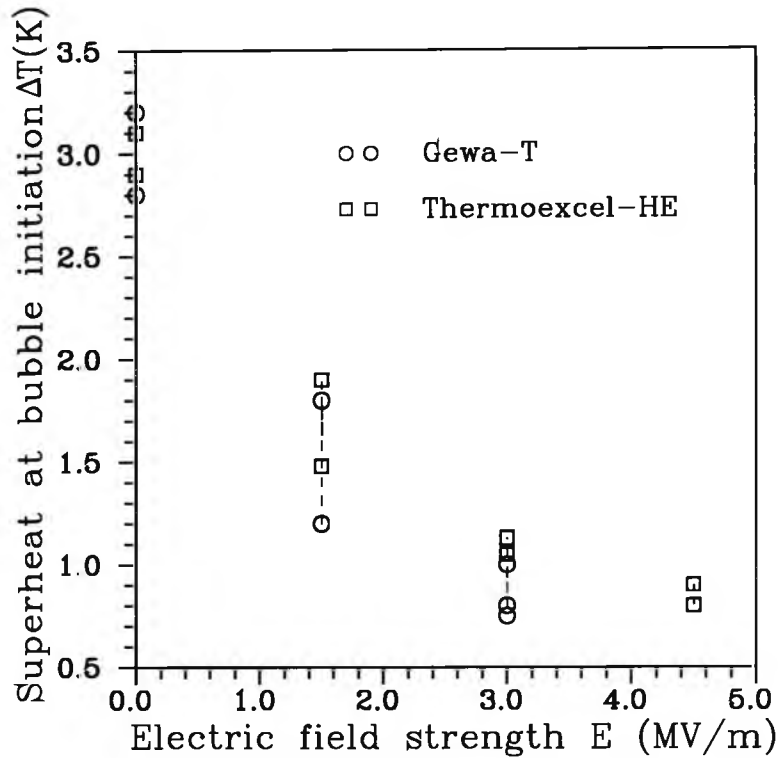


Figure 5.11: Effect of electric field on superheat for bubble initiation

### 5.3.4 EHD as a control mechanism

Different heat transfer performance was obtained by changing the applied field strengths when the heat flux was kept constant. Figures 5.12 and 5.13 show the heat transfer coefficient ratio versus electric field strength for the Thermoexcel-HE and the Gewa-T, surfaces respectively. These indicate that heat transfer coefficients are a function of field strength at constant heat flux conditions; the slope is reduced as the heat flux value increases. This means that the performance of nucleate boiling under EHD conditions is adjustable and controllable. This seems to be an important EHD effect quite distinct from the enhancement itself. The potential of EHD techniques as a control mechanism could be attractive for renewable energy applications, thermal control in space stations and the heat transfer control for electronic equipment. Of course, the electrode system for EHD thermal control in a practical system should be well designed and the reliability needs to be further studied.

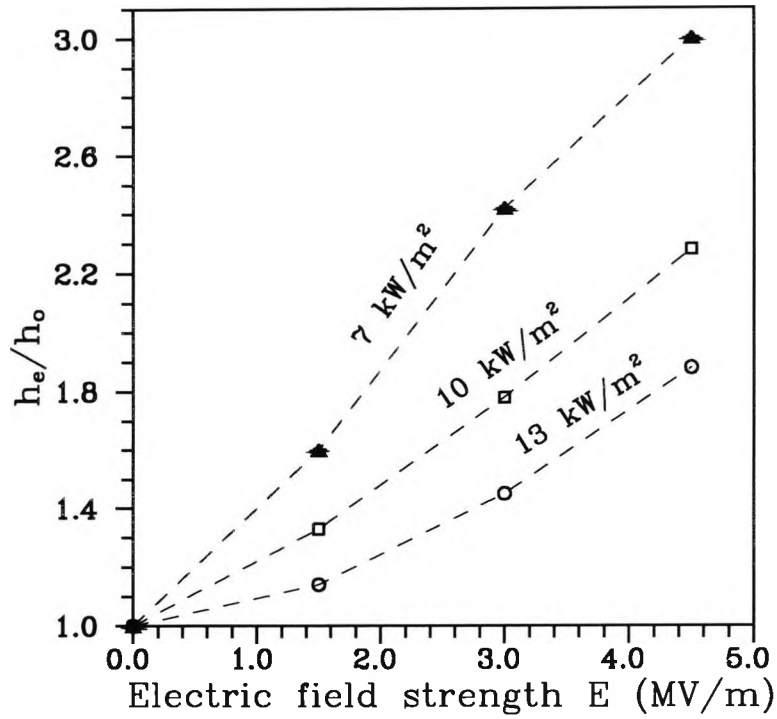


Figure 5.12: Ratio of heat transfer coefficients versus field strengths for the T-HE tube

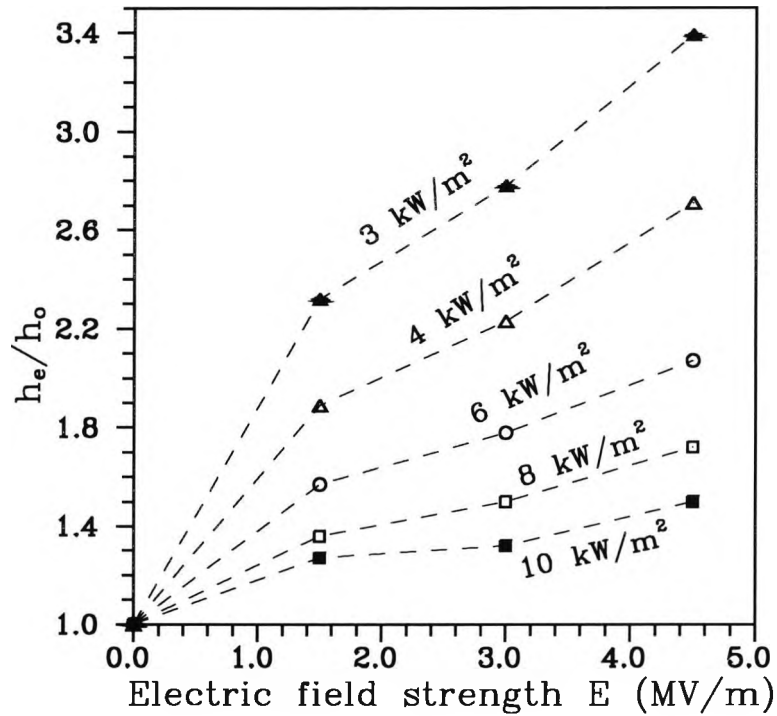


Figure 5.13: Ratio of heat transfer coefficients versus field strengths for the G-T tube

### 5.3.5 The effect of surface geometry

The effect of surface geometries on EHD boiling heat transfer was studied by comparing the heat transfer performance for different surfaces. This can show not only the interesting comparison of how much improvement passive enhanced surfaces give over smooth ones but also how even the smooth case is improved by a factor of about two when an EHD effect was applied. These were done using the tube rating concept defined in equation (5.6).

Figures 5.14 and 5.15 show respectively results for the Thermoexcel-HE (T-HE) and the Gewa-T (G-T), compared with the smooth (SM) surface described in Table 5.1, both with and without EHD.

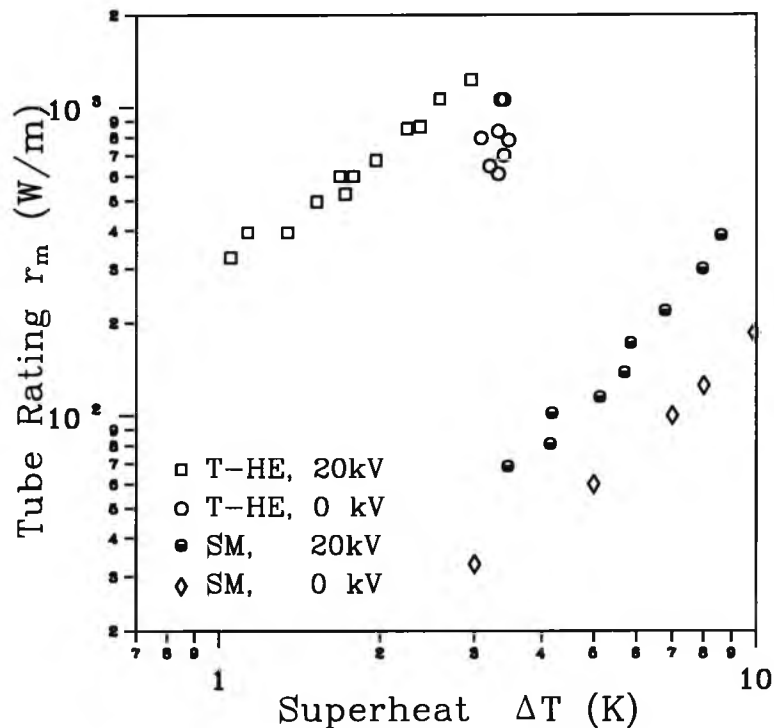


Figure 5.14: Results for the T-HE compared with that for the smooth tube

The increased enhancement for these passive enhanced surfaces is obvious, the boiling starting at much lower superheat and the tube rating being much higher than with a smooth surface. It is seen from the figures that, when the surfaces were subjected to a uniform electric field, the net EHD effect for the passive enhanced surfaces is much more significant than for the smooth one.

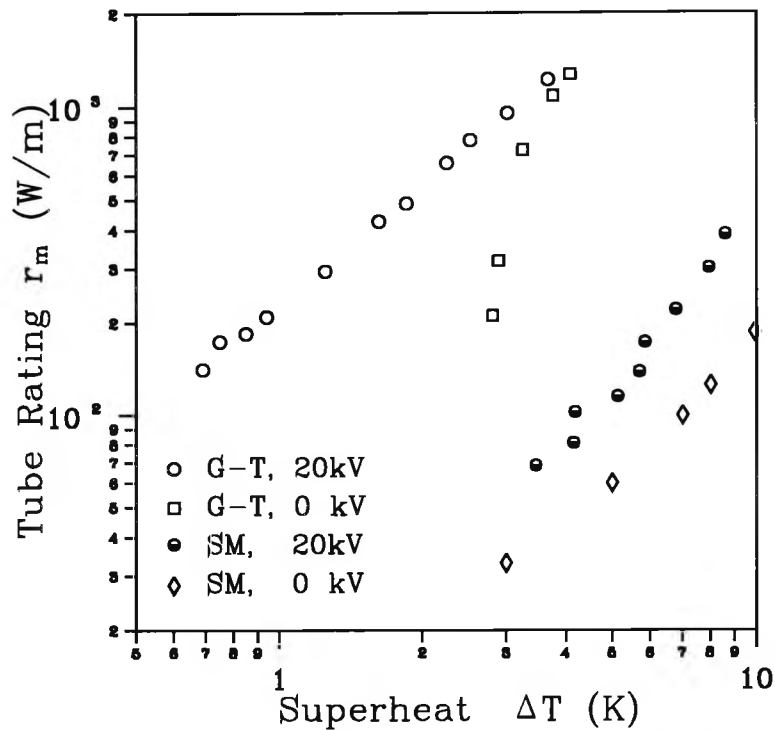


Figure 5.15: Results for the G-T compared with that for the smooth tube

Comparisons for the performance between the Thermoexcel-HE (T-HE), the Gewa-T (G-T), the low-fin (L-F) and the Thermoexcel-C (T-C) surfaces, were also carried out using the concept of tube rating. Figure 5.16 shows the comparison between the T-HE and the Gewa-T at 0 and 20kV (3 MV/m). The figure indicates that the boiling performance for the T-HE and the Gewa-T is comparable and quite close at the zero field condition. When the field strength increases to 3 MV/m (20kV), the performance of the T-HE seems to be better than for the Gewa-T. At the same superheat level, the heat flux of the T-HE was higher than for the Gewa-T. Also, the peak flux of the T-HE was higher than for the Gewa-T. This suggests that there is a *different* EHD effect for different surface geometries.

Figure 5.17 gives a comparison between the two Thermoexcel surfaces, the T-HE and the T-C at 0 to 30kV (4.5 MV/m). It can be seen that although the T-C had an inferior performance with no electric field because its original design was for condensation purpose, it was comparable with the T-HE at 20kV (3 MV/m); when the field strength increased to about 4.5 MV/m (30kV) (the T-C was only

increased to about 4.1 MV/m (27kV)), the EHD enhancement effect for the T-C became more significant.

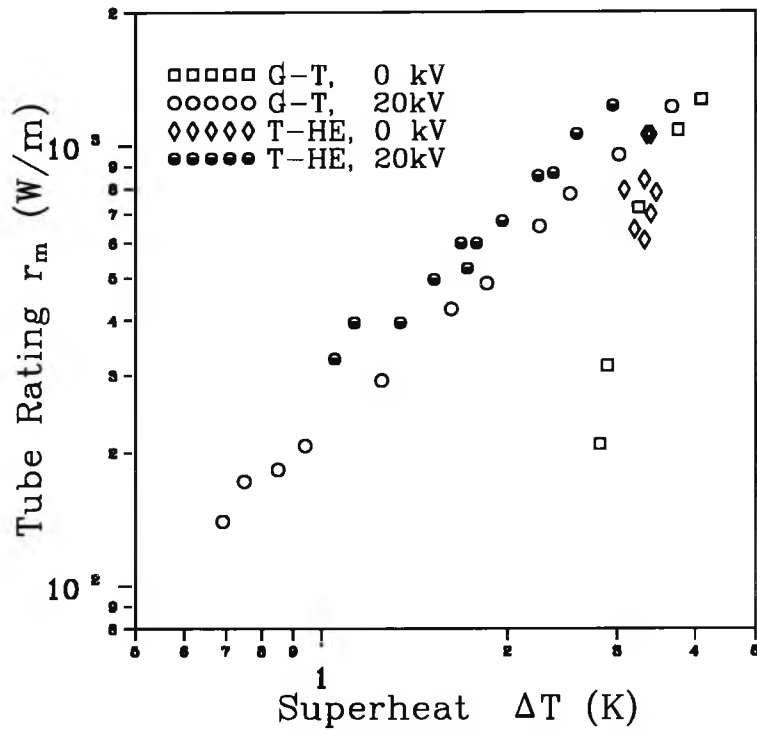


Figure 5.16: Results for the T-HE compared with that for the G-T

Figure 5.18 gives the comparison for the Gewa-T and the low-fin tubes. The former was developed from the latter, as mentioned in chapter 3. It can be seen from the figure that although the Gewa-T surface offered good heat transfer results, with and without EHD, the net EHD effect of the low-fin seems to be a little larger than for the Gewa-T, and particularly in the high superheat area. These could further suggest that the EHD effect on the enhancement of nucleate boiling is geometry dependent.

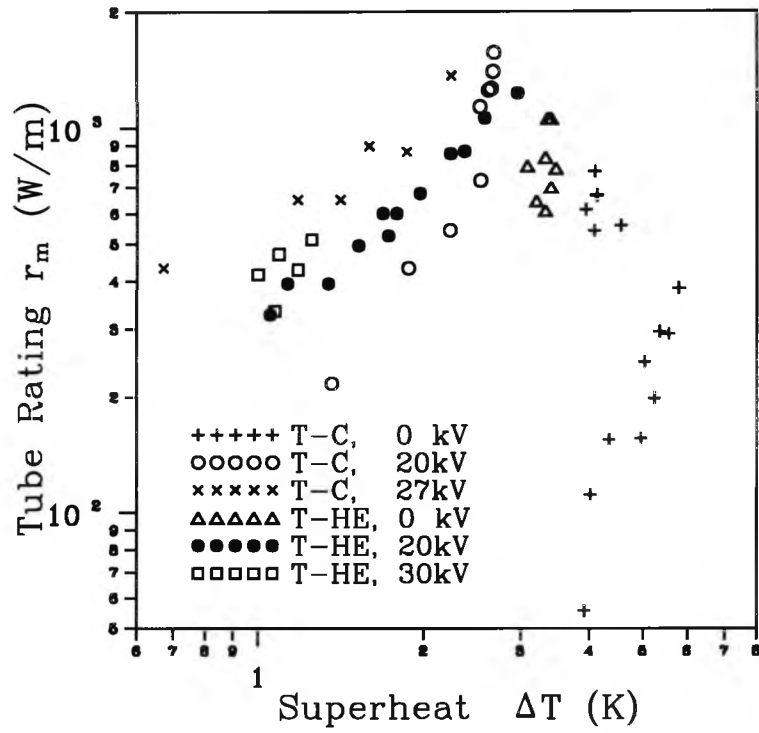


Figure 5.17: Results for the T-HE compared with that for the T-C

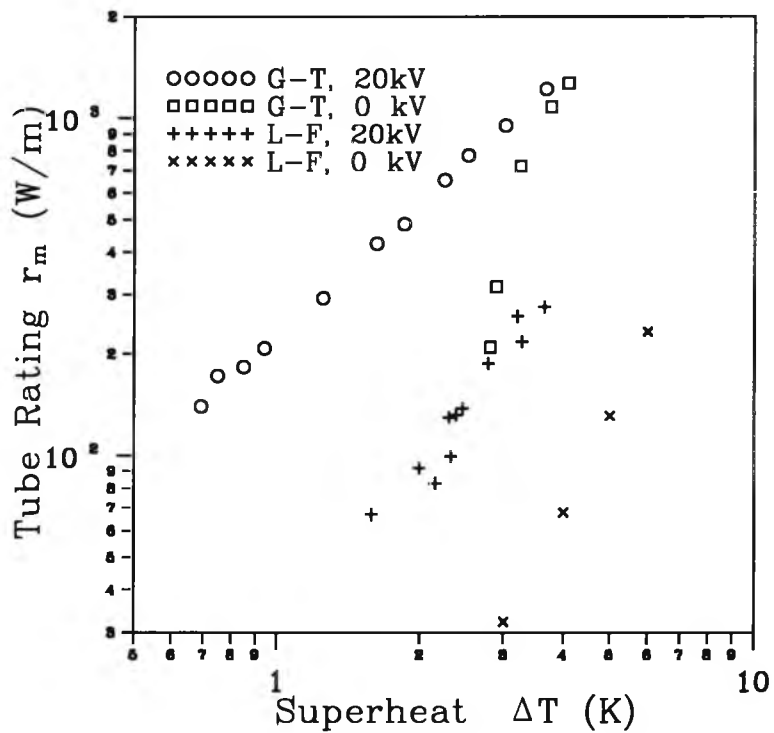


Figure 5.18: Results for the G-T compared with that for the L-F

### 5.3.6 The compound effects

The compound effects on nucleate boiling are suggested when both the effect of passive enhanced surfaces and the effect of EHD enhancement are considered. Concerning passive enhanced surfaces, the T-HE and the Gewa-T tubes have offered the best heat transfer performance in the comparisons, as shown in Figure 5.19, which gives the tube rating comparison for different tube surfaces without EHD. This has also been proved by many other experimental results for nucleate boiling research (Bergles, 1989 and Webb and Pais, 1992).

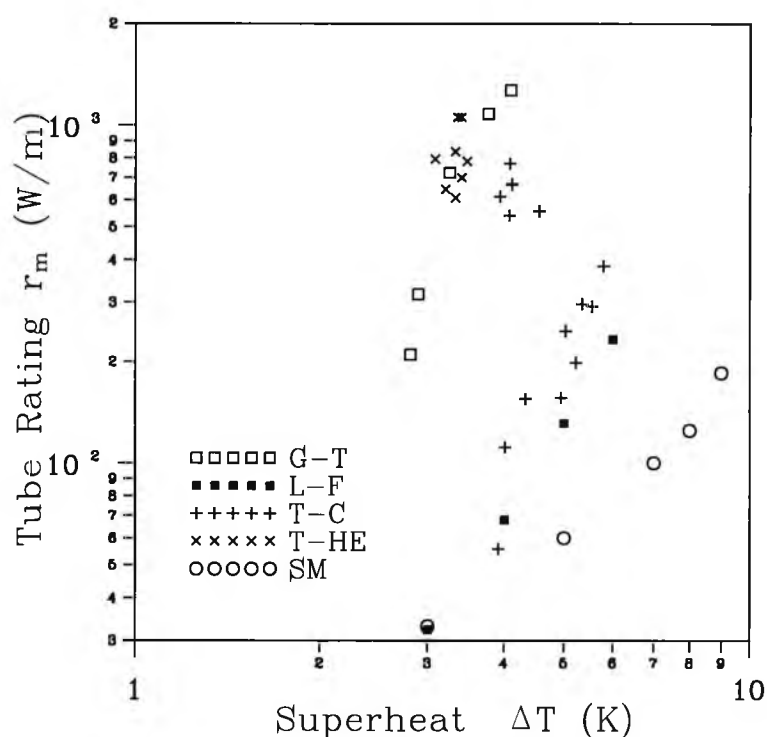


Figure 5.19: Tube rating versus superheat for different surfaces at zero field

In Chapter 4, the EHD effect on nucleation was predicted, in which the EHD nucleus radius was smaller and EHD nucleation rate was higher than those without EHD. Also, the EHD effect at these surfaces was indirectly predicted by calculating potential distributions. The predicted results for boiling surfaces have indicated that the equi-potential contours are becoming slightly closer when the surface geometry changes from the Gewa-T like surface to low-fin surfaces and to the smooth. This could increase the EHD effect on the surfaces inside cavities, in particular,

on the bottom surface of cavities. But at the same time, as shown in Figure 5.19, the passive enhanced effect is being decreased. Also, the potential contour figures highlight the very high potential gradient at the shoulders area compared to that over the rest of the field. This was particularly significant at the Gewa-T surface which has a group of tiny cavity slots on the tube surface causing the heating surface area to be increased and affecting the contact angles of the generated bubbles. When the system was in the presence of an electric field, the high potential gradient at the shoulders could strongly affect the contact angle by decreasing the surface tension at liquid-vapour interface, as expressed in

$$\cos(\theta) \propto 1/(\sigma_o - \Delta r \epsilon_o \Delta \epsilon E^2) \quad (5.10)$$

Clearly, the experimental results reported in this chapter (Figures 5.7 to 5.18) have shown a kind of compound effect of both EHD and passive enhancement on the nucleate boiling.

The results for the T-C could give a good explanation for the compound effect. The first effect for this surface on nucleate boiling, the passive enhancement effect, is that the boiling performance at zero field is not as good as that for the Gewa-T and the T-HE, but is a little better than for the low-fin. This is because of its surface geometry and its original design purpose for condensation. Compounding the second effect, the EHD enhancement effect, the tube rating result is comparable with the Gewa-T and T-HE at 3 MV/m (20kV) and more significant at about 4.5 MV/m (30kV), as shown in Figure 5.19.

After all this, comparisons in Figures 5.19 and 5.20 for different surfaces at different levels of applied potential have indicated that an even better performance might be achieved with the design of a surface geometry specifically for use with EHD.

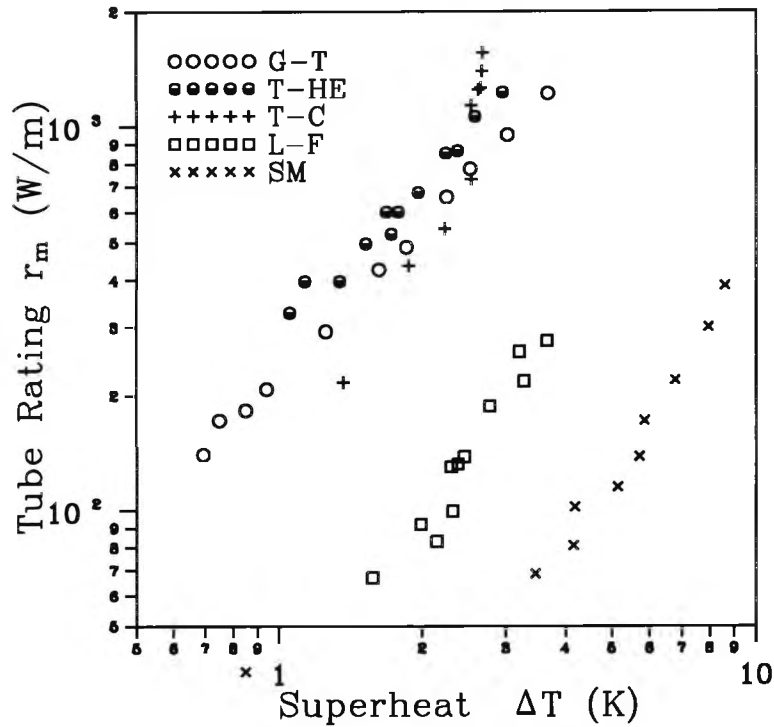


Figure 5.20: Tube rating versus superheat for different surfaces,  $E=3.0$  MV/m

### 5.3.7 Electric power consumption

It is interesting to note that the electric power consumption for the employment of high voltage in the experiments was very small and negligible. The maximum electric current reading for applying a 30kV (4.5 MV/m) field was less than  $2.5\mu\text{A}$ .

## 5.4 Conclusions

The EHD effect of nucleate boiling at low superheat surfaces, Thermoexcel-HE (T-HE) and Gewa-T, were studied experimentally. To study the heat transfer performance, the experiments were carried out in a single tube test rig and to compare with the earlier results for other surfaces, such as the smooth, the low-fin and the Thermoexcel-C (T-C), obtained under the same test rig, the same working fluid and the same experimental conditions, Refrigerant R114 was employed as

working fluid. From the experimental results and the discussion, the following conclusions can be reached:

- The boiling hysteresis for both the Thermoexcel-HE and the Gewa-T, which exists at zero field strength, can be eliminated by utilizing EHD.
- EHD enhancements of nucleate boiling for both the Thermoexcel-HE and the Gewa-T surfaces are significant at low superheat conditions.
- The EHD boiling enhancement improves with applied voltage but decreases with heat transfer rate. Nucleate boiling seems therefore to be controllable by applying a variable EHD effect under constant heat flux conditions.
- The EHD effect on nucleate boiling gives different results for different surface geometries. This results from the compound effect of both passive and EHD enhancement on nucleate boiling. Therefore, a surface geometry designed specifically for EHD applications may give even better performance.

## **Part II**

# **Effects of an Electric Field on Crystallization Processes from Industry Melts**

# Chapter 6

## Part Two Introduction

It is well known that crystallization must surely rank as the oldest unit operation, in the chemical engineering sense. Today there are few sections of the chemical industry that do not, at some stage, utilize crystallization as a method of production, purification or recovery of solid material. Apart from being one of the best and cheapest methods available for the production of pure solids from impure solutions, crystallization has the additional advantage of giving an end product that has many desirable properties. This kind of end product can be seen not only in the chemical industry but also in metallurgy, medicine and food industries. Uniform crystals have good flow, handling and packaging characteristics; they also have an attractive appearance, and this latter property alone can be a very important sales factor.

The industrial applications of crystallization are not necessarily confined to the production of pure solid substances. Many techniques for large-scale purification and solidification have been developed in recent decades. Industrial crystallization processes mostly dealt with the crystallization of solid phase from a supersaturated or supercooled liquid phase (another type of crystallization of solid substances induced from a supersaturated vapour is normally called sublimation). For the purpose of application, the liquid for crystallization is generally identified as either a melt or a solution.

A solution is a homogeneous mixture of two or more substances. The constitu-

ents of liquid solutions are frequently called solvents and solutes. Owing to the widespread and often indiscriminate use of the word "melt", it is difficult to give a precise definition of the term. Strictly speaking, a melt refers to a liquid close to its freezing point, but in its general industrial application it tends to encompass homogeneous multicomponent liquid mixtures that would individually solidify on cooling to ambient temperatures. Melt crystallization is a common term applied to the controlled cooling crystallization and separation of such systems with the objective of producing one or more of the components in relatively pure form.

Basically, a melt crystallization on cooling consists of two stages called nucleation and crystal growth. Normally, the condition of supercooling alone is not sufficient cause for a system to begin to crystallize. Before crystals can develop there must exist in the melt a number of minute solid bodies, called embryos, nuclei or seeds, that act as centres of crystallization. To initiate the nuclei is termed nucleation. As soon as stable nuclei, i.e. particles larger than the critical size, have been formed in a supercooled system, they begin to grow into crystals of visible size. Clearly, nucleation plays an critical role during a melt crystallization process.

Nucleation may occur spontaneously or it may be induced artificially. Many techniques to induce nucleation have been studied and developed; these include agitation, mechanical shock, friction and extreme pressure within the solution or melts. The influence of some other external stimulus, such as electric and magnetic fields, spark discharges, ultra-violet light, X-rays,  $\gamma$ -rays, sonic and ultrasonic irradiation, have also been studied for many years, but the effects of these on nucleation were generally commented on as erratic.

Concerning the effects of an electric field on crystallization, it seems to be not very scientific if it was simply said to have erratic effects. In fact, some consistent results have been reported since it was studied. Although the published literatures on this subject is not as large as that on EHD heat transfer, some results have been reported and published and this will be reviewed in the next chapter.

In this part of the thesis, the research interest came from the significant effects of EHD on heat transfer. In particular, the EHD effect on nucleate boiling of dielectric fluids has reminded us to think about the general effect of an electric field on phase change processes in dielectric liquids. For this reason, the effect of electric fields on crystallization should be regarded as a valid choice for the extension of the research on EHD phase change heat transfer.

In the present research, the effects of an electric field on melt crystallization are studied. The experimental melts were selected from industrial material which could be classified as dielectrics and has typical crystalline properties, such as the polymorphic behaviour and recrystallization, etc. and these will be introduced and discussed in detail in Chapter 8.

The crystallizations from the melts reported in the following chapters are concerned with multicomponent liquid mixtures that solidify on cooling. The effects of an electric field on the samples' crystallization have been firstly studied experimentally and assessed by both the time-temperature cooling curves and Differential Scanning Calorimetry (DSC) methods. Considering the effects of multi-factors on crystallization, a novel experimental design using the Taguchi method has been completed and the experiments have been carried out. A new method for assessing the DSC results of the Taguchi experiments is particularly developed and the relative results are reported. Some theoretical work was also undertaken and is introduced in chapter 11.

# Chapter 7

## Research History and Progress

The effect of an electric field on crystallization process has been studied for many years. The research has involved both theoretical and experimental studies. Some results have been published, but in general, up to now, the references reported are still very limited.

### 7.1 Historical Review

The first study in this field was the work of Kondoguri (1926 and 1928) who studied the effect of electric and magnetic fields on crystallization and found that the fields can accelerate the action on crystallization of under-cooled liquids. In his earlier study, drops of molten salol and piperine were compressed between glass slides and placed in electric and magnetic fields during cooling. He found that the number of crystalline centres of under-cooled piperine and salol is considerably increased by electric and magnetic fields. The investigation was reported exhaustively with following results :

- For equal time intervals, the number of crystals forming is approximately proportional to the strength of the electric field;
- For constant field strength, the number increases with time, up to a limited value;
- An increase in the electric field produces an increase in the number of crystalline centres until a new saturated value is reached.

After that, Kondoguri (1936) also studied the crystallization of sulphur on cooling in an electric field. He reported that, when exposed to an electric field, the number of crystalline centres was increased if the field was normal to the sulphur film and decreased if the field is parallel.

Since then, some researchers, mainly in Russia and east Europe, such as Goskii (1932, 1955 and 1969), Berlaga (1940), Chesnokov et al (1956), Kozlovskii (1962), Prishchena (1964), Abdullaev and Odobesku (1967) and Shubnikov and Parvov (1969), have done similar experimental studies on crystallization in dielectrics. They reported that an electric field can cause changes in parameters of a crystallizing system and in crystallization rate.

Chesnokov (1956) studied the linear rate of crystallization experimentally using salol and betol as dielectrics. He applied a continuous electric field (such as d.c.) in a parallel or a perpendicular direction to the investigated layer and applied alternating field only in a perpendicular direction. It was noted that a shift of the curves appears in the first case towards the higher temperature, while for the second case it shifts towards the lower ones and the amount of shift depends on the frequency. They also found that the activation energy of the dielectric melt increased under a continuous field and decreases under an alternating field.

Growther and Saunders (1973) performed an experimental study of ice crystal growth in a uniform electric field. An earthed microscope was used in the experimental observation. They found that needle type ice crystals increased their growth rate by more than thirty times in electric fields of over 46 kV/m, while small hexagonal plate crystals were unaffected by the electric field.

Since the middle of the 1970s, a series of research results on the crystallization of dielectric liquids on cooling affected by applying electric fields was published by Lychev et al (1976, 1977, 1978, 1979a, 1979b and 1979c). For this reason, Lychev and his group could be thought to be the first who did more systematic and rel-

atively detailed studies on dielectric crystallization in an electric field. He and his colleague (1976 and 1977) examined a single component melt – crystal system lying between two vertical plates connected to a d.c. supply. Using a thermodynamics method, they derived some basic expressions for the relationship between the pressure of crystallization or the specific heat of crystallization and the strength of the electric field. On the basis of nucleation theory, they also derived a basic expression for the critical size of a solid phase nucleus in the electric field.

Furthermore, Lychev et al developed a function expression for the nucleation formation rate or nucleation velocity  $I(T)$  and the temperature of crystallization in the electric field. As the results of their theoretical study, they reported that a homogeneous electric field applied to a supercooled dielectric melt has a substantial effect on the parameters of crystallization, the number of nuclear centres, the critical dimensions, and the work and nucleus formation rate. They developed a concept of the equilibrium temperature in the electric field, namely,  $T_E$ . They reported that an electric field applied to a dielectric melt at the temperature below some value of  $T_E$  increases the number of crystallization centres, while at the temperature above  $T_E$  it reduces the number of centres. These results were particularly emphasized to be dielectric properties-dependent. After all, an external electric field may accelerate dielectric crystallization in a temperature interval and these characteristics are dielectric properties-dependent; for different dielectrics the results may be totally different. It was also reported that their results achieved complete qualitative agreement with experiments.

Later, Lychev and Cheremisin (1978, 1979a and 1979b) particularly studied the electric field effect on dielectric crystallization kinetics. On the basis of the fluctuation theory of supercooled melt crystallization, they introduced dielectric properties and the strength of electric field to the formulae of the parameters of phase transformation kinetics, i.e., the nucleation rate and the linear rate of crystallization. Then, they obtained the expression for a critical strength of the electric field at constant temperature conditions for the maximum nucleation rate or the maximum linear rate of crystallization, respectively. They also discussed the rela-

tions in which the linear rate of crystallization or the nucleation rate changes with temperature when the electric field strength was constant.

However, Lychev et al did not consider the change of the surface energy when the system was subjected to an electric field. This was completed by Aliksabov and Shklyar (1980) and Shklyar (1989). That the coefficient of the surface strength depends on the tension of the external electric field was suggested by Frenkel (1946). Aliksabov and Shklyar (1980) considered an experimental system which was similar to the one Lychev et al used and placed it in a uniform electric field. They firstly showed experimentally the influence of the change of the surface energy in the electric field. After that, Shklyar (1989), followed the work of Lychev, took the change of surface energy into account in the expressions of critical size of a crystal, the nucleation rate and other important parameters. As a result, he derived a temperature formula at which, when the external electric field did not change, the velocity of critical embryo creation took its maximum value.

As an another contribution in this research field, Lychev et al (1979a) took into account the effect of an electric field on massive crystallization kinetics. On the basis of the statistical theory, they discussed some important parameters as follows: (1) The minimum time  $\tau_{min}$  of complete crystallization in the volume and the relative strength of the electric field. (2) The maximum crystal size  $l_{max}$ , the number of crystals  $N$  in a given volume at the end of crystallization and the relative strength of electric field. In their studies, the parameters of dielectric characteristics,  $\beta$ , were particularly emphasized in the case of  $\beta > 0$  or  $\beta < 0$ . It was reported that the electric field effect on dielectric crystallization had totally different results when the  $\beta$  value was different. This was reported to be entirely in agreement with the experimental results of Geller et al (1975), Rogass et al (1976) and Kozlovskii, et al (1976).

Similarly, the massive crystallization in an electric field was also considered by Iliev et al (1989), but another concept called total crystallization was used. As an important parameter, the concept of total crystallization  $a = V_{cr}/V_o$ , where  $V_o$  is

the original volume of melt and  $V_{cr}$  is the volume of crystallization, was discussed by Avrami (1940) and Gutsov (1971). The value of total crystallization changes over the time course and the time dependence  $a(t)$  has a typical *S* - *shape* curve. This was described by Avrami's equation. Iliev and Kontrov (1989) obtained and compared  $a(t)$  curves for, with and without, the application of an electric field. The results indicated that with an electric field, the total crystallization takes a shorter time to reach a saturated value than in the absence of a field. Because Avrami's equation is based on the nucleation rate being constant over time, it is actually only for the steady state occurrence of crystallization processes. Gutsov et al (1970 and 1968) suggested that non-steady-state effects should be taken into account in all cases of phase-formation, particularly in the crystallization of various melts. Then they developed approximate expressions for the degree of crystallization in a non-steady-state process. On this basis, Iliev et al also considered the crystallization process for a non-steady-state period in an electric field and obtained the relevant  $a(t)$  curve.

In the meantime, static electric field effects on the nucleation rate of both polar and nonpolar crystalline polymorphs for dielectric crystallization were studied by American researchers (Marand et al., 1988 and 1989) who studied isothermal crystallization of undercooling Poly (vinylidene fluoride) ( $PVF_2$ ) in the presence of high static electric fields. Firstly, primary nucleation of  $PVF_2\gamma$ -phase crystals from the melt was observed by polarised optical microscopy, thermal analysis, and wide-angle X-ray diffraction. Then a modification of the classical theory of homogeneous nucleation of a crystalline phase was proposed to account for the experimental observations. They derived a relation predicting ratios of nucleation rates in the presence and absence of the field for both polar and nonpolar crystalline polymorphs as functions of crystallization temperature and the field strength. The theoretical predictions indicated that a static electric field will increase the nucleation rate of polar  $\gamma$ -phase and will decrease the nucleation rate of a nonpolar  $\alpha$ -phase. This was confirmed by the fact observed experimentally. For the experiments, the effect of crystallization temperature and electric field strength on the crystal phase content and morphology were also reported. The  $\gamma$ -phase nucleation

process was examined directly by polarised optical microscopy and indirectly by small-angle light scattering. The crystal phase content was assessed by differential scanning calorimetry (DSC). The results indicated that the  $\gamma$ -phase nucleation density and  $\gamma$ -phase content increase with electric field strength and that the higher the crystallization temperature, the larger the effect of the field.

The practical application of an electric field effect on crystallization is very limited and no large scale application has been reported up to now (Mullin, 1993), while research work on the electric field enhancement of glass forming processes for practical application purposes was reported. This was followed by a series of experiments carried out by Kontrov et al (1980a and 1980b) and Penchev et al (1980 and 1982) under laboratory, pilot-plant and industry conditions. The results indicated that there was an improvement in the mechanical strength and thermal-shock resistance of some types of glassware following the action of an electric field in the hot state. After that, Iliev et al (1981a, 1981b, 1981c 1983 and 1987) did further studies. Their work was aimed at elucidating the mechanism of the action of an electric field and finding a method of controlling the crystallization process. An hypothesis to explain crystallization in glass forming melts under the action of an electrostatic field was developed during their work. This was based on the fact that the energy of the electric field in a dielectric (they considered the silicate glasses melt as a dielectric system) changes with the emergence of a new phase. Iliev et al (1989) gave detailed information about the effect of an electric field on the crystallization process in an ionic glass-forming melt. They obtained very positive results that include: (1) In an ionic glass-forming melt the critical size of the crystallization nuclei and the thermodynamic potential of crystallization decrease with the formation of critical nuclei in the electric field with a constant potential at the electrodes; (2) The specific heat and the crystallization temperature are increased, i.e. the energy benefit from the crystallization and supercooling process increased; (3) The nonsteady-state time is reduced; (4) The tendency of glass-forming melts to crystallization is increased.

## 7.2 The Mechanism Study

The theoretical studies for the mechanism of an electric field effect on dielectric crystallization have long been thought to be an important subject. Some researchers like Lychev et al (1976 to 1979) believed that the mechanism should be based on the fact that the energy of the electric field in a dielectric melt changes with the emergence of a new phase (crystal phase). They examined a single component melt-crystal system and derived an expression for the additional energy as

$$\Delta w_{1-2} = \Delta\mu_{1-2} - \Delta\mu_{1-2}^{\circ} \quad (7.1)$$

where  $\Delta\mu_{1-2}$  and  $\Delta\mu_{1-2}^{\circ}$  represent the chemical potential changes in the presence and in the absence of an electric field, respectively; and the additional energy was further expressed as

$$\Delta w_{1-2} = w_2 - w_1 = \frac{\epsilon_0}{2}(\chi_2 V_2 - \chi_1 V_1)E^2 = \beta E^2 \quad (7.2)$$

where  $\chi_i$  is the dielectric susceptibility,  $V_i$  is the specific (per molecule) volume of the  $i$ -th phase, and  $\epsilon_0$  is the dielectric constant (vacuum permittivity), and  $\beta$  is a coefficient dependent on dielectric properties. If dielectrics are denser in the solid state,  $\beta > 0$  while for less dense dielectrics,  $\beta < 0$ .

For a system with no permanent polarization, Guggenheim (1967) gave a basic expression for an infinitesimal change in the internal energy.

$$dU^e = TdS - pdV + V_c E dD \quad (7.3)$$

where  $V_c$  is the volume of the system that is subject to the electric field.  $D$  is the electric induction,  $D = \epsilon_0 \epsilon E$ .

Following Guggenheim's notation, the change of free energy for a system with permanent polarization was also obtained by Marand et al (1988 and 1989) as

$$F^e = F^{\circ} - V_c \left( \overline{P}_o E + \frac{\epsilon_0 \epsilon E^2}{2} \right) \quad (7.4)$$

here the additional free energy of the dielectric melt in an electric field was described as

$$w_i = \overline{P}_o E - \frac{1}{2} V_c \epsilon_0 \epsilon_i E_o^2 \quad (7.5)$$

where  $V_c$  is the volume of the system that is subject to the field;  $\overline{P}_o$  is the permanent polarization of the system,  $\epsilon_o$  and  $\epsilon_i$  are the vacuum dielectric constant and the relative dielectric constant of the system for the  $i$ -th phase, respectively.

Similar derivation for the additional energy was also done by Iliev et al (1989) who obtained an expression as

$$\Delta w_{1-2} = \Delta W_{1-2} \frac{V_1}{V_K} \quad (7.6)$$

where  $V_1$  is the volume of a single particle; it has the same values for different phases;  $V_K$  is the volume of the newly formed complex; and  $\Delta W_{1-2}$  is the phase formation energy of the dielectric field changes.

$$\Delta W_{1-2} = W_2 - W_1 = \frac{\epsilon_o}{2} \int_{V_K} (\epsilon_2 - \epsilon_1) E_2 E_1 dV \quad (7.7)$$

With the formation of spherical acicular (parallel and perpendicular to the field bias) crystallization nuclei in a supercooled melt in a uniform electric field, an actual expression was given as

$$\Delta w_{1-2} = \delta \epsilon_o (\epsilon_2 - \epsilon_1) E^2 \quad (7.8)$$

where the proportionality coefficient  $\delta$  depends on the geometry of the nuclei, dielectric permittivities and the geometry of the electrodes which produce the field and on the extent to which the melt fills the interelectrode volume.

On the above basis, the critical radius of crystal nucleus and the nucleation rate under the action of an electric field could be derived.

However, the above researchers did not consider the effect of surface energy changes affected by an electric field on the phase change process. This was completed by Aliksabov and Shklyar (1980) and Shklyar (1989). They applied the formula suggested and described by Frenkel (1946), in which the surface tension depends on the strength of an external electric field, as

$$\sigma_1 - \sigma_1^o = - \int_{-\infty}^{\infty} \epsilon_o \epsilon E^2 dx \quad (7.9)$$

where  $\sigma_1^o$  is the coefficient of the surface tension of liquid (melt) in the absence of the electric field. When the system is placed in the uniform electric field, they obtained the expression

$$\sigma_1 = \sigma_1^o - \frac{L}{4\pi} \epsilon_o \epsilon E^2 \quad (7.10)$$

where L is the distance between the vertical surfaces which create the field. Actually, for the coefficient of surface tension at the melt-crystal system interface in the electric field, the evidence can also be obtained from the work of Avrami (1940) where it was expressed as

$$\sigma^e = \sigma_1 \left( \frac{\rho_2}{\rho_1} \right)^{\frac{2}{3}} \left( \frac{c_p}{\eta} \right) \quad (7.11)$$

where  $\rho_{1,2}$ ,  $c_p$  and  $\eta$  are the density of melt or crystal phase, the specific heat of the crystallization, and the specific heat of evaporation, respectively.  $\eta$  can be expressed as

$$\eta = \eta_o - dE^2 \quad (7.12)$$

where

$$d = \epsilon_o(\chi_1 V_1 - \chi_3 V_3) \quad (7.13)$$

where the subscript 3 is for vapour phase.

### 7.3 Critical Nucleus Size

The critical size of a solid phase nucleus in the absence of an electric field has been defined in the text books of chemical engineering or crystallization. An authoritative one could be the work of Mullin (1993), in which a crystal nucleus was assumed to be spherical, the critical radius was then defined as

$$r_{cr}^o = \frac{-2\sigma^o}{\Delta G^o} \quad (7.14)$$

where  $\sigma^o$  and  $\Delta G^o$  are the coefficient of surface tension and the change of the Gibbs free energy in the absence of the electric field, respectively.

$r_{cr}^o$  was also described by Frenkel (1946) as

$$r_{cr}^o = \frac{2\sigma^o V}{c_p^o(T_o - T)} \quad (7.15)$$

where  $T_o$  is the melting point,  $T$  is the temperature at which the nuclei appear and  $c_p^o$  is the specific heat.

Similarly, considering the chemical potential changes when the system was in the presence of an electric field in the above equation, the critical radius of a solid phase nucleus in the electric field was derived by Lychev et al (1977 and 1979) as

$$r_{cr}^e = \frac{2\sigma^e V_2}{\Delta\mu^o - \beta E^2} \quad (7.16)$$

where  $\sigma^e$  is the coefficient of surface tension at the melt-crystal interface in the electric field.

An important result of this equation is that the effect of the electric field on crystal critical nucleus would be different for different conditions. When  $\beta > 0$ ,  $\Delta\mu^e < \Delta\mu^o$ , so that  $r_{cr}^e > r_{cr}^o$ , that is, the crystallization in an external electric field would take place at larger crystal sizes of the nuclei than in the absence of a field; on the contrary, when  $\beta < 0$ , then  $\Delta\mu^e > \Delta\mu^o$ , so that  $r_{cr}^e < r_{cr}^o$ . This means that, in this situation, the crystallization in an electric field will take place at smaller critical sizes of the nuclei than in the absence of a field. Because of this, the work required,  $Q^e$ , to form a nucleus in an electric field will also be less than the work  $Q_o$  in the absence of an electric field.

$$Q^e = \frac{4}{3}\pi\sigma r_{cr}^e < Q_o = \frac{4}{3}\pi\sigma^o r_{cr}^o \quad (7.17)$$

Taking into account the effect of electric fields on surface tension, the critical radius was derived by Shklyar (1989) as

$$r_{cr}^e = \frac{2V_2}{\Delta\mu^o - \beta E^2} \left(\frac{\rho_2}{\rho_1}\right)^{\frac{2}{3}} \left(\sigma_1^o - \frac{L\epsilon_o\epsilon}{4\pi} E^2\right) \frac{c_p^o - \beta E^2}{\eta_o - dE^2} \quad (7.18)$$

## 7.4 Kinetics of the Crystallization Process

According to Frenkel's fluctuation theory, the velocity of crystallization or the kinetics of phase transformation are usually characterised by two different quantities, namely the birth rate of crystallization centres or the rate of nucleation, which was

expressed as  $I$ , and their linear crystallization velocity or linear crystallization rate, which was expressed as  $\nu$ .

In the crystallizing process an important role is played by the activation energy of diffusion of particles across the interface between phases; these have been described by Frenkel (1946). Taking into account the effect of an external electric field, the relative expressions were derived by Chesnokov (1956), Lychev (1976 and 1977) and Iliev et al (1981).

### 7.4.1 Activation energy and diffusion coefficient

When an external electric field is applied to a dielectric melt, the activation energy necessary for a molecule to pass from the liquid phase to the solid phase was described as

$$U^e = U^o - \Delta U = U^o - \gamma E^2 \quad (7.19)$$

where  $U^o$  is the activation energy in the absence of the field,  $\gamma$  is the coefficient.  $\gamma$  was expressed by Lychev (1976 and 1977) as

$$\gamma = \frac{1}{2} \epsilon_o \chi_1 V_1 \quad (7.20)$$

In another reference (Lychev, 1979a), it was expressed as

$$\gamma = \left( \frac{U^o}{c_p^o} \right) \beta \quad (7.21)$$

( $\beta$  is the parameter defined before.) Nevertheless, Iliev (1989) reported that  $\gamma$  depends on the dielectric constant  $\epsilon$ , the arrangement and the configuration of the electrodes.

Accordingly, on the basis of Frenkel's theory, the diffusion coefficient was described by the above researchers as

$$\begin{aligned} D_e \sim \exp\left(-\frac{U^e}{\kappa T}\right) &= \exp\left(-\frac{U^o - \Delta U}{\kappa T}\right) \\ &= D_o \exp\left(\frac{\gamma E^2}{\kappa T}\right) \end{aligned} \quad (7.22)$$

where  $\kappa$  is the Boltzmann constant, and  $D_o$  is the diffusion coefficient in the absence of the field.

## 7.4.2 The rate of nucleation

The rate of nucleation in the absence of an electric field was described in the classical kinetics theory of phase transition. On this basis, several models for the case of nucleation rate in the presence of an electric field were developed.

### The classical models

Assuming that the velocity of crystallization is the same as that in any other transition process associated with the existence and growth of the embryos of a new phase (YY) amidst the initial one (XX), such as from the vapour phase to the condensed liquid phase, the following expression for the formation rate of crystalline nuclei from a melt in the absence of an electric field were given by Frenkel (1946) as

$$I_o = \text{const.} \exp \left[ -\frac{1}{\kappa T} \left( U^o + \frac{4\pi}{3} r_{cr}^2 \sigma^o \right) \right] \quad (7.23)$$

If the critical size  $r_{cr}$  is expressed as a function of the degree of supercooling, it can be described as

$$I_o = \text{const.} \exp \left\{ -\frac{1}{\kappa T} \left[ U^o + \frac{4\pi \sigma^o}{3} \left( \frac{2\sigma^o V_2 T}{c_p^o (T_o - T)} \right)^2 \right] \right\} \quad (7.24)$$

where  $\kappa$  is the Boltzmann constant,  $T_o$  the melting point, T the temperature at which the crystallization centre appears,  $\sigma^o$  the surface tension at the melt-crystal boundary,  $c_p^o$  the specific heat of crystallization and  $V_2$  the specific (per molecule) volume of the solid phase.

Similar expression can also be found from the work of crystallization, in which it was expressed as (Mullin, 1993)

$$I_o = \text{const.} \exp \left[ -\frac{16\pi(\sigma^o)^3}{3\kappa T^* \Delta H_f^2 T_r (\Delta T_r)^2} \right] \quad (7.25)$$

where  $T^*$  is the solid-liquid equilibrium temperature expressed in Kelvins,  $\Delta H_f$  is the latent heat of fusion and  $T_r$  is the reduced temperature defined by  $T_r = T/T^*$  and  $\Delta T_r = (T^* - T)/T^*$ , that is  $\Delta T_r = 1 - T_r$ .

### Lychev's model

On the basis of the Frenkel's model, parameters  $T$ ,  $T_o$ ,  $c_p^o$ , and  $U^o$  in the above expression were substituted into the ones for an electric field with strength  $E$ , then the equation for nucleation rate in an electric field was described by Lychev (1976 and 1977)

$$I_e = I_e(T, E) = \text{const. exp} \left\{ -\frac{1}{\kappa T} \left[ U^o - \gamma E^2 + \frac{A}{\left[ T - T_{oe} \left( 1 - \frac{\beta E^2}{c_p^o} \right) \right]^2} \right] \right\} \quad (7.26)$$

where

$$A = \frac{16\pi(\sigma^e)^3 V_2^2 T_{oe}^2}{3(c_p^o)^2} \quad (7.27)$$

where  $T_{oe}$  was defined as the equilibrium temperature in the absence of an electric field.

They suggested from the partial analysis results that there should be a critical temperature  $T_E$ , namely

$$T_E = T_{oe} \left[ 1 - \frac{\beta E^2}{c_p^o} - \frac{\sigma^e V_2}{c_p^o} \left( \frac{32\pi\beta}{3\gamma} \right)^{\frac{1}{3}} \right] \quad (7.28)$$

When  $T < T_E$ ,  $dI_e/dE > 0$  and for  $T > T_E$   $dI_e/dE < 0$ ; these could mean that an electric field applied to a dielectric melt at a temperature below some value  $T_E$  could increase the number of crystallization centres and the rate of nucleation as a function of the field could also be increased; while, for  $T > T_E$  the rate of nucleation as a function of the field and the number of crystallization centres could be decreased. These results reported were for the case of the parameter  $\beta > 0$ ; for the case of  $\beta < 0$ , the results were not discussed in detail but were simply concluded as that there would be an opposite effect from the case of  $\beta > 0$ .

Another formula was also published by Lychev et al (1979a and 1979b) and the rate of nucleation was expressed as

$$I_e(T, E) = \text{Const. exp} \left\{ -\frac{1}{RT} \left[ U^o + \gamma E^2 + \frac{A}{\left[ T_{oe} \left( 1 + \frac{\beta E^2}{c_p^o} \right) - T \right]^2} \right] \right\} \quad (7.29)$$

where  $V_2$  is specific volume of the solid phase,  $R$  the gas constant and  $A$  has the same expression as before. It was deduced from this equation that the rate of nucleation in an electric field at  $T = const$  for dielectric with  $\beta > 0$  would first increase with increase in the field strength,  $E$ , and then decrease. The maximum value of  $I_e(T)$  was suggested to be at

$$E_{(I_e)}^* = \sqrt{\frac{1}{3} \left( \frac{2A}{\gamma \Delta T_o^2} - \frac{c_p^o \Delta T_o}{\beta T_{oe}} \right)} \quad (7.30)$$

where  $\Delta T_o = T_{oe} - T$ .

### Shklyar's model

Followed the work on Lychev's model, the electric field effect on the surface tension  $\sigma$  was considered by Shklyar (1989) and the rate of nucleation was then expressed as

$$I_e = Const. \exp \left\{ -\frac{1}{RT} \left[ U^o + \gamma E^2 + \frac{A \sigma^e}{\left[ T_{oe} \left( 1 + \frac{\beta E^2}{c_p^o} \right) - T \right]^2} \right] \right\} \quad (7.31)$$

where  $A$  has the same expression as Eq.(7.27) and

$$\sigma^e = \left( \frac{\rho_2}{\rho_1} \right)^{\frac{2}{3}} \left( \sigma_1^o - \frac{L\epsilon}{4\pi} E^2 \right) \frac{c_p^o - \beta E^2}{\eta_o - dE^2} \quad (7.32)$$

It was discussed that, when the external electric field does not change, the rate of nucleation takes its maximum value in the following temperature

$$T_{I_e}^* \approx T_{oe} \left( 1 - \frac{\beta E^2}{c_p^o} \right) - 2 \left( \frac{A}{\lambda} \right)^{\frac{1}{3}} \quad (7.33)$$

where

$$A = A_o \left( 1 - \frac{L\epsilon}{4\pi \sigma_1^o} E^2 \right)^3 \frac{\left( 1 - \frac{\beta E^2}{c_p^o} \right)^3}{\left( 1 - \frac{dE^2}{\eta_o} \right)^3} \quad (7.34)$$

$$A_o = \frac{16\pi \sigma_o^3 V_2 T_{oe}^2}{(3c_p^o)^3} \quad (7.35)$$

$$\sigma_o = \sigma_1^o \left( \frac{\rho_2}{\rho_1} \right)^{\frac{2}{3}} \left( \frac{c_p^o}{\eta_o} \right) \quad (7.36)$$

$\lambda \approx 292.6 \text{ kJ/mole.K}$  for supercooled organic liquids.

### A model for homogeneous primary nucleation

This model was developed by American researchers Marand, Stein and Stack (1988). An electric field effect on both polar and nonpolar crystalline polymorphs was considered. They followed the scheme developed by Isard (1977) and extended his treatment to the case where the nucleus polarisation is not only of the induced type but may also have a permanent contribution. They noted that the change from a homogeneous medium in zero field to a nucleated medium in a field  $E_o$  can occur by two different routes as shown in the schematic Figure 7.1.

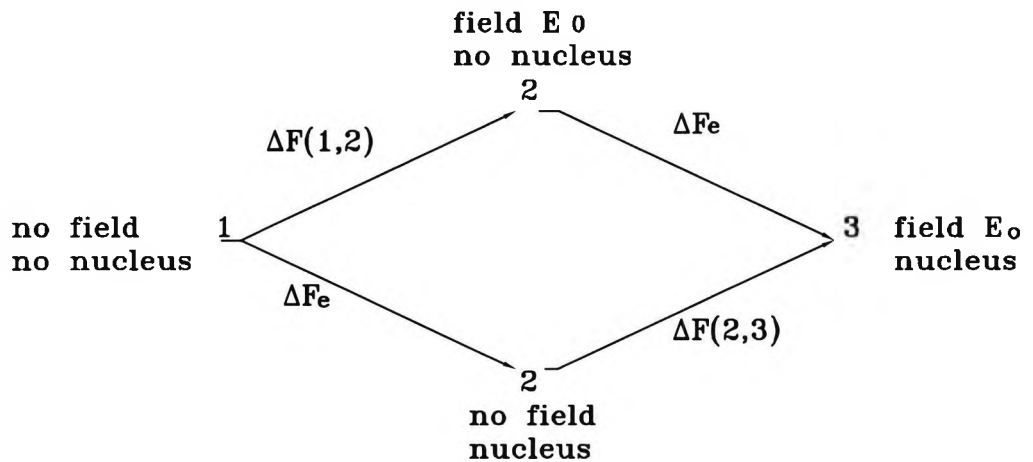


Figure 7.1: The routes for a homogeneous medium in zero field to a nucleated medium in a field E

By means of the thermodynamic analysis, the final expression for the free energy of formation of a nucleus was obtained as

$$\Delta F_e = -NAL(\Delta f + \bar{P}E_o) + 2NAf_{end} + 2L\sqrt{NA\pi}f_{side} \quad (7.37)$$

where  $NAL$  is the critically stable size of embryos(volume), N the number of strands, L the length, and A the cross-sectional area, respectively.  $f_{end}$  and  $f_{side}$  are

the end-surface and side-surface free energies, respectively.  $\Delta f$  is the free energy of melting of a boundless unit volume of crystal.  $\bar{P}$  is the polarisation. For the nonpolar ( $\gamma$ ) phase,  $\bar{P} = \bar{P}_P$  (permanent polarisation) and for the polar ( $\alpha$ ) phase,  $\bar{P} = \bar{P}_i$  (induced polarisation). The polarisations  $\bar{P}_i$  and  $\bar{P}_P$  were expressed as

$$\bar{P}_i = \epsilon_o \epsilon_a \left( \frac{\epsilon_c - \epsilon_a}{\epsilon_c + \epsilon_a} \right) E_o \quad (7.38)$$

$$\bar{P}_P = \frac{2\epsilon_a}{\epsilon_a + \epsilon_c} \bar{P}_c \quad (7.39)$$

where  $\epsilon_o, \epsilon_a$  and  $\epsilon_c$  express the vacuum, the melt and the crystal dielectric permittivities, respectively;  $\bar{P}_c$  is the permanent polarisation of the nuclei.

Therefore, in order to assess the relative change of the nucleation rate with undercooling or with field strength, the logarithm of the ratio of the nucleation rates with ( $I_e$ ) and without ( $I_o$ ) electric field as a function of the field strength was described as

$$\log_{10} \left( \frac{I_e}{I_o} \right) = \frac{1}{2.303\kappa T} \left[ \left( \frac{1}{\Delta f} \right)^2 - \left( \frac{1}{\Delta F_e^*} \right) \right] \quad (7.40)$$

where

$$\Delta f = \frac{\Delta h \Delta T}{T_m^o} \quad (7.41)$$

Here  $T_m^o$  is the equilibrium melting temperature, and  $\Delta T = T_m^o - T$ ;  $\Delta h$  is the enthalpy of melting and

$$\Delta F_e^{cr} = \frac{8\pi f_{end} f_{side}^2}{(\Delta f + \bar{P} E_o)^2} \quad (7.42)$$

is the free energy change upon formation of a critical nucleus in the electric field. The compared results are shown as Figure 7.2.

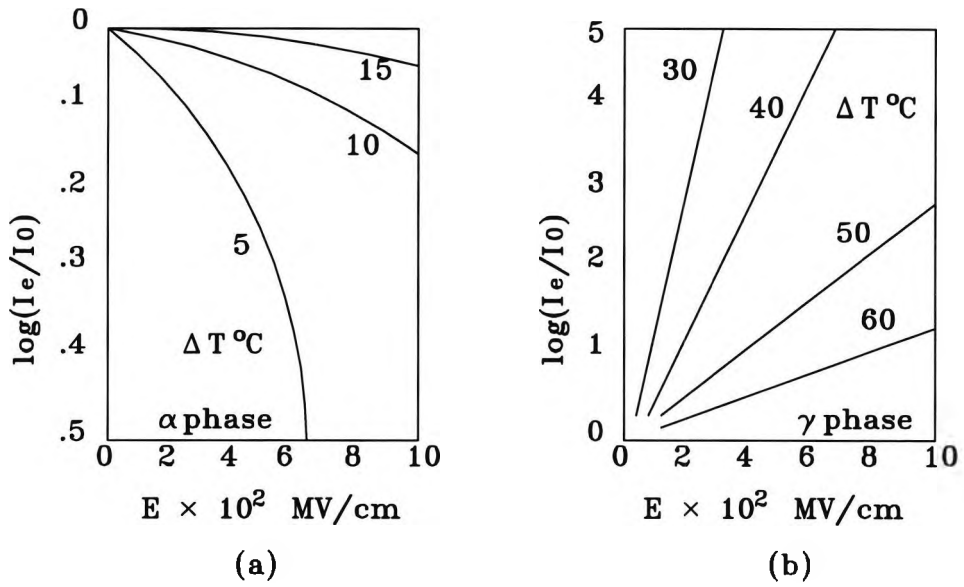


Figure 7.2: Effect of electric field strength on nucleation rates ratio  $I_e$  for various undercoolings. (a) nonpolar  $\alpha$  phase; (b) polar  $\gamma$  phase.

### 7.4.3 Linear crystallization rate

The linear crystallization rate or linear crystallization velocity was defined as a velocity with which the boundary surface between the melt and the crystallized mass of substance moves forward under microscopic conditions. The fluctuational theory of supercooled-melt crystallization gave an expression (Frenkel, 1946) as

$$\nu(T) = K \exp \left\{ -\frac{1}{\kappa T} \left[ U^\circ + \frac{\pi \chi^2 F T_o}{c_p^o (T_o - T)} \right] \right\} \quad (7.43)$$

where  $K$  is a constant,  $\kappa$  is the Boltzmann constant,  $T_o$  and  $T$  are melting point and the temperature at which the crystallization centre appears, respectively,  $\chi$  is specific perimeter energy,  $U^\circ$  is the activation energy necessary for an atom to pass from the melt phase to the solid phase and  $F$  is the area over which a monomolecular layer of one mole of material extends.

Considering the electric field influence, the linear crystallization was described by Lychev et al (1979a and 1979b) as

$$\nu(T, E) = K \exp \left\{ -\frac{1}{RT} \left[ U^o + \gamma E^2 + \frac{B}{T_{oe} \left( 1 + \frac{\beta E^2}{c_p^o} \right) - T} \right] \right\} \quad (7.44)$$

where

$$B = \frac{\pi \chi^2 F T_{oe}}{c_p^o} \quad (7.45)$$

On the basis of this equation, for the case of  $\beta > 0$  and  $T = const.$ , a maximum value for function  $\nu(E)$  was suggested, this was at

$$E_{(\nu_e)}^* = \sqrt{\frac{1}{2} \left( \frac{B}{\gamma \Delta T_o} - \frac{c_p^o \Delta T_o}{\beta T_{oe}} \right)} \quad (7.46)$$

The function  $\nu$  would increase for  $E < E_{\nu_e}^*$ , and decrease for  $E > E_{\nu_e}^*$ . It was also reported that for  $E < E_{\nu}$  then  $\nu > \nu_o$  and for  $E > E_{\nu}$  then  $\nu < \nu_o$ , where  $E_{\nu} = \sqrt{2} E_{\nu_e}^*$ .

When  $E = const.$ , the relationship between the linear rate  $\nu$  and temperature  $T$  was also derived, i.e.  $\nu$  rises with temperature for  $T < T_{\nu}^*$  and decreases for  $T > T_{\nu}^*$ ; when  $T = T_{\nu}^*$ ,  $\nu(T) = \nu_{max}$  where

$$T_{\nu}^* \approx T_{oe} - \sqrt{\frac{B}{\lambda}} + \frac{\beta E^2}{c_p^o} T_{oe} \quad (7.47)$$

When  $E = 0$ ,  $\nu_o(T)$  has a maximum at

$$T_{o, \nu_{max}}^* \approx T_{oe} - \sqrt{\frac{B}{\lambda}} \quad (7.48)$$

Hence a concluded result was suggested as that an external electric field could shift the maximum value on the curve of linear crystallization rate against temperature toward higher temperature for dielectric with  $\beta > 0$ , and toward low temperatures for dielectrics with  $\beta < 0$ . This shift should be of magnitude

$$\Delta T_{max} \approx \frac{\beta E^2}{c_p^o} T_{oe} \quad (7.49)$$

Furthermore, it was also shown that at temperatures  $T < T_{\nu}$ , the curve of  $\nu(T)$  in an electric field (with  $E = const.$ ) lies below the corresponding curve of  $\nu_o(T)$  in the absence of a field, while at  $T > T_{\nu}$  it lies above the curve of  $\nu_o(T)$ . where

$$T_{\nu} = T_{oe} \left( 2 + \frac{\beta E^2}{c_p^o} \right) - \sqrt{\frac{B}{\lambda} + 3T_{oe}^2 \left( 1 + \frac{\beta E^2}{c_p^o} \right)} \quad (7.50)$$

This suggested that for  $\beta > 0$ , the electric field decreases the linear crystallization rate of the dielectric at small supercooling rates and increases it at large supercooling rates.

#### 7.4.4 Kinetics of massive crystallization

The effect of an electric field on the kinetics of massive crystallization were considered by Lychev (1979a) and Iliev and Kontrov (1989), who followed the idea of total crystallization described by Avrami's equation (Avrami, 1940). The total crystallization was defined as

$$a = \frac{V_{cr}}{V_o} \quad (7.51)$$

where  $V_o$  is the original volume of the melt and  $V_{cr}$  is the volume of the crystallized material. This value changes over the course of time and was described by Avrami's equation

$$a(t) = 1 - \exp(-kI^l\nu^m t^n) \quad (7.52)$$

where  $k$ ,  $m$ , and  $n$  are coefficients depending on the configuration of the nucleus and the nucleation mechanism which is: thermal, when ever-new nuclei arise during the crystallization period, or athermal, when a simultaneous increase of the specified number of nuclei begins at a given zero moment; while  $l$  is equal to 1 for the thermal and to 0 for the athermal crystallization mechanism.

Similarly, another parameter called the fraction of the mother-liquor volume that is uncrystallized at time  $t$  and the time of complete crystallization  $\tau$  was described by Kolmogorov (1947) as

$$b(t) = \exp\left(-\frac{\pi}{3}I_o\nu_o^3 t^4\right) \quad (7.53)$$

$$\tau = \frac{1.37}{(I_o\nu_o^3)^{\frac{1}{4}}} \quad (7.54)$$

Obviously, in general, the relation can be easily derived as

$$b(t) = 1 - a(t) \quad (7.55)$$

Moreover, other important crystallization parameters of the material are the maximum crystal size  $l_{max}$  and the number of crystals  $N$  in a given volume at the end of crystallization. These parameters determine the structure of the crystallized solid phase. The relative expressions were described by Kolmogorov (1947) as

$$l_{max} = 1.57 \left( \frac{\nu_o}{I_o} \right)^{\frac{1}{4}} \quad (7.56)$$

and

$$N = 0.121 \left( \frac{I_o}{\nu_o} \right)^{\frac{3}{4}} \quad (7.57)$$

Using these formulae, the rates of phase transformation of material in the volume in the presence and absence of an electric field were compared. This is shown in Figure 7.3 which gives the comparison results for the time dependence of the total crystallization.

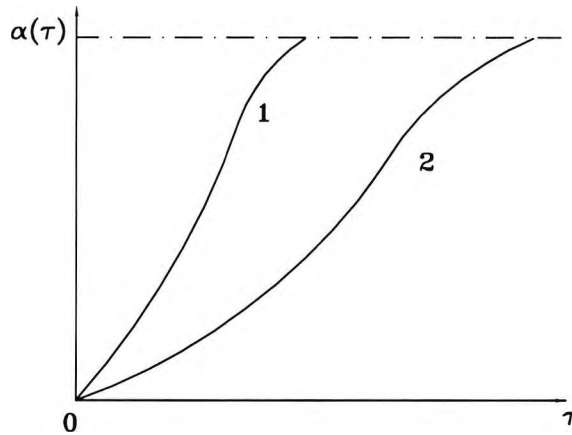


Figure 7.3: The time dependence of the total crystallization. (1) with an electric field; (2) without a field.

For optimizing the complete crystallization, based on equations 7.29 and 7.44, the analysis results (for  $\beta > 0$ ) were reported by Lychev (1979a) as

$$\left. \begin{array}{ll} b_e(t) < b_o(t) & \text{for large supercooling } (T > T_\nu), \quad E = \text{const.} \\ \tau_e < \tau_o & \text{for weak field } (E < E_I, E_\nu), \quad T = \text{const.} \end{array} \right\} \quad (7.58)$$

$$\left. \begin{array}{ll} b_e(t) > b_o(t) & \text{for small supercooling,} \quad E = \text{const.} \\ \tau_e > \tau_o & \text{for strong field,} \quad T = \text{const.} \end{array} \right\} \quad (7.59)$$

This suggested that, with increase in the electric field strength,  $E$ , the time of complete crystallization,  $\tau$ , falls at first and then begins to rise. As a result, the minimum time,  $\tau_{min}$ , of the complete crystallization in the volume could be obtained at the relative strength of the electric field represented as

$$E_{min}^{\tau} \approx \sqrt{\frac{c_p^o}{\beta T_{oe}} \frac{A}{(12\lambda\Delta T_o^2 - 3B)}} \quad (\Delta T_o > 1^\circ C) \quad (7.60)$$

Similarly, on the basis of equations 7.29 and 7.44, the maximum crystal size  $l_{max}$  and the number of crystals  $N$  in a given volume at the end of crystallization and the relative strength of the electric field was also analyzed for the case of  $\beta > 0$ . The results indicated that with increase in the field strength  $E$ , at constant  $T$ ,  $l_{max}$  decreases and  $N$  increases when  $E < E_{max}^l$  where

$$E_{max}^l = \sqrt{\frac{c_p^o}{\beta B} \left( \frac{2A}{T_{oe}} - \Delta T_o \right)} \quad (7.61)$$

However,  $l_{max}$  increases and  $N$  decreases when  $E > E_{max}^l$ .

It was also reported that when  $E < E_e$  or  $T < T_e$ , then  $l_{max}^e < l_{max}^o$  and  $N > N_o$ , while when  $E > E_e$  or  $T > T_e$ ,  $l_{max}^e > l_{max}^o$  and  $N < N_o$ ; where

$$E_e = \sqrt{\frac{c_p^o \Delta T_o}{\beta T_{oe}} \left( \frac{2A - B\Delta T_o}{B\Delta T_o - A} \right)} \quad (7.62)$$

$$T_e \approx T_{oe} - \frac{B}{24A} \beta E^2 c_p^o T_o^2 \quad (7.63)$$

These indicated that, for the case of  $\beta > 0$ , the crystals obtained in weak fields (or at small supercooling) would be finer than those in strong fields (or at large supercooling). The changes of field strength or superheat may decrease or increase the size of the crystals, i.e. may change the structure of the solid phase obtained.

It was noted that the Avrami equation is actually for the steady-state occurrence of the crystallization process in which it is assumed that the nucleation rate is constant over time. It was established after the passage of some time called the nonsteady-state period and this affects the total occurrence of the crystallization

process. Therefore, the nonsteady-state effects were considered in all cases of phase formation, particularly in the crystallization of viscous melts (Gutsov, 1971) and the approximate expression for the degree of crystallization in a nonsteady-state crystallization process and with thermal nucleation was suggested as

$$a(t) = \begin{cases} 0 & 0 \leq t \leq g\tau \\ 1 - \exp[-kI\nu^m(t - g\tau)^n] & g\tau \leq t < \infty \end{cases} \quad (7.64)$$

where  $g = \pi^2/6$ . This equation shows that the presence of nonsteady-state effects moves the S-shaped curve of  $a(t)$  a distance of  $g\tau$  towards large values of time. This is shown in Figure 7.4.

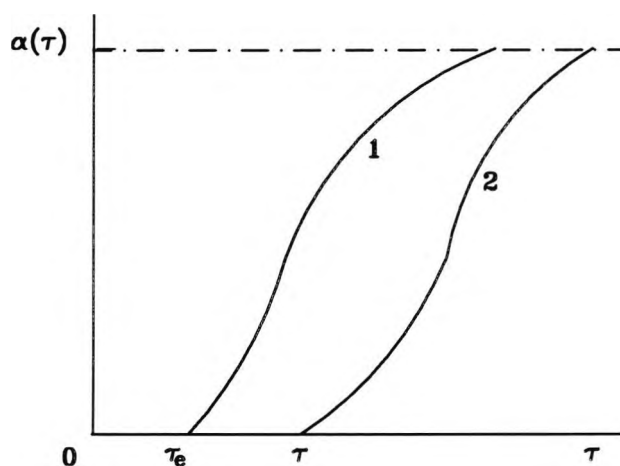


Figure 7.4: Time dependence of the degree of total crystallization with non-steady state thermal nucleation. (1) with an electric field; (2) without the field.

## 7.5 The Assessment of Experimental Results

The crystals from dielectric melts were normally obtained from experiments under cooling. The effects of an electric field on dielectric crystallization were realised by putting the dielectric melt into the space between two electrodes which were normally the plate ones. Reviewing the experimental studies on crystallization affected by an electric field, it was seen that the experimental facilities were rather simple and the methods were more or less the same; the problem was how to assess

the experimental results.

Probably, one of the most important aspects of the industrial manufacture of crystallization or crystallization research is the ability to measure the physical properties of the materials — both the basic components and the final products. As the industry has progressed and crystallization products become more sophisticated, so too have the methods used for assessing physical properties. Nowadays there are many kinds of method which are employed to assess the crystallization results. Such methods range from time-temperature cooling curve measurements to more sophisticated “molecular” techniques such as nuclear magnetic resonance (NMR) and X-ray diffraction.

The time-temperature cooling curve measurement method could be called the most basic assessment for the crystallization. The changes in temperature with time during cooling can give the basic information of the crystallization. Actually, to assess the effects of an electric field on dielectric crystallization, researchers mentioned above used to use this general macroscopic method, of which the parameters, such as temperatures or pressures were measured along the time course and different electric field strength, this was reported in the references mentioned above.

By using “molecular” techniques like NMR and X-ray diffraction, information about the state of individual atoms and molecules can be obtained and from which solid/liquid contents and structures can be calculated. However, these properties are measured from the basic molecular information and the methods can only be considered indirect.

The Differential Scanning Calorimetry (DSC) method has been extensively used to assess the crystallization products. The instruments used were mostly Perkin Elmer differential calorimeters. The principles of DSC and its application to dielectric crystallization have been described in many references, such as Haighton and Vermaas (1969) and Hamoson and Rothbart (1969). The effect of an electric field on crystallization could be indirectly assessed by DSC, and this was reported by

Marand et al (1988 and 1989). The assessments for the same samples were also carried out using an optical microscope directly and using wide-angle X-ray diffraction (WAXD) indirectly by the same researchers. However, it does not report how to connect the experimental system with an electric supply for a kinetic crystallization process.

## 7.6 Summary

The research history and progress for the effects of an electric field on crystallization have been reviewed. On this basis, some important results can be summarized as follows. However, it should be pointed that because only limited references have been published, and some of them were published by the same researchers, the summarized results have not given a consistent conclusion yet.

### The general conclusions

1. An electric field, particularly a direct current field, has a significant effect on the crystallization of dielectrics.
2. The electric field effects on the crystallization of dielectrics depend on dielectric properties, such as the permittivity, the dielectric susceptibility and the specific volume for different phases. For  $\beta > 0$  or  $\beta < 0$ , the effect may be different; while in both cases, an electric field can have a positive effect on the crystallization of dielectrics, this is subject to some conditions.
3. An electric field may have a different effect on different crystal phases, such as polar phase or non-polar phase.

### Effects on critical size of nuclei

For  $\beta < 0$ , the crystallization in an electric field takes place at smaller critical size of the nuclei than in the absence of a field. For  $\beta > 0$ , the result should be the opposite.

### **Effects on nucleation rate**

The critical temperature: An electric field (of strength  $E$ ) applied to a dielectric melt ( $\beta > 0$ ) at a temperature below some value  $T_E$  (the critical temperature) ( $T < T_E$ ) increases the crystallization centres and the nucleation rates. While, for  $T > T_E$  the nucleation rate and the crystallization centres are decreased. In the case  $\beta < 0$ , it was said the result is different and the analysis is analogous.

At a certain temperature, there is an optimum field strength for the maximum nucleation rate. For  $\beta > 0$ , the nucleation rate increases with the electric field strength when  $E < E^*$ , but decreases with the field strength when  $E > E^*$ . For  $\beta < 0$ , the result can also be predicted according to the model.

### **Effects on linear crystallization**

For the case of  $\beta > 0$ , at a certain temperature condition,  $\nu_{max}$  is reached at an optimum field strength  $E_\nu^*$ . For  $E < E_\nu^*$ ,  $\nu_E$  increases. While for  $E > E_\nu^*$ ,  $\nu_E$  decreases.

When the electric field is constant, there is a critical temperature  $T^*$  for the maximum linear crystallization rate. The rate increases for  $T < T^*$  and decreases for  $T > T^*$ .

### **The Effect on crystallization time**

The time for the total crystallization in the presence of an electric field is shorter than that in the absence of a field. For  $\beta > 0$ , this happens when  $E < E^*$  (namely weak field). For  $\beta < 0$ , the results are reversed.

### **The effect on polymorphism**

An electric field has an effect on crystallization polymorphism. For  $PVF_2$  (a kind of dielectric), the field increases the nucleation rate of polar phase ( $\gamma$ -phase) and decreases the nucleation of non-polar phase ( $\alpha$ -phase).

# Chapter 8

## Experimental Samples

### 8.1 Introduction

The experimental samples were selected from industry melts called cocoa butter and its mixtures such as chocolate. A major reason for this choice is to simplify the sample preparation process because these samples are easy to prepare in the laboratory; the melt point is only about 35 – 40 °. More importantly, the specific properties of cocoa butter on crystallization, such as the polymorphism behaviour, result in another major factor of this choice. Of course, if the enhancement effect on crystallization of cocoa butter and chocolate can be understood experimentally, it would be valuable for the food industry and particularly for the confectionery industry.

Since the early 1900's, chocolate confectionery has grown and diversified into an important factor in the world economy. Due to its aesthetic flavour appeal, chocolate is the major ingredient in many confections and is also used as a flavouring agent in the baking and beverage industry. Nowadays there are millions of people who enjoy chocolate confections in their daily life and even billions of people who do like chocolate products. Consumers enjoy eating chocolates because they taste good and produce a feeling of satisfaction and pleasure.

The pleasure derived from consuming chocolate may also be due to the cocoa butter which is a major part of the product formulation. *Theobroma cocoa* is the source

of the cocoa bean. Cocoa beans are cultivated in the tropical regions of Western Africa, Brazil, and many other locations within 20° north or south of the equator. The dried cocoa beans entering Europe and the U.S.A. are processed into various products. To ensure cleanliness and quality, the beans are processed through air lifts, screens, and magnetic separators to remove fibre, stones, and immature small beans. Once the beans are cleaned, roasting is carried out to develop flavour and aroma. Roasting facilitates the removal of the shell during winnowing and also reduces the moisture content of the bean. The beans are then passed through breakers and winnowing machines which operate by cracking the shell and bean into large pieces. The fractured shell and bean fragments are separated by sieving and air elutriation. The separation process is dependent on a difference in density between the bean cotyledon fragments and the shell. The fragments, known as nibs, are converted into a fluid paste known as chocolate liquor. This phase contains approximately 55% fat and 45% finely ground cocoa solids. In the production of milk chocolate, the addition of sugar, milk solids, and additional cocoa butter are added to the liquor prior to refining. After a small particle size ( $<25\mu\text{m}$ ) has been established in the refiners, the chocolate blend is conched. Along with producing the desired flavour, conching helps to form a continuous fat phase that evenly coats the sugar and cocoa solids thus producing a flowable liquid.

The last critical processing steps are tempering and final solidification of the confectionery product. Tempering is a process undertaken to produce a proper amount of stable cocoa butter seed crystals which will initiate crystallization in the remaining liquid butter mass. Immediately after tempering, the chocolate is moulded and cooled to approximately 16°C for proper set and contraction. It has been reported that cocoa butter crystallization has a key effect on tempering (Hans, 1989).

Cocoa butter plays a very important role in chocolate solidification. The effect of cocoa butter in chocolate solidification has been theoretically understood since the 1950s. Formulated chocolate is essentially composed of cocoa, sugar, milk solid (milk chocolate), vanillin and lecithin, all of which are suspended in a crystalline matrix of cocoa butter. When chocolate solidifies, it is the crystalline cocoa butter

that affects the product's surface finish, color, and shelf-life stability.

However, cocoa butter has complex properties. It contains specific triacylglycerols (TAGs) of Sat-O-Sat type such as POP, POS(2-oleoyl-palmitoyl-1-stearoyl-glycerol), and SOS, the total of which reaches 80%. Cocoa butter as a mixture of POP, POS and SOS can crystallize in numerous crystalline forms; this is called its polymorphic behaviour or polymorphism. Much research work has been done to understand and identify the polymorphism and other properties, while it is basically confirmed that only one of these forms is the desired stable form.

It has been found that chocolate with crystals in the less stable form has a tendency to be soft and also undergo crystal transitions; for instance it causes fat bloom, which could adversely affect product appearance. In order to ensure that the final chocolate product is in the proper crystalline form, it is very necessary to arrange some careful thermal treatments to control the polymorphic crystallization of cocoa butter.

In current practice, the confectionery (chocolate) industry uses “tempering methods” to control the polymorphic crystallization of cocoa butter. Another technique, namely “seeding”, was also introduced. It is aimed at simplifying the chocolate solidification by adding the seed crystal powders in the molten chocolate.

Using an electrostatic field to enhance cocoa butter and chocolate crystallization is a new test in confectionery industry. The potential of this test may substitute traditional ‘tempering’ process so as to shorten the manufacture period. The other benefit of applying an electric field, such as killing the small microbes, has also been reported.

In the present research, the effects of electric fields on the crystallizations of cocoa butter and chocolate are studied experimentally. In experiments, cocoa butter is selected as the basic sample and chocolate as its mixture.

## 8.2 Composition of Cocoa butter

Cocoa butter, obtained by hydraulic compression of cocoa nib, is a light yellow fat, exhibiting a distinct brittle fracture below 20°C, a fairly sharp complete melting point about 35°C, with an incipient fusion or softening around 30-32°C. Solidification and melting characteristics of fat crystals are influenced by the composition and positioning of the fatty acids on the glycerol (Toll, 1978).

It is generally accepted that cocoa butter is composed of six fatty acids, namely, stearic (S), oleic (O), palmitic (P), linoleic (Li), arachidic (A), and myristic (M). Of these six fatty acids, palmitic, oleic and stearic acids comprise approximately 95% of the total fatty acids composition. The majority of cocoa butter triglycerides fit the 2-monounsaturated triglyceride structure. The triglycerides POP, POS and SOS comprise approximately 70-80% of cocoa butter composition. Hilditch and Stainsby (1936) and Meara (1949) established that percentages of the constituent glycerides were as shown in Table 8.1, with approximately variations.

Table 8.1: The percentages of the constituent glycerides

glycerides	percentage (%)
trisaturated	2.5 to 3.0
triunsaturated (triolein)	1.0
diunsaturated:	
stearo-diolein	6-12
palmito-diolein	7-8
monounsaturated:	
oleo-distearin	18-22
oleo-palmitostearin	52-57
oleo-dipalmitin	4-6

The configuration of these diglycerides has been the subject of much research by a number of workers using modern analytical techniques, including Chapman (1957),

Lutton (1957), Savary and Flanzky (1957), Schofield and Outton (1959), and Steiner and Bonar (1961). Kattenberg (1981) has analyzed cocoa butters from various cocoa-growing areas and his findings are summarized in Table 8.2. Figure 8.1 shows the growth of percent solid phase temperature of cocoa butter.

Table 8.2: Triglyceride composition of cocoa butter

bean original	trisaturated %	monounsaturated %	diunsaturated %	polyunsaturated %
Ghanaian	1.4	77.2	15.3	6.1
Ivory coast	1.6	77.7	16.3	4.4
Cameroun	1.3	75.7	18.1	4.9
Brazil	1.0	64.2	26.8	8.0

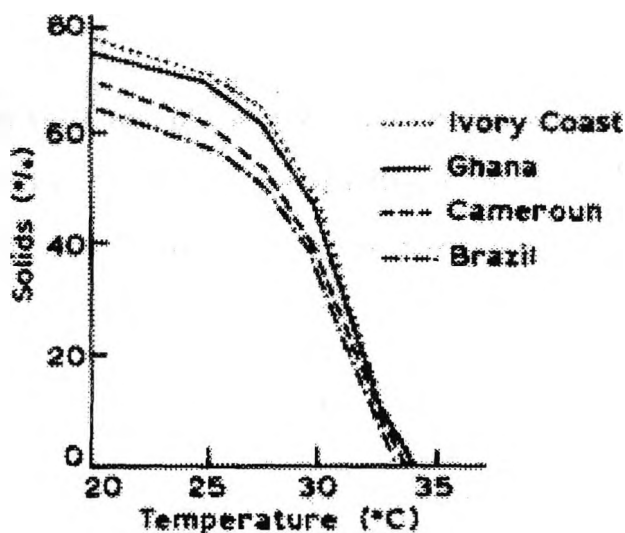


Figure 8.1: Graph of percent solid phase versus temperature of cocoa butters (Kattenberg, 1981)

## 8.3 Polymorphic Property of Cocoa Butter

### 8.3.1 The polymorphism of POP, POS and SOS

The Sat-O-Sat TAGs exhibit essentially common polymorphic behaviour, although some differences are present. Their structural properties are a prerequisite for understanding the polymorphism of cocoa butter.

The literature on the polymorphism of Sat-O-Sat TAGs contains serious contradictions. This is mainly attributed to the uncertain purity of samples employed. Using very pure samples with X-ray diffractometry (XRD), differential scanning calorimetry (DSC) and optical microscopy, the occurrence of the five basic polymorphs of POP and SOS, namely, alpha ( $\alpha$ ), pseudo-beta ( $\beta$ )-prime, beta ( $\beta$ )-2 and beta ( $\beta$ )-1 were confirmed. In POP, there are two pseudo- $\beta$ -prime forms, while in POS there is only one beta form (Sato et al., 1989).

### 8.3.2 Classification for cocoa butter crystal

For a long time, one of the most controversial areas in confection science has been the discrepancy found in cocoa butter crystal classifications. Since the discovery of polymorphism, many scientists have reported different numbers of polymorphs and conflicting melting points for the various crystalline forms found in cocoa butter.

In 1951, four crystalline forms with different melting points were observed by Vaeck (1951) and labelled as gamma( $\gamma$ ), alpha( $\alpha$ ), beta double prime( $\beta''$ ) and beta( $\beta$ ). Nine years later, Vaeck (1960) again examined cocoa butter and concluded that there were four polymorphic forms, but that the melting points were slightly different than previously reported. In 1966, fifth and sixth polymorphic forms were observed by Wille and Lutton (1966); however, the nomenclature denoting the various crystalline forms was changed to Roman numerals. The most recent work of Lovegren et al (1976) revealed six polymorphic forms, but in this case the nomenclature was exactly opposite to that proposed by Wille and Lutton. In addition to these scientists, others have reported classifications dealing with cocoa but-

ter polymorphism (Duck, 1964; Chapman et al., 1971; Witzel and Becker, 1969; Huyghebaert and Hendrickx, 1971). The various classifications and temperatures of cocoa butter crystalline forms are listed in Table 8.3.

Table 8.3: Classification of cocoa butter crystallization forms

Vaeck (1951)	Vaeck (1960)	Duck (1964)	Wille and Lutton (1966)	Chapman et al. (1971)	Lovegren et al. (1976)
$\gamma$ 18.0	$\gamma$ 17	$\gamma$ 18.0	I 17.3	I	VI 13.0
$\alpha$ 23.5	$\alpha$ 21-24	$\alpha$ 23.5	II 23.3	II	V 20.0
			III 25.5	III	IV 23.0
$\beta''$ 23.0	$\beta'$ 28	$\beta''$ 28.0	IV 27.5	IV 25.6	III 25.0
$\beta$ 34.5	$\beta$ 34-35	$\beta'$ 33.0	V 33.8	V 30.8	II 30.0
		$\beta$ 34.4	VI 36.3	VI 32.2	I 33.5

Nowadays it is generally believed that cocoa butter possesses six different crystalline states although melting points and nomenclature may differ greatly (Wille and Lutton, 1966). In the mean time, the six polymorphic forms observed by Wille and Lutton have been quoted by many references (Hans, 1989; Sato, 1991; and Manning, 1984). On this basis, another six forms were also classified by Davis and Dimick in 1986 (Dimick and Manning, 1987) as shown in Table 8.4.

Table 8.4: Davis and Dimick's classification on crystal forms of cocoa butter

forms	I	II	III	IV	V	VI
melt point °C	13.1 <sup>a</sup> /17.6 <sup>b</sup>	17.7/19.9	22.4/24.5	26.4/27.9	30.7/34.4	33.8/34.1

<sup>a</sup> Onset or transition temperature determined by DSC.

<sup>b</sup> Maximum peak temperature determined by DSC.

The polymorphic form of cocoa butter in the end products is form V, since this form has the most desirable melting and solidification behaviour compared to other

polymorphs. Form V is, however, not the most stable polymorph; that is form VI. According to polymorphic stabilization, form V transforms to form VI either through solid-state or through melt mediated transformations. The transformation to form VI gives rise to undesirable physical properties of the end products. In particular, it causes fat bloom. It was reported that the occurrence and transformation of less stable forms to form V also result in undesirable effects, such as non-temper type fat bloom (Manning, 1984).

### 8.3.3 Cocoa butter and POP, POS, SOS molecules

Each of the cocoa butter crystals was related to one of the polymorphic modifications of the Sat-O-Sat TAGs by Sato (1991). This is partly based on the polymorphic behaviour of mixtures of POP/POS/SOS in the ratio 18.2/47.8/34.0, which is the same as for cocoa butter (Sagi et al., 1989). Sato et al believed that

1. Form I of cocoa butter corresponds to sub-alpha ( $\alpha$ ) of Sat-O-Sat which transforms to alpha ( $\alpha$ ) on heating.
2. Forms II, V and VI correspond to  $\alpha$ ,  $\beta$ -2 and  $\beta$ -1, respectively. It is very important to note that form V and form VI are independent polymorphic forms. ( It was reported that this fact had so far been disregarded in chocolate sciences. Instead, form V and form VI were considered to differ in the concentration ratios of POP/POS/SOS due to self-fractionation.
3. Forms III and IV seem to be equivalent to two pseudo- $\beta$ -prime forms of POP as for as the similarity in their XRD short spacing patterns and the double length structure is concerned.

## 8.4 Physical Properties of Cocoa Butter

Many analyses which are concerned with the physical properties of cocoa butter have been published by (Fincke, 1965; Jensen, 1931; Pearson, 1970; and Minifie, 1989). The main physical and chemical constants show little variation but modern methods of analysis have shown some differences in glyceride structure and there

has been considerable study of the physical properties, including rate of crystallization, cooling curves, hardness, and contraction. These properties show significant variations (Minifie, 1989).

### 8.4.1 Properties of cocoa butter

Some typical published parameters for the properties of cocoa butter are given in Tables 8.5 and 8.6 (Minifie, 1989).

Table 8.5: Solid fat of cocoa butter

temperature °C	20	25	30	32.5	35
solid Fat %	76	69	32	8	0

Table 8.6: Some properties of commercial cocoa butter

acid number	1-4	melting point	32-34 °C
saponification number	190-198	(incipient fusion)	31.2-32.7°C
iodine number	33-40	$c_p$ (liquid)(J/g)	2.07 (34-45°C)
specific gravity	0.856-0.975	$c_p$ (solid)(J/g)	2.22 (5-20°C)
unsaponifiable meter %	0.2-0.6	viscosity (50°C)	≈ 0.1
refractive Index (40°C)	1.456-1.458	viscosity (20°C)	solid
density	0.88-0.964	titer	45-50°C
free fat acids	15 %	fatty acids	51.5-53.5°C
fatty acids(flow point)	49-51°C		

### 8.4.2 Cooling curves

Cocoa butter has unique supercooling properties, which means that the liquid fat in an undisturbed condition will remain in the liquid state well below its melting point. When cooled and stirred under rigidly controlled conditions, time and temperature can be plotted graphically.

As some new techniques were developed, such as the diffraction pattern temperature camera (DPT) to study X-ray patterns, it is possible to record continuously the X-ray patterns as a function of the temperature and time on a moving film. In this way, the crystallization and recrystallization can be studied under dynamic conditions. Some results are shown in Figure 8.2 (Hans, 1989). In the experiments the temperature conditions used for the well-known Shukoff cooling curve, which is often used to assess cocoa butter, are simulated in the DPT camera. And the results are on the same time scale superimposed on the Shukoff cooling curve of butter used for the X-ray studies. For the purpose of comparison, the cooling curve for olive oil has also been included.

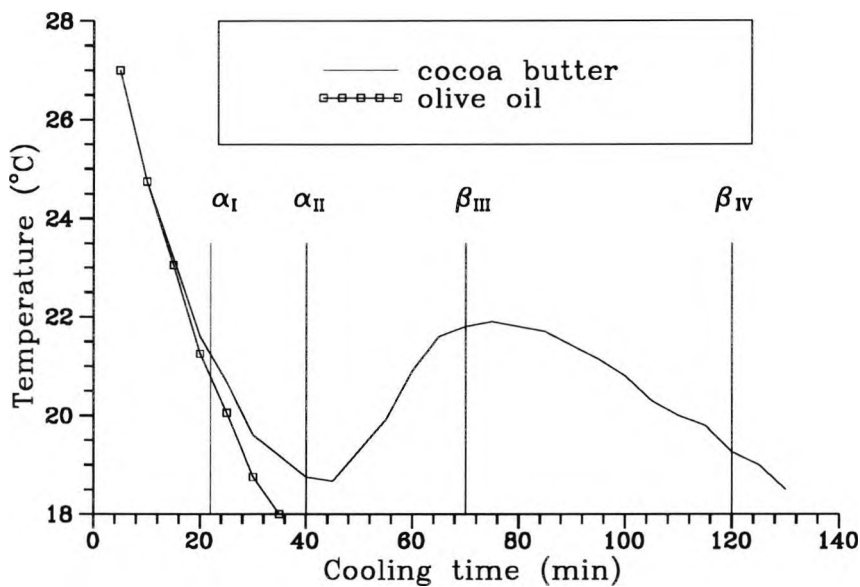


Figure 8.2: Shukoff cooling curve (phase transitions during cooling, Diffraction Pattern Temperature (DPT) x-ray studies)

It was reported that at the point where the cocoa butter curve deviates from the olive oil curve the cocoa butter starts to crystallize (Hans, 1989). According to the DPT-pattern between this starting point and the minimum of the curve only alpha ( $\alpha$ ) crystals are formed. So the primary crystallization of cocoa butter takes place in the  $\alpha$  modification. In the next part of the curve recrystallization takes

place from  $\alpha$  to beta ( $\beta$ )-prime(III). The slope of the curve is used to calculate the Shukoff  $dT/dt$  ratio. In other words the Shukoff  $dT/dt$  is a measure of the rate at which the cocoa butter recrystallizes from  $\alpha$  to  $\beta$ -prime. The  $dT/dt$  ratio can be quite different for various cocoa butters, which indicates that the rate of recrystallization of these butters will vary too.

### 8.4.3 The speed of crystallization

This is a factor that has become increasingly important. In the early days of development of equivalent fats, it was soon noted that this property was independent of glyceride structure. The temperature and cooling curve give some information, but recently developed instruments measure the increase in viscosity or resistance to mixing when the fat is allowed to crystallize under specific conditions of temperature and movement (Minifie, 1989).

### 8.4.4 Contraction

Cocoa butter has the valuable property of contraction on solidification, which enables the moulding of chocolate blocks and bars into the attractive confections displayed in shops and stores.

Proper contraction depends on correct seeding of the liquid fat or tempering of chocolate. The solidification of cocoa butter or chocolate to bring about this contraction, and also to give a smooth crystalline solid that will keep satisfactorily without fat bloom (discoloration), depends on the production of the stable polymorphic form of the fat during cooling and setting. This was studied by Minifie (1989) by determining linear and volumetric contraction of seeded cocoa butter under different cooling conditions. Others were also reported by Minifie (1989) and Lovegren (1965). The relevant results are given in Tables 8.7 and 8.8.

However, up to now no published work for the dielectric properties, which is essential for the applications of an electric field in the confectionery, is reported.

Table 8.7: Percentage of contraction volume

cooling time (min)	contraction volume (%)	
	(18°C)	(10°C)
25	1.8	4.1
50	4.1	7.4
100	7.4	7.7

Table 8.8: Percentage of liquid phase cocoa butter with temperature

temperature (°C)	liquid phase (%)		
	well tempered c.b. (Lovegren and Feuge)	solidified c.b. (average of various workers)	cocoa butter/butter fat (82 % or 18 %) as in England milk chocolate
0	0.6	–	–
5	1.9	–	–
10	4.1	11	19
15	6.8	14	25
20	10.8	15	30
25	16.7	20	37
30	36.1	38	75
34.1	100	–	–

## 8.5 Dielectric Property

A dielectric is a common material in our life. Most fats could be classified as dielectrics. Studying dielectric properties could provide an important approach to the understanding of the structure of matter. In particular, on the basis of the review work in Chapter 7 of Part two, an electric field has a significant influence on the crystallization of dielectrics. It was reported that this effect depends on the dielectric properties, such as the permittivity, the dielectric susceptibility, etc.

It was also reported that an electric field may have a different effect on different crystal phases for dielectrics, such as polar phase or non-polar phase. All of this information suggests that understanding dielectric properties should be the essential for the study of electric field effects on cocoa butter and chocolate.

An experimental study for the macroscopic dielectric properties of cocoa butter and chocolate in both solid and liquid state were carried out in the Laboratory of the Electronics Department, City University. The study particularly focuses on the dielectric constant (or relative permittivity) and the susceptibility of the cocoa butter and the chocolate.

### 8.5.1 Relative permittivity

The experimental method was originally discovered by Faraday, in which the capacitance of a condenser is increased if the space between the conductors (electrodes) is filled with a dielectric material. If  $C_o$  is the capacitance of the condenser with the region between the electrodes evacuated and  $C$  is its capacitance when this region is filled with a dielectric; then the ratio

$$\frac{C}{C_o} = \epsilon \quad (8.1)$$

is found to be independent of the shape or the dimension of the conductors and is called the dielectric constant or relative permittivity (Anderson, 1964; Zaky and Hawley, 1970).

The capacitance  $C_o$  in the equation can be expressed as

$$C_o = \frac{\epsilon_o a}{d} \quad (8.2)$$

where  $a$  is the area of the parallel plates,  $d$  the distance apart in vacuum. So the relative permittivity can be expressed as

$$\epsilon = \frac{Cd}{\epsilon_o a} \quad (8.3)$$

where  $\epsilon_o = 8.854 \text{ pF/m} = 8.854 \cdot 10^{-12} \text{ F/m}$ .

### 8.5.2 Complex permittivity

The  $\epsilon$  value is the relative permittivity in a static (or d.c) field. When an alternating field is applied across the condenser, it was defined as

$$\epsilon = \epsilon' - i\epsilon'' \quad (8.4)$$

where  $\epsilon'$  is the real part of relative permittivity,  $\epsilon''$  is the dielectric loss and  $i^2 = -1$ . The loss tangent is normally expressed as

$$\tan(\delta) = \frac{\epsilon''}{\epsilon'} \quad (8.5)$$

$$\epsilon' = \frac{C}{C_0} \quad (8.6)$$

$$\epsilon'' = \frac{1}{\omega RC_0} \quad (8.7)$$

where  $\delta$  is the angle between the total displacement current and its loss component;  $R$  is the resistance of the dielectric;  $\omega = 2\pi f$  where  $f$  is the frequency of the current.

### 8.5.3 Dielectric Susceptibility

The dielectric susceptibility of the material is clearly given by (Anderson, 1964)

$$\frac{(\text{bound charge density})}{(\text{free charge density})}$$

and is expressed as

$$\chi = \epsilon' - 1 \quad (8.8)$$

Then the polarisation vector can be obtained as

$$\bar{P} = \chi\epsilon_0 E \quad (8.9)$$

### 8.5.4 Experimental arrangement

Two kinds of cocoa butter, namely Nederland and Ghanian cocoa butter, and one kind of chocolate, namely milk chocolate, in both solid and liquid states, were studied by means of an Automatic Meter (LCR4210). The experimental system and the capacitor mould are respectively shown in Figure 8.3 (a) and (b). For the capacitor mould, two  $30 \times 30$  mm copper plates were used as electrodes, and

the cocoa butter or the chocolate filled the gap between the electrodes. For solid cocoa butter, the geometry is  $30 \times 30 \times 6$  mm; for solid chocolate,  $30 \times 30 \times 9.6$  mm. For the liquids, a perspex mould was used to keep the liquids (cocoa butter or chocolate) in the same geometry as that of the mould ( $30 \times 30 \times 3$  mm).

During the experiments, a.c fields with frequencies of 100Hz, 1kHz and 10kHz were applied, respectively.

In order to confirm the experimental results, a  $100\mu F$  standard capacitor was firstly measured; then a mica ( $30 \times 30 \times 3.19$ ) sample of which the dielectric constant is well known. The results and the original data matched each other. This is shown in Table 8.9.

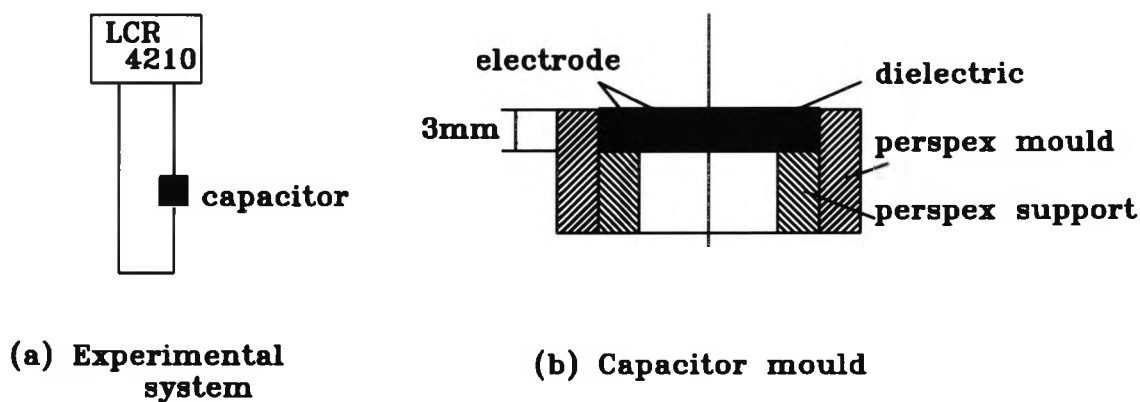


Figure 8.3: Experimental arrangement for measuring dielectric properties

Table 8.9: Standard capacitor and mica permittivity

frequency	100 Hz	1 kHz	10 kHz
standard capacitor (100 $\mu\text{F}$ )	101.2 ( $\mu\text{F}$ )	99.9 ( $\mu\text{F}$ )	99.8 ( $\mu\text{F}$ )
Dielectric constant mica ( $\epsilon' = 5 - 7$ )	6.1	5.6	5.5

### 8.5.5 Results and discussion

The results for the dielectric properties of the solid cocoa butters and the chocolate are presented in Table 8.10. The results for the liquid cocoa butters and chocolate are presented in Figure 8.4. The room temperature for all measurements is 20-21°C.

Table 8.10: Real part of dielectric constant  $\epsilon'$ , loss  $\epsilon''$  and loss tangent  $\tan(\delta)$

	Hz	$\epsilon'$	$\chi$	$\epsilon'' \times 10^2$	$\tan(\delta) \times 10^2$
Nederland (c.b.)	100	4.4	3.4	–	–
	1 k	4.1	3.1	–	–
	10k	4.0	3.0	1.5	0.37
Ghanaian (c.b.)	100	4.4	3.4	–	–
	1 k	4.2	3.2	–	–
	10k	4.1	3.1	1.5	0.36
milk chocolate	100	4.9	3.9	–	–
	1 k	4.9	3.9	–	–
	10k	4.9	3.9	9.6	1.96

The results in Table 8.10 indicate that Nederland and Ghanaian cocoa butter show similar dielectric constants or relative permittivity. While the milk chocolate has a relatively higher dielectric constant than the cocoa butter, it has a higher conductivity also. For both the cocoa butter and the chocolate, the dielectric constants

and the susceptibilities in the liquid state are larger than those in the solid state.

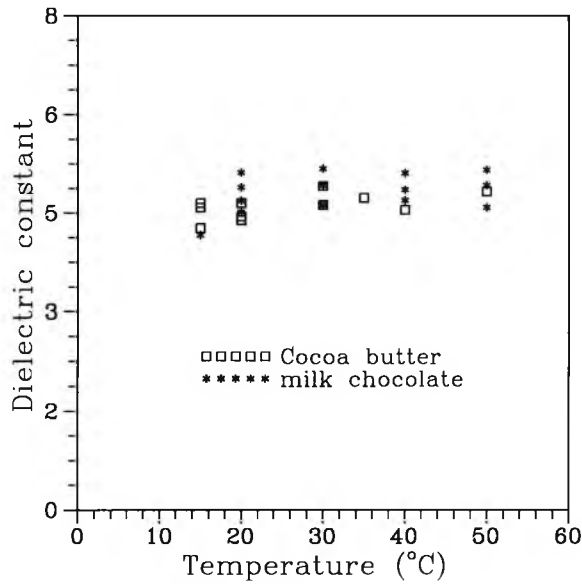


Figure 8.4: Dielectric constant of liquid samples

It can be seen from Figure 8.4 that the dielectric constants of liquid cocoa butter and chocolate do not vary greatly with temperature. It can also be proved that the permittivities vary little with pressure.

Although the results show slight changes of the relative permittivity with the changes of frequency, these are negligible in view of the experimental accuracy.

According to the dielectric theory, as reviewed in Chapter 3, the cocoa butter and chocolate may be classified as non-polar dielectrics (or slightly semi-polar). Basically, most substances which have a dielectric constant lying between 2 and 10 are good insulators; and such materials are termed non-polar because the constituent molecules do not bear a permanent dipole moment (Grant et al. 1978). The relative permittivities of Nederland and Ghanian cocoa butter and the milk chocolate are just in this range.

Another important difference between polar and non-polar materials is that the former are strongly dependent upon various physical parameters such as temperature, pressure, and frequency of applied field; whereas the electric properties of a non-polar material are largely independent of them. From this point of view, the cocoa butter and chocolate studied may be classified as non-polar (or slightly semi-polar because the slight changes of the relative permittivity with the changes of frequency) dielectrics.

It is well known that a non-polar dielectric is one whose molecules possess no permanent dipole moment unless they are in the presence of an electric field. In this case the field induces molecular dipole moments by perturbing the electron cloud around the nucleus so as to produce a separation of the centre of negative charge and the centre of positive charge. This is shown in Figure 3.3 of Part 1. For cocoa butter and chocolate, the mechanism should be similar. The polarization phenomenon, such as the electronic displacement or electro-convection, has been clearly observed when cocoa butter has been subjected to an electric field. This is described in the late chapter.

## **8.6 Chocolate Production**

### **8.6.1 Tempering**

Tempering is the controlled formation of a sufficient number of stable crystal seeds and to promote controllable crystallization. The conventional process of tempering involves cooling chocolate from  $50^{\circ}\text{C}$  to  $32^{\circ}\text{C}$  with constant agitation. Once  $32^{\circ}\text{C}$  is reached the temperature is then decreased to  $28^{\circ}\text{C}$  to produce stable cocoa butter seed crystals. After seed formation, the temperature is increased to working temperature which is usually between  $29^{\circ}\text{C}$  and  $32^{\circ}\text{C}$  depending on the chocolate formation (Kleinert, 1970). On reheating, the unstable crystals are melted and the stable crystals remain and act as seed for further crystallization. It is believed that during batch tempering the crystals increase in size and number (Mitchell, 1968). At this point, the chocolate is poured into moulds, vibrated to move air,

and cooled to approximately  $16^{\circ}\text{C}$ . Cooling is undertaken to remove the heat of crystallization. This latent heat must be removed to ensure the formation of the largest number of small stable crystals. During cooling, contraction occurs which is important for manufacturing reasons and also can be an indication of proper temper. Exactly which crystal form is desired at the completion of tempering is still speculative; for instance, Vaeck (1960) believed that  $\beta'$  and  $\beta$  crystals are present in the final tempered product, while Wille and Lutton (1966) believed that form V is the crystal desired in the final product. It was mentioned above that the latter suggestion is generally accepted.

Fat crystals should be small for visual appearance, but also for texture and mouth-feel reasons. A poorly tempered chocolate sample may have defects, such as large crystal size, poor snap, low gloss, and other undesirable characteristics. Problems may occur during tempering for numerous reasons. The presence of unstable crystals after tempering may cause production problems due to absence of contraction during cooling. The amount of stable seed formed and the manner in which the product is cooled have a large effect on product quality. Insufficient cooling may lead to large crystal formations and bloom. The addition of foreign fat in confectionery products may affect the tempering procedure and product appearance. For example, addition of milk fat to a milk chocolate reduces the tempering temperature by approximately  $1^{\circ}\text{C}$  (Koch, 1956). During tempering there should be adequate agitation to ensure proper heat transfer between the chocolate product and the cooling medium. Mechanical agitation usually involves a narrow working area which constantly fractures fat crystals as they are being formed. As a result, crystal fragments are uniformly dispersed, producing optimum crystal seed. So Feuge et al. (1962) believe that it is possible to temper cocoa butter through a mechanical process that influences polymorphic transition.

There are numerous methods used to temper chocolate. The single stream continuous tempering starts with non-crystalline chocolate at  $49^{\circ}\text{C}$  and cools it to  $28^{\circ}\text{C}$ , inducing the formation of  $\beta''$  and unstable  $\alpha$  crystals (Nelson, 1967). Upon entering the coater, the temperature is slowly increased to  $32^{\circ}\text{C}$  to melt out the  $\alpha$  crystals

and to retain the  $\beta'$  and  $\beta$ . The product is then moulded and gently cooled. Shock cooling, in contrast to slow cooling, reduces temper due to the increased amount of unstable crystals.

In practice, tempering of chocolate is carried out in scraped cooling (Hans, 1989). In Figure 8.5 a model is shown of the conditions in such a cooler.

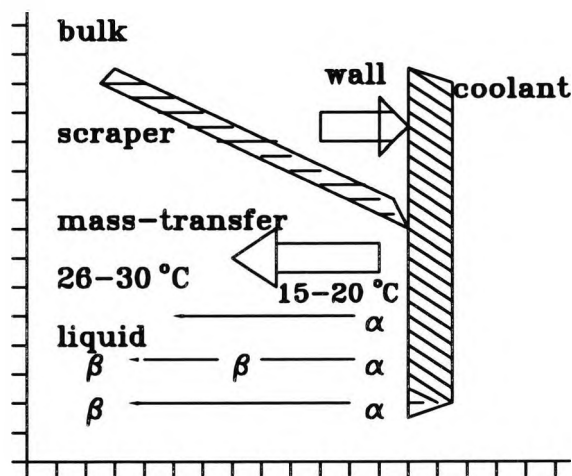


Figure 8.5: Crystallization during tempering in a scraped cooler

In the bulk stream the temperatures are 25 to 33°C, and no primary crystallization will take place, because the temperatures are well above the alpha ( $\alpha$ )-melting point. The temperature on the wall is below 20°C. Here primary crystallization can take place in the alpha ( $\alpha$ ) configuration. The scraping will cause mass transfer towards and away from the wall and the crystals are forced back into the bulk stream. The greater part will just melt and only a few will survive by recrystallization into the stable ( $\beta$ )-modification either via the  $\beta$ -prime or directly. The amount of  $\beta$ -crystals formed will strongly depend on the rate of recrystallization. A higher rate of recrystallization will result in more crystals in the bulk stream. More crystals in the bulk stream after tempering will increase the rate of solidification.

ation; this means better contraction in the mould and this will give smaller (and therefore more) crystals in the chocolate. This means a harder end product will be obtained.

### 8.6.2 Fat bloom

Fat bloom is a problem that causes the glossy surface of chocolate to become dull and covered with a grey film. This discoloration resembles the bloom on grapes, thus it was termed "bloom" (Cerbulis,1957). The most typical fat bloom occurs when normally-fabricated chocolate is stored for a long duration at elevated temperatures(25-35°C). It is well known that, through the fat bloom of this kind, the polymorphic form of cocoa butter of the bloomed and non-bloomed portions are form V and VI, respectively. More fat bloom phenomena are observed during the solidification process of chocolate without proper tempering procedures. For example, when chocolate which is first melted above 36°C, was solidified directly at about 25°C, the fat bloom occurs. In this case, the polymorphic form of the bloomed portion is not everywhere of form VI. It is sometimes form V or even form IV.

The mechanism leading to bloom formation is still a controversy today (Manning, 1984). Numerous theories have been proposed to explain the problem of bloom formation (Whymper, 1933; Becker, 1958; Kleinert, 1961; Vaeck, 1960 and Jewell, 1972) ). In view of these, the basic mechanism of the fat bloom may be growth of more stable forms after either melting or dissolution of less stable forms, as shown in Figure 8.6 (Sata, et al., 1989). The conversion through melting would occur when chocolate is subjected to cyclic temperature fluctuations, which pass through the melting points of forms III, IV or V. The dissolution process occurs via liquid oil fractions of low-melting components of cocoa butter. This is due to the fact that the less stable forms are more soluble than the more stable ones.

In both cases, slow growth of the more stable forms results in the formation of large crystals, particularly on the chocolate surface with free spaces for crystalliz-

ation. The nuclei for the fat blooming crystals would form either via solid-state polymorphic transformation or via spontaneous nucleation of more stable forms. The TAG molecules reach the newly-growing crystals through a volume diffusion process in the liquidus oil fraction.

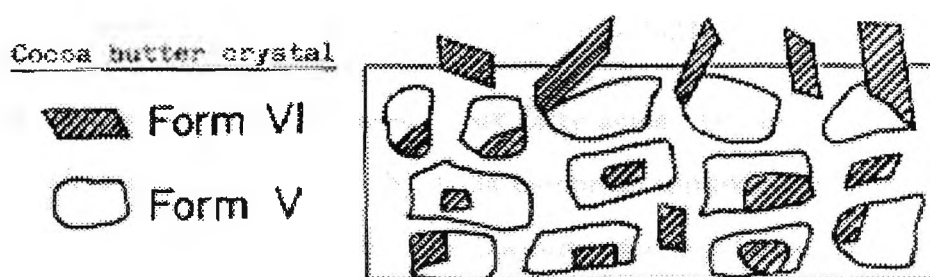


Figure 8.6: A model of fat bloom formation

The fat bloom formation is influenced by the crystallization processes of cocoa butter. It was predicted that the less stable forms crystallize more rapidly than the more stable forms (Sato, et al., 1989). For example, form II of cocoa butter crystallizes predominantly, when the molten cocoa butter is cooled below  $20^{\circ}\text{C}$ . Forms III and IV are predominant at the melt crystallization around  $25^{\circ}\text{C}$ . Once crystallized, these metastable forms convert very easily to more stable forms, always accompanied with newly grown crystals of form V or form VI which cause fat bloom.

## 8.7 Summary

1. The major fat in chocolate is cocoa butter. Formulated chocolate is essentially composed of cocoa, sugar, milk solid, vanilline and lecithin, all of which are suspended in a crystalline matrix of cocoa butter.
2. Cocoa butter is composed of six fatty acids. Of these acids, palmitic (P),

oleic (O), and stearic (S) acids comprise approximately 95% of the total fatty acids composition. The majority of cocoa butter triglycerides fit the 2-monounsaturated triglyceride structure. The triglycerides POP, POS and SOS comprise approximately 70-80% of cocoa butter composition.

3. Cocoa butter possesses six different crystalline forms, labelled I to VI. The polymorphic form of cocoa butter in the end product is form V, but the most stable polymorph is form VI.
4. Each of the cocoa butter crystals is related to one of the polymorphic modifications of Sat-O-Sat TAGs on the basis of which the polymorphic behaviour of the mixture system of POP/POS/SOS has the same ratio as cocoa butter.
5. The cooling properties of cocoa butter, i.e. the relation between time and temperature, can be plotted graphically. On this basis, the cooling properties of cocoa butter can be assessed by the well-known Shukoff cooling curve. By comparing with the cooling properties of olive oil, the starting point of cocoa butter crystallization can be identified. Using some modern techniques, such as DPT camera and X-ray studies, the polymorphic properties of cocoa butter can be identified and plotted on the curves. The slope in the curve can be used to calculate the ratio  $dT/dt$  which is a measure of the rate of cocoa butter recrystallization from  $\alpha$  to  $\beta$ -prime.
6. Cocoa butter has a valuable property of contraction on solidification. The contraction volume increases with cooling time. The specific volume of cocoa butter in the crystal (solid) state is smaller than that in the liquid (molten) state.
7. Dielectric properties of cocoa butter and chocolate have been studied experimentally. Dielectric constants and susceptibilities for both the cocoa butter and the chocolate studied are smaller in the solid state than in the liquid state. The relative permittivities of the cocoa butter and the chocolate should be classified as non-polar (or slightly semi-polar) dielectrics.
8. The tempering process is a special thermal treatment to control the poly-

morphic crystallization of cocoa butter. There are numerous methods used to temper chocolate. Basically, the following function is necessary :

- (a) Increase the stable crystals in size and number.
  - (b) The crystals should be small for visual appearance, but also for texture and mouthfeel reasons.
  - (c) Remove the heat of crystallization successfully to ensure the formation of the largest number of small stable crystals.
9. The basic mechanism of the fat bloom may be growth of more stable forms after melting of less stable forms. The fat bloom formation can be influenced by the crystallization processes of cocoa butter. Proper tempering of chocolate can reduce the fat bloom phenomena.

# Chapter 9

## Experimental Study on Crystallization

### Crystallization of Cocoa Butter/Mixture in the Presence of an Electric Field

#### 9.1 Introduction

This study is on the basis of the fact that cocoa butter and its mixture, such as chocolate, can be classified as dielectrics and all of the substances in chocolate are suspended in a crystalline matrix of cocoa butter. In the first place, the effect of an electric field on cocoa butter crystallization is studied. Then the crystallization properties and the cooling rates of cocoa butter mixture (with different percentages of chocolate) in the presence of an electric field are examined. The objectives are as follows:

1. Comparing the cooling rates of the cocoa butter (or its mixture with different percentages of chocolate) and the olive oil (with and without an electric field) to identify the behaviour of  $\alpha$ -crystals (the starting and the ending points).
2. Understanding the characteristics of polymorphic crystallization of the cocoa butter and its mixture under the action of an electric field.

3. Studying the effect on the processes of cutting off the field.
4. Comparing the results of using different electrodes and at different cooling levels.
5. Examining the possibility of using an electric field instead of the tempering process to enhance the chocolate crystallization.

## 9.2 Experimental Method and the System

### 9.2.1 Experimental system and equipment

The experimental system, as shown in Figure 9.1, was designed for both cocoa butter and chocolate crystallization with or without an electric field. Basically, it consists of three parts, namely, the high voltage generating and supplying system, the cooling system and the test rig, as well as the data acquisition and processing system.

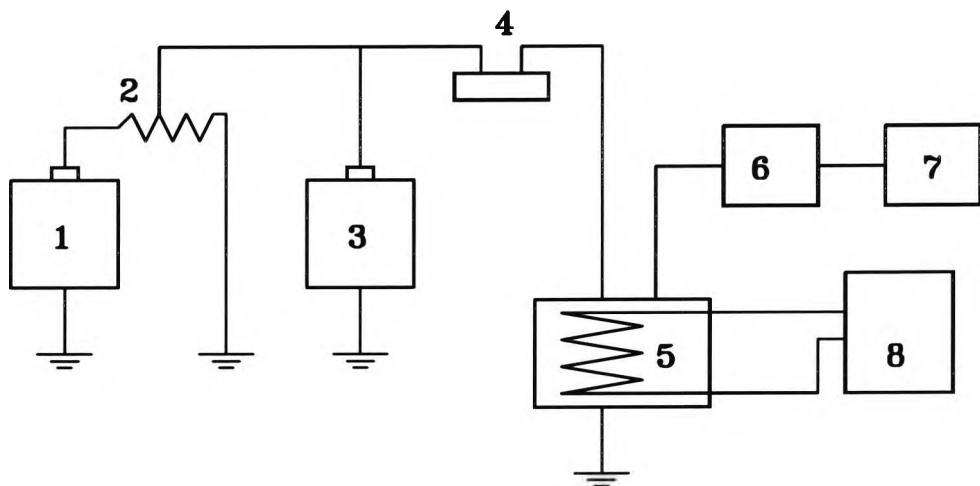
The high voltage supply is obtained from a "Sames" electrostatic generator for d.c. potential. This is capable of supplying positive d.c. up to 80kV with a maximum current of 200  $\mu A$ . The high voltage is fed through a potential divider to the electrode and is measured by a "Pye" electrostatic voltmeter of 40kV maximum RMS indication. Electric current measurements are taken using a d.c. Microammeter calibrated to BS89 with a maximum reading of 200  $\mu A$ . The electrical equipment and connections are also shown schematically in Figure 9.1.

A Faraday cage is built to insulate the experimental rig and high voltage equipment from the surroundings and allow operation. All zero potential parts of the high voltage circuit are earthed.

The test rig in the experimental system is shown schematically in Figure 9.2. It includes a sample container (crucible) which is made of stainless steel, a plastic cooling water container, a coil radiator and perspex supports, as well as an elec-

trode.

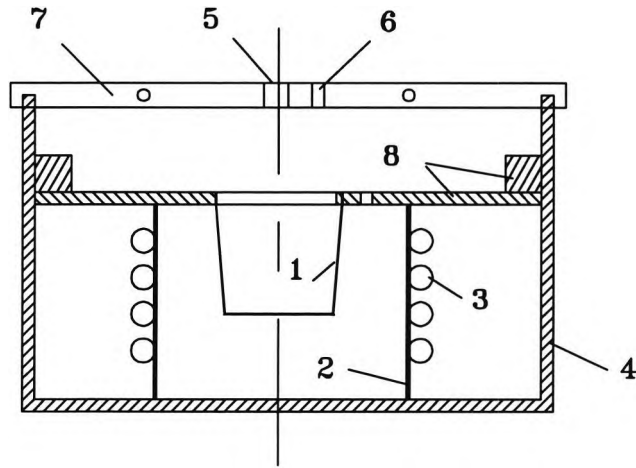
The temperature of the cooling source and cooling rate are adjusted by a coil radiator which is connected with a water refrigerator system. The temperature variation of the cooling source can be controlled in the range of  $\pm 0.3\text{ }^{\circ}\text{C}$ .



**1. High voltage supply; 2. Potential divider; 3. High voltage meter; 4. Ammeter; 5. Test rig.; 6. Data acquisition system; 7. Computer; 8. Water refrigerator system.**

Figure 9.1: The experimental system for crystallization with or without an electric field

The temperatures of the system (cocoa butter or chocolate samples, the cooling source, and the environment) are measured by means of a group of copper-constantan thermocouples and recorded by a PC computer by means of an SI 3531F Data Acquisition system. Therefore, the temperature variation can be monitored every minute or in some other time interval. The thermocouples outside the cocoa butter are well insulated so that the high voltage charge can be avoided.



- |                              |                    |
|------------------------------|--------------------|
| 1. Stainless steel crucible  | 5. Electrode       |
| 2. Stainless steel container | 6. Perspex support |
| 3. Coil radiator             | 7. Thermocouples   |
| 4. Plastic container         | 8. Perspex support |

Figure 9.2: The test rig for crystallization in the presence of an electric field

### 9.2.2 Electrodes

In order to reach different field strengths and different field directions in the experiments, a series of electrodes are designed and applied. Figure 9.3 shows these electrodes.

Electrode No. 1 is a rod electrode which is made of brass. Electrode No. 2 is a “bucket” structure electrode, which increases the field intensity because the gap is smaller. Electrode No. 3 and No. 4 are plates with “ $\perp$ ” electrodes made of brass and stainless steel, respectively. These electrodes can be moved along a vertical

direction and the field intensity is adjustable. Electrode No. 5 is a cylinder, made of stainless steel, which has six ribs vertically distributed in the cylinder surface. Electrode No. 6 is a semi-ball electrode made of aluminium alloy.

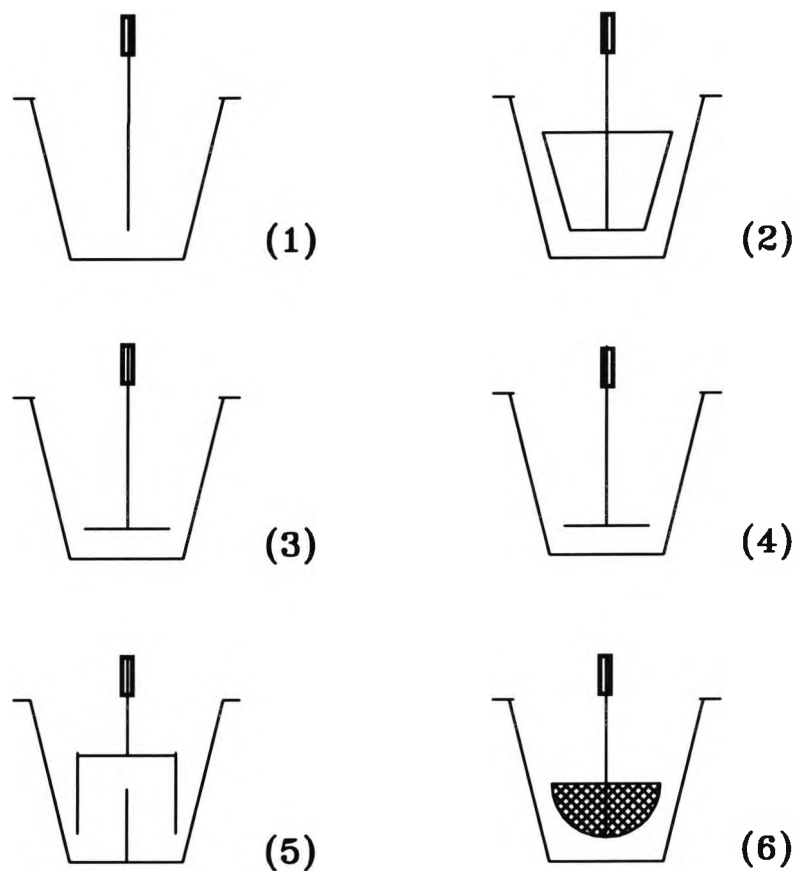


Figure 9.3: Electrodes used in experiments. (1) brass rod electrode; (2) stainless steel bucket structure electrode; (3) brass plate electrode; (4) stainless steel plate electrode; (5) stainless steel cylindrical structure electrode and (6) ball electrode.

An electrode system used for DSC sample preparation consisted of a “⊥” shape one as the positive and another with a flat bottom as the negative. This is shown in Figure 9.4.

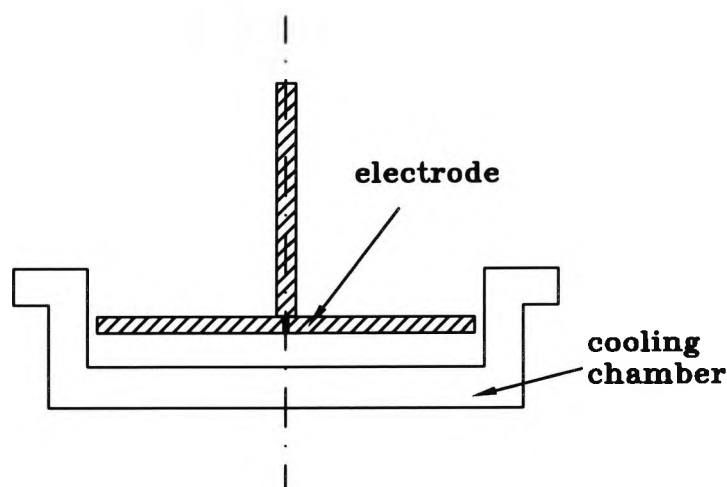


Figure 9.4: An electrode system for DSC sample preparation

### 9.2.3 Experimental method and procedures

The experimental method was a basic time-temperature measurement based on the sample temperature changes during a cooling process. A sample for crystallization would start at a temperature higher than its melting point. Cooling would then produce a gradual lowering of temperature until crystals start to be formed, when the latent heat of crystallization will be released, causing an increase of temperature since the heat energy release rate will be greater than the heat transfer due to cooling. A larger increase would indicate to more stable crystal forms. Recording the changes of sample temperature versus the cooling time will help an understanding of the basic behaviour of the crystallization.

There is no doubt that this time-temperature measurement during cooling is a basic and easy way to probe the effect of an electric field on cocoa butter and its mixture (chocolate) crystallization. Of course, the accurate measurement for the temperature and the time should be a most important basis for the results assessment. Fortunately, the thermocouple which had been carefully calibrated against the British Standards calibrated mercury thermometer reading was employed helping to measure temperature accurately and the data processing system connected with the computer could measure the time-dependent temperature as accurately as possible (the temperature could be recorded every half minute).

The experiments were carried out using the experimental system described above. Firstly, the samples (cocoa butter or chocolate) was heated to get a completely molten state; for cocoa butter, over  $35^{\circ}\text{C}$ ; for chocolate, over  $55^{\circ}\text{C}$ . Secondly, the molten samples were put into the sample container (the stainless steel crucible, 40ml) in the experimental system. Then, the electrode was attached and high voltage d.c. was applied (if with an electric field). Before the experiment began, the field strength was decided. This depended on the distance,  $x$ , between the positive electrode and the negative electrode because the field strength is equal to the value of the voltage of the field supply per charging distance ( $V/x$ ). The position of the thermocouple junction in the experimental sample for the temperature measurement, ( $x_1$  and  $x_2$ ), was also decided very carefully before the test, so that the results could be compared. The parameters  $x_1$ ,  $x_2$ , and  $x$  are schematically shown in Figure 9.5. During the experiments, the cooling source temperature was kept constant. The temperature was read every minute by the data-logger and computer system automatically. By changing the cooling source temperature, different cooling rates could be obtained.

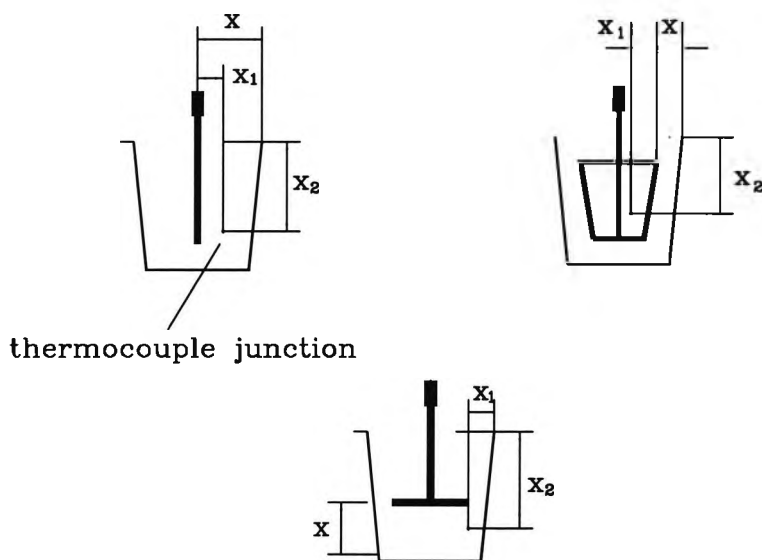


Figure 9.5: Positions of electrode and thermocouple junction

### 9.3 The Behaviour of Olive Oil

Olive oil with  $\epsilon = 3.1$  (Gemant, 1933) is a kind of dielectric liquid which does not have crystalline forms during a cooling process. This property attracted researchers to use it to compare and understand the crystallization properties of other liquids during the cooling process. In particular, it is useful to identify the polymorphic crystallization of cocoa butter. To help to understand the crystallization of cocoa butter and its mixtures in the presence of an electric field, the behaviour of the olive oil in the high voltage electric field at different cooling rates was studied. The experimental results are presented in Figures 9.6 to 9.8, respectively.

Figure 9.6 shows the cooling curves for olive oil with No.1 electrode at different voltages. The results indicate that the cooling rate increases with the applied voltages and in a stronger field, this increase is more significant than in a weaker field. Figure 9.7 can more clearly express these properties, in which the cooling

time versus electric field strengths for different cooling levels was described. It was very obvious during the experiments that the electroconvection phenomena were significant when the supplied voltage was increased. This is because of the polarization of the olive oil in the presence of the electric fields. When the fields were cut off, the polarization phenomenon stopped immediately. This suggests that the olive oil should be a non-polar dielectric. Using No. 2 electrode, cooling rates for the olive oil when the fields were cut off at different times are shown in Figure 9.8. This result gives the conclusion that the cooling rate for olive oil is enhanced by the electric field and relies on its continuation.

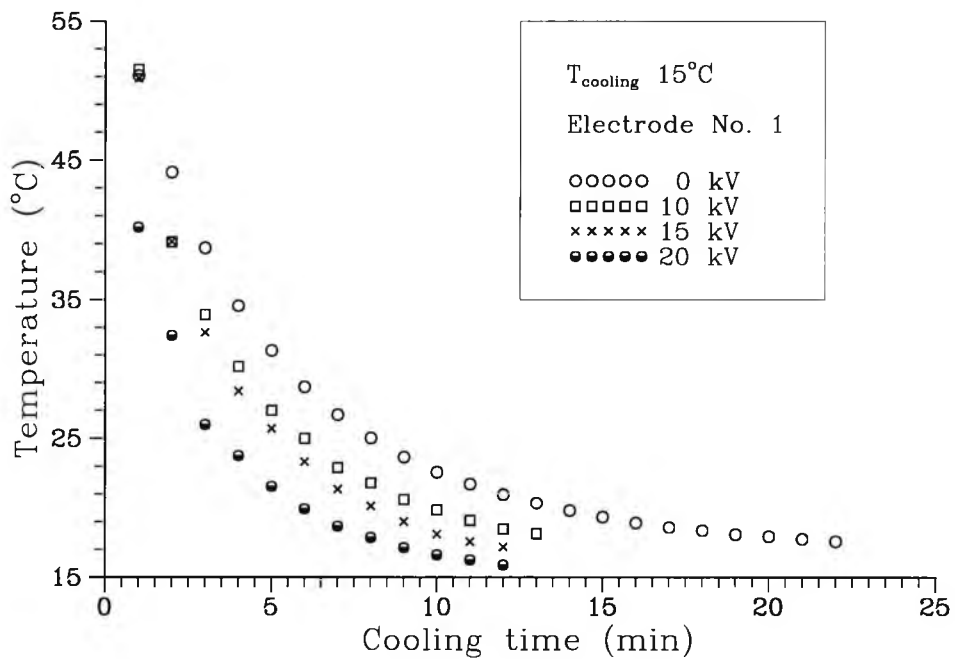


Figure 9.6: Cooling curves for olive oil at different field potentials ( $x=18\text{mm}$ ,  $x_1 = 10\text{mm}$  and  $x_2 = 18\text{mm}$ )

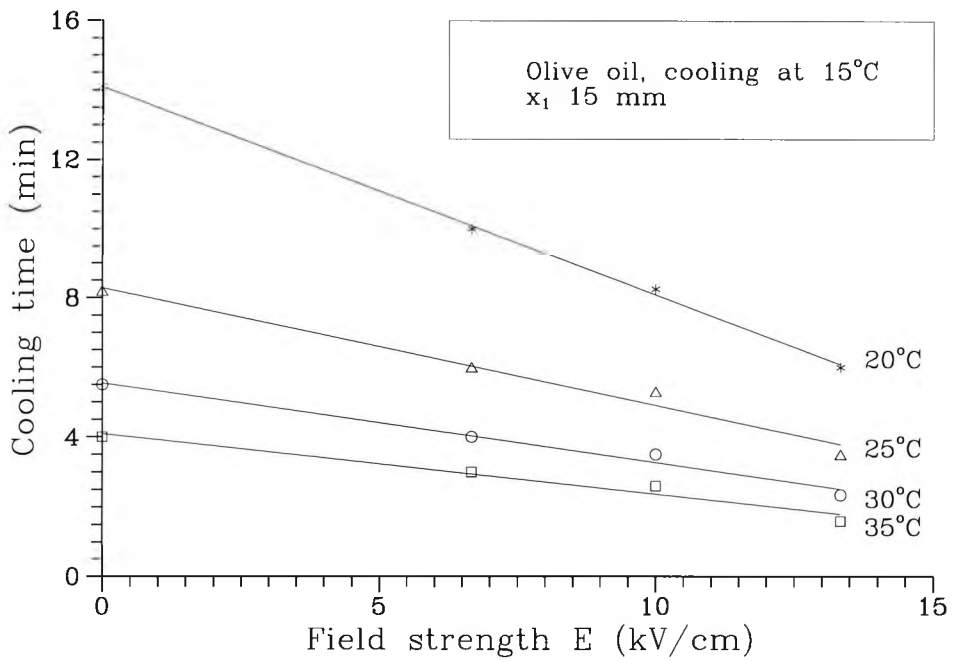


Figure 9.7: Cooling time versus field strength for olive oil at different cooling levels

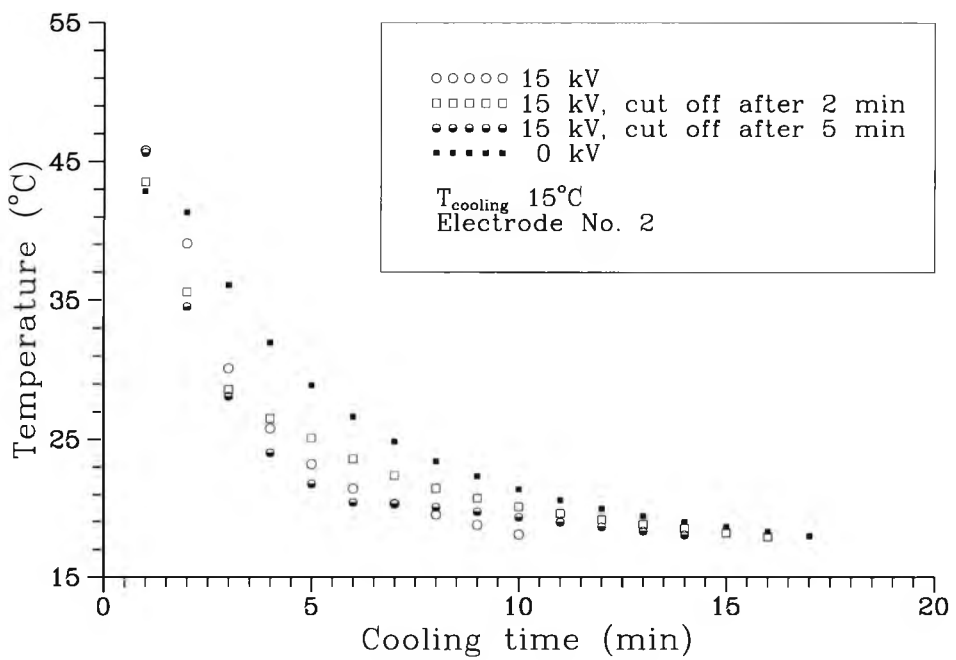


Figure 9.8: Cooling curves for olive oil with an electric field and cutting off the field supply at different times

## 9.4 Cocoa Butter Crystallization

The properties of cocoa butter crystallization affected by the electric fields were studied experimentally with different conditions; these include the general time-temperature measurements for the crystallization, Differential Scanning Calorimetry (DSC) assessments, the effect of noncontinuous field application on crystallization, called the cutting off effect, and the effect of employing different electrodes. The results are shown in Figures 9.9 to 9.27, respectively.

### 9.4.1 The cooling curves

The cooling curves for Ghanaian cocoa butter with 0 kV, 10kV and 15kV d.c. electric field using a brass rod electrode and the comparison with the cooling curves for olive oil are presented in Figures 9.9 to 9.12.

On the basis of the “Shukoff Cooling Curve”, as shown in Figure 8.2, the crystallization behaviour, such as the starting and the ending of the  $\alpha$ -crystals and the  $\beta$ -III (stable) crystals, can be identified from the cooling curves for cocoa butter and olive oil.

Figure 9.9 shows the cooling curves with 0 kV and its reproducibility. Figure 9.10 gives the comparison between the 0 kV curves and the Shukoff cooling curves. The differences may result from the difference between the experimental samples and was also relevant to the cooling source temperature. Figure 9.10 shows the results obtained at a cooling source temperature 15°C. Nevertheless, it can be seen from the figure that this result is consistent with the Shukoff cooling curve. Therefore, it can be a basis for comparison and to identify the behaviour of crystal forms; this is as marked in Figure 9.10. At the experimental cooling condition, the  $\alpha$ -crystal started at about 15 min and ended at about 40 min; the stable  $\beta$ -crystal form were completed (giving up the most latent heat during the crystallization) at about 77 min.

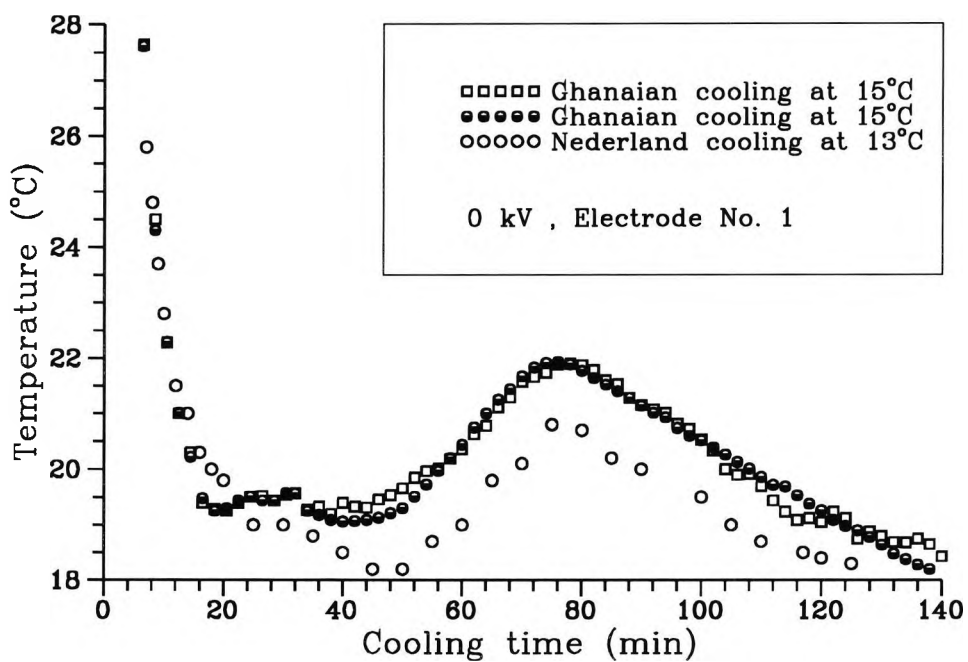


Figure 9.9: Cooling curves for cocoa butter with 0 kV field

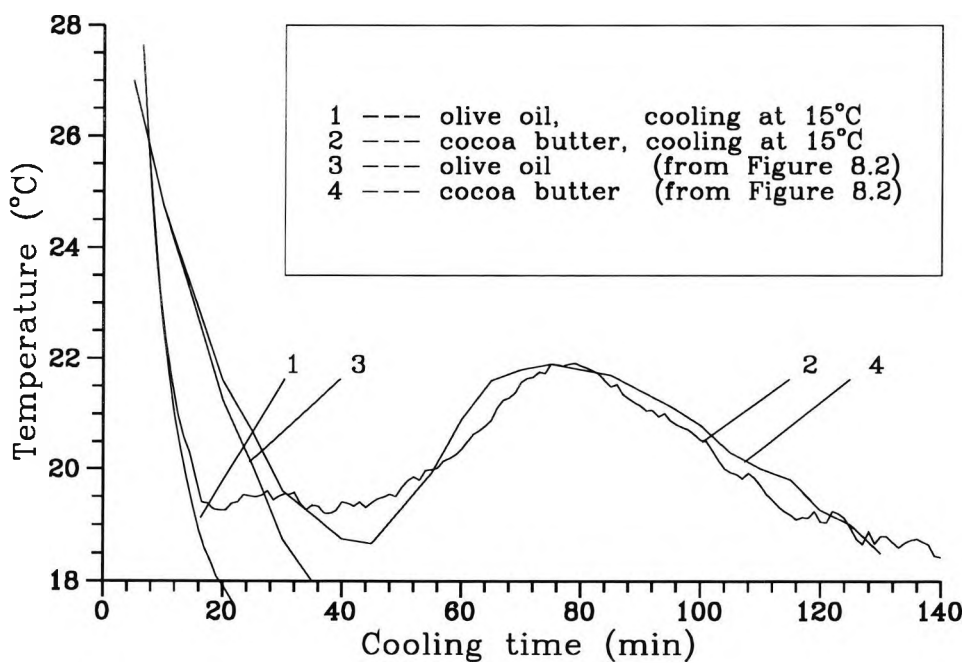


Figure 9.10: Comparison between the 0 kV curve and "Shukoff cooling curve"

Figures 9.11 and 9.12 show the cooling performance of the same sample under the action of an electric field of 10 kV and 15 kV, respectively. The reproducibilities of the experiments are also shown in the figures. It is interesting to note that, by the electric field effect, the time of both the start and end point of  $\alpha$ -crystals marked as  $\alpha_I$  and  $\alpha_{II}$ , respectively, appeared earlier than without the field. The appearing time for stable  $\beta$ -crystals marked as  $\beta_{III}$  and  $\beta_{IV}$ , respectively, was even shorter in the electric field. It was about 65 min when applying 10 kV field and only about 40 min when applying 15 kV.

Similar results for different cocoa butter and under different experimental conditions were also obtained. It is clearly seen that, as the strength increases, the time for the crystals appearing is getting short. Figures 9.13 and 9.14 show these properties for Ghanaian and Nederland cocoa butter, respectively.

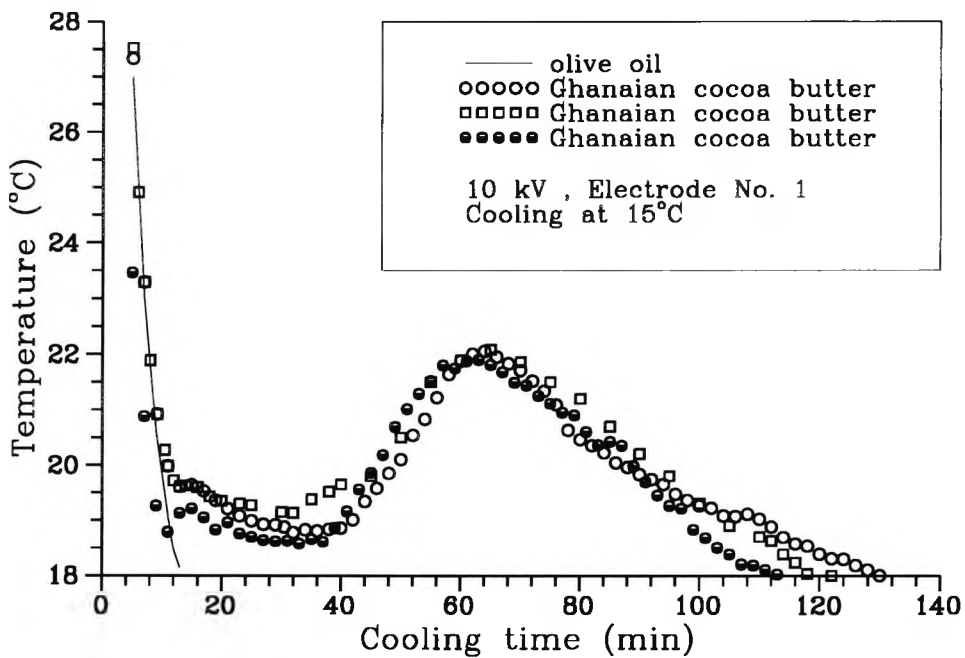


Figure 9.11: Cooling curves for cocoa butter with 10 kV field

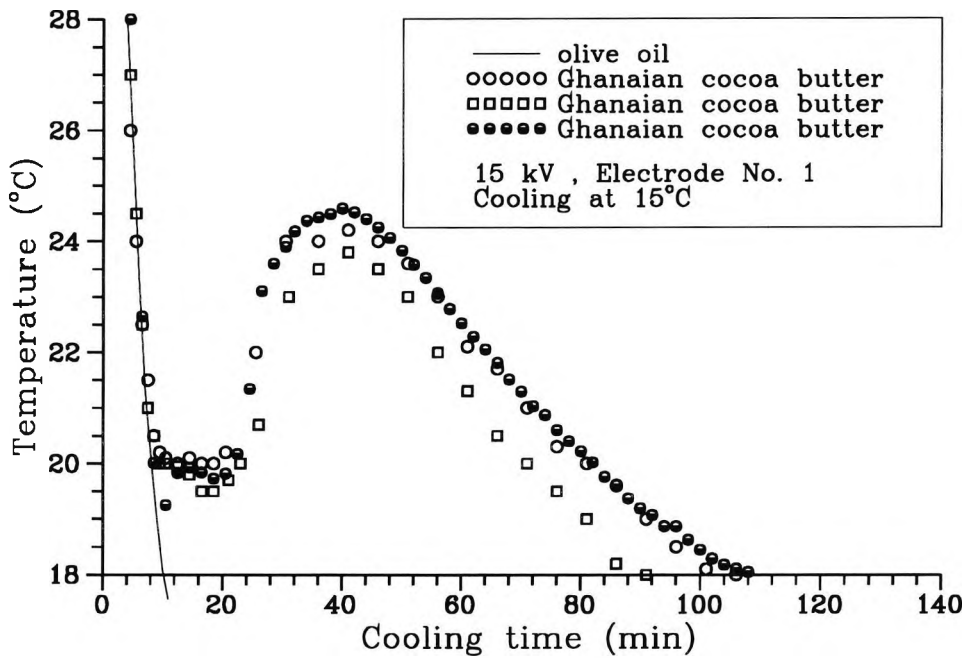


Figure 9.12: Cooling curves for cocoa butter with 15 kV field

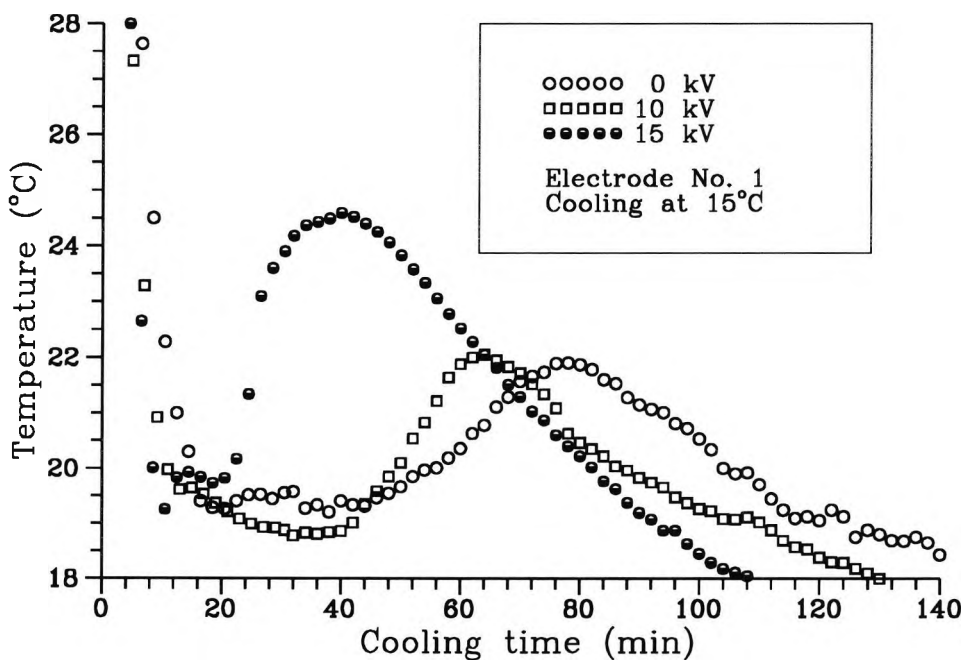


Figure 9.13: Cooling curves for Ghanaian cocoa butter at different voltages

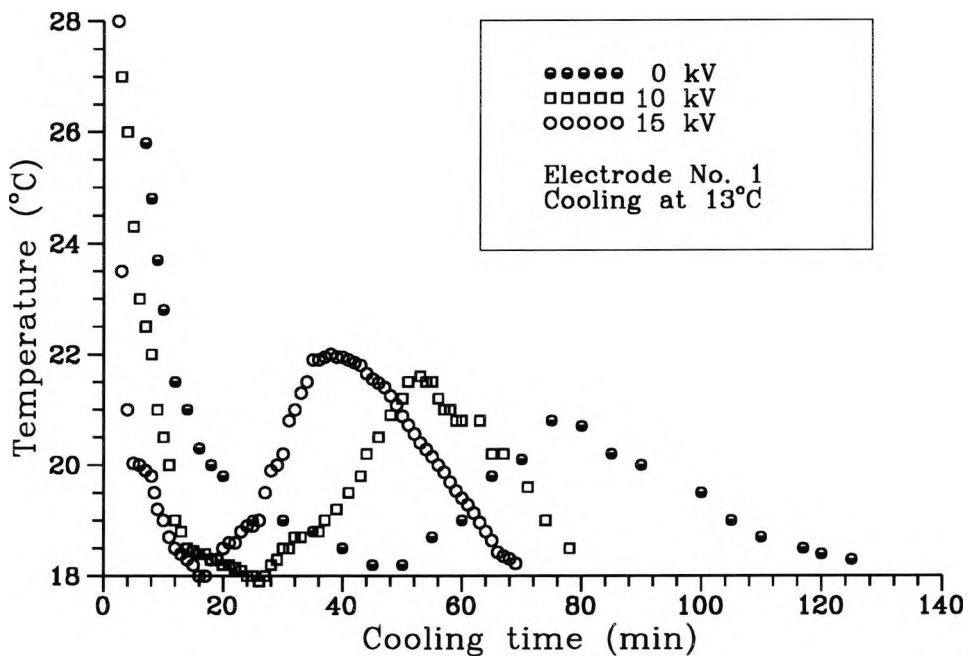


Figure 9.14: Cooling curves for Nederland cocoa butter at different voltages

Figures 9.15 and 9.16 show comparisons of the crystallization properties in the presence of the electric fields between these two kinds of cocoa butter. Although the effects of an electric field produce similar shapes of curve, small changes can be seen between the different types of cocoa butter. These indicate that the effect of electric fields on cocoa butter crystallization is significant. The major characteristics of the effects are inducing stable crystals and accelerating the crystallization. Figure 9.17 shows the cooling curves for cocoa butter using two types of electrode, one brass rod electrode which generated a field strength of 0.84 kV/cm when the electrode potential was 15kV; another a stainless steel with “bucket” frame (shape) electrode which generated about 2.2 to 2.5 kV/cm localised field. The results also indicate that the time for stable crystal appearance for polymorphism in cocoa butter samples changes with the applied field strength; a high strength field could help to induce stable crystals in a shorter time.

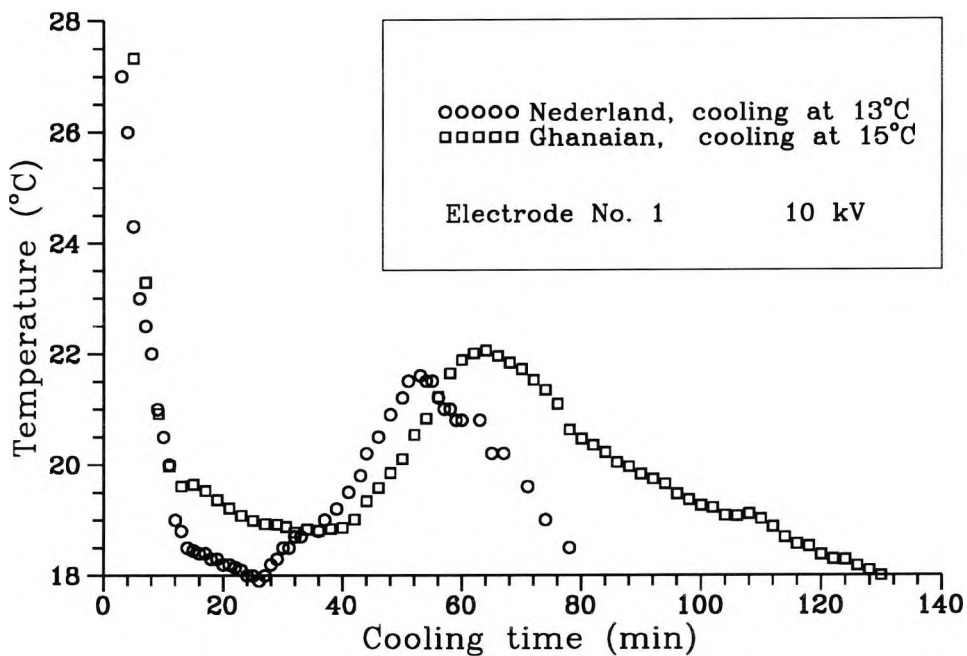


Figure 9.15: Comparison of cooling curves between Ghanaian and Nederland cocoa butter at 10 kV

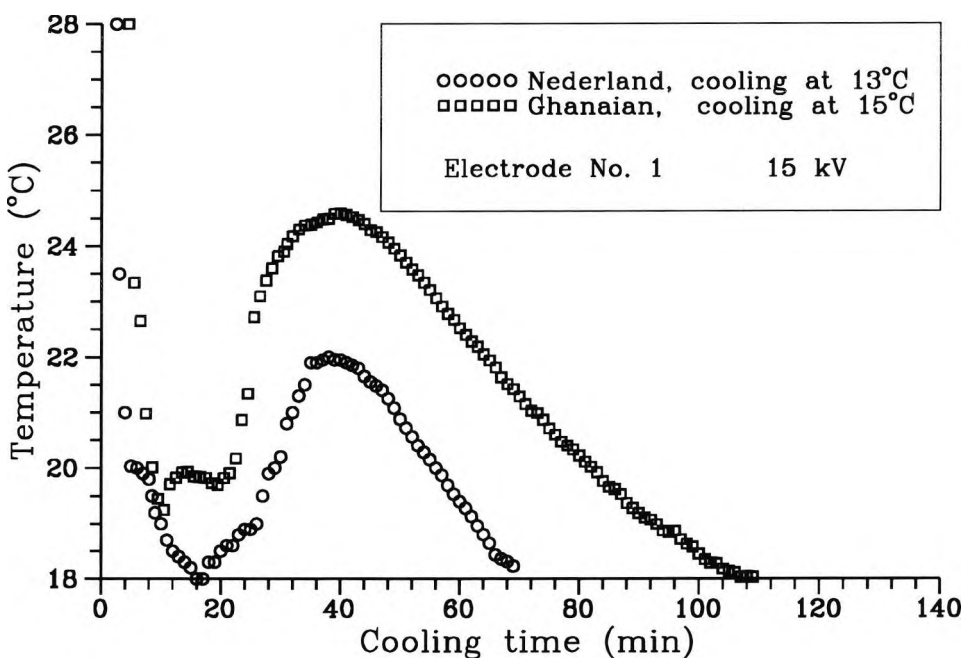


Figure 9.16: Comparison of cooling curves between Ghanaian and Nederland cocoa butter at 15 kV

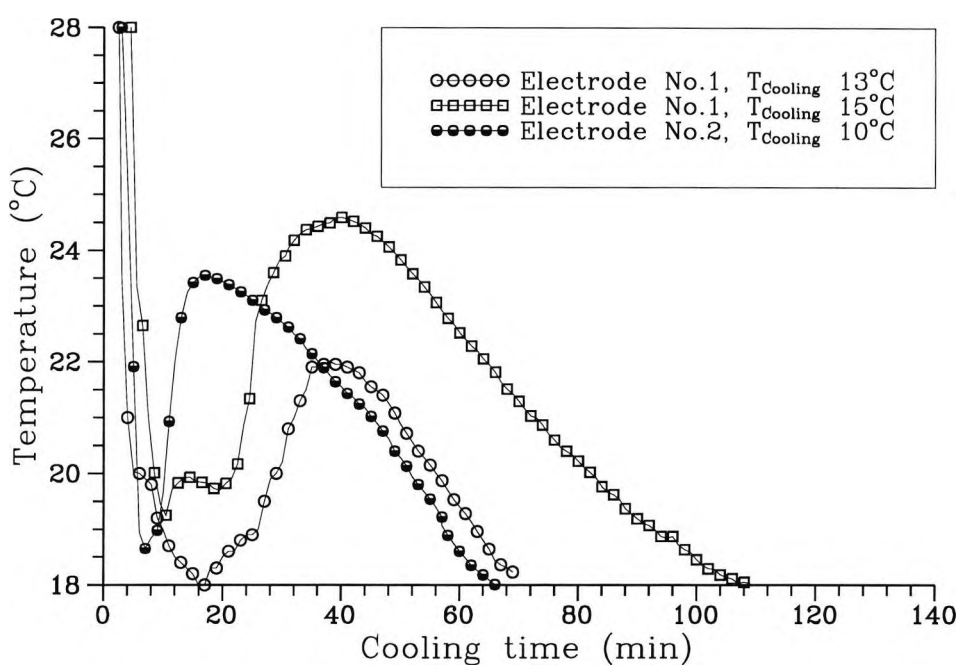


Figure 9.17: Cooling rate for cocoa butter using different electrodes at 15 kV

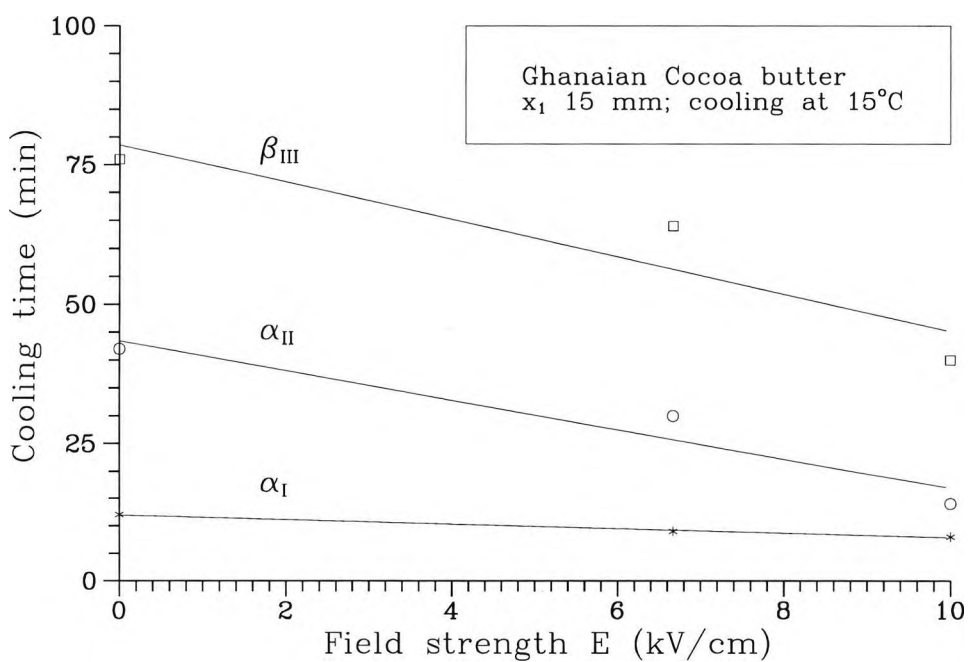


Figure 9.18: Cooling time versus the field strengths for different crystal forms

For Ghanaian cocoa butter, the properties of the crystals, such as the starting of the  $\alpha$ -crystals ( $\alpha_I$ ), the ending of the  $\alpha$ -crystals ( $\alpha_{II}$ ) and the appearance of the  $\beta_{III}$  crystals (they give up the most amount of heat during the process so that the temperature is the highest), with different field strengths are shown in Figure 9.18. These results indicate that, as the field strength increases by means of increasing the voltage supplied, the cooling times for both the  $\beta_{III}$  crystals and the  $\alpha_{II}$  crystals appearing are reduced greatly. The time for  $\alpha_I$  crystals appearing is less dependent on the field strength.

#### 9.4.2 DSC analysis

The experimental results were also checked and analyzed by Differential Scanning Calorimetry (DSC). This was done by using a DSC7 testing system which will be described in detail in Chapter 10. The samples were the same for the cooling curve experiments and were prepared in the experimental system introduced above using the “L” shape stainless steel electrode, as described in Figure 9.4, and applying an electric field from 0 kV to 15 kV. The cooling source was kept at 15°C and the distance between the electrode and the container was  $x=4$  mm. Each sample was treated for 20 min and then an immediate check on the DSC was carried out. Some of the analysis results are shown in Figures 9.19 and 9.20, respectively.

The peak heat flows per unit sample weight during the heating process for different samples were shown in Figure 9.19 and all are superimposed in Figure 9.20. These results indicate that, among the three samples, the one treated by the field with 15 kV had the most stable crystals because the highest heat flow was needed to melt the crystals whose peak molten temperature was 33°C. This temperature for the sample treated by 10 kV was 31.7°C and for the untreated one was only 20.77°C. In particular, it could be confirmed from the DSC charts that the crystallization temperature was about 22.5 - 36°C for the sample treated by 15 kV, about 22.5 - 34°C for the one treated by 10 kV and about 10 - 25°C for the untreated sample (0 kV).

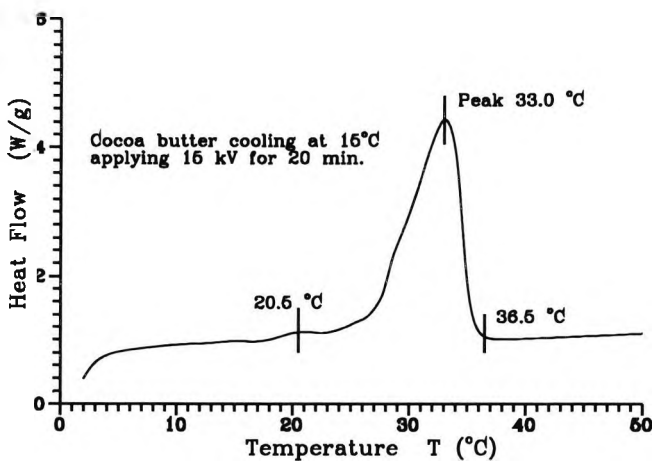
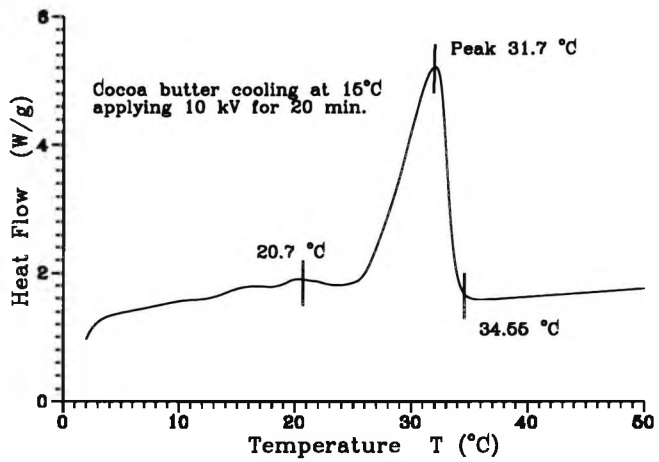
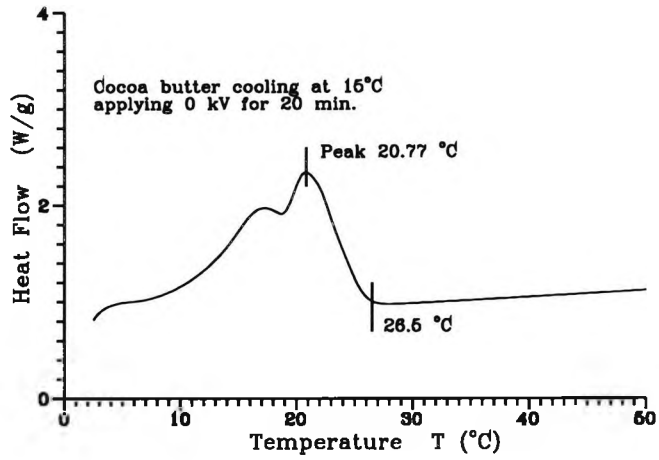


Figure 9.19: Results of DSC analysis

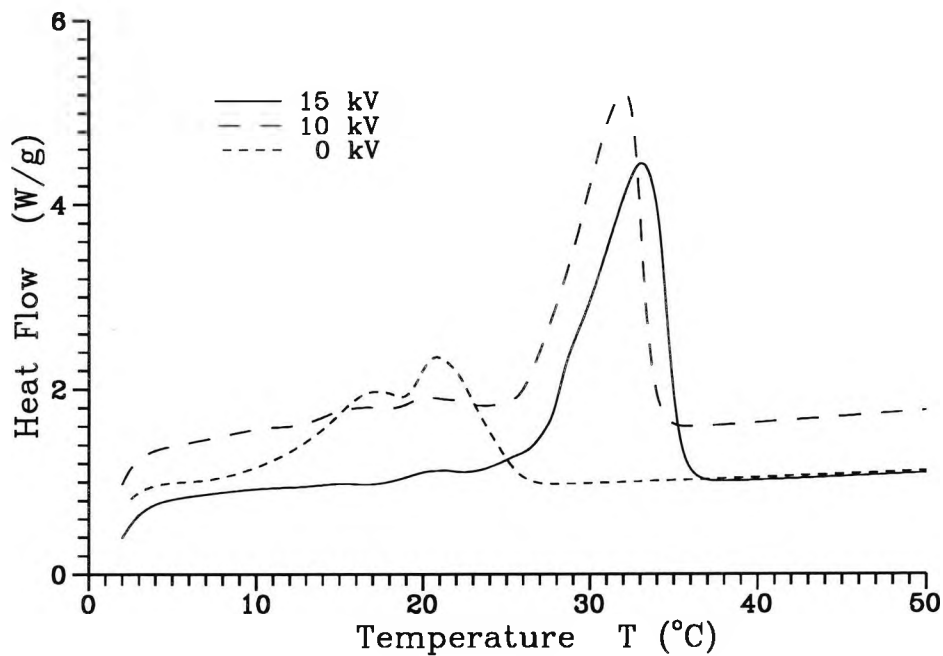


Figure 9.20: Comparison of DSC results for different samples

### 9.4.3 The cutting off effects

The effects of cutting off an electric field which is applied to the processes of cocoa butter crystallization were studied using the rod electrode. The results are presented in Figures 9.21 and 9.22. Figure 9.21 shows the cooling curves of the cocoa butter when the electric field was cut off at the times with “ $\alpha_I$ ”, “ $\alpha_{II}$ ”, “ $\beta_{III}$ ” and “ $\beta_{IV}$ ” crystals respectively, beginning to appear, on the basis of the cooling behaviour at 15 kV field. The results seem to suggest that field supply should not be stopped before  $\beta_{III}$  crystals had been crystallized.

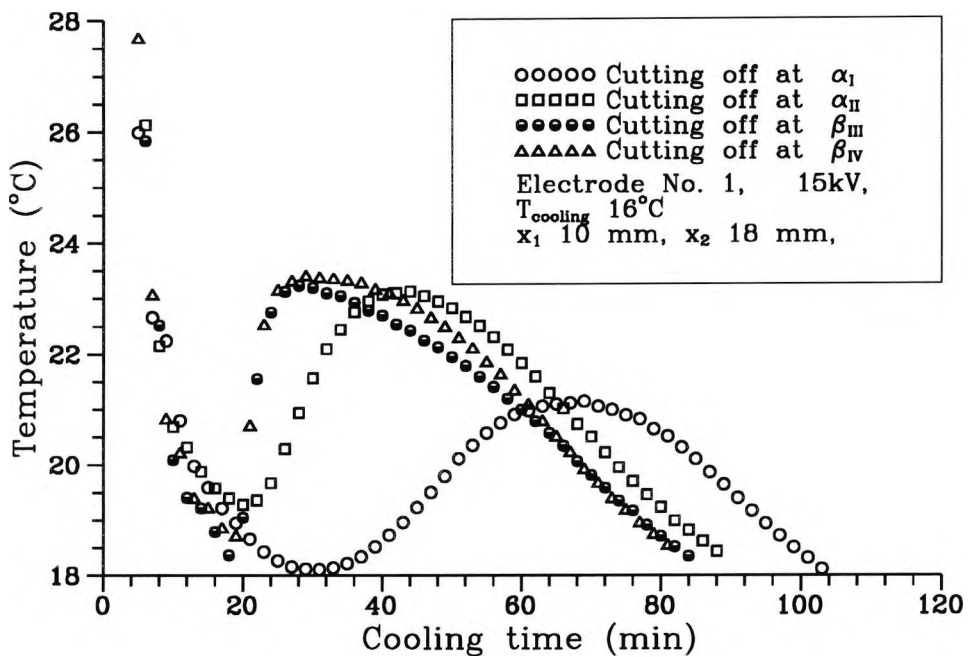


Figure 9.21: Cooling curves for cocoa butter when the field was cut off at different times

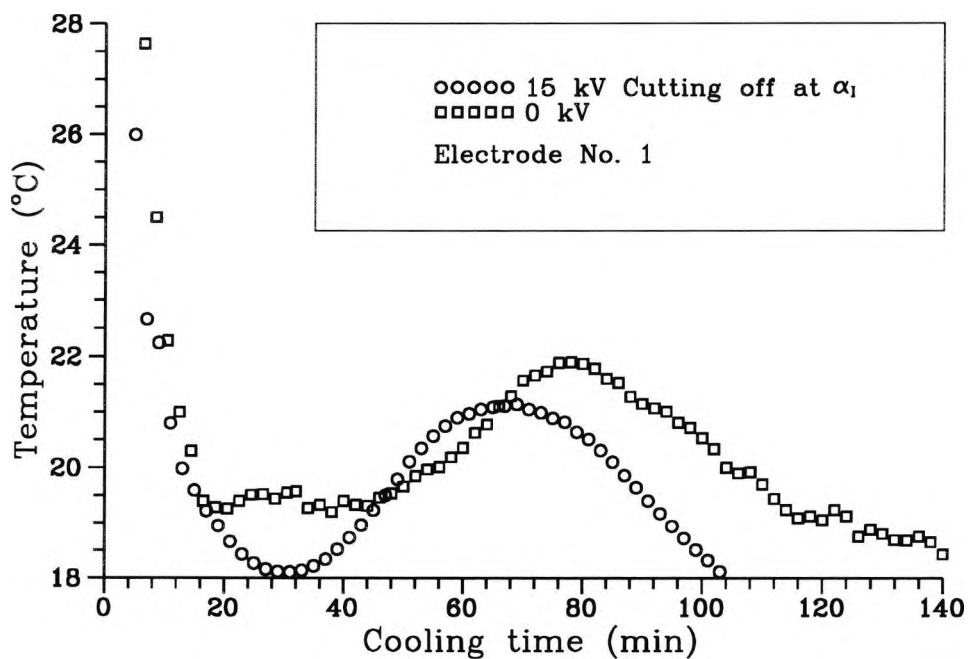


Figure 9.22: Comparison between 0 kV curve and the curve for which the field was cut off at the beginning of the crystallization

Figure 9.22 shows the comparison of the cooling curves for the cocoa butter with 0 kV and with the field (15kV) cutting off at the appearance of the  $\alpha$ -crystals. The above results indicate the following points:

1. The field cutting off effect for cocoa butter is different from the one for olive oil. For olive oil, the electroconvection is stopped immediately when the field is cut off; no phase change happens (as shown in Figure 9.8).
2. For Cocoa butter, the crystals' behaviour is not terminated immediately when the field is cut off. The nucleus centres are stimulated at the beginning when the field is applied. After the field is cut off, the stimulated nucleate centres or crystals still grow much faster than without an electric field (0kV) (shown in Figure 9.22).
3. The crystallization polymorphism is different when the field is cut off at different times. The later the field is cut off, the better properties of crystallization can be reached. For example, as shown in Figure 9.21, cutting off the field at the time of " $\alpha_{II}$ " crystals appearing (on the basis of the original cooling curves with 15kV), the  $\beta_{III}$  crystals appear 30 min earlier than when the field is cut off at the time when the original " $\alpha_I$ " crystals appear.
4. The best result is with the field being cut off at the time when its highest temperature is reached (" $\beta_{III}$ "). It can be seen from Figure 9.21 that the cooling rate is nearly equal to the one when the field is cut off at the time " $\beta_{IV}$ ". Actually, it is similar to the original cooling curves with 15 kV during the whole process. The similar result was also obtained using a "bucket" shape stainless steel electrode (electrode No. 2); this is shown in Figure 9.23.

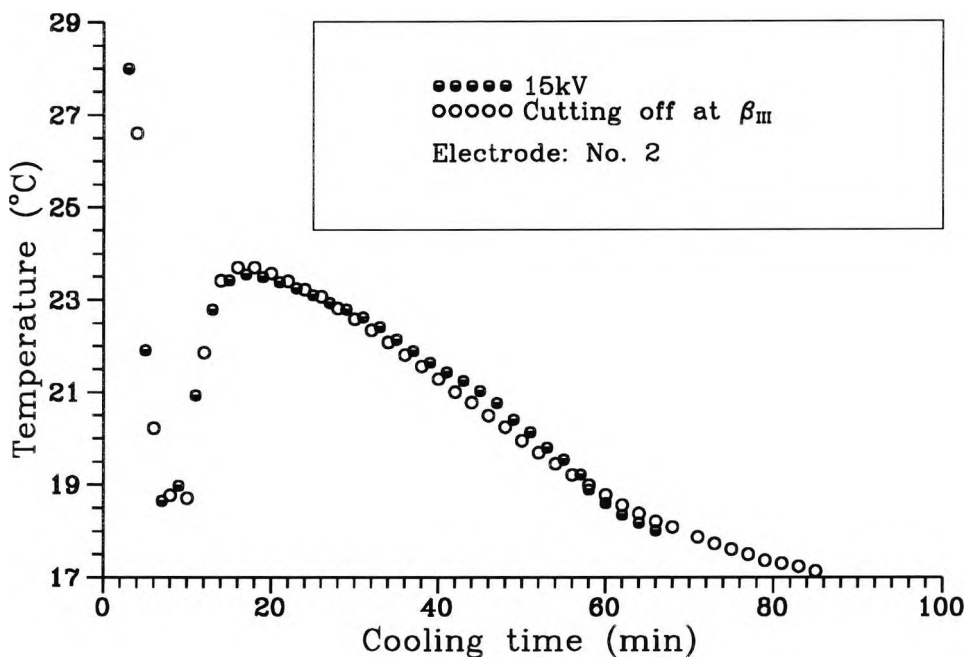


Figure 9.23: Field was cut off at the point with the highest temperature

#### 9.4.4 The electrode effect

The experimental results for electrode effects on crystallization were obtained and shown in Figures 9.24 to 9.27, respectively. Figure 9.24 shows the cooling curves for a “ $\perp$ ” shape stainless steel electrode with different electric field strengths (the position of the electrode was changed). As the strength is increased, the  $\beta_{III}$  crystals appear at higher temperature. This means the stronger field could be more helpful to induce  $\beta_{III}$  crystals, so that more heat is given up. Similar results were obtained from comparing the cooling curve of the cocoa butter using a “bucket” shape (electrode No. 2), a “cylinder” shape (electrode No. 5) or the “ $\perp$ ” shape (electrode No. 4) electrodes, respectively, as shown in Figure 9.25.

The results of using brass electrodes (electrode No. 1 and No. 3) are presented in Figure 9.26. This result also indicates that, for the same material electrodes, as long as the field strength is different, the properties for the crystallization will be quite different.

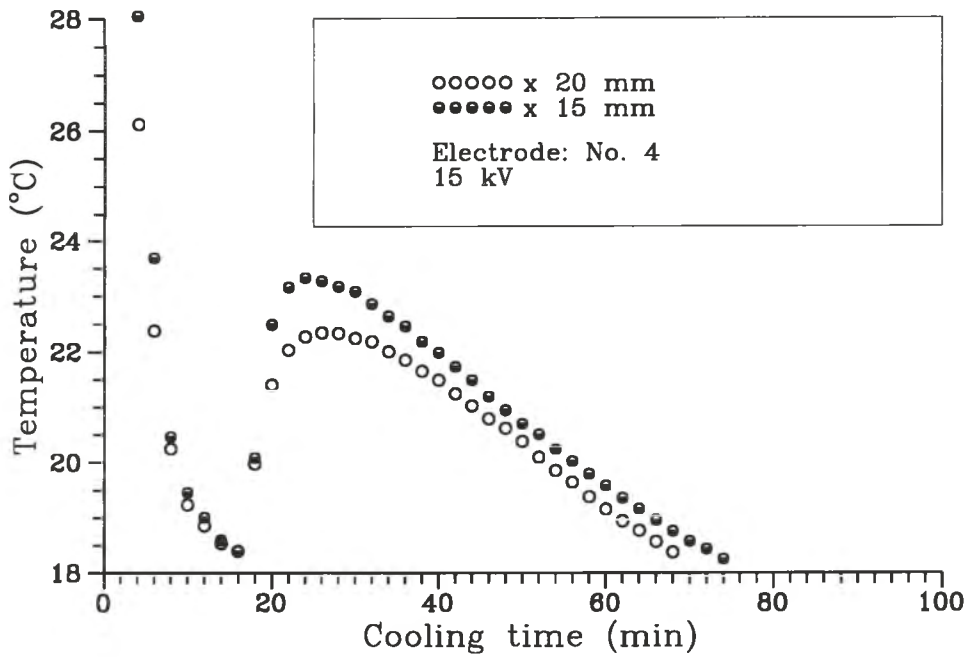


Figure 9.24: Cooling curves for cocoa butter crystallization using a "⊥" shape electrode at different field strengths

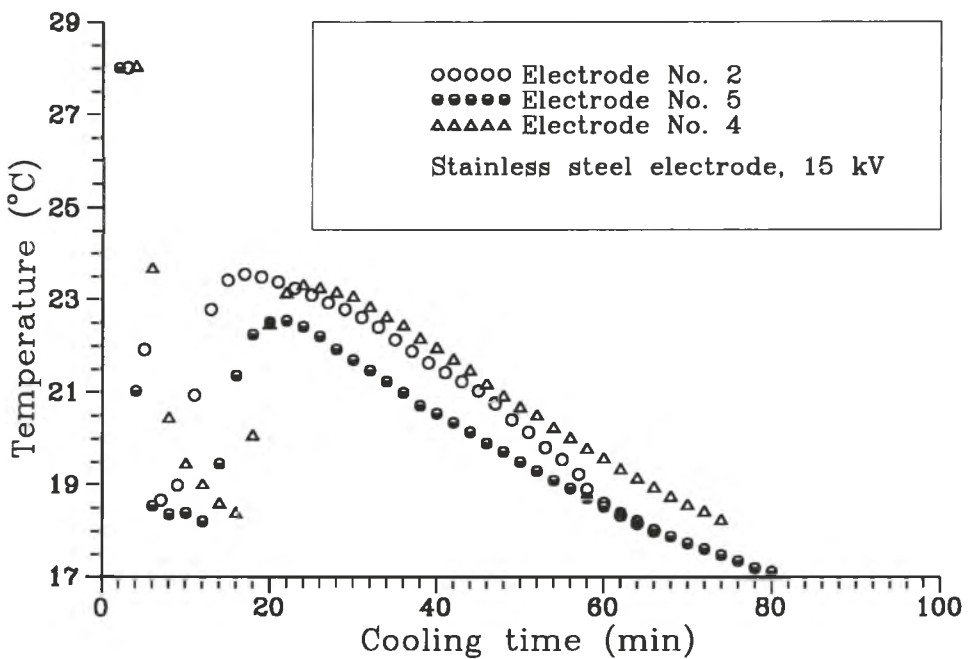


Figure 9.25: Cooling curves for cocoa butter crystallization using stainless steel electrodes

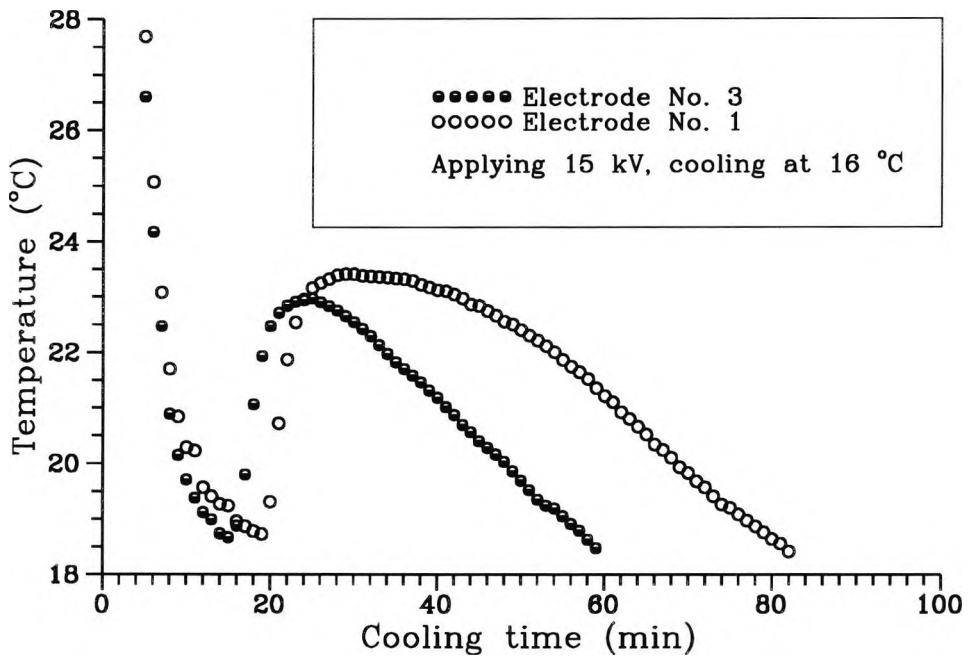


Figure 9.26: Cooling curves for cocoa butter crystallization using the electrode with same material but different geometries

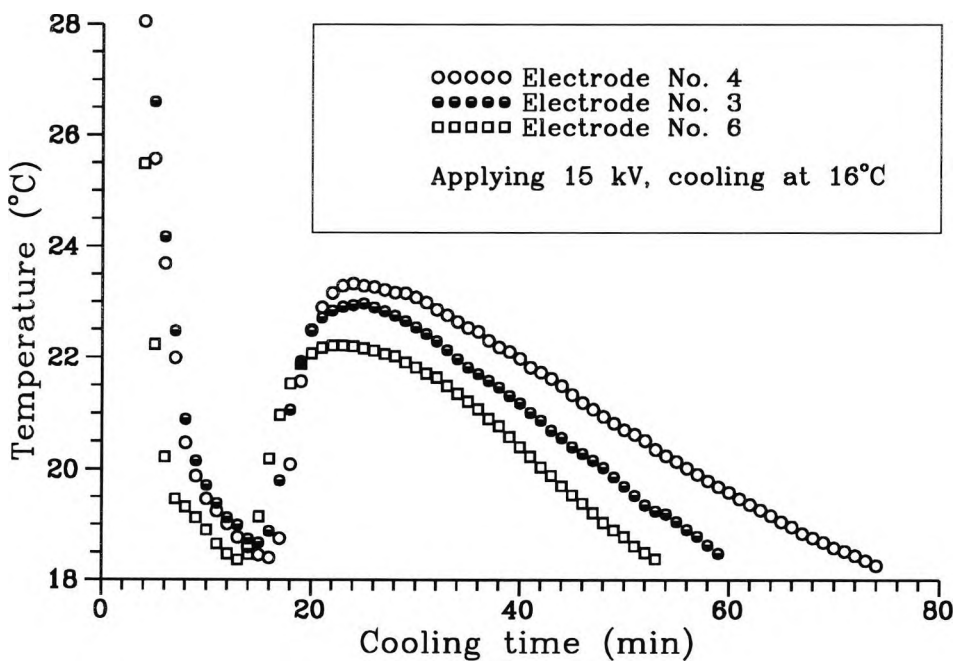


Figure 9.27: Cooling curves for cocoa butter crystallization using the electrode with same geometry but different material

Figure 9.27 shows the cooling curves for the cocoa butter crystallization using the electrodes with similar geometries and different materials at the same electric field strength. The results indicate that, under the same field strength, the stainless steel electrode has the best effect on the crystallization, then the brass one; the aluminium alloy electrode has the weakest effect on the crystallization compared with the other two kinds of electrodes used in the experiments.

It should be mentioned that no abnormal deposit on the electrodes was found during the experiments.

## 9.5 Crystallization of Cocoa Butter Mixture

The effect of cocoa butter on chocolate tempering has been clearly understood. This is based on a model in which all the other constituents of chocolate are suspended in the crystalline matrix of cocoa butter. The fact that cocoa butter crystallization can be enhanced under the action of applying electric fields can be concluded from above results. On this basis, the effect of the electric fields on cocoa butter mixture (by adding chocolate) crystallization and the field effect on chocolate tempering were studied.

Figures 9.28 to 9.31 show the cooling curves for cocoa butter with different percentages of chocolate using two types of electrode, one a rod electrode (No. 1), the other a "bucket" shaped electrode (No. 2), at an applied voltage of 15 kV. The results indicate that the higher the percentages of cocoa butter in chocolate, the earlier the  $\beta_{III}$  crystals appear. This seems to mean that, when the strength of the field is constant, the electric field effect would be getting gradually weaker with the decrease of the percentages of cocoa butter in the chocolate.

With the same percentages of cocoa butter and using different electrodes, different results for the chocolate crystallization and the tempering were obtained. This is

as shown in Figure 9.32 and also in Figures 9.28 and 9.29, the effect of the field on chocolate tempering and crystallization using the “bucket” electrode is much more significant than using the rod electrode. It should be noted that the field strength of the “ bucket” one at 15kV is nearly 2.5 times as high as with the rod electrode. This indicates that for chocolate tempering and crystallization enhancement, even higher field strength should be applied.

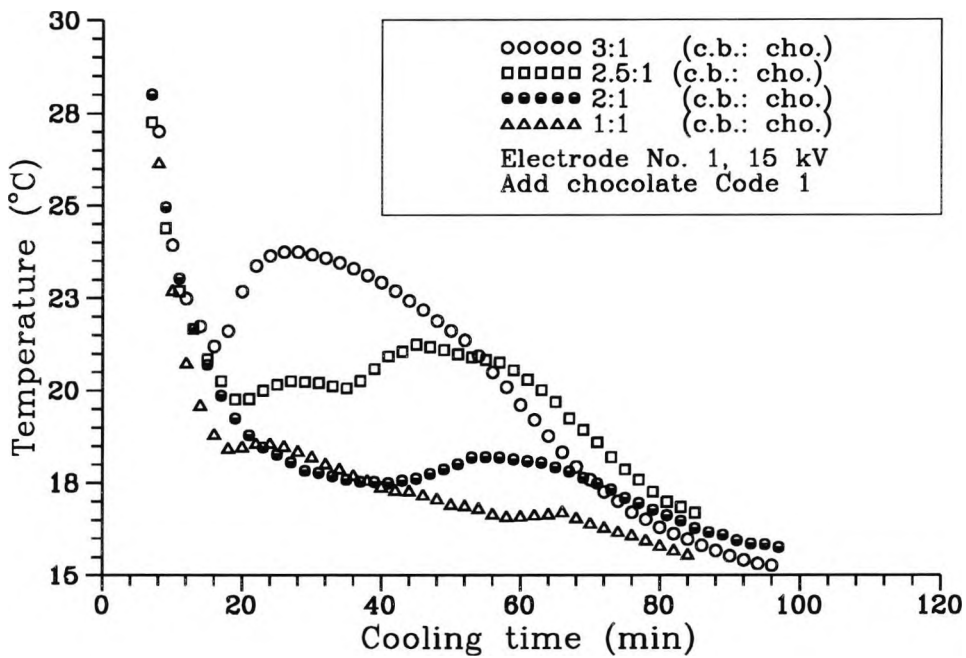


Figure 9.28: Cooling curves for cocoa butter with different percentages of chocolate using a rod electrode at 15 kV

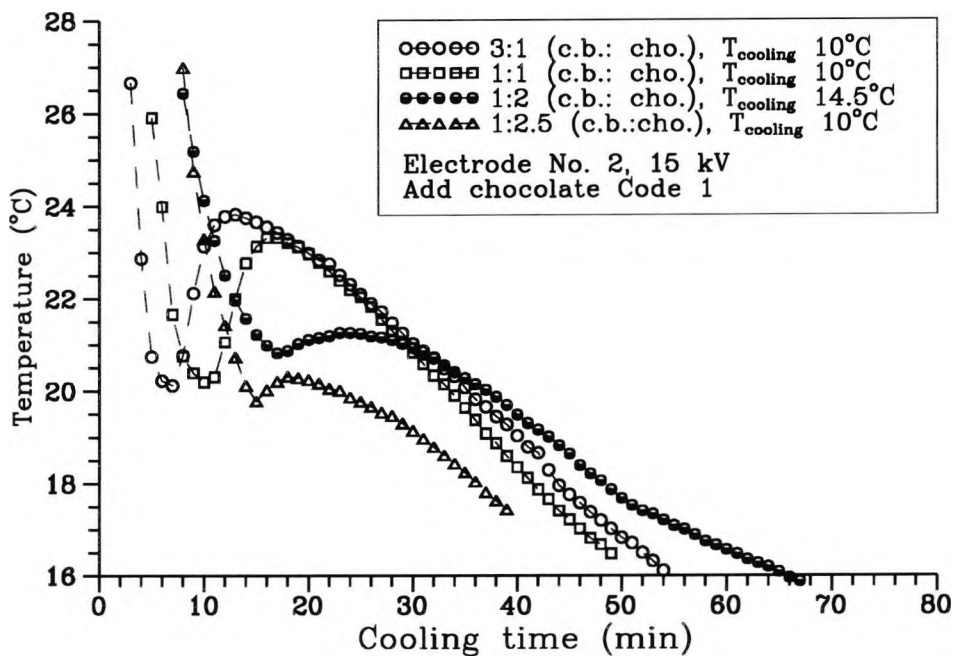


Figure 9.29: Cooling curves for cocoa butter with different percentages of chocolate using a “bucket” shape electrode at 15 kV

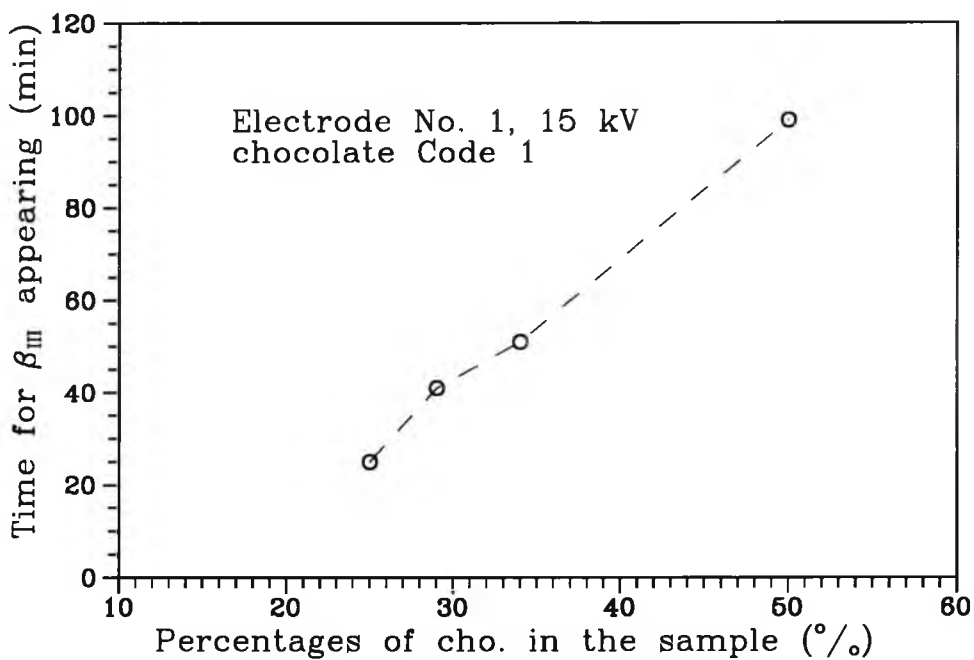


Figure 9.30: The time for  $\beta_{III}$  crystals appearing versus percentages of chocolate in samples

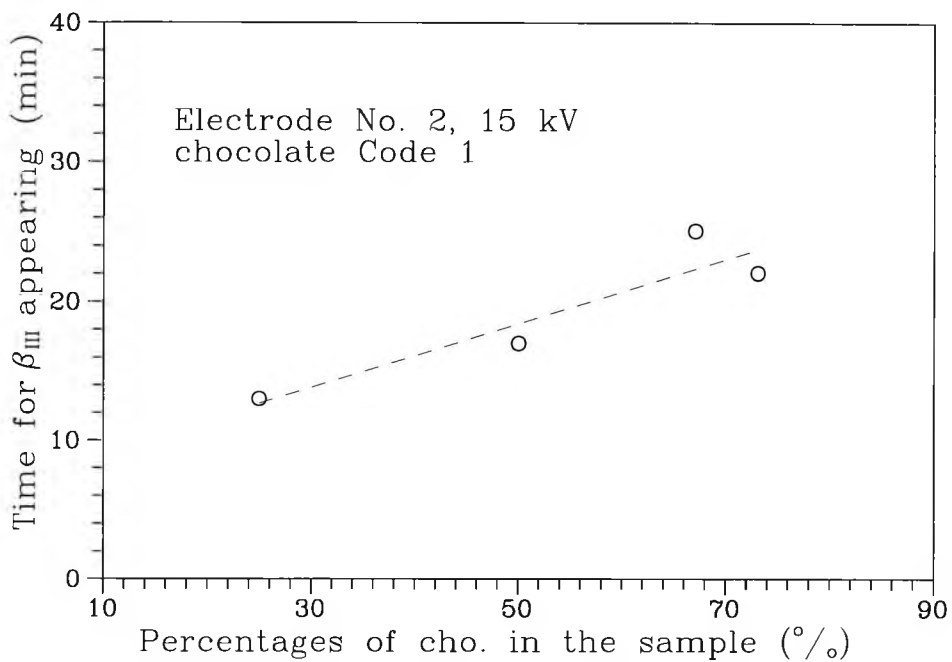


Figure 9.31: The time for  $\beta_{III}$  crystals appearing versus percentages of chocolate in samples

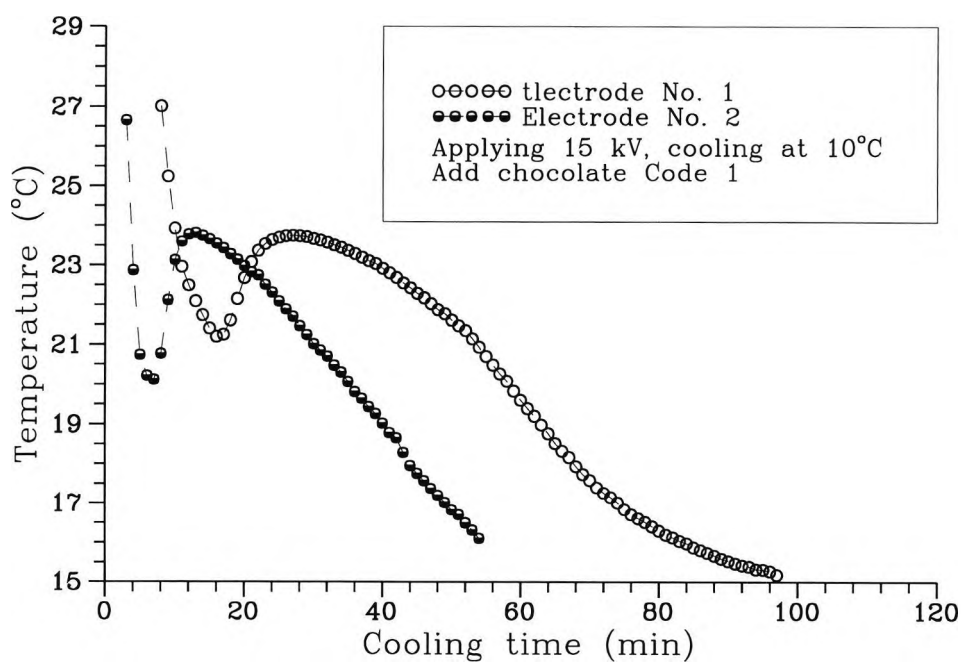


Figure 9.32: Cooling curves for cocoa butter mixture with 25% of chocolate using different electrodes at 15 kV

Figure 9.33 shows the cooling curves for cocoa butter mixture (with 50% of chocolate at different cooling rates. The result suggests that the deeper cooling during the chocolate crystallization in the presence of the electric field may enhance the  $\alpha$  and  $\beta_{III}$  crystals, but the end of the product  $\beta_{IV}$  should be examined.

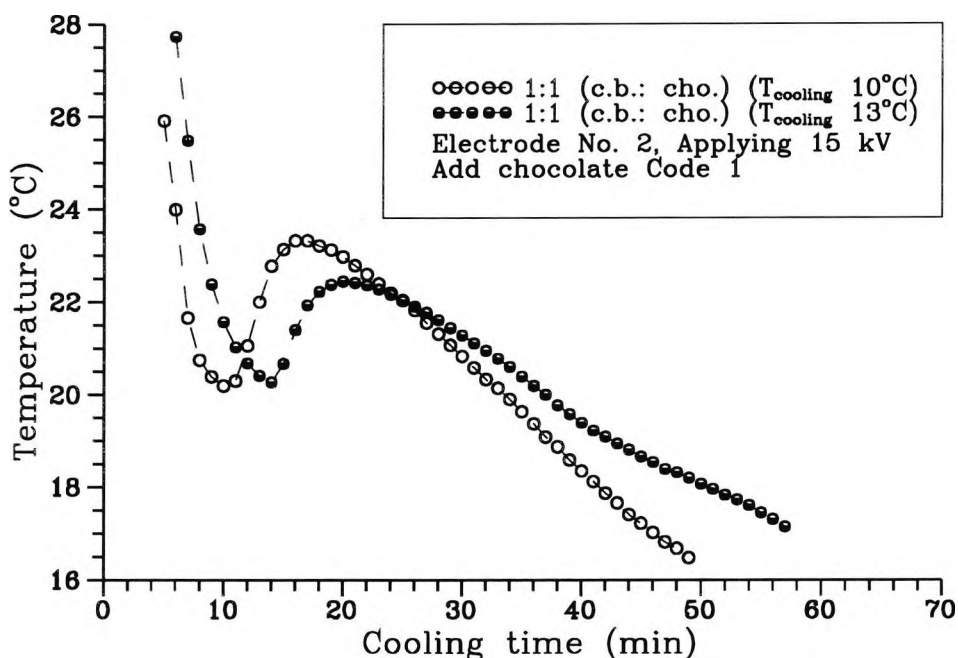


Figure 9.33: Cooling curves for cocoa butter mixture with 50% of chocolate using different electrodes at 15 kV

The cutting off effect for cocoa butter mixture was also studied and this is shown in Figure 9.34. This indicates that, cutting off the field at the highest temperature point (for  $\beta_{III}$  appearing), the obtained cooling curve is similar to the one applying the continuous field; however the  $\beta_{IV}$  crystals may be better.

The effect of an electric field on cocoa butter mixture was also examined by using different types of chocolate, marked as Code 1 and Code 2, respectively. The different codes were classified based on the prescriptions of which Code 1 was a kind of milk chocolate and Code 2 was a kind of American dark one. Figure 9.35 shows the results for the sample with the same percentages of chocolate Code 1 and Code 2 and using same electrode. The tempering for Code 1 seems be better than for Code 2.

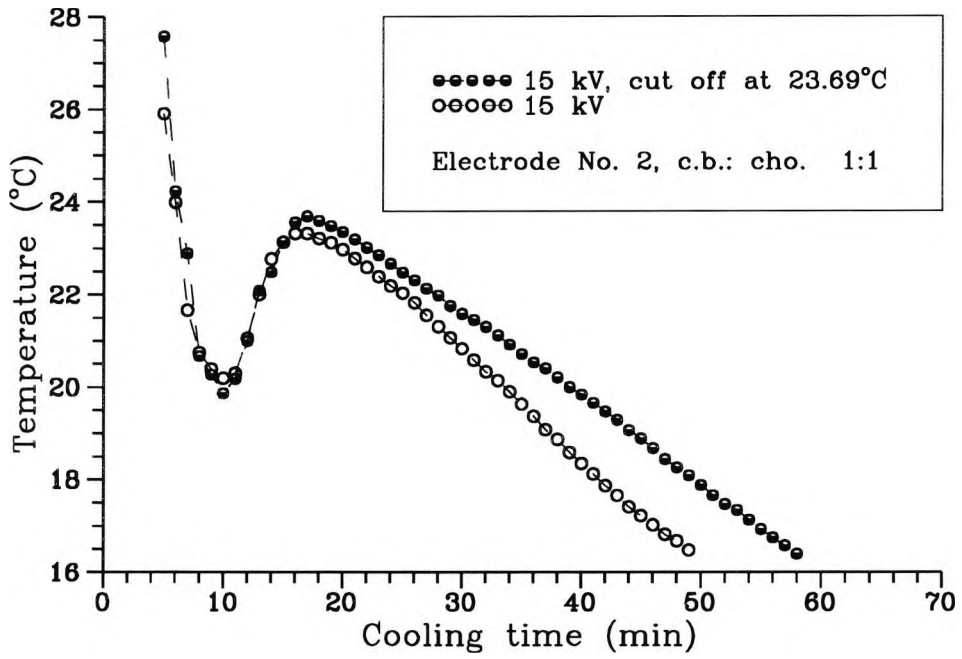


Figure 9.34: The cutting off effect for cocoa butter mixture with 50% of chocolate in the presence of an electric field

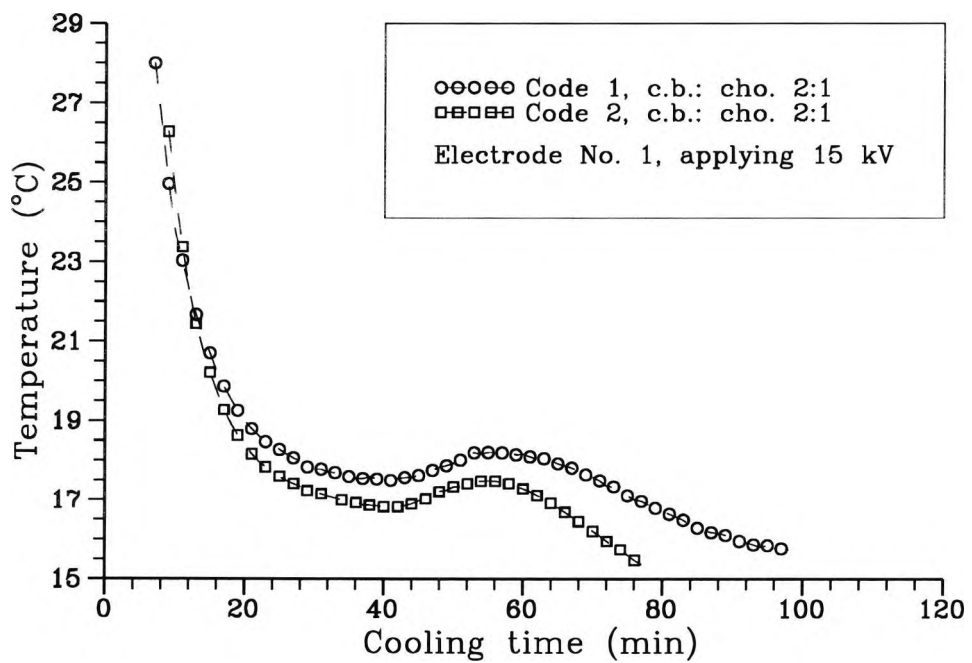


Figure 9.35: Cooling curves for cocoa butter mixture with different codes of chocolate

Figure 9.36 shows the cooling curves for samples with different percentages of the chocolate Code 2 using electrode No. 2 at 15 kV. The comparison for the cocoa butter samples with different Codes' chocolate using the same electrode is given in Figure 9.37.

Figure 9.38 shows the cooling curves of the cocoa butter mixture using a "ball" shaped electrode. The results are similar to that discussed before.

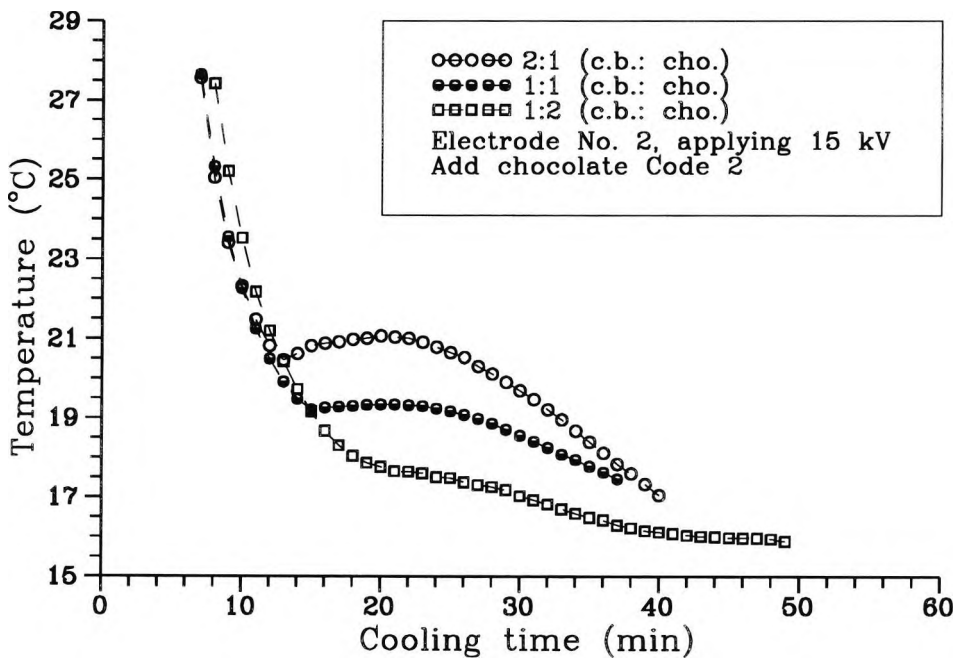


Figure 9.36: Cooling curves for cocoa butter mixture with chocolate Code 2 in the presence of an electric field

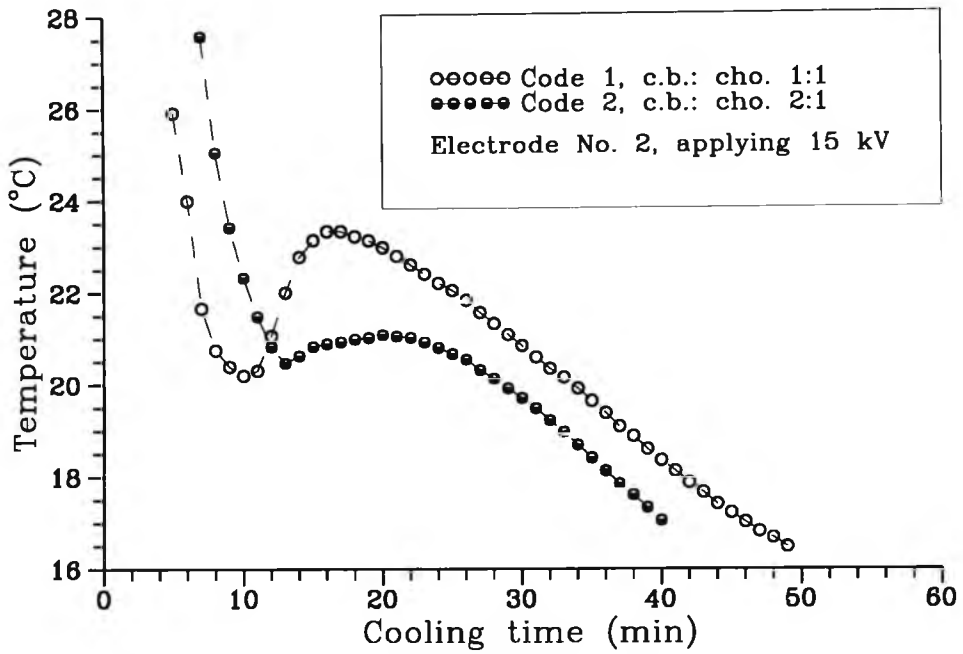


Figure 9.37: Comparison for the crystallization of cocoa butter mixture with different codes of chocolate using the same electrode

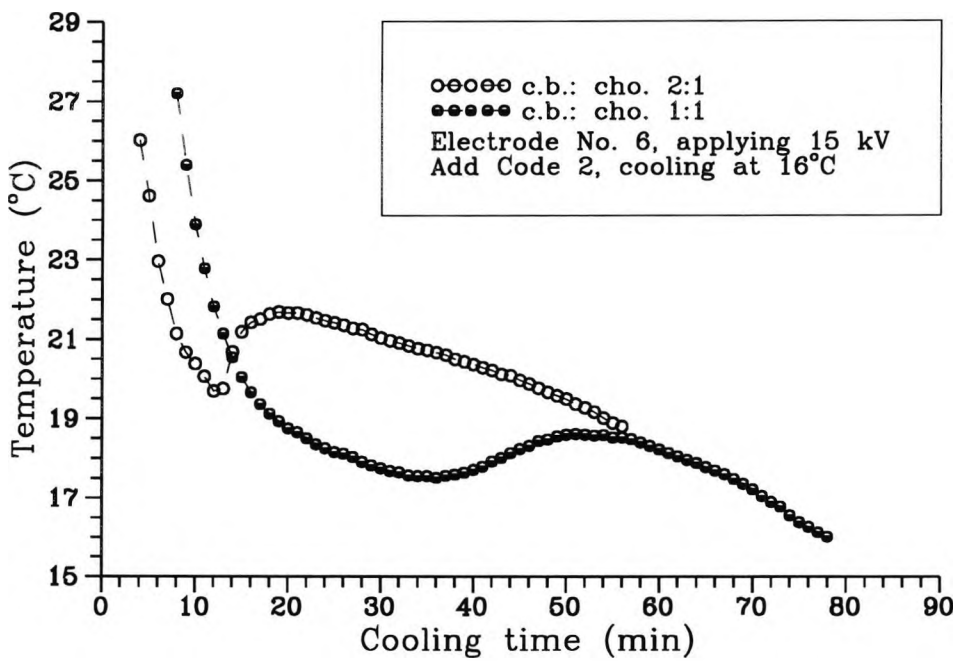


Figure 9.38: Cooling curves for cocoa butter mixture using a "ball" shaped electrode

## 9.6 Conclusions

1. The cooling rate of olive oil, which is a dielectric liquid and without crystallization during cooling, increases with the strength of the applied field. The electroconvection in the oil is the major effect of the field on olive oil.
2. The effect of the electric fields on the cocoa butter crystallization is very significant. As the strength of the applied fields increases, both the  $\alpha$  and  $\beta$ -prime (form III) crystals appear earlier. This indicates that the nucleate centres are stimulated and the speed of the crystals growth is enhanced.
3. When the applied fields are cut off at a certain time, the electroconvection phenomena in the olive oil disappear immediately, but the nucleate centres and the crystals growth for cocoa butter still share the benefit of the field. Cutting off the field at the moment of which the highest temperature appears because of the latent heat of crystallization, the cooling curve for crystallization is similar to the one in which the field is applied to the end.
4. Among the electrodes used in experiments, the stainless steel ones seem to be the best for the application of an electric field on crystallization.
5. In the experiment, the higher intensity field seems to have a stronger effect on crystallization and tempering of the cocoa butter mixture (chocolate). On this basis, an even higher strength of the electric field could be applied to enhance the real chocolate crystallization.

# Chapter 10

## Experiments on Untempered Chocolate for Different Conditions

### 10.1 Introduction

The effects of an electric field on cocoa butter mixture with different percentages of chocolate have been described and analyzed in Chapter 9 by the time-temperature cooling performance. The results seem to be attractive because the cocoa butter mixture with 50% of chocolate was shown being tempered under the action of an electric field and the crystallization seems to be enhanced by increasing the field strengths. This would encourage people to understand the effect on real chocolate crystallization which could be classified as a kind of crystallization of dielectric liquid mixed with the full amount of uncrystallized material.

Based on this background, it is necessary to investigate the electric field effects on the crystallization of untempered chocolate with normal fat content under different conditions. Indeed, from this point of view, a schedule of experiments is essential. Considering various factors which may affect experimental results, the original experimental conditions were chosen as shown in Table 10.1, which is a design of 5 factors  $\times$  4 levels. However, these full factorial experiments would number 1024 ( $4^5$ )

and it would take about 2.5 years time to complete the laboratory work. There is no doubt that much time and energy would be taken and the compound effect from the uncertainties of each result on the overall experimental uncertainty would result in an extremely difficult analysis.

To solve this problem and to improve the efficiency and minimise the experimental cost, the Taguchi method was studied and applied.

Table 10.1: The experimental conditions

Factor\Level	L <sub>1</sub>	L <sub>2</sub>	L <sub>3</sub>	L <sub>4</sub>
A (kV)	0	10	15	25
B (°C)	0	5	10	15
C (°C)	28	30	35	42
D (min)	2	5	10	20
E (mm)	4	6	10	13

In the Table, factor A represents the voltage of the applied field, B the coolant temperature, C the original temperature of the sample, D the time of applying the field and factor E the thickness of the samples.

Initially, Taguchi methods were developed in Japan in the late 1950s. Since then they have been extensively applied in quality control engineering in manufacturing industries, firstly in Japan, later (in the 1980s) in the USA. Great achievements in quality control and cost saving have been reported (Burgam, 1985).

Another important problem parallel with the experimental design is the assessment of the experimental results. In chapter 9, this was mainly completed by the analysis of time-temperature cooling curves. As discussed before, this method looks quite helpful in understanding the crystallization behaviour and identifying the different effects of an electric field on crystallization for different samples. However, the time-temperature curves depend on the accurate measurement of temperature

changes in experimental samples during cooling processes and this was normally done using a thermocouple. Problems would emerge when increasing electric field strengths or reducing samples' volume because this would result in either the thermocouple junction being broken down or the measurement being unstable. For the above reason, Differential Scanning Calorimetry (DSC) was employed to assess the experimental results designed using the Taguchi method. Although DSC is a very efficient method for assessing the polymorphic behaviour of crystallization, it is indeed a new subject to pick up the optimal result or to find the relationship among the DSC results obtained by the large amount of experiments.

This chapter is concerned with the novel approach of applying Taguchi methods to the experimental DSC testing of electric field effects on the crystallization of untempered chocolate and will deal with the design of experiments, the DSC results and the relevant Taguchi analysis methods.

## **10.2 Experimental Design Using the Taguchi Method**

### **10.2.1 Taguchi method and orthogonal arrays**

The use of orthogonal arrays is one of the main tools of Taguchi methods. Put simply, an orthogonal array is an experimental design representation to allow a mathematically independent assessment of the effect of each of the factors. Orthogonality means that factors can be evaluated independently of one another; the effect of one factor does not influence the estimation of the effect of another factor. Orthogonal arrays can be traced back to Euler's Graeco-Latin squares, but in Euler's time they were only known as a type of mathematical game. The idea of using orthogonal arrays for the design of experiments was studied independently in the USA and Japan during World War II.

Taguchi has simplified the derivation of the experimental designs by providing

linear graphs with orthogonal arrays. The arrays that he uses are often called fractional factorial designs because they are a particular combination of trials from a full factorial. Savings are enormous, compared to full factorial designs, as only a very small fraction of possible test conditions need to be investigated. For example, a factorial experiment where 7 factors were investigated at 2 levels could be carried out in just 8 tests compared to 128 ( $2^7$ ) for the full factorial (Taguchi, 1987). The reason for this large difference in the number of experiments is due to the fact that only the main effects of each factor are generally investigated.

It has been proved that, by adopting the use of orthogonal arrays, a large number of factors can be investigated simultaneously. It has been shown that an orthogonal array is on average greater than 90% as efficient as running a full factorial experiment, and this small loss in efficiency is more than justified when the experiment costs are compared. It should be mentioned that Taguchi uses orthogonal arrays for a very different purpose from most traditional approaches. Evaluating the effect of factor levels with respect to robustness is particularly emphasized.

### **10.2.2 Orthogonal array selection**

On the basis of the full factorial experiments arrangement shown in Table 10.1, an L16 ( $4^5$ ) orthogonal array was selected for the design of the experiments, as shown in Table 10.2.

In the table, the numbers A, B, C, D and E represent different factors which should be considered in experiments and the numbers 1 to 4 are discrete parameter levels for each of the variables involved. The trial number indicates the number of the experiment.

Table 10.2: The orthogonal array L16 ( $4^5$ )

Trial no.\Factor	A	B	C	D	E
1	1	1	1	1	1
2	1	2	2	2	2
3	1	3	3	3	3
4	1	4	4	4	4
5	2	1	2	3	4
6	2	2	1	4	3
7	2	3	4	1	2
8	2	4	3	2	1
9	3	1	3	4	2
10	3	2	4	3	1
11	3	3	1	2	4
12	3	4	2	1	3
13	4	1	4	2	3
14	4	2	3	1	4
15	4	3	2	4	1
16	4	4	1	3	2

### 10.2.3 The experimental arrangement

The experimental arrangement on the basis of the orthogonal array L16 ( $4^5$ ) is as shown in Table 10.3.

In Table 10.3, factor A is the applied electric field (kV); B the coolant temperature ( $^{\circ}\text{C}$ ); C samples temperature ( $^{\circ}\text{C}$ ); D the time of treatment (min); and factor E the thickness of the samples (mm).

Table 10.3: The experimental arrangement

Trial no.\Factor	A	B	C	D	E
1	0	0	28	2	4
2	0	5	30	5	6
3	0	10	35	10	10
4	0	15	42	20	13
5	10	0	30	10	13
6	10	5	28	20	10
7	10	10	42	2	6
8	10	15	35	5	4
9	15	0	35	20	6
10	15	5	42	10	4
11	15	10	28	5	13
12	15	15	30	2	10
13	25	0	42	5	10
14	25	5	35	2	13
15	25	10	30	20	4
16	25	15	28	10	6

### 10.3 Experimental Detail

The experimental system was designed for accuracy and convenience of sample treatment. This included the following factors: to realise a higher field strength (a small thickness sample treated by applying a very high voltage) without the field breaking down during treatment; ease and accuracy of controlling the temperature of the cooling source; and ease of controlling and changing the thickness of samples. Also the sample preparation for DSC should be comparable.

### 10.3.1 The test rig system and equipment

Basically, the function of the test rig system was similar to the one described in last Chapter, but no computer and data log were connected because the time-temperature data were not measured during the experiments. Instead of this, a Grant water bath system, as shown in Figure 10.1, with temperature control was employed to control the cooling source temperature. In fact, this water bath has both heating and cooling functions which enable the cooling source temperature to increase or decrease to a designed value. The accuracy of temperature for the cooling source could be ensured at about  $\pm 0.1^{\circ}\text{C}$  and was sufficient for the experimental requirement.

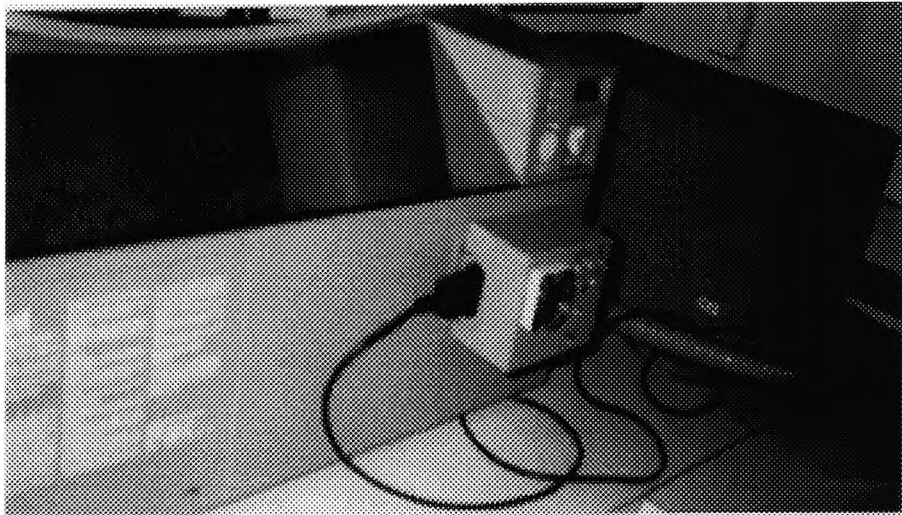


Figure 10.1: The water bath system used in experiments

Similar to the traditional Faraday cage described before, a cabinet was used, as shown in Figure 10.2, which has the same function as the Faraday cage and consisted of eight perspex windows. The high voltage generator located on the top of the cabinet, as shown in Figure 10.2, was a GLASSMAN high voltage product (output voltage is 0 – 40kV for d.c. with maximum current  $100\mu\text{A}$ ) and the ap-

plied potential is easy to adjust outside the cabinet. All zero potential parts of high voltage circuit were earthed.



Figure 10.2: The high voltage cabinet used in experiments

The electrode system used for sample treatment, as shown in Figure 10.3 and Figure 10.4, consisted of a “ $\perp$ ” shape electrode as the positive of which the electrode shaft was insulated, a plastic (perspex) disc for controlling the sample depth (thickness) and also as the insulator between the electrodes, and a cooling chamber as the negative electrode through which the cooling water flowed to cool the experimental samples. In particular, a flat radiator ( $400 \times 250$ ) shown in Figure 10.4 was connected in parallel with the electrode system. This could ensure the environmental temperature inside the cabinet was close to the cooling source temperature so as to eliminate the environmental effect on the crystallization and to avoid the condensation on electrodes which would give false results for dielectric crystallization in the presence of an electric field.

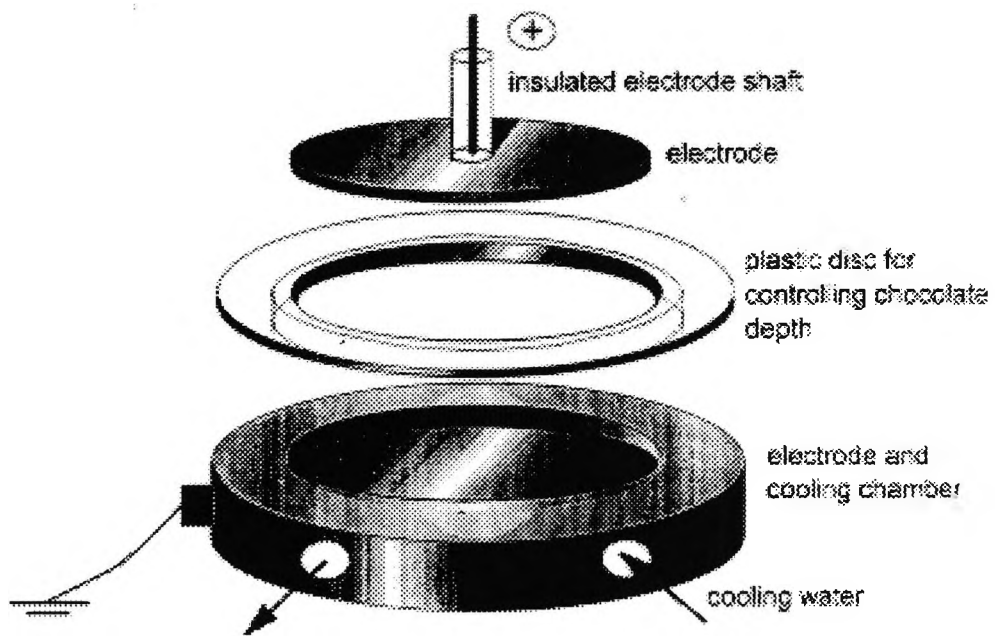


Figure 10.3: The electrode system for DSC sample treatment

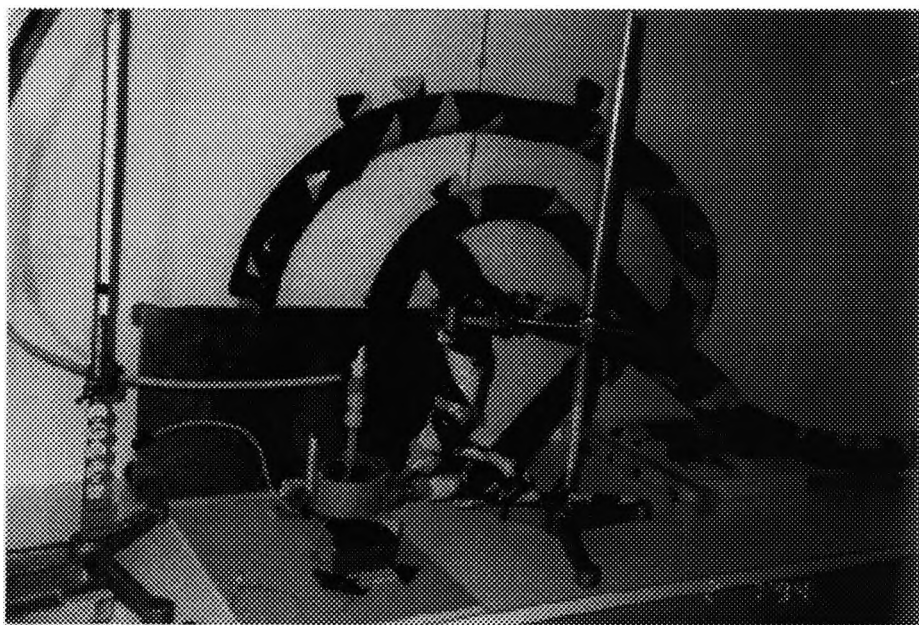


Figure 10.4: The electrode assembly and the parallel radiator inside the cabinet

### 10.3.2 Sample preparation

The sample preparation process can be clearly described by the process flow chart shown in Figure 10.5. At first, the chocolate was heated to 45°C to obtain the fully molten and untempered chocolate. Then the molten chocolate was cooled down to 42, 35, 30 and 28°C, respectively for the different trial requirements. After that, a check for tempering was normally needed because the tempered chocolate would result in an assessment difficulty when the results were compared. This was done by means of a “temper machine” where the time-temperature curve and the slope were checked. The next stage was the sample treatment inside the high voltage cabinet on different conditions as designed. When a treated sample was ready, it was normally divided into two separate samples by a symmetry line along the sample diameter. One would immediately be assessed by the DSC, another would be kept in a refrigerator (about 5–7°C) for 24 hours for crystal growing and then be assessed by the DSC for comparison.

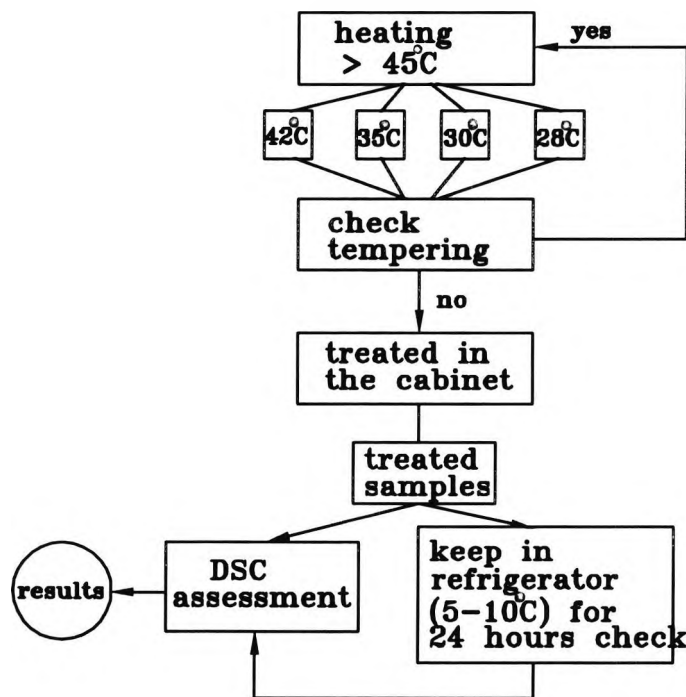


Figure 10.5: The flow chart of the sample preparation process

### 10.3.3 Differential scanning calorimetry (DSC)

DSC has been used for many years in the characterization of confectionery fats, cocoa butter and pure triglycerides. The basic principle is to measure the energy difference needed to keep a sample and a reference (usually air) at the same temperature during heating and/or cooling. The DSC calorimeter used in the experiments was a Perkin Elmer DSC7 module with a PC computer as shown in Figure 10.6.

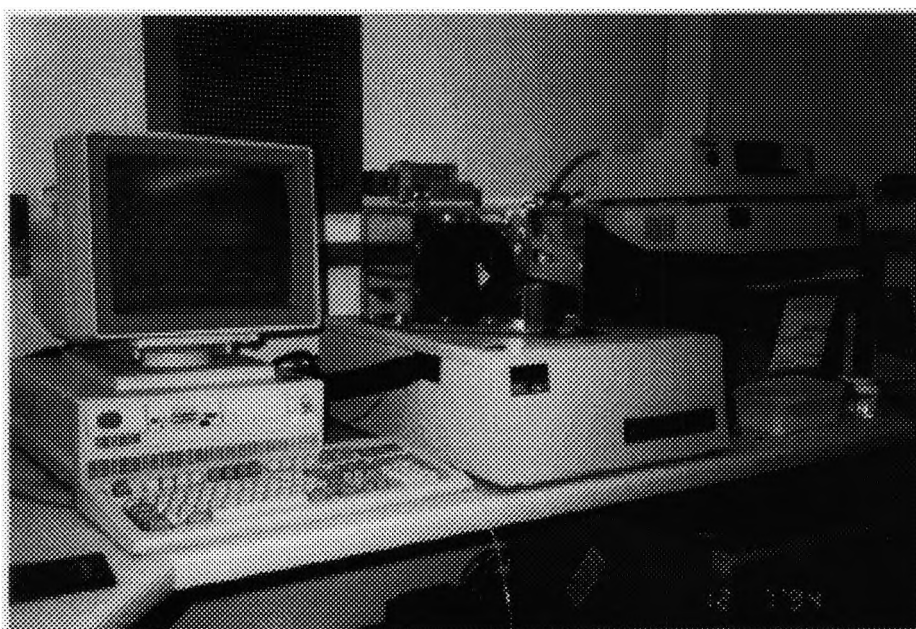


Figure 10.6: The DSC7 testing system

Temperature and energy were calibrated prior to measurement using gallium and indium standards. Samples of each treatment chocolate (about 4 - 8 mg) were accurately weighed by an electric microweigh meter shown in Figure 10.7 into aluminium pans. An empty pan was used as the reference. In addition, samples of each prepared chocolate were heated in the DSC at 10°C/min to produce melting point data of the most stable ( $\beta$  form V and VI) polymorphic form.



Figure 10.7: The microweigh meter used for DSC sample weighing

## 10.4 DSC Results and Comparisons

### 10.4.1 Normalization

The normalized thermograms of DSC results for the immediate assessment after the Taguchi experiments are shown in Figures 10.9 to 10.24, respectively. Each of these Figures was obtained from the original experimental data,  $Q_0$ , which consists of 900 data, being divided by the sample weight, GM, and its data point scaling factor, QY. This can be expressed as

$$Q(T_i) = \frac{Q_0(T_i)}{GM \cdot QY} \quad (10.1)$$

where the value of QY is generated by the DSC software automatically and varies for different experiments.

Normally, DSC results are compared on the basis of normalised curves and the straightforward qualitative comparison of any two DSC curves would not be difficult. However, it seems to be impossible to obtain a comparison result over 16 curves because of the fact that only tiny differences exist among the them. The 16 experiments analyzed here were subjected to a full quantitative Taguchi analysis because of the way in which the 16 tests were designed and because so many possible contributory tests are omitted in the Taguchi technique.

### 10.4.2 The definition of a baseline

In order accurately to compare the DSC results of Figures 10.9 to 10.24, a baseline,  $QB$ , for each graph was decided. This was done on the basis of the minimum difference between  $Q(T_i \leq 36^\circ\text{C})$  and  $QB$ . Therefore, the comparable value of heat flow becomes

$$q(T_i) = Q(T_i) - QB \quad (10.2)$$

The definition of  $Q(T_i)$  and  $QB$  is given in Figure 10.8.

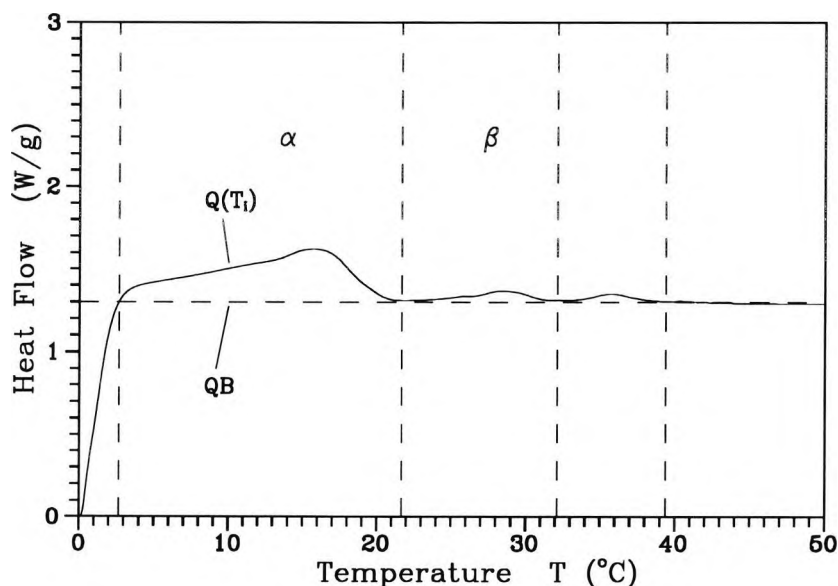


Figure 10.8: The definition of  $Q(T_i)$  and  $QB$

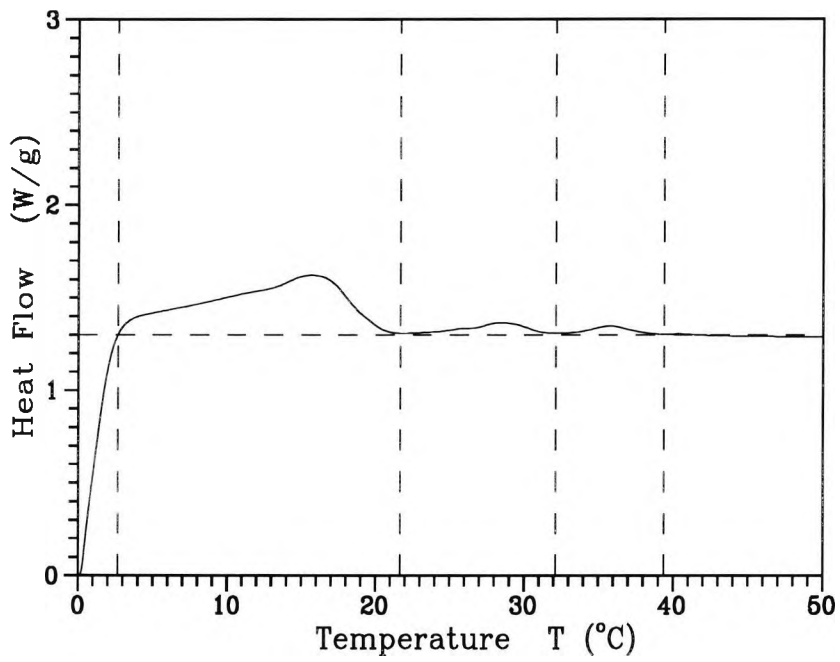


Figure 10.9: The thermogram for the sample of trial No. 1

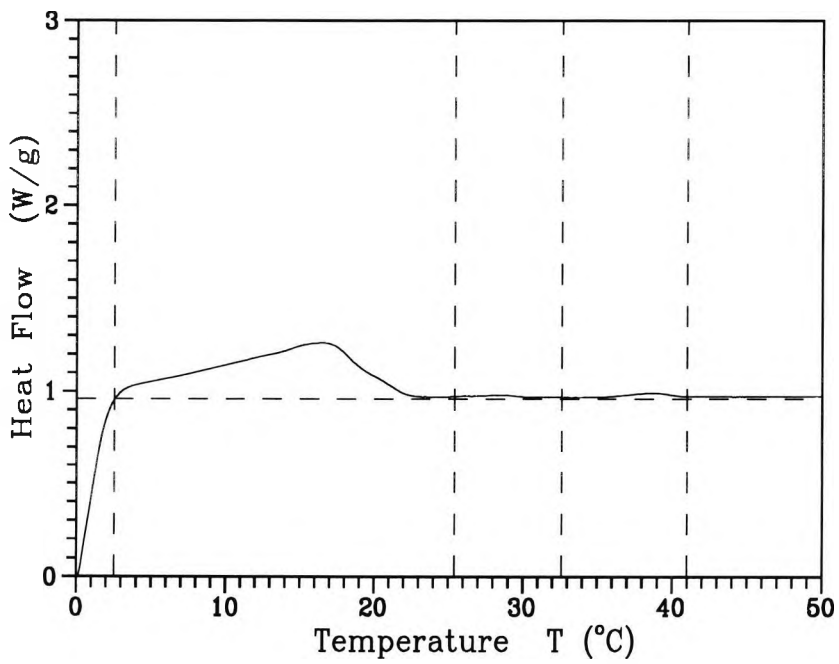


Figure 10.10: The thermogram for the sample of trial No. 2

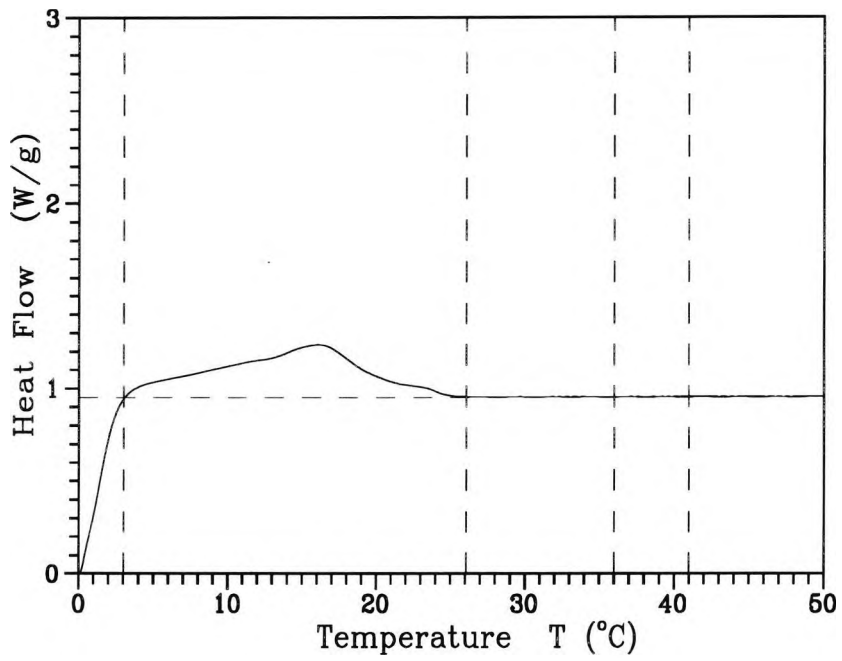


Figure 10.11: The thermogram for the sample of trial No. 3

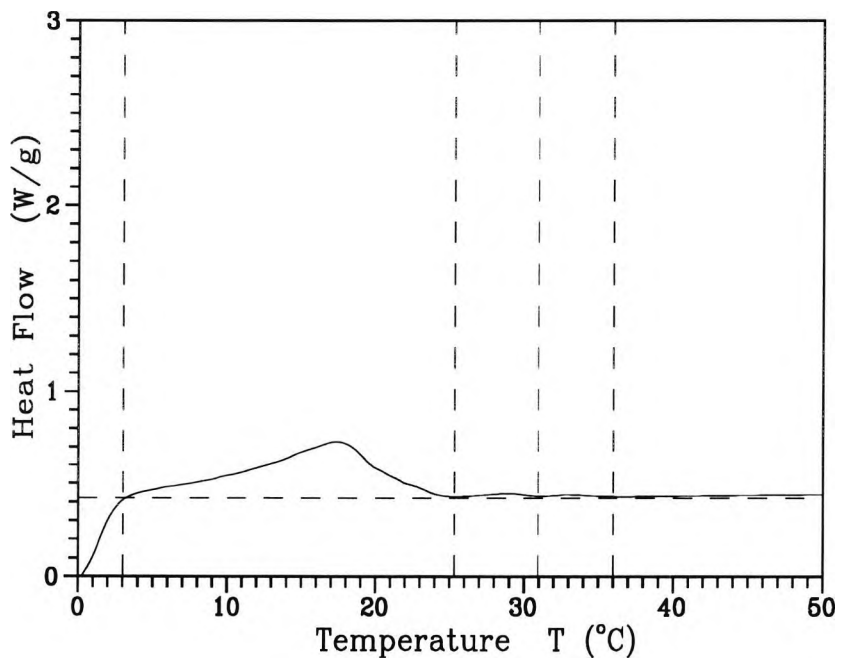


Figure 10.12: The thermogram for the sample of trial No. 4

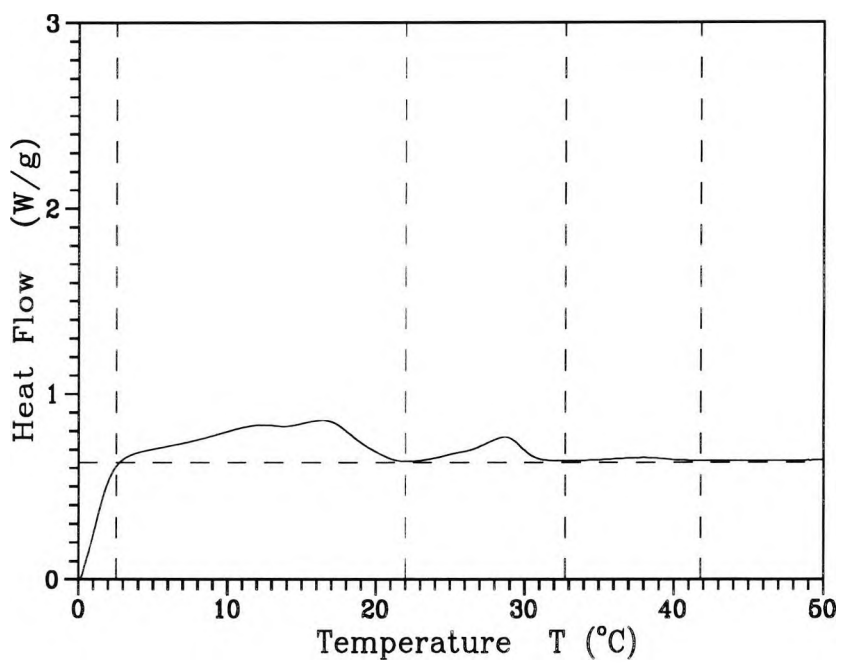


Figure 10.13: The thermogram for the sample of trial No. 5

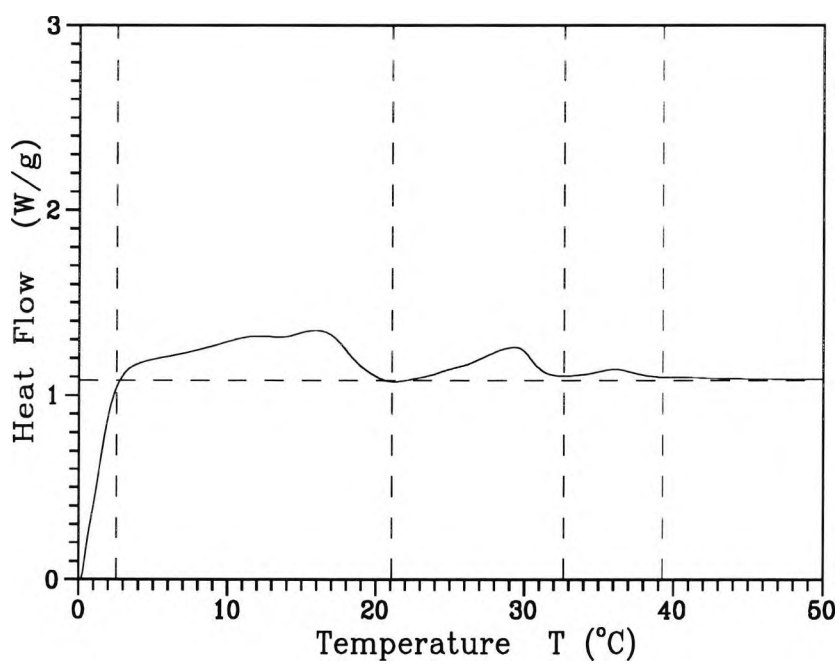


Figure 10.14: The thermogram for the sample of trial No. 6

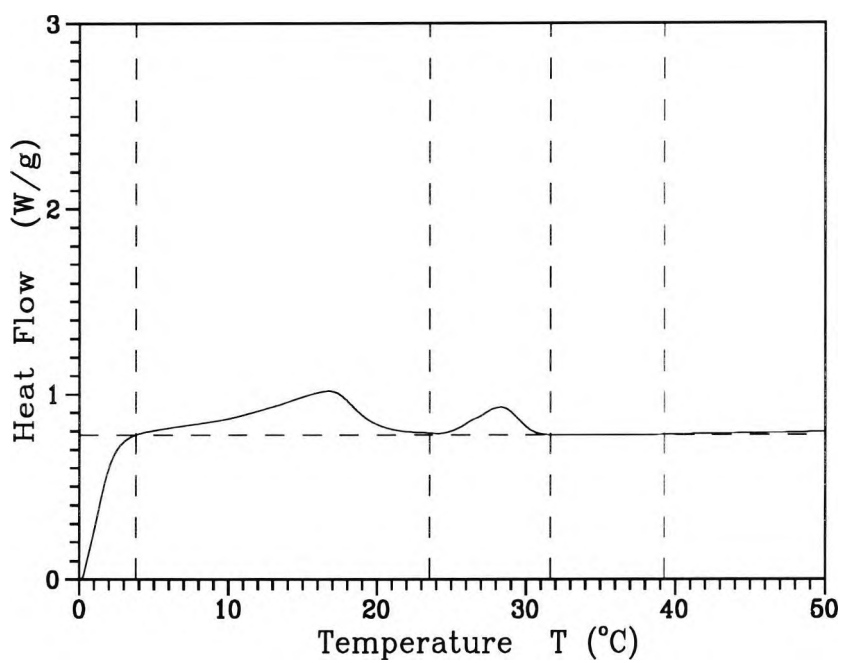


Figure 10.15: The thermogram for the sample of trial No. 7

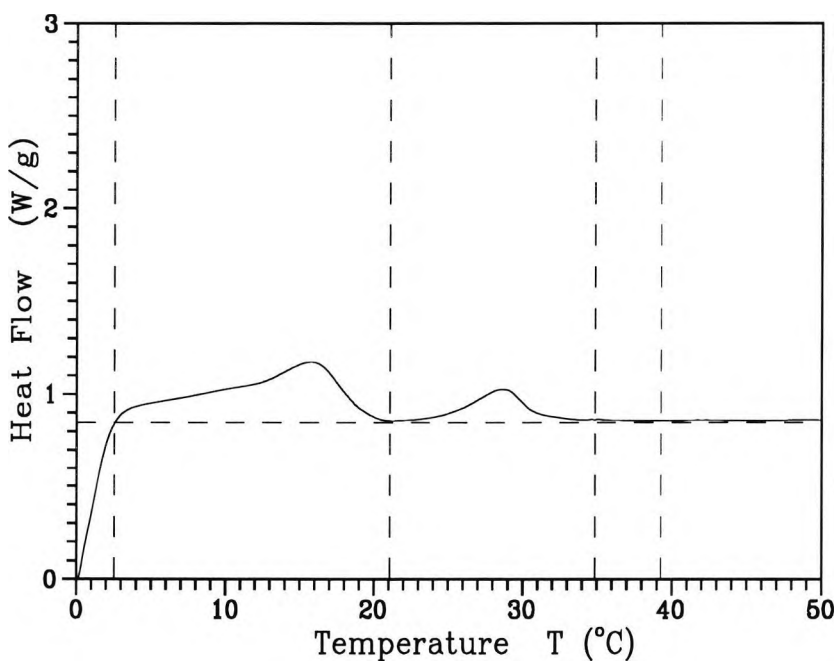


Figure 10.16: The thermogram for the sample of trial No. 8

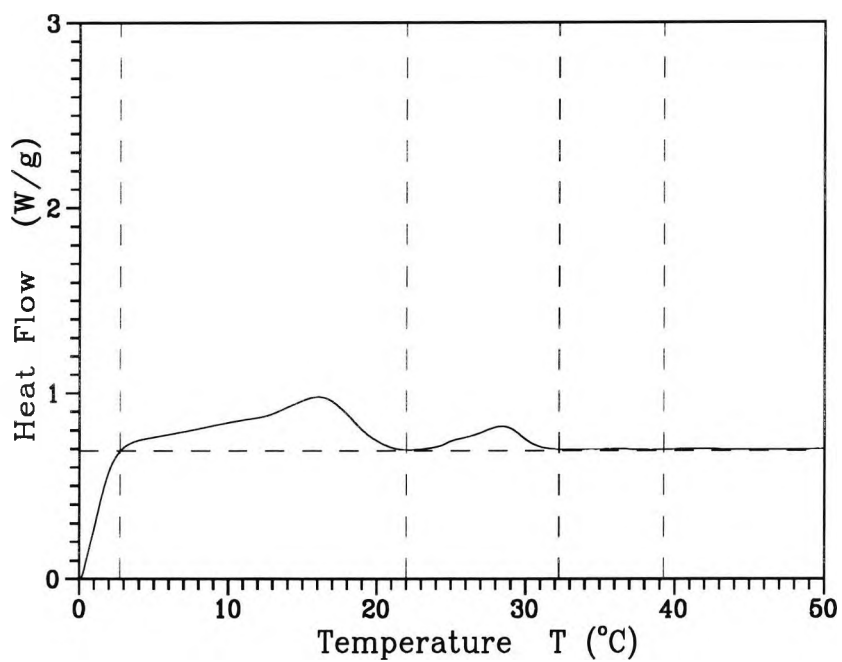


Figure 10.17: The thermogram for the sample of trial No. 9

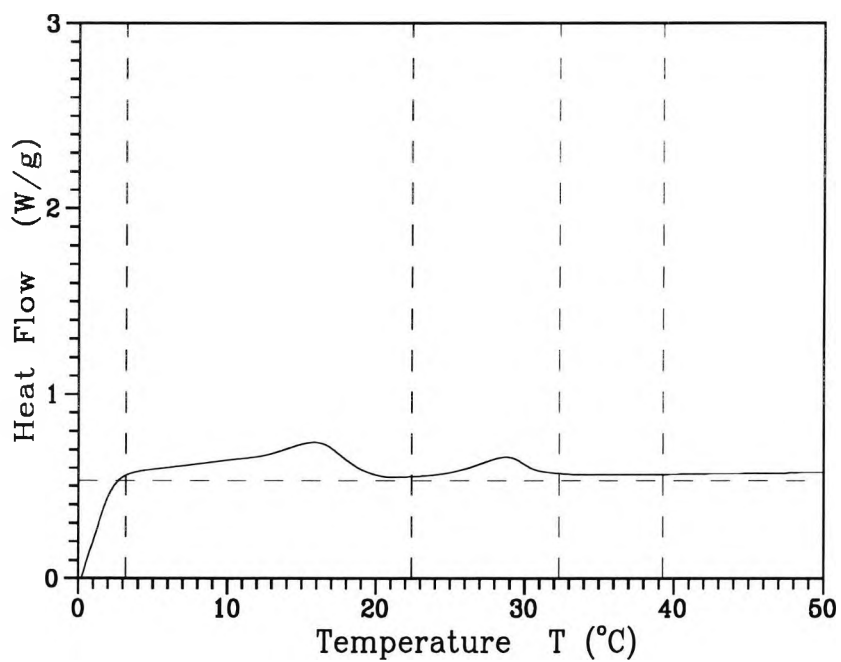


Figure 10.18: The thermogram for the sample of trial No. 10

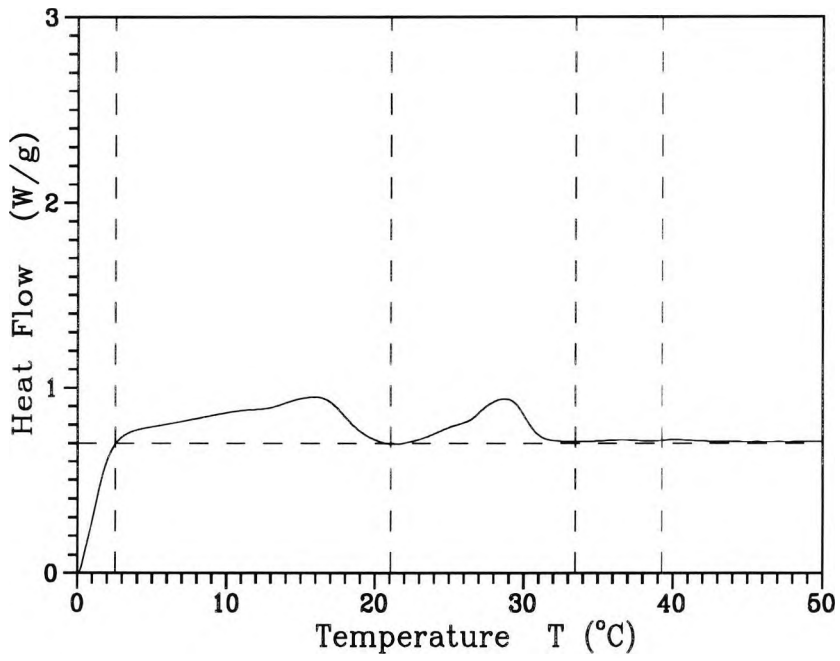


Figure 10.19: The thermogram for the sample of trial No. 11

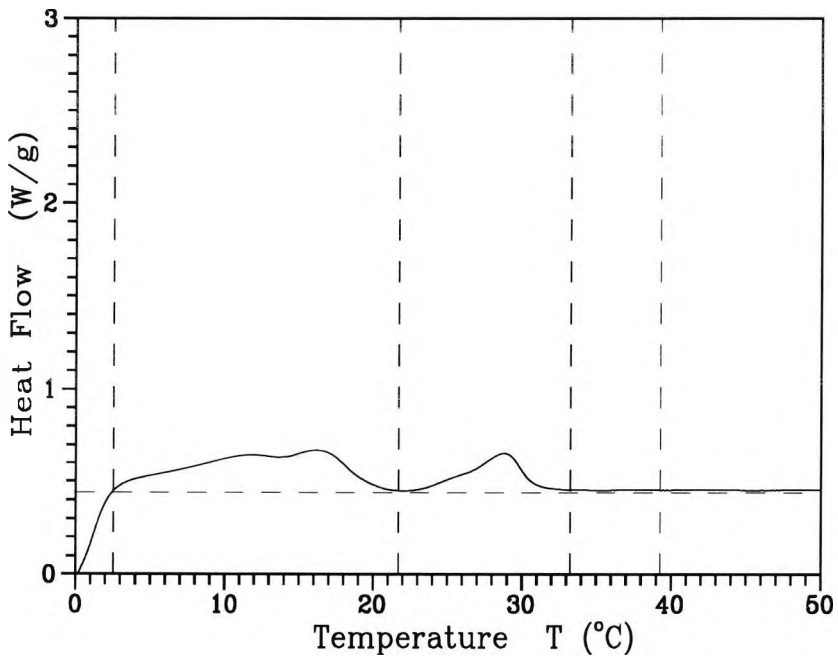


Figure 10.20: The thermogram for the sample of trial No. 12

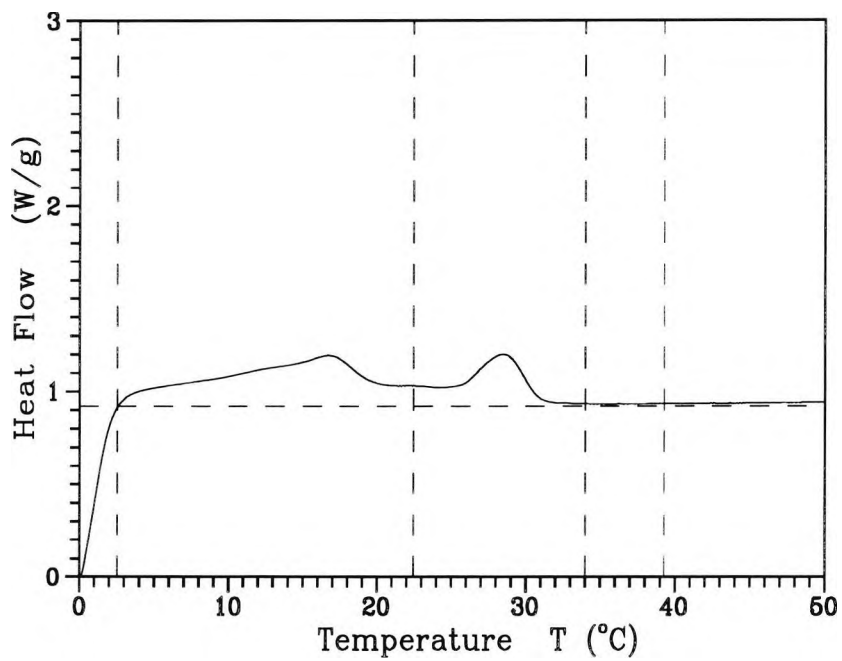


Figure 10.21: The thermogram for the sample of trial No. 13

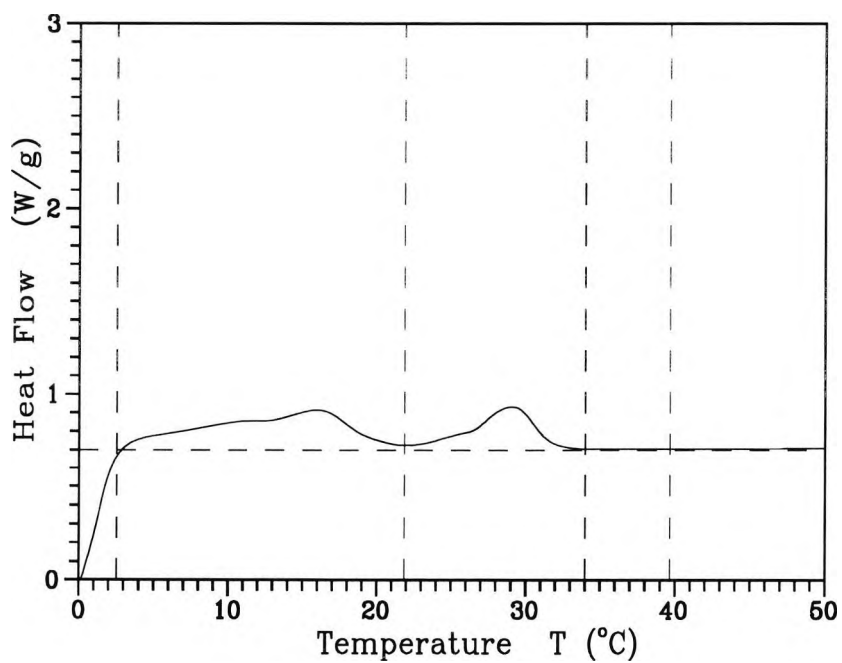


Figure 10.22: The thermogram for the sample of trial No. 14

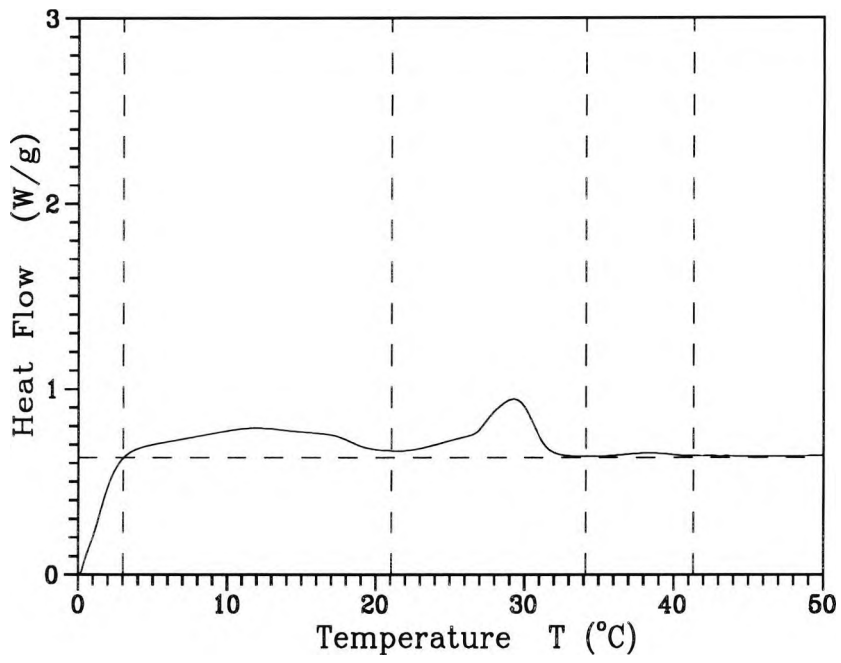


Figure 10.23: The thermogram for the sample of trial No. 15

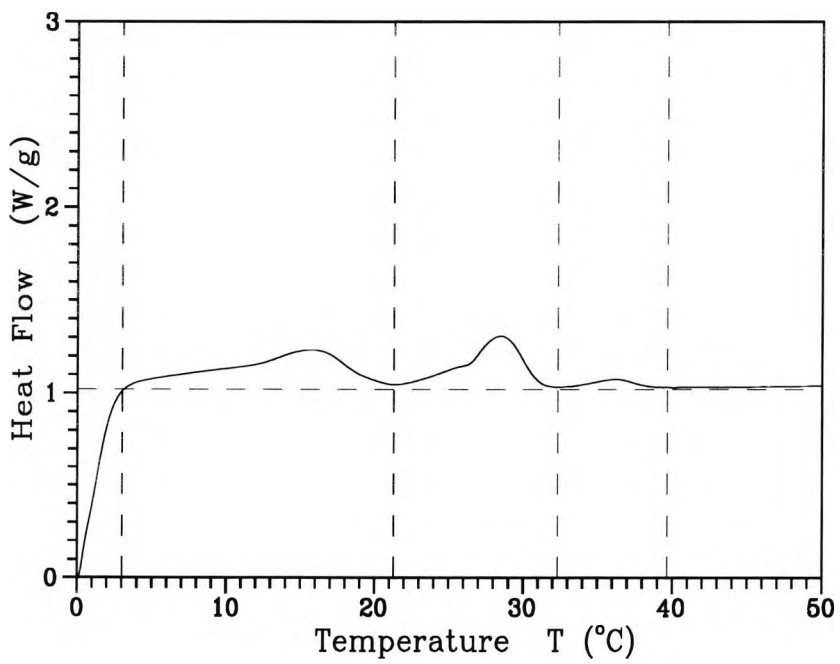


Figure 10.24: The thermogram for the sample of trial No. 16

The DSC thermograms for samples after 24 hours were also obtained and these results were generally much more impressive than those for immediate assessment. Figure 10.25 shows an example which is a comparison for the result of experiment trial No. 15.

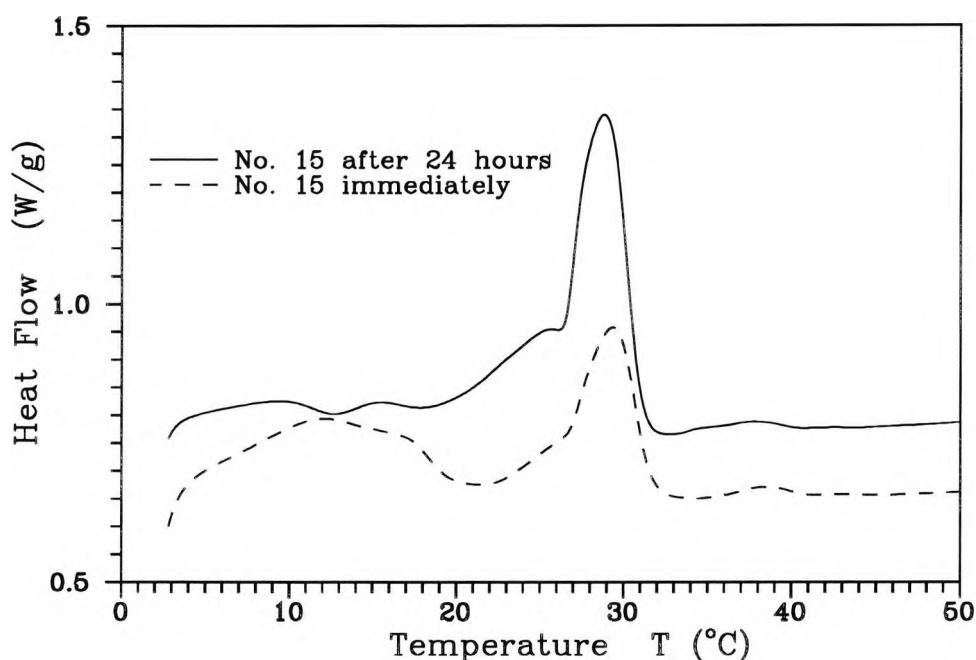


Figure 10.25: An example of the DSC result for the 24-hour-sample and the comparison

### 10.4.3 The criterion for comparisons

In view of the heat flows accompanying the heating process during a DSC analysis, as shown in Figures 10.9 to 10.24, the crystals of treated samples can be generally divided into two classes. One is unstable crystals, which normally have maximum heat flow at about 17°C; another is relatively stable crystals, whose maximum heat flow appears at about 29-30°C. Furthermore, the plotting method used for Figures 10.9 to 10.24 means that the heat energy flows during crystal melting will be represented by the area under the curves:

$$W = \int_{T_0}^{T_n} Q(T) dT \quad (10.3)$$

For the unstable crystals, defined as  $\alpha$ -crystals,

$$W_\alpha = \int_{T_l}^{T_m} Q(T) dT \quad 0 < l < \dots < m; \quad (10.4)$$

Similarly, for the stable crystals, defined as  $\beta$ -crystals,

$$W_\beta = \int_{T_m}^{T_s} Q(T) dT \quad m < \dots < s < n; \quad (10.5)$$

Considering the selected baseline QB, the criterion for the comparisons can be decided as

$$\eta = \frac{W'_\beta}{W'_\alpha} = \frac{\int_{T_m}^{T_s} q(T) dT}{\int_{T_l}^{T_m} q(T) dT} \quad (10.6)$$

#### 10.4.4 Numerical Integration

There are many methods for numerical integration. One of the most widely known and used techniques in the numerical integration over a finite interval is Simpson's rule (Davis and Rabinowitz, 1984). It divides the total interval into many smaller intervals and approximates the area under them. If  $f(x) \in C^4[a, b]$ ; then

$$\int_a^b f(x) dx - \frac{b-a}{6} \left[ f(a) + 4f\left(\frac{a+b}{2}\right) + f(b) \right] = -\frac{h^4}{180} f^4(\xi) \quad (10.7)$$

where  $a < \xi < b$ . Therefore the Simpson approximation

$$\int_a^b f(x) dx \approx \frac{b-a}{6} \left[ f(a) + 4f\left(\frac{a+b}{2}\right) + f(b) \right] \quad (10.8)$$

is accurate for all polynomials of degree three or less.

where  $a = x_0 < x_1 < \dots < x_{2N-1} < x_{2N} = b$

be a sequence of equispaced point in  $[a, b]$ :

$$x_{i+1} - x_i = h, \quad i = 0, \dots, 2N - 1. \quad (10.9)$$

Set  $f_i = f(x_i)$ . Then the compound Simpson's rule is

$$\int_{x_0}^{x_{2N}} f(x)dx \approx \frac{h}{3} [f_0 + 4(f_1 + f_3 + \dots + f_{2N-1}) + 2(f_2 + f_4 + \dots + f_{2N-2}) + f_{2N}] \quad (10.10)$$

In the case of the DSC results, the functions of each  $f(x) = q(T)$  are unknown. However the equispaced temperature intervals in the experiments were small enough to be used directly in a Simpson's rule calculation without bothering to establish a functional relationship first. The interval in experiments was:

$$h = T_{i+1} - T_i = 0.067^\circ C \quad (10.11)$$

On the basis of above, a Fortran 77 program was developed and the calculations were carried out. Table 10.4 lists the calculation results for Figures 10.9 to 10.24.

Table 10.4: Results of the numerical integration

Trial no.	Orthogonal array	$W'_\alpha^{(1)}$	$W'_\beta^{(1)}$	$\eta^{(1)}$	$W'_\alpha^{(2)}$	$W'_\beta^{(2)}$	$\eta^{(2)}$
1	1 1 1 1 1	3.413	0.337	0.099			
2	1 2 2 2 2	3.406	0.102	0.030	3.374	0.200	0.059
3	1 3 3 3 3	3.238	0.066	0.021			
4	1 4 4 4 4	3.054	0.102	0.033			
5	2 1 2 3 4	2.562	0.508	0.198			
6	2 2 1 4 3	3.046	0.894	0.294			
7	2 3 4 1 2	1.982	0.518	0.261			
8	2 4 3 2 1	3.017	0.852	0.282			
9	3 1 3 4 2	2.727	0.586	0.215			
10	3 2 4 3 1	1.937	0.877	0.452			
11	3 3 1 2 4	2.569	1.112	0.433	2.879	0.919	0.319
12	3 4 2 1 3	2.673	0.955	0.357	2.231	1.326	0.594
13	4 1 4 2 3	3.223	1.423	0.441	3.507	1.360	0.388
14	4 2 3 1 4	2.301	1.167	0.507			
15	4 3 2 4 1	1.922	1.517	0.789			
16	4 4 1 3 2	2.049	1.350	0.659	2.079	1.123	0.540

In the Table  $\eta^{(k)}$  ( $k=1, 2$ ) denotes the different runs of the experiments, respectively.

The integration results for the thermograms of 24-hour samples were also obtained by calculation and are given in Table 10.5.

Table 10.5: Results of the numerical integration for 24-hours thermograms

Trial no.	Orthogonal array	$W'_\alpha$	$W'_\beta$	$\eta^{(1)}$
1	1 1 1 1 1	–	2.872	–
2	1 2 2 2 2	2.439	0.787	0.323
3	1 3 3 3 3	3.087	1.456	0.471
4	1 4 4 4 4	4.305	0.462	0.107
5	2 1 2 3 4	–	2.908	–
6	2 2 1 4 3	–	2.717	–
7	2 3 4 1 2	0.841	1.986	2.362
8	2 4 3 2 1	–	2.383	–
9	3 1 3 4 2	–	2.951	–
10	3 2 4 3 1	–	1.689	–
11	3 3 1 2 4	–	3.481	–
12	3 4 2 1 3	1.013	1.053	1.040
13	4 1 4 2 3	0.415	1.154	2.780
14	4 2 3 1 4	0.643	0.920	1.430
15	4 3 2 4 1	–	2.332	–
16	4 4 1 3 2	–	3.625	–

## 10.5 Analysis Method and Results

### 10.5.1 The method

Firstly the ratio of stable crystals to unstable ones, the  $\eta$  values, were divided into 4 levels for each factor. In the case of Table 10.4, the total  $\eta$  values for different

factors at different levels were calculated as

$$A_1 = \sum_{i=1}^4 \eta_i; \quad A_2 = \sum_{i=5}^8 \eta_i; \quad (10.12)$$

$$A_3 = \sum_{i=9}^{12} \eta_i; \quad A_4 = \sum_{i=13}^{16} \eta_i;$$

$$\begin{aligned} B_1 &= \eta_1 + \eta_5 + \eta_9 + \eta_{13} \\ B_2 &= \eta_2 + \eta_6 + \eta_{10} + \eta_{14} \\ B_3 &= \eta_3 + \eta_7 + \eta_{11} + \eta_{15} \\ B_4 &= \eta_4 + \eta_8 + \eta_{12} + \eta_{16} \end{aligned} \quad (10.13)$$

$$\begin{aligned} C_1 &= \eta_1 + \eta_6 + \eta_{11} + \eta_{16} \\ C_2 &= \eta_2 + \eta_5 + \eta_{12} + \eta_{15} \\ C_3 &= \eta_3 + \eta_8 + \eta_9 + \eta_{14} \\ C_4 &= \eta_4 + \eta_7 + \eta_{10} + \eta_{13} \end{aligned} \quad (10.14)$$

$$\begin{aligned} D_1 &= \eta_1 + \eta_7 + \eta_{12} + \eta_{14} \\ D_2 &= \eta_2 + \eta_8 + \eta_{11} + \eta_{13} \\ D_3 &= \eta_3 + \eta_5 + \eta_{10} + \eta_{16} \\ D_4 &= \eta_4 + \eta_6 + \eta_9 + \eta_{15} \end{aligned} \quad (10.15)$$

$$\begin{aligned} E_1 &= \eta_1 + \eta_8 + \eta_{10} + \eta_{15} \\ E_2 &= \eta_2 + \eta_7 + \eta_9 + \eta_{16} \\ E_3 &= \eta_3 + \eta_6 + \eta_{12} + \eta_{13} \\ E_4 &= \eta_4 + \eta_5 + \eta_{11} + \eta_{14} \end{aligned} \quad (10.16)$$

Then, the fractions were obtained as

$$\begin{aligned} \overline{A}_j &= \frac{1}{4}A_j; \quad \overline{B}_j = \frac{1}{4}B_j; \\ \overline{C}_j &= \frac{1}{4}C_j; \quad \overline{D}_j = \frac{1}{4}D_j; \\ \overline{E}_j &= \frac{1}{4}E_j; \end{aligned} \quad (10.17)$$

## 10.5.2 The results

The results were obtained from above calculation. When using  $\eta_i = \eta_i^{(1)}$ , the data of results are given in Table 10.6. This Table shows that if the experimental conditions are changed from  $A_1=0\text{kV}$  to  $A_2=10\text{kV}$ ,  $A_3=15\text{kV}$  and  $A_4=25\text{kV}$ , ignoring all other parameters, the fraction  $\eta$  values increase from 4.58% to 25.88%, 36.43% and 59.9%, respectively. Similarly for the other experimental conditions.

Table 10.6: Response Table – Mean (I)

Fraction	j=1 (%)	j=2 (%)	j=3 (%)	j=4 (%)
$\overline{A_j}$	4.58	25.88	36.43	59.9
$\overline{B_j}$	23.83	32.08	37.60	33.28
$\overline{C_j}$	37.13	34.35	25.63	29.68
$\overline{D_j}$	30.60	29.65	33.25	33.28
$\overline{E_j}$	40.55	29.13	27.83	29.28

Using the data of both  $\eta_i^{(1)}$  and  $\eta_i^{(2)}$ , let

$$\eta_i = \overline{\eta}_i = \frac{1}{2}(\eta_i^{(1)} + \eta_i^{(2)}) \quad (10.18)$$

then the results as given in Table 10.7 were obtained.

Table 10.7: Response Table – Mean (II)

Fraction	j=1 (%)	j=2 (%)	j=3 (%)	j=4 (%)
$\overline{A_j}$	4.95	25.88	37.98	57.78
$\overline{B_j}$	23.18	32.45	36.18	34.78
$\overline{C_j}$	34.23	37.70	25.63	29.03
$\overline{D_j}$	33.58	27.95	31.78	33.28
$\overline{E_j}$	40.55	28.03	30.15	27.85

The results given in Tables 10.6 and 10.7 are also as shown in Figures 10.26 to 10.30, respectively. These will give a group of figure for the criterion  $\eta_i^k$  versus different experimental factors.

### 10.5.3 Discussions

Results in Tables 10.6 and 10.7 indicate that, among the five factors, the effect of factor A (applied electric field) on the  $\eta$  values is the most significant. As the field potential increases, the number of stable crystals increases and the number of unstable crystals decreases. These results, as shown in Figure 10.26, are consistent with the single experiment results for chocolate or cocoa butter.

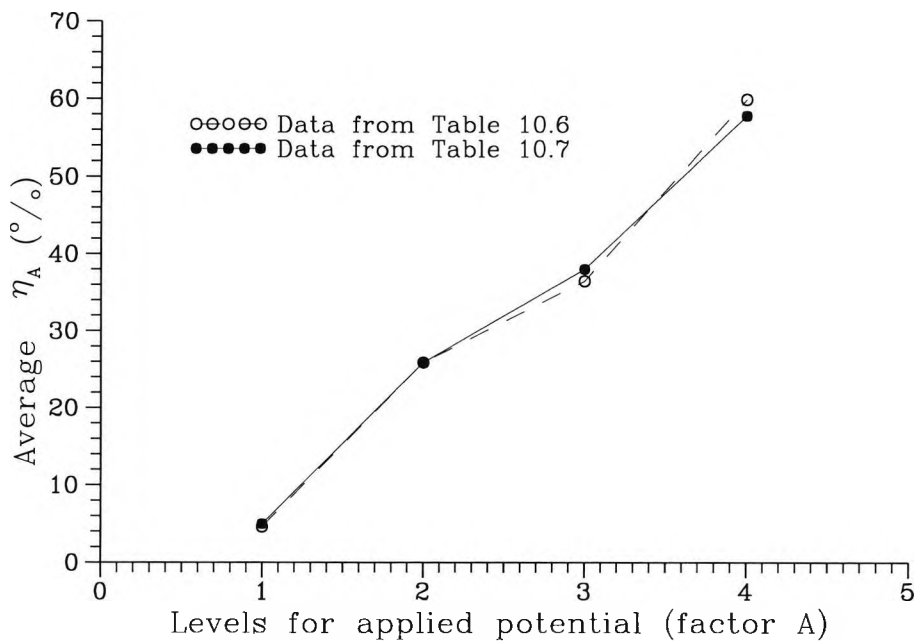


Figure 10.26: Analysis result  $\eta_A$  versus experimental levels for voltages of the applied field (factor A); (1: 0kV, 2: 10kV, 3: 15kV, 4: 25kV)

The effects of both the coolant temperature and sample temperature on the  $\eta$  values are not very significant but are distinguishable. Figure 10.27 indicates that the number of stable crystals has a maximum value at level 3 (10°C) in the experiments. If considering the linear best fit curves shown in the Figure, the number of stable crystals seems to be higher when the coolant temperature increases in a reasonable

range. On the contrary, as shown in Figure 10.28, the  $\eta$  values are relatively lower when the sample temperature remains at a higher level.

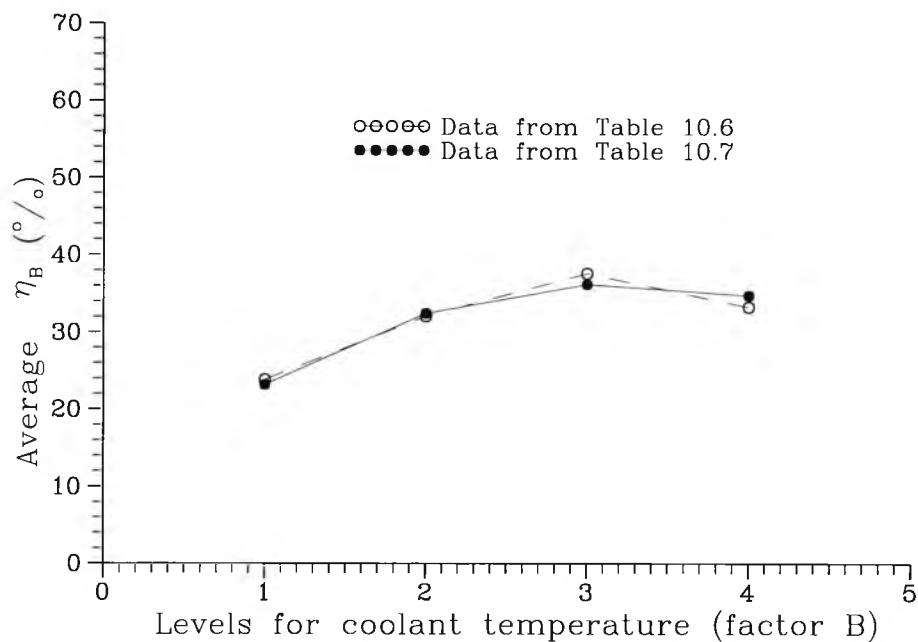


Figure 10.27: Analysis result  $\eta_B$  versus experimental levels for the coolant temperature (factor B); (1: 0°C, 2: 5°C, 3: 10°C, 4: 15°C)

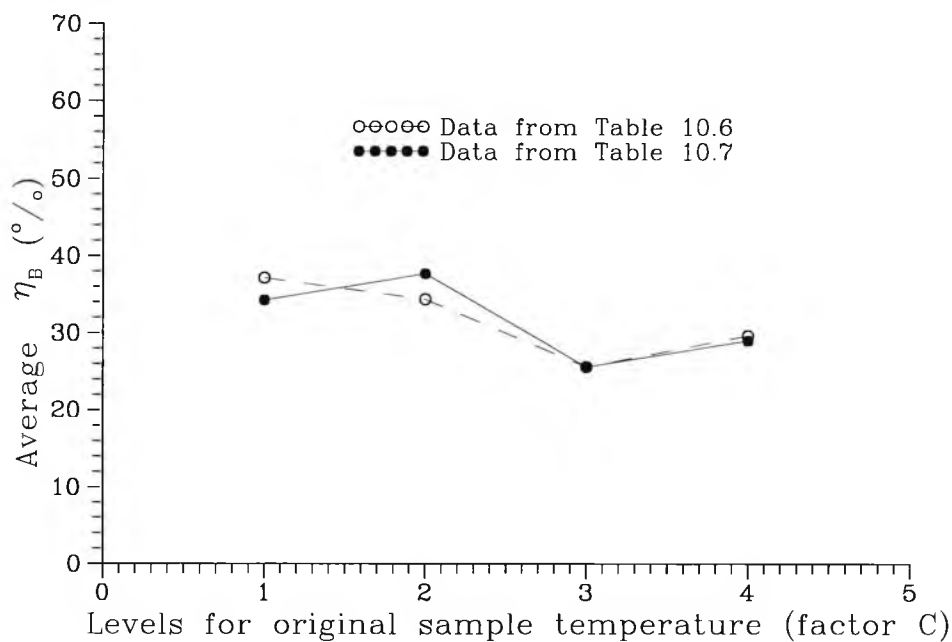


Figure 10.28: Analysis result  $\eta_C$  versus experimental levels for the original temperature of samples (factor C); (1: 28°C, 2: 30°C, 3: 35°C, 4: 42°C)

The time for the sample treatment seems to be unimportant for the  $\eta$  values. In view of Figure 10.29, the number of stable crystals increases very slightly when the treatment time changes from 10 min changes to 20 min.

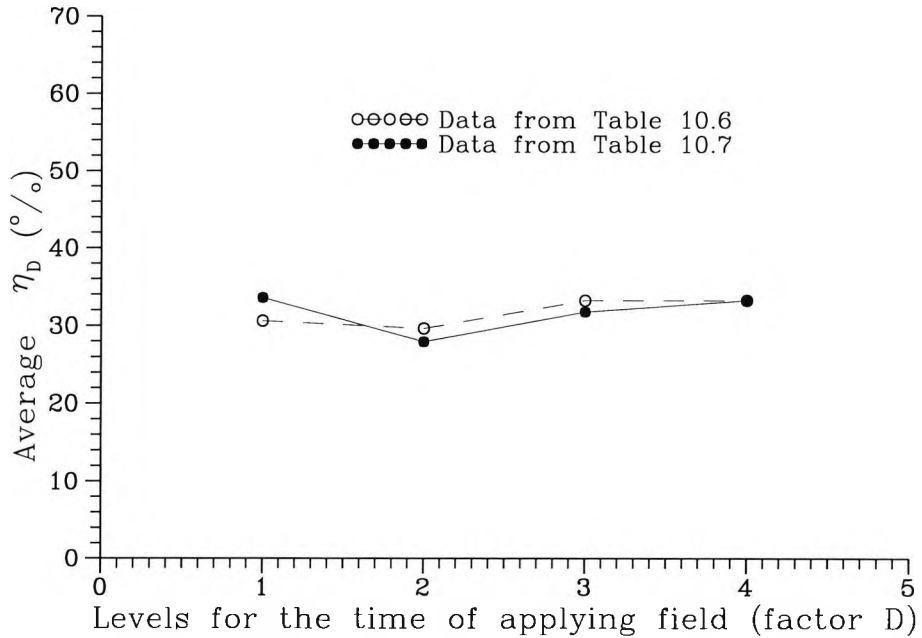


Figure 10.29: Analysis result  $\eta_D$  versus experimental levels for the time of applying field (factor D); (1: 2min, 2: 5min, 3: 10min, 4: 20min)

The thickness of samples also has an effect on the  $\eta$  values. The number of stable crystals has a highest value at level one (4 mm), then it reduces as the sample thickness increases. This can be seen from the linear best fit curve shown in Figure 10.30. Actually, the data in this figure show nearly constant  $\eta$  values for levels 2 to 4. This may result from the experiments in which the DSC samples were taken from nearly the same position of treatment samples.

Obviously, from the information given in Table 10.6 and Figures 10.26 to 10.30, it is still difficult to say which trial of the experiments is the optimum. If only the fraction differences are taken into account, the experimental arrangement ( $A_4, B_3, C_1, D_4, E_1$ ) seems to be the best. In fact, the small difference between  $\overline{D}_4$  and  $\overline{D}_3$  is negligible, but the time for the treatment is 20 min and 10 min, respectively. Therefore the arrangement ( $A_4, B_3, C_1, D_3, E_1$ ) may be more reasonable. It can

be seen from Table 4 that this arrangement is quite close to the result of trial No. 15. Clearly the result of trial No. 15 has the maximum  $\eta$  value in the experiments (0.789). Considering the linear best fit data given in Table 10.7, the arrangement of (A<sub>4</sub>, B<sub>3</sub>, C<sub>1</sub>, D<sub>3</sub>, E<sub>1</sub>) is still acceptable.

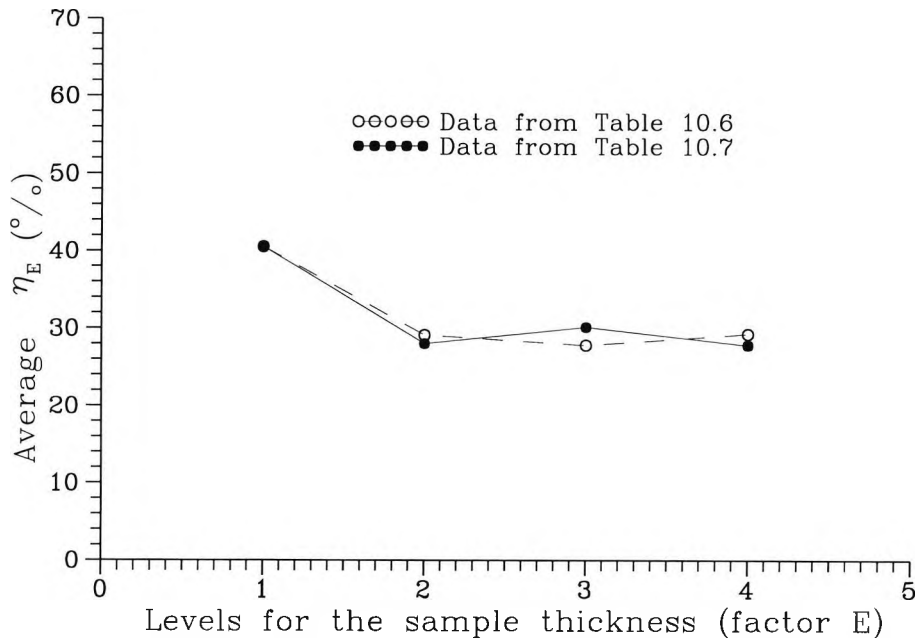


Figure 10.30: Analysis result  $\eta_E$  versus experimental levels for the thickness of samples (factor E); (1: 4mm, 2: 6mm, 3: 10mm, 4: 13mm)

Concerning the DSC data of 24-hour samples, the criterion of comparisons does not exist for all cases because the intergration results listed in Table 10.5 have shown that the value  $w'_\alpha$  was zero for many trials. For this reason, the analysis was done using the value  $w'_\beta$  as the criteriron for comparison. Figure 10.31 shows the analysis results calculated on the basis of Table 10.5. This is a plot for the integration value  $w'_\beta$  versus experimental levels for different factors. It can be noted that the effect of factor C, D and E respectively on the stable crystals for 24-hour samples is very similar to that for the immediate assessments shown as Figures 10.28 to 10.30. Although the effect of factor A on stable crystals for this analysis seems to be not as significant as that for the immediate testing shown in Figure 10.26, the changes of linear best fit curves are basically similar. However, the effect of factor

B on stable crystals shows a different changes from that shown in Figure 10.27.

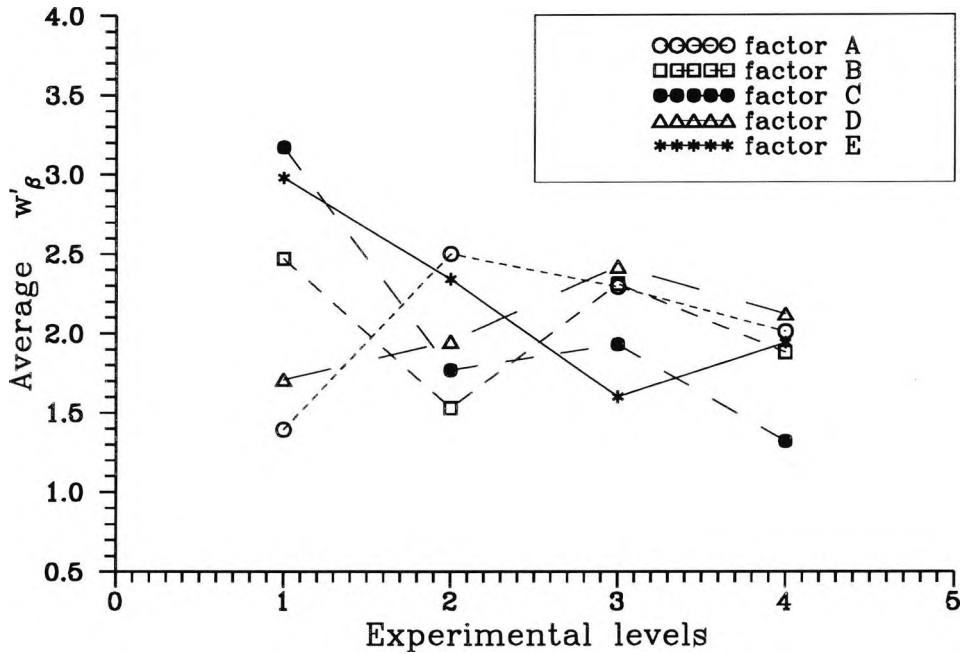


Figure 10.31: Analysis result  $w'_\beta$  versus experimental levels for different factors

## 10.6 Summary

In this chapter, a novel approach of applying the Taguchi method to the experimental design and results analysis was carried out. To investigate the effect of an electric field on the crystallization of untempered chocolate on different conditions, five factors and four levels were considered and an L16 ( $4^5$ ) matrix of orthogonal experiments were designed and carried out. Differential scanning calorimetry (DSC) was employed to assess the experimental results for both the immediate samples and the 24-hour ones.

To deal with the different DSC results, which are in the form of thermograms, based on the Taguchi experiments, a criterion for comparison was developed and

the numerical intergration was done. As the final stage, the integrated results were analyzed by the Taguchi way, in which the effects of different factors, such as the applied potential, the coolant temperature, the sample initial temperature, the time of treatment and the sample thickness, on the comparison criterion were discussed and concluded.

As a results of this analysis, the relations for the calculation criteria  $\eta_i$  versus the experimental factors can be obtained. On this basis, the optimal result can be identified. Of course, to confirm the optimum arrangement, a lot of further work is needed.

# Chapter 11

## Theoretical Approach

### 11.1 Introduction

The theoretical analysis for all situations of electric fields acting on crystallization with polymorphic behaviour is complex due to the interactive influences of thermal (heating/cooling), electrical and chemical potential fields on dielectric melts or liquids. Any practically realized effect of electric fields on crystallization can, at present, only be modelled with considerable simplification of the true situation. This chapter describes the basis of the mathematical models used to analyse several of the situations investigated or reported in earlier chapters. In particular, the process for single crystal form among the polymorphs was studied.

### 11.2 Derivation of Basic Relations

To simplify the problem, here, the crystallization with a single crystal form from a dielectric melt with or without permanent polarization in the presence of an electric field was considered. Based on the experimental results reported in chapters 9 and 10, a supposition was developed, in which the additional energy of an electric field when it is applied to a dielectric melt changes with the emergence of a new crystal phase and results in the change of crystallization rate.

### 11.2.1 The changes of chemical potential

It is well known from the theory of chemical dynamics (Mullin, 1993) that the major driving force for the crystallization of a melt or liquid is the difference of chemical potentials per molecule developed from the phase change, namely

$$\Delta\mu = \mu_1 - \mu_{2\infty} \quad (11.1)$$

where the subscripts 1 and 2 denote melt phase and crystal phase, respectively.

For a single component melt-crystal system, the chemical potential per molecule of the  $i$ -th phase in an external electric field can be expressed as

$$\mu_i(p, T, E) = \mu_i^o(p, T) + w_i(E) \quad (11.2)$$

where  $\mu_i^o$  is the chemical potential of the  $i$ -th phase in the absence of an electric field;  $w_i$  is the additional energy of an  $i$ -th phase molecule due to the polarization and  $E$  is the electric field strength. The subscript  $i = 1$  is for melt phase and  $i = 2$  for crystal phase.

This additional energy has been discussed by several researchers as reviewed in chapter 7 and similar definitions have been given but different expressions were presented. Basically, it can be derived from the equilibrium thermodynamics theory. An infinitesimal change in the internal energy with no permanent polarization was derived by Guggenheim (1967),

$$dU^e = TdS - pdV + V_cEdD \quad (11.3)$$

and the free energy and free enthalpy were then respectively expressed as

$$F^e = U - TS - V_cED \quad (11.4)$$

$$G^e = U + pV - TS - V_cED \quad (11.5)$$

where  $V_c$  is the volume of the system that is subject to the electric field and  $D$  is the electric induction.

However, when considering the dominant effect of dielectric polarization in an electric field, the electric induction  $D$  in the above equations should be replaced by the dielectric polarization  $\overline{P}$ , and then expressed as

$$dU^e = TdS - pdV + V_c E d\overline{P} \quad (11.6)$$

where  $\overline{P} = D = \epsilon_o \epsilon E - \epsilon_o E$ ; and

$$dF^e = -SdT - pdV - V_c \overline{P} dE \quad (11.7)$$

$$dG^e = -SdT + Vdp - V_c \overline{P} dE \quad (11.8)$$

for a non-polar dielectric melt which has no permanent polarization;

$$D = \epsilon_o \epsilon E + \overline{P}_o \quad (11.9)$$

with the permanent polarization, where  $\overline{P}_o$  is the permanent polarization.

Therefore, the Gibbs free energy in the presence of an electric field can be obtained by integration of the previous equation as

$$G_i^e = G_i^o - \frac{1}{2} V_i \epsilon_o (\epsilon_i - 1) E^2 = G_i^o - \frac{1}{2} V_i \epsilon_o \chi_i E^2 \quad (11.10)$$

for non-polar and

$$G_i^e = G_i^o - V_i \left( \overline{P}_o E + \frac{1}{2} \epsilon_o \chi_i E^2 \right) \quad (11.11)$$

for polar liquid. In the above equations,  $\chi = \epsilon - 1$  is the dielectric susceptibility.

According to the literature (Turnbull, 1956 and Frenkel, 1946), the chemical potential difference per molecule could be denoted by the Gibbs free energy difference per unit volume of the new phase in the bulk as

$$-\frac{\Delta G^o}{V_2} = \frac{(\mu_1^o - \mu_{2\infty}^o)}{v_2} \quad (11.12)$$

that is

$$\Delta \mu^o = -\kappa_v \Delta G^o \quad (11.13)$$

where  $\kappa_v = v_2/V_2$  is a constant.

Considering a non-polar dielectric melt, if the electric field is supposed to be uniform, the potential change from liquid phase ( $i = 1$ ) to solid phase ( $i = 2$ ) is then expressed as

$$\begin{aligned}\Delta\mu(p, T, E) &= \Delta\mu^o(p, T) - \frac{\kappa_v \epsilon_o}{2} (\chi_2 V_2 - \chi_1 V_1) E^2 \\ &= \Delta\mu^o(p, T) + \frac{\kappa_v \epsilon_o}{2} V_1 (\chi_1 - \chi_2 \xi_v) E^2\end{aligned}\quad (11.14)$$

so that the additional energy is

$$\Delta w_{1-2} = \frac{\kappa_v \epsilon_o}{2} V_1 (\chi_1 - \chi_2 \xi_v) E^2 \quad (11.15)$$

where  $\xi_v$  is the ratio of the volume contraction and was defined as  $\xi_v = V_2/V_1$ .

### 11.2.2 The change of temperature with field strength

Thermodynamic relations can be obtained from the basic chemical potential expression during crystallization in the presence of an electric field. If assuming the system pressure before and after applying the field is the same, i.e.  $p=p^o=\text{constant}$  (which is close to the conditions of the experiments described in chapters 9 and 10), differentiating equation (11.14) with respect to  $E$ , gives

$$\left(\frac{\partial \Delta\mu}{\partial T}\right)_p \frac{dT}{dE} = \kappa_v \epsilon_o (\chi_1 - \chi_2 \xi_v) V_1 E \quad (11.16)$$

According to the definition of free enthalpy, the first term on the lefthand side of this equation can be expressed as

$$\left(\frac{\partial \Delta\mu}{\partial T}\right)_p = -\kappa_v (S_2 - S_1) \quad (11.17)$$

where  $S_i$  ( $i = 1$  and  $2$ ) is the entropy of  $i$ -th phase, so that

$$\frac{dT}{dE} = \frac{\epsilon_o V_1}{S_2 - S_1} (\chi_2 \xi_v - \chi_1) E \quad (11.18)$$

After integrating, the change in temperature of crystallization in the electric field can be obtained as

$$T = T^o + \frac{\epsilon_o V_1}{2(S_2 - S_1)} (\chi_2 \xi_v - \chi_1) E^2 \quad (11.19)$$

where  $T^o$  is the temperature of crystallization in the absence of an electric field.

The entropy change can be denoted by the heat of crystallization (the latent heat) which is liberated during crystallization divided by the crystallization temperature

$$S_2 - S_1 = -\frac{\Delta Q_{sol}}{T} \quad (11.20)$$

Therefore, equation (11.19) is expressed as

$$T = T^o - \frac{\epsilon_o V_1 T}{2\Delta Q_{sol}} (\chi_2 \xi_v - \chi_1) E^2 \quad (11.21)$$

By multiplying equation (11.19) by the entropy change of the crystallization, ( $S_1 - S_2$ ), the relation for the crystallization heat (the latent heat) before and after applying the field can be obtained

$$|\Delta Q_{sol}| = |\Delta Q_{sol}^o| - \frac{\epsilon_o V_1}{2} (\chi_2 \xi_v - \chi_1) E^2 \quad (11.22)$$

where  $\Delta Q_{sol}^o$  is the crystallization heat in the absence of an electric field.

Combining equations (11.21) and (11.22), we obtain

$$T = \left( \frac{\Delta Q_{sol}}{\Delta Q_{sol}^o} \right) T^o \quad (11.23)$$

It is clear that if the expression  $(\chi_2 \xi_v - \chi_1) < 0$  in equation (11.22), the heat of crystallization in the presence of an electric field will be larger than that in the absence of the field; so the temperature of crystallization will be a slightly higher than without the field. This is consistent with the experimental results reported in chapter 9. In that case, the  $\alpha$  and  $\beta_{III}$  crystals appear earlier and the crystallization temperatures are higher under the action of an electric field than that without the field.

### 11.2.3 The change of pressure with field strength

Similar to the above analysis, differentiating equation (11.14) with respect to  $E$  for  $T = T^o$ , we obtain

$$\frac{dp}{dE} = \frac{\epsilon_o V_1}{V_1 - V_2} (\chi_2 \xi_v - \chi_1) E \quad (11.24)$$

so that

$$p = p^o + \frac{\epsilon_o}{2} \left( \frac{\chi_2 \xi_v - \chi_1}{1 - \xi_v} + 1 \right) E^2 \quad (11.25)$$

where  $p^{\circ}$  is the pressure of crystallization in the absence of an electric field.

This equation indicates that applying an electric field, in most cases, will result in a big change in the crystallization pressure, because in most cases, the relation

$$|\epsilon_2\xi_v - \epsilon_1| \gg (1 - \xi_v)$$

seems to be always satisfied. Indeed, the extreme pressure would help to induce nucleation and result in crystallization enhancement. This has been proved by the early experiments of Young (1911) and Berkeley (1912) and has been written into the textbook (Mullin, 1993). In the case of  $(\epsilon_2\xi_v - \epsilon_1) < 0$ , the pressure of crystallization in the presence of an electric field will be lower than that without the field. In the case of cocoa butter described in chapter 9, when the field was at 15 kV (3.75 MV/m), the pressure would change about two times as high as that in the absence of the field.

### 11.3 The Rate of Nucleation

On the basis of the nucleation theory, the rate of nucleation,  $J$ , the number of nuclei formed per unit time per unit volume, can be expressed in the form of the Arrhenius reaction velocity equation commonly used for the rate of a thermally activated process (Mullin, 1993)

$$J = C \exp\left(\frac{-\Delta G}{kT}\right) \quad (11.26)$$

where  $C$  is a constant;  $k$  is the Boltzmann constant, the gas constant per molecule ( $1.3805 \times 10^{-23}$  J/K =  $R/N$ , where  $R$  is the universal gas constant =  $8.314$  kJ  $K^{-1} \text{mol}^{-1}$  and  $N$  = the Avogadro number =  $6.023 \times 10^{23}$   $\text{mol}^{-1}$ ); and  $\Delta G$  is the Gibbs free energy based on the critical size of nuclei.

However, for dielectric melt crystallization, it was noted that melts frequently demonstrate abnormal nucleation characteristics (Tamman, 1925) (see Mullin, 1993). The rate of nucleation usually follows an exponential curve as supercooling increased, but reaches a maximum and subsequently decreases. Tamman suggested

that this behaviour was caused by the sharp increase in viscosity with supercooling which restricted molecular movement and inhibited the formation of ordered crystal structures. Turnbull and Fisher (1949) qualified this behaviour with a modification as

$$\begin{aligned} J &= C' \exp\left(\frac{-\Delta G + \Delta G'}{kT}\right) \\ &= C' \exp\left[-\frac{16\pi\sigma^3 v^2}{3k^3 T^3 (\ln S)^2} + \frac{\Delta G'}{kT}\right] \end{aligned} \quad (11.27)$$

where  $T$  denotes the temperature,  $S$  the degree of supersaturation and  $\sigma$  the interfacial tension. This modified equation includes a “viscosity” term. When  $\Delta G'$ , the activation energy for molecular motion across the embryo-matrix interface, is exceptionally large and the other exponential term is small (because under these circumstances  $S$  is generally very large),  $\Delta G'$  then becomes the dominant factor in the equation and a decrease in nucleation rate is predicted.

Clearly, considering the relatively high viscosities of dielectric melts (cocoa butter is nearly solid at 20°C), the model for the rate of nucleation should require the change of activation energy to be taken into account.

When an external electric field is applied to a dielectric melt with a unit volume, the activation energy for a molecule to pass from the bulk melt to the crystal phase can be described by

$$\Delta G' = \Delta G'_o - \delta G' = \Delta G'_o - \gamma E^2 \quad (11.28)$$

where  $\Delta G'_o$  is the activation energy in the absence of the field;  $\gamma$  is a coefficient and can be expressed on the basis of the derivation of chemical potential changes as

$$\gamma = \frac{1}{2}\epsilon_o(\chi_2\xi_v - \chi_1) \quad (11.29)$$

So that the rate of nucleation can be expressed as

$$J \sim \exp\left[\frac{M(\Delta G'_o - \gamma E^2 - \Delta G)}{R\rho_1 T}\right] \quad (11.30)$$

where  $M$  is the relative molecular weight (kg/mol) and  $\rho_1$  is the density of the melt. And on the basis of the crystallization theory (Mullin, 1993), the  $\Delta G$  in this

equation can be also expressed as

$$\Delta G = \frac{16\pi M\sigma^3}{3RT(\Delta Q_{sol})^2 T_r (\Delta T_r)^2} \quad (11.31)$$

where  $T_r = T_c/T$  and  $\Delta T_r = \Delta T/T$ ;  $T_c$  is cooling temperature and  $\Delta T$  is the supercooling.

If we take the rate of nucleation as a function of two variables, the crystallization temperature  $T$  and the electric intensity  $E$ , then according to the maxi-criterion, the optimum  $T$  and  $E$  could be found, to obtain the maximum rate of nucleation, i.e.

$$\frac{\partial^2 J}{\partial T^2} < 0 \quad (11.32)$$

and

$$\left(\frac{\partial^2 J}{\partial T^2}\right) \left(\frac{\partial^2 J}{\partial E^2}\right) - \left(\frac{\partial^2 J}{\partial T \partial E}\right)^2 > 0 \quad (11.33)$$

Unfortunately, for the case of cocoa butter, there is no published information for its relative molecular weight, so this calculation could not be carried out.

## 11.4 Heat and Mass Transfer Analysis for Crystal Growth

As soon as stable nuclei, (i.e. particles larger than the critical size) have been formed in a supercooled system, they begin to grow into crystals of visible size. There are many classical theories to explain the mechanism of the growth and these have been extensively reviewed by many researchers, such as Well (1946), Lewis (1980) and Chernov (1980 and 1989).

Based on the diffusion-reaction theories, the rate of crystallization from a melt could be thought to depend on the rate of heat transfer from the crystal face to the bulk of the liquid (Mullin, 1993). As the process is generally accompanied by the liberation of crystallization heat, the surface of the crystal will have a slightly higher temperature than the supercooled melt. These conditions are shown in Figure 11.1, where the melting point of dielectric crystals in the absence of an electric field is

denoted by  $T^*$ , and the temperature of the bulk of the superheated melt by  $T$ . Therefore, the overall degree of supercooling is  $(T^* - T)$ . The temperature at the surface of the crystal, the solid-liquid interface, in the absence of an electric field is denoted by  $T_{sl}$ , so the driving force for heat transfer across the effective film of the melt or liquid close to the crystal surface is  $(T_{sl} - T)$ . The rate of heat transfer in the absence of an electric field, then, can be expressed as

$$\frac{dq}{dt} = hA(T_{sl} - T) \quad (11.34)$$

where  $A$  is the area of growing solid surface, and  $h$  is a film coefficient of heat transfer and is defined by

$$h = \frac{\kappa}{\delta} \quad (11.35)$$

where  $\kappa^\circ$  is the thermal conductivity without the field,  $\delta$  is the effective film thickness for heat transfer.

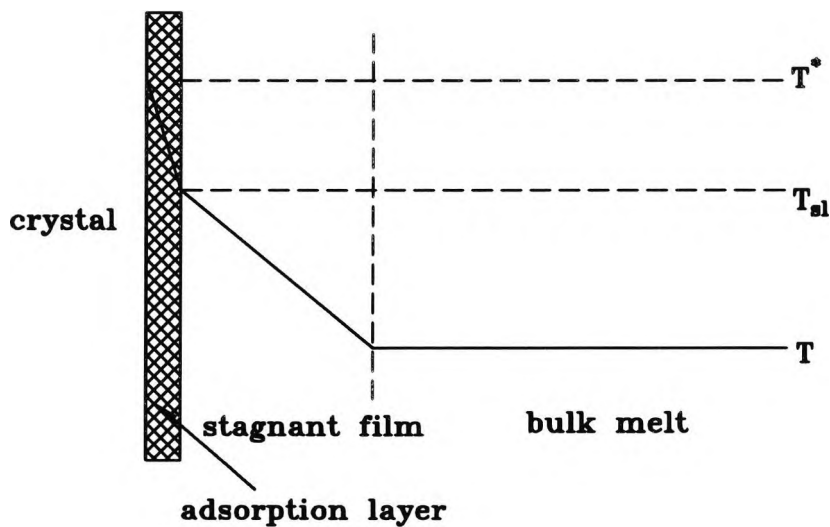


Figure 11.1: Conditions of heat transfer

Obviously, if the thickness of effective film is reduced, the film coefficient of heat transfer will be increased and so will the interfacial temperature,  $T_{sl}$ , which will

tend to the value near to that of melting point  $T^*$ . Traditionally, this could be realized by agitation. In fact, it could be also obtained by applying the electric field effect.

When the crystal-melt system was in the presence of an electric field, the bulk liquid would be polarized. In that case, the polarization vector  $\bar{P}$  was effective, and it may be interpreted as the dipole moment per unit volume

$$\bar{P} = N\bar{u} \quad (11.36)$$

where  $N$  is the number of dipoles per unit volume of the dielectric melt,  $\bar{u}$  is the electric dipole moment and can be represented as

$$\bar{u} = q_e d \quad (11.37)$$

where  $q_e$  is the electric charge and  $d$  is the distance between the positive and negative charges.

If  $E'$  represents the local electric field strength acting on the dipole, the torque  $W$  could be obtained as

$$W = \bar{u} \times E' \quad (11.38)$$

The torque would simply tend to align the dipole in the field direction (right-hand rule). Therefore, the force acting on the dipole could be obtained as

$$\begin{aligned} F &= F_- + F_+ = E'(-q) + [E' + (d \cdot \nabla)E'](+q) \\ &= qd \cdot \nabla E' = \bar{u} \cdot \nabla E' \end{aligned} \quad (11.39)$$

For simplicity, if we assume

$$\bar{u} = \alpha E' \quad (11.40)$$

where  $\alpha$  could be called the polarizability, then the force

$$F = \alpha E' \cdot \nabla E' \quad (11.41)$$

The exact determination of  $E'$  in this equation could be very difficult, because in dielectric melt the field acting on a particle might be expected to be modified by

the polarization of the surrounding particles. However, for a non-polar dielectric, a reasonable approximation of the local field is the Mossotti field (first suggested by Mossotti in 1850) given by

$$E' = E + \frac{\bar{P}}{3\epsilon_o} = \frac{1}{3}(\epsilon + 2)E \quad (11.42)$$

where  $E$  is the applied field intensity and the polarization  $\bar{P}$  is related to  $E$  by the equations defined before and can be further expressed as

$$\bar{P} = (\epsilon - 1)\epsilon_o E = N\alpha E' \quad (11.43)$$

Substituting the Mossotti field, we obtain

$$\frac{N\alpha}{3\epsilon_o} = \frac{\epsilon - 1}{\epsilon + 2} \quad (11.44)$$

so the force per dipole is obtained as

$$F = \frac{\epsilon_o (\epsilon - 1)(\epsilon + 2)}{6N} \nabla E^2 \quad (11.45)$$

or per volume force

$$F = \frac{\epsilon_o}{6} (\epsilon - 1)(\epsilon + 2) \nabla E^2 \quad (11.46)$$

In the bulk melt of a crystal-melt system, the force is proportional to the gradient of the square of the field; the direction of the force is independent of the polarity of the field. Also, since the force arises from the action of the electric field on individual dipoles, the force on a unit volume of bulk melt might be expected to be orders of magnitude greater than that on a unit volume of crystal phase in the adsorption layer. Therefore, the electric force will have a strong effect on the stagnant or effective film in the bulk melt. This will result in an instability in the film and reduce the thickness so that the increase in film coefficient and the temperature of the crystal-melt interface will tend to the value of the melting point  $T^*$ . As a result, the rate of crystallization from the melt will be increased.

The most basic evidence of these could be found from the work of Tamman (1925) in which he suggested that the maximum rate of crystallization would occur at a melt temperature,  $T$ , given by

$$T = T^* - \left( \frac{\Delta Q_{sol}}{C_m} \right) \quad (11.47)$$

where  $\Delta Q_{sol}$  is the heat of crystallization (latent heat) and  $C_m$  is the mean specific heat capacity of the melt.

Similarly, the crystal growth rate or the linear growth rate of crystallization, which is normally denoted by mass per unit time, can be expressed as a function of the overall temperature driving force (Mullin, 1993) by

$$\frac{dm}{dt} = K_G A (T^* - T)^g \quad (11.48)$$

where  $A$  is the crystal surface area,  $K_G$  is an overall mass transfer coefficient for crystal growth and exponent  $g$  generally has a value in the range 1.5 to 2.5.

Clearly, the crystal growth rate mainly depends on the overall mass transfer coefficient,  $K_G$ , and the driving force  $(T^* - T)$ . For a given material at a given cooling condition, like the experiments described in chapter 9, the melting temperature and the bulk melt temperature have relative constant values; and the overall mass transfer coefficient will be directly affected by applying an electric field. The mechanism would be the same as that for heat transfer.

# Chapter 12

## Conclusions of the Thesis

The work described in this thesis was directed primarily towards investigating the effect of an electric field on two kinds of phase change processes in industry. One is the effect on nucleate boiling heat transfer, the other is the effect on crystallization from industrial dielectric melt. Some general points have been demonstrated in the experimental work and other conclusions can be drawn or discussed from both the experimental and the theoretical approach.

### 12.1 Conclusions for EHD Effect on Nucleate Boiling at Low Superheat Surfaces

#### 12.1.1 General conclusions for experimental study

The effect of an electric field on nucleate boiling at low superheat surfaces in heat exchangers has been studied experimentally in a single tube test rig by applying a 0 kV to 30 kV circumferencial uniform electric field. Two kinds of low superheat surface, the Thermoexcel-HE and the Gewa-T, were tested using refrigerant 114 as working fluid to compare the results with those for other surfaces using the same working fluid. Conclusions can be drawn from the experimental study as:

1. The boiling hysteresis for both the Thermoexcel-HE and the Gewa-T, which exists at zero field strength, can be eliminated by utilizing EHD.

2. EHD enhancements of nucleate boiling for both the Thermoexcel-HE and the Gewa-T surfaces are significant at low superheat conditions.
3. The EHD boiling enhancement improves with applied voltage but decreases with heat transfer rate. Nucleate boiling seems therefore to be controllable by applying a variable EHD effect under constant heat flux conditions.
4. The EHD effect on nucleate boiling gives different results for different surface geometries. This results from the compound effect of both passive and EHD enhancement on nucleate boiling. Therefore, a surface geometry designed specifically for EHD applications may give even better performance.

### **12.1.2 The effect of surface geometries on EHD application**

Conclusions of the effect of surface geometries on EHD application have been reached by analyzing equi-potential contours calculated using a CFD method. Generally, the local field near the surfaces, in particular near the surfaces of the cavities, is not uniform. Different equi-potential contour distributions could be obtained by applying the electrode potential to different surfaces. This includes:

1. The contour plots highlight the very high potential gradient existing near the shoulders area on these passive surfaces. The localised field gradients of the shoulders area are much higher than the far-field gradients. Such a high potential gradient should strongly affect contact angles by decreasing surface tensions at liquid-vapour interface.
2. With the localised field distribution on passive surface cavities, high field gradients exist next to the shoulders area and relatively lower ones inside the cavities. These differences of field gradient would help to drive the generated bubble sliding into the cavities to grow and move and result in heat transfer enhancement.
3. Comparisons for the relative increase of localised field gradient close to the shoulders area and the far-field gradients for different surfaces have shown

quite different results. This suggests that applying EHD techniques to a dielectric fluid at passive enhanced surfaces should lead to the development of an ideal surface shape for optimum performance. The enhancement would result in a compound effect both of EHD enhancement and passive enhancement on nucleate boiling.

### **12.1.3 EHD enhancement on bubble nucleation**

The theoretical model for nucleation is on the basis of equilibrium thermodynamics and fluid fluctuation theories. The calculated results from the model have indicated that, in the action of an electric field, the critical bubble nucleus becomes smaller and the nucleation rate is increased. This seems to be the basis for the EHD enhancement of nucleate boiling. The analysis of the bubble movement by predicting the field distribution around a spherical bubble has indicated that the bubbles would be affected by the compound or cumulative factors of buoyancy and EHD forces. The resultant effect would enhance nucleate boiling heat transfer.

## **12.2 Conclusions for Effects of an Electric Field on Crystallization**

### **12.2.1 The effect on no-crystallization dielectric oil**

Electroconvection is the major effect of applying an electric field on no-crystallization dielectric oil. Experimental results have indicated that the cooling rate of olive oil, which is a dielectric liquid and without crystallization, increases with the strength of the applied field. This enhancement effect for convection will not be continuous when the field is cut off.

### **12.2.2 The effect on polymorphism crystallization of dielectric melt**

#### **Increasing the rate of crystallization**

The effect of the electric fields on cocoa butter crystallization is very significant. As the strength of the applied fields increases, both the  $\alpha$  and  $\beta$ -prime (form III) crystals appear earlier. This indicates that the nucleate centres are stimulated and the speed of the crystals growth is enhanced.

#### **The cut-off effect**

When the applied fields are cut off at a certain time, the electroconvection phenomena in the olive oil disappear immediately, but the nucleate centres and the crystal growth of cocoa butter still share the benefit of the field. Cutting off the field at the moment the highest temperature appears (because of the latent heat of crystallization), gives a cooling curve for crystallization similar to the one in which the field is applied to the end.

### **12.2.3 The effect on dielectric melt mixture**

The effect of an electric field on dielectric melt crystallization decreases with the percentage of added mixtures. For the case of cocoa butter and chocolate, the effect of an electric field on the rate of crystallization of cocoa butter is significant but becomes smaller when the percentages of chocolate are increased.

### **12.2.4 The method for DSC assessment using the Taguchi method**

To deal with the different DSC results, which are in the form of thermograms, based on the Taguchi experiments, a criterion for comparison was developed and the numerical intergration was done. As the final stage, the integrated results were analyzed by the Taguchi method, in which the effects of different factors, such as the applied potential, the coolant temperature, the sample initial temperature, the

time of treatment and the sample thickness, on the comparison criterion were discussed and concluded.

As a result of these analyses, the relations for the calculation criteria  $\eta_i$  versus the experimental factors can be obtained. On this basis, the optimal results can be further obtained.

### **12.2.5 Theoretical approach**

The theoretical approach has indicated that the benefits of an electric field to enhance the general crystallization process depend on conditions such as the dielectric properties, the volume contraction properties, etc. For the case of cocoa butter, the effect of applying an electric field on crystallization is beneficial.

Based on diffusion theory, the rate of crystallization from a melt can be predicted from the rate of heat and mass transfer. The results indicated that applying an electric field to a dielectric melt should enhance crystallization processes.

# References

- ABDULLAEV, G.B. and ODOBESKU, A.I. (1967). *Papers at the Third Scientific-Technical Conference of Kishinev Polytechnic Institute*, Kishinev, 123.
- AHSMANN, G. and KRONING, R. (1950). The influence of electric fields on convective heat transfer in liquids. *Appl. Sci. Res.*, **A2**, 235-244.
- ALIKSABOV, V.D. and SHKLYAR, V.S. (1980). Crystallization of dielectric in an electric field. *News AH. CCCP. Inorganic Material* **16**, pp. 402 (in RUSSR).
- ALLEN, P.H.G. (1959). Electric stress and heat transfer. *Br. J. Appl. Physics*, **10**, 347-351.
- ALLEN, P.H.G. and COOPER, P. (1987). The potential of electrically enhanced evaporators. *Procs. 3rd Int. Symp. on the Large Scale Applications of Heat Pumps*. Oxford, P2, 221-229.
- ALLEN, P.H.G. and COOPER, P. Electrohydrodynamic (EHD) effects on condensing and evaporating Freons. *Video held by ASME Heat Transfer Films Library*, Mechanical and Aerospace Engineering. The University of Tennessee, Knoxville, Tenn. 37996-2210.
- ANDERSON, J.C. (1964). *Dielectrics*. Chapman and Hall Ltd.
- ASCH, V. (1966). Electrokinetic phenomena in boiling 'Freon-113'. *J. Appl. Phys.*, **37**, 2654-2658.
- AVRAMI, M. (1940). Kinetics of phase change. II. Transformation-time relations for random distribution of nuclei. *J. Chem. Phys.*, **8-2**, pp. 212-224.
- BABOI, N.F., BOLOGA, M.K. and KLYUKANOV, A.A. (1968). Some features of ebullition in an electric field. *Appl. Electr. Phenom.*, (USSR), **20**, 57-70.
- BARLETTA, A. and ZANCHINI, E. (1993). On the stress tensor for a dielectric fluid in an electrostatic field. *Int. J. of Heat and Technology*, **11**, No. 1-2, pp. 159-176.
- BASU, D.K. (1973). Effect of electric field on boiling hysteresis in carbon tetrachloride. *Int. J. Heat Mass Transfer*, **16**, 1322-1324.

- BECKER, K. (1958). The causes of fat bloom in coated and solid chocolates. *Rev. Int. Choc.*, **13**, pp. 254.
- BERGHMANS, J. (1976). Electrostatic fields and the maximum heat flux. *Int. J. Heat Mass Transfer*, **19**, 791-797.
- BERGLES, A.E. (1985). Techniques to augment heat transfer. *In: Handbook of Heat Transfer Applications*, 2nd edition, Rohsenow, W.M., Hartnett, J.P. and Ganic, E.N. (eds.) McGraw Hill.
- BERGLES, A.E. (1989). The challenge of enhanced heat transfer with phase change. *Trans. VII Congresso Nazionale Sulla Trasmissione Del Calore*, Florence, 1-12.
- BERKELEY, The Earl of, (1912), Solubility and supersolubility from the osmotic standpoint. *Philosophical Magazine*, **24**, 254-268.
- BERLAGA, R.Ya. (1940). *Tr. Odess. Gos. Univ. Fiz.*, **2**, 11.
- BOCHIROL, I., BONJOUR, E. and WEIL, L. (1960). Etude de l'action de champs electriques sur les transferts de chaleur dans les liquides bouillants. *C. R. Hebd. Seances Acad. Sci. (Paris)*, 76-78.
- BONJOUR, E., VERDIER, J. and WEIL, L. (1962). Electroconvection effects on heat transfer. *Chem. Eng. Prog.*, **58**, 63-66.
- CERBULIS, J., CLAY, C. and MACK, C.H. (1957). The composition of bloom fat in chocolate. *J. Am. Oil. Chem. Soc.*, **43**, pp. 533.
- CHAPMAN, D. et al. (1957). *J. Chem. Soc.*, 1502.
- CHAPMAN, G.M., AKEHURST, E.E. and WRIGHT, W.B. (1971). Cocoa butter and confectionery fats studies using programmed temperature X-ray diffraction and differential scanning calorimetry. *J. Am. Oil. Chem. Soc.*, **48**, pp. 824.
- CHELKOWSKI, A. (1980). Dielectric Physics. ELSEVIER Scientific Publishing Company, Amsterdam-Oxford-New York.
- CHESNOKOV, L.I. (1956). The effect of an electric field on the linear rate of crystallization of supercooled melts. *Scientific Works of the Belorussian Polytechnic Institute*, **55**, 136-145.

- CHEUNG, K.H., OHADI, M.M. and DESSIATOUN, S. (1995). Compound enhancement of boiling heat transfer of R-134a in a tube bundle. *ASHRAE TRANS.*, 1995, **101**, Pt. 1. (CH-95-14-1).
- CHOI, H.Y. (1962). Electrohydrodynamic boiling heat transfer. *Ph.D. Thesis*, Dept. Mech. Eng., M.I.T., Cambridge.
- CHUBB, L.W. (1916). Improvements relating to methods and apparatus for heating liquids. U.K. Patent No. 100, 796.
- COOPER, P. (1986). Electrically enhanced heat transfer in shell/tube heat exchanger. *Ph.D Thesis*, University of London.
- COOPER, P. (1990). EHD enhancement of nucleate boiling. *Trans. ASME, J. Heat Transfer*, **112**, 458-464.
- CORNWELL, K. (1990). The role of sliding bubbles in boiling on tube bundles. *9th Int. Heat Transfer Conf.*, **3**, pp. 455-460.
- CORTY, C. and FOUST, A.S. (1955). Surface variables in nucleate boiling. *Chem. Eng. Progr. Symp. Ser.* **51**, no. 17.
- DAMIANIDIS, C., COLLINS, M.W., KARAYIANNIS, T.G. and ALLEN, P.H.G. (1991). EHD enhancement of heat transfer in evaporators and condensers. *Proc. 11th Int. of Heating, Refrigerating and Air-conditioning (Interklima 91)*, Zagreb, June, pp. 10-26.
- DAMIANIDIS, C., KARAYIANNIS, T.G., AL-DADDAH, R.K., JAMES, R.W., COLLINS, M.W. and ALLEN, P.H.G. (1992). EHD boiling enhancement in shell-and tube evaporators and its application in refrigeration plants. *ASHRAE Trans.*, **98**, Part 2, 462-472.
- DUCK, W.N. (1964). Determination of solid fat in melted fat, their role in formation and polymorphic form by viscometry. *Master Thesis*, Franklin and Marshall College, Lancaster, PA. Pgs. 72.
- DULIKRAVICH, G.S., AHUJA, V. and LEE, S. (1993), Simulation of electrohydrodynamic enhancement of laminar flow heat transfer. *J. Enhanced Heat Transfer*, **1**, no. 1, 115-126.

- ELLION, M.E. (1954). A study of the mechanism of boiling heat transfer. Jet Propulsion Laboratory Memo 20-80, California Inst. of Tech.
- FARBER, E.A. and SCORAH, R.L. (1948). Heat transfer to water boiling under pressure. *Trans. ASME*, **70**, 369-384.
- FEUGE, R.O., LANDMANN, W. and LOVEGREN, N.W. (1962). Tempering triglycerides by mechanical working. *J. Am. Oil. Chem. Soc.*, **39**, pp. 310.
- FINCKE, A. (1965). *Handbuch der kakaoerzeugnisse* (2nd ed.), Springer-Verlag, Berlin.
- FORSTER, H.K. and ZUBER, N. (1955). Dynamics of vapour bubbles and boiling heat transfer. *A.I. Ch.E. J.*, **1**, pp. 531-535.
- FORSTER, H.K. and Greif, R. (1959). Heat transfer to a boiling liquid; mechanism and correlations. *Trans. ASME, Ser.C.J. Heat Transfer*, **81**, pp. 43-53.
- FRENKEL, J. (1946). *Kinetic Theory of Liquids*, Oxford.
- FRITZ, W. (1935). Maximum volume of vapour bubbles. *Phys. Z.*, **36**, pp. 379-384.
- GAERTNER, R.F. (1962). Distribution of active sites in the nucleate boiling of liquids. *A. I. Ch. E., Preprint 5*, Fifth National Heat Transfer Conference, Houston.
- GELLER, I.Kh., KOLOMIETS, B.T. and POPOV, A.I. 1936 (1975), *Izv. Akad. Nauk SSSR, Neorgan. Mater.*, **11-11**.
- GEMANT, A. (1933). *Liquid Dielectrics*. Chapman and Hall Ltd.
- GORENFLO, D., BLEIN, P., ROTT, W., SCHOMANN, H. and SOKOL, P. (1990). Pool boiling heat transfer from a Gewa-T-x finned tube to propane and propylene. *Eurotherm No. 8, Advances in Pool Boiling Heat Transfer*, Paderborn, FRG. May 11-12, 1990.
- GORSKII, F.K. and MIKHNEVICH, G.L. (1932). *Zh. Eksp. Teor. Fiz.*, **2**, 264.
- GORSKII, F.K. (1955). The effect of various physical factors on the crystallization parameters of a material. *Scientific Works of the State Medical Institute, Belorussian SSR, Minsk*, **15**, 308-327.

- GORSKII, F.K. and BASHUN, M.L. (1969). The Mechanism and Kinetics of Crystallization. *Nauka i Tekhnika*, Minsk, 346.
- GRANT, E.H., SHEPPARD, R.J. and SOUTH, G.P. (1978). Dielectric Behaviour of Biological Molecules in Solution. Clarendon Press, Oxford.
- GRIFFITH, P. (1956). The dynamics of bubbles in nucleate boiling. *D.Sc. Thesis*, Mech. Eng. Dept., Massachusetts Institute of Technology.
- GROWTHER, A.G. and SAUNDERS, C.P.R. (1973). Ice crystal growth in electric fields. *J. Meteorol. Soc.*, Japan, **51-5**, 318-324.
- GUGGENHEIM, E.A. (1967), *Thermodynamics*, 5th ed., North-Holland.
- GUTSOV, I.S. and TOSHEV, S. (1968). Nestatsionarno zarodishobrazuvane pri formirane na izotpi i kristanni fazi. Bulgarian AN, Izvan na. *Izv. na Otd. za Khimi. za khim. Nauki*, **1**, Bk. 4, pp. 133-145.
- GUTSOV, I.S. and KASHCHIEV, D. (1970). Sumarna kritallizatsiya kinetichna ustoychivost na preoxhlazhdeni stopilki pri nestatsionarno zarodishobrazuvane. *Bolg. Akad. Nauk. Izv. na Otd. za Khim. Nauki*, **3**, Bk. 4, pp. 645-659.
- GUTSOV, I.S. (1971). Izsledovane na kristallizatsionniya protses v "v viskosna st" kloobrazuvashcha stopilka. Doctoral Dissertation ( in Bulgarian ), Univ. of Sofiya.
- HAHNE, E. and MULLER, J. (1983). Boiling on a finned tube and a finned tube bundle. *Int. J. Heat Mass Transfer*, **26**, pp. 849-859.
- HANS, R.K. (1989). The effect of cocoa butter on chocolate tempering and bloom. *The Manufacturing Confectioner*, May, pp. 77-81.
- HILDITCH, T.P. and STAINSBY, W.J. (1936). *J. Soc. Chem. Ind.*, **55**, 95T.
- HSU, Y.Y. (1962). On the size range of active nucleation cavities on a heating surface. *Trans. ASME, Ser. C., J. Heat Transfer*, **84**, 207-216.
- HUYGHEBAERT, A. and HENDRICKX, H. (1971). Polymorphism of cocoa butter shown by differential scanning calorimetry. *Lebensm - Wiss. u. technol.*, **4**: 59.
- ILIEV, V.A., KONTROV, S.I. and PENCHEV, P.R. (1981a). *Nauchna Sesiya VMEI*, Sofiya, pp.28-35.

- ILIEV, V.A. and KONTROV, S.I. (1981b), *Sb. Rezyume na dokl. Yubileina Nauchna Sesiya, VMEI*, **4**, Varna, pp. 174-175.
- ILIEV, V.A. and KONTROV, S.I. (1981c), *Nauchna Tr., Yubileina Nauchna Sesiya, VNVAU*, **12**, T'rnovo, pp. 49-55.
- ILIEV, V.A. and KONTROV, S.I. (1983), *Nauchna Sesiya, VMEI, Varna*, pp. 38-41.
- ILIEV, V.A., KONTROV, S.I. and A.K. IVANOV, A.K. (1987), *Nauchna Sesiya, VMEI, Varna*, pp. 61-67.
- ILIEV, V.A. and KONTROV, S.I. (1989). Effect of an electric field on crystallization processes in a glass-forming melt. *Fiz. Khim. Stekla*, **15-2**, pp. 544-548.
- ISARD, J.U. (1977). *Phil. Mag.*, **35**, pp. 817.
- JENSEN, H.R. (1931). *Chemistry flavoring and manufacture of chocolate, confectionery and cocoa*. Blackistons, Philadelphia.
- JEWELL, G.G. (1972). Some observations on bloom on chocolate. *Rev. Int. Choc.*, **27**, pp. 161.
- JOHNSON, R.L. (1968). Effect of an electric field on boiling heat transfer. *AIAA Journal*, **6**, 1456-1460.
- JONES, T.B. (1978). Electrohydrodynamically enhanced heat transfer in liquids – a review. *Advances in Heat Transfer*. **14**, 107-148.
- KARAYIANNIS, T.G., COLLINS, M.W. and ALLEN, P.H.G. (1989). Electrohydrodynamic enhancement of nucleate boiling heat transfer in heat exchangers. *Chem. Eng. Comms.*, **81**, 15-24.
- KARAYIANNIS, T.G., AL-DADAH, R.K., JAMES, R.W. and ALLEN, P.H.G. (1993). Electrohydrodynamic boiling heat transfer enhancement in heat exchangers. *ASME WAM.*
- KARLEKAR, B.V. (1983). *Thermodynamics for Engineers*, Prentice-Hall, inc. Englewood Cliffs, N.J. 07632.
- KATTENBERG, H.R. (1981). The quality of cocoa butter. *Manf. conf. Jan.*

- KAWAHIRA, H., KUBO, Y. and YOKOYAMA, T. (1987). The effect of an electric field on boiling heat transfer of refrigerant-11. *Proc. IEEE/IAS Annual Meeting*, Atlanta, October, pp. 1446-1454.
- KHAMSKII, E.V. (1969). *Crystallization from Solutions*, Consultants Bureau, New York.
- KLEINERT, J. (1961). Studies on the formation of fat bloom and methods of delaying it. *Rev. Int. Choc.*, **9**, pp. 329.
- KLEINERT, J. (1970). Cocoa butter and chocolate: the correlation between tempering and structure. *Rev. Int. Choc.*, **25**, pp. 386.
- KOCH, J. (1956). Chocolate tempering in theory and practice. *Rev. Int. Choc.*, **11**, pp. 344.
- KONDONDOGURI, V.V. (1926). Influence of electric and magnetic fields on solidification of under-cooled piperine and salol. *Zh. Russ. Fiz.-Khim. O-va., Chast. Fiz.*, **58**, 279.
- KONDONDOGURI, V.V. (1928). Influence of electric and magnetic fields on the crystallization of under-cooled liquids. *Z. Phys.*, **47**, 589.
- KONDONDOGURI, V.V. (1936). The crystallization of under-cooled sulfur in electric fields. *Phys. Z. Sowjetunion*, **9**, 603.
- KONTROV, S.I., PENCHEV, P.R., et al. (1980). *Sb. Dokl. Yubileina Nauchna Sesiya, VNVAU*, **8**, Part 3, D. Mitropoliya, pp. 30-34.
- KONTROV, S.I., PENCHEV, P.R., et al. (1980). *Nauchna Sesiya, VNVAU, Shumen*, pp. 72-76.
- KOZLOVSKII, M.I. (1962). *Crystallization and Phase Transition. Izd. ANBSSR*, Minsk, 404.
- KOZLOVSKII, M.I., BURCHAKOVA, V.I. and MALENT'EV, I.I. (1976). Electric fields and crystallization. *Shtiintsa, Kishinev*.
- LANDAU, L.D. and LIFSHITZ, E.M. (1960). *Electrodynamics of Continuous Media*. Pergamon Press, New York.

- LOVEGREN, N.V. and FEUGE, R.O. (1965). *J. Am. Oil. Chem. Soc.*, **43**, pp. 491.
- LOVEGREN, N.V., GRAY, M.S. and FEUGE, R.O. (1976). Effect of liquid fat on melting point and polymorphic behaviour of cocoa butter and a cocoa butter fraction. *J. Am. Oil. Chem. Soc.*, **53**, pp. 108.
- LOVENGUTH, R.F. and HANESIAN, D. (1971). Boiling heat transfer in the presence nonuniform, direct current electric fields. *Ind. Eng. Chem. Fundam.*, **10**, 570-576.
- LUTTON, E.S. (1957). *J. Am. Oil. Chem. Soc.*, **34**, pp. 521.
- LYCHEV, A.P., RUDENKO, Yu.S. and CHEREMISIN, A.I. (1976). Thermodynamics of crystallization of dielectrics in an electric field. *Kris, Svoistva, Kristallov*, **6**, 29-34.
- LYCHEV, A.P., RUDENKO, Yu.S. and CHEREMISIN, A.I. (1977). Effect of an electric field on crystallization. *Izv. Vyssh. Uchebn. Zaved., Fizika*, **4**, 29-32.
- LYCHEV, A.P. and CHEREMISIN, A.I. (1978). The action of a constant magnetic field on crystallization. *Electrochemistry in Industry and Biology*, 38-40.
- LYCHEV, A.P. and CHEREMISIN, A.I. (1979a). Electric field effect on crystallization kinetics. *Izv. Vyssh. Uchebn. Zaved., Fizika*, **2**, 63-67.
- LYCHEV, A.P. and CHEREMISIN, A.I. (1979b). Crystallization kinetics of dielectrics in an electric field – Effect of the kinetic parameters. *Krist. Svoistva Kristallov*, **6**, 3-9.
- LYCHEV, A.P. and CHEREMISIN, A.I. (1979c). Crystallization kinetics of dielectrics in an electric field – Effect of the field on the kinetics of mass crystallization. *Krist. Svoistva Kristallov*, **6**, 8-12.
- MANNING, D.M. (1984). Thermal and compositional properties of cocoa butter during static and dynamic crystallization. *Ph.D Thesis*, The Pennsylvania State University.
- MARAND, H.L. STEIN, R.S. and STACK, G.M. (1988). Isothermal crystallization of Poly(vinylidene fluoride) in the presence of high static electric fields.

- I. Primary nucleation phenomenon. *J. of Polymer Science: Part B: Polymer Physics*, **26**, pp. 1361-1383.
- MARAND, H.L. STEIN, R.S. and STACK, G.M. (1989). Isothermal crystallization of (PVF<sub>2</sub>) in the presence of high static electric fields. (II): Effect of crystallization temperature and electric field strength on the crystal phase content and morphology. *J. of Polymer Science: Part B: Polymer Physics*, **27**, pp. 1089-1106.
- MARKELS, M. and DURFEE, R.L. (1964). The effect of applied voltage on boiling heat transfer. *A. I. Ch. E. J.*, **10**, 106-109.
- MCADAMS, W.H., WOODS, W.K and BRYAN, R.L. (1941). Vaporization inside horizontal tubes. *Trans. ASME*, **63**, 545-552.
- MEARA, M.L. (1949). *J. Chem. Soc.*, 2154.
- MILLER, I.A. (1981). Electrohydrodynamic enhancement of forced convection heat transfer to low viscosity liquids flowing in annuli. *Ph.D Thesis*, University of Bristol.
- MINIFIE, B.W, (1989). *Chocolate, Cocoa, and Confectionery - science and technology. 3rd edition*, Published by Van Nostrand Reinhold.
- MITCHELL, D.G. (1968). Practical chocolate tempering. *Proceedings from the 22nd Annual PMCA Production Conference*.
- MULLIN, J.W. (1993). *Crystallization*, Third Edition (3 Rev. ed.), Butterworth Heinemann.
- NAKAYAMA, W., DAIKOKU, T., KUWAHARA, H. and NAKAJIMA, T. (1980). Dynamic model of enhanced boiling heat transfer on porous surface — Part I and II. *J. Heat Transfer*, **102**, 445-456.
- NELSON, R. (1967). New developments in true continuous tempering and cooling of chocolate. *Proceedings from 21st Annual PMCA Production Conference*.
- NUKIYAMA, S. (1934). Maximum and minimum values of heat transmitted from metal to boiling water under atmospheric pressure. *J. Soc. Mech. Engrs. Japan*, **37**, 367.

- OGATA, J., IWAFUJI, Y., SHIMADA, Y. and YAMAZAKI, T. (1992). Boiling heat transfer enhancement in tube-bundle evaporators utilizing electric field effects. *ASHRAE Trans.*, **98**, pt. 2.
- OGATA, J. and YABE, A. (1993a). Basic study on the enhancement of nucleate boiling heat transfer by applying electric fields. *Int. J. Heat Mass Transfer*, **36**, 3, 775-782.
- OGATA, J. and YABE, A. (1993b). Augmentation of boiling heat transfer by utilizing the EHD effect – EHD behaviour of boiling bubbles and heat transfer characteristics. *Int. J. Heat Mass Transfer*, **36**, 3, 783-791.
- OHADI, M.M., PAPAR, R.A., NG, T.L., FAANI, M.A. and RADERMACHER, R. (1992). EHD enhancement of shell-side boiling heat transfer coefficients of R-123/oil mixture. *ASHRAE Trans.*, **98-2**.
- OLINGER, J.L. and COLVER, C.P. (1971). A study of the effect of a uniform electric field on nucleate and film boiling. *Chem. Eng. Prog. Symp. Ser.*, **67**, 113, pp. 19-29.
- PEARSON, D. (1970). *Chemical Analysis of Foods*, Churchill, London (new edition 1981).
- PEEBLES, F.N. and GARBER, H.J. (1953) Studies on the motion of gase bubbles in liquids. *Chem. Eng. Progr.*, **49**, pp. 88-97.
- PENCHEV, P.R., KONTROV, S.I., et al. (1980). Nauchna Sesiya, VNVAU, Shumen, pp. 48-52.
- PENCHEV, P.R., KONTROV, S.I., et al. (1982). Nauchna tr. Yubileina Nauchna Sesiya, Vol. 12, V. T'rnovo, pp. 61-66.
- POHL, H.A. (1978). Dielectrophoresis, The Behaviour of Neutral Matter in Nonuniform Electric Fields. Cambridge Univ. Press.
- PRISHCHENA, L.T. (1964). Mechanism and Kinetics of Crystallization. Minsk, 282.
- RAYLEIGH, L. (1917). Pressure due to collapse of bubbles. *Phil. Mag.*, **34**, pp. 94-98.

- ROGASS, H., LAUCKNER, J. and FINKE, J. (1976). *Phys. Status Solidi*, **36**, 1, K9.
- ROHSENOW, W.M. and Clark, J.A. (1951). Heat transfer and pressure drop data for high heat flux densities to water at high sub-critical pressures. *In: Heat Transfer and Fluid Mechanics Inst.*, pp. 193-207, Stanford University Press.
- ROHSENOW, W.M. (1952). A method of correlating heat transfer data for surface boiling of liquids. *Trans. ASME*, **74**, pp. 969-976.
- RUTKOWSKI, J. (1977). The influence of electric field on heat transfer in boiling cryogenic liquid. *Cryogenics*, 242-243.
- RUTKOWSKI, J. (1980). The influence of electric field on heat transfer in boiling cryogenic liquid. *Cryogenics*, 75-78.
- SAGI, N., ARISHIMA, T., MARI, H. and SATO, K. (1989). Polymorphism of mixture of POP, POS and SOS. *J. Jpn. Oil. Chem. Soc.*, **38**, pp. 306-311.
- SATO, K., ARISHIMA, T., WANG, Z.H., OJIMA, K., SAGI, N. and MORI, H. (1989). Polymorphism of POP. and SOS. I. Occurrence and Polymorphic Transformation. *J. Am. Oil. Chem. Soc.*, **66**, pp. 664-674.
- SATO, K. (1991). Polymorphism of cocoa butter and formation of fat bloom. *2nd International Congress on Cocoa and Chocolate*.
- SAVARY, P. and FLANZY, J. (1957). *Desnuelle Biochem., Biophys, Acta*, **24**, 414.
- SCHMIDT, E. and LEIDENFROST, W. (1953). Der einfluss elektrischer felder auf den warmetransport in flussingen elektrischennichtleitern. *Forsch. Geb. Ingenieurwes.*, **19**, 65-80.
- SCHOFIELD, C.A. and DUTTON, H.J. (1959). *J. Am. Oil. Chem. Soc.*, **36**, pp. 325.
- SCRIVEN, L.E. (1959). On the dynamics of phase growth. *Chem. Eng. Sci.*, **10**, pp. 1-13.
- SENFTLEBEN, H. and BRAUN, W. (1936). Der einfluss elektrischer felder auf den warmestrom in gasen. *Z. Phys.*, **102**, 480-500.

- SENFLEBEN, H. and LANGE-HAHN, R. (1958). Der einfluss elektrischer felder auf den warmeubergang in flussigkeiten. *Z. Naturforsch.*, Teil., A13, 99-105.
- SHKLYAR, V.S. (1989). Crystallization of dielectrics in an electric field. *Teor. Osn. Khim. Tekhnol.*, **23-5**, 688-689.
- SHUBNIKOV, A.V. and V.F. PARVOV, V.F. (1969). Nucleation and Growth of Crystals. *Nauka*, Moscow, 23.
- SMYTH, C.P. (1955). International Chemical Series – Dielectric Behaviour and Structure. McGraw-Hill, Inc.
- STEINER, E.H. and BONAR, A.R. (1961). *J. Sci. Fd. Agr.*, **12**, pp. 247.
- STRATTON, J.A. (1941). Electromagnetic Theory. McGraw-Hill Book Company, Inc, New York and London.
- TOLL, J. (1978). Fat crystallography. *Manufacturing Confectioner*, **58**: 57.
- TONG, L.S., CURRIN, H.B., LARSEN, P.S. and SMITH, O.G. (1965). Influence of axially non-uniform heat flux on DNB. *A. I. Ch. E. Preprint 17*, Eighth National Heat Transfer Conference, Los Angeles.
- UEMURA, M., NISHIO, S. and TANASAWA, I. (1990). Enhancement of pool boiling heat transfer by static electric field. *10-EH-13*, pp. 75-80.
- VAECK, S.C. (1951). The polymorphism of certain natural fats: Cocoa butter. *Rev. Int. Choc.*, **6**: 100.
- VAECK, S.C. (1960). Cocoa butter and fat bloom. *Manufacturing Confectioners*, **40**: 35.
- VOLMER, M. (1939). Kinetik der phasenbildung. in *Die Chemische Reaktion*, **4**, edited by K.F. Bonhoeffer, Leipzig, Steinkopf.
- WALLACE, D.C. 1972, *Thermodynamics of Crystals*, John Wiley and Sons, Inc.
- WANG, S.Y., ALLEN, P.H.G. and COLLINS, M.W. (1989). Prediction of the effect of electrohydrodynamic (EHD) enhancement on fluid flow and heat transfer. *Heat Transfer 90' Conf.*, Southampton, UK. in *Advanced Computational Methods in Heat Transfer*. **2**, 231-238. Springer-Verlag, 1990.

- WARK, J.W. (1933). The physical chemistry of flotation, I. *J. Phys. Chem.*, **37**, pp. 623-644.
- WASTON, R.K. (1961). Influence of an electric field upon the heat transfer from a hot wire to an insulating liquid. *Nature* (London, **189**, 563-564.
- WEBB, R.L. (1981). The revolution of enhanced surface geometries for nucleate boiling. *Heat Trans. Eng.*, **2**, 46-69.
- WEBB, R.L. and PAIS, C. (1992). Nucleate pool boiling data for five refrigerants on plain, integral-fin and enhanced tube geometries. *Int. J. Heat Mass Transfer*, **15**, 8, 1893-1904.
- WHYMPER, R. (1933). The Problem of Chocolate Fat Bloom. The Manufacturing Confectioner Publishing Company, Chicago, IL.
- WILLE, R.L. and LUTTON, E.S. (1966). Polymorphism of cocoa butter. *J. Am. Oil Chem. Soc.*, **43**, pp. 491 - 496.
- WINER, M. (1967). An experimental study of the influence of a nonuniform electric field on heat transfer in a dielectric fluid. Rep. No. EM 17-24. TRW Systems, Redondo Beach, California.
- WINSMER, K.L. (1922). Pressure-volume relation of superheated liquids. *J. Phys. Chem.* **26**, 301.
- WITZEL, H. and BECKER, K. (1969). Uaer die kristallstruktur der kakao butter, *Fette Seifen Anstrichmittel*, 71: 507.
- YABE, A. and MAKI, H. (1988). Augmentation of convective and boiling heat transfer by applying an electro-hydrodynamical liquid jet. *Int. J. Heat Mass Transfer*, **31**, 407-417.
- YABE, A. (1991). Active heat transfer enhancement by applying electric field. *Proc. 3rd ASME-JSME Thermal Engineering Joint Conference*, Reno. U.S.A. **3**, pp. xv-xxii.
- YABE, A., TAKETANI, T., MAKI, H., TAKAHASHI, K. and NAKADAI, Y. (1992). Experimental study of electrohydrodynamically(EHD) enhanced evaporator for nonazeotropic mixtures. *Trans. of ASHRAE*, **98-2**, pp. 455-461.

- YABE, A. (1993). Mechanism of electro-hydrodynamically (EHD) enhanced boiling and condensation. *Computer and Computing in Heat Transfer Science and Engineering*, ed. by W. Nokayamal and K.T. Yang. CRC.
- YAMASHITA, K., KUMAGAI, M. and SEKITA, S. (1991). Heat transfer characteristics on an EHD condenser. *ASME/JSME Thermal Engineering Proceedings*, **3**-ASME, pp. 61-67.
- YAN, Y.Y., KARAYIANNIS, T.G., ALLEN, P.H.G., COLLINS, M.W. and NEVE, R.S. (1994). EHD enhancement of boiling heat transfer at low superheat surfaces in heat exchangers. *In: Heat Exchanger Technology — Recent developments*, (October 1993 Paris). pp 111-117. Eds. C. Marvillet and R. Vidil (Eurotherm). Editions Europeens Thermique et Industries, F-75016, Paris.
- YAN, Y.Y., KARAYIANNIS, T.G., COLLINS, M.W., ALLEN, P.H.G., NEVE, R.S. and AL-DADDAH, R.K. (1995a). EHD enhanced heat exchangers — new challenging equipment for renewable energy applications. *Proc. ICEE-95, (E008)*, May 8-10, Shanghai.
- YAN, Y.Y., NEVE, R.S. and COLLINS, M.W. (1995b). The compound effect of EHD enhancement on nucleate boiling at low superheat surfaces, *In: IMechE Conference Transactions, 1995-2*, C510/039/95, (The 4th U.K. National Conference on Heat and Mass Transfer, IMech and IChem, Sept. 1995), pp. 261-265.
- YILMAZ, S., HWALCK, J.J. and WESTWATER, J.W. (1980). Pool boiling heat transfer performance for commercial enhanced tube surfaces. *ASME Paper 80-HT-41*.
- YOKOYAMA, T., YAMAZAKI, T., KUBO, Y., OGATA, J., KAWADA, A. and OOKI, Y. (1987). The effect of an electric field on boiling heat transfer of fluorocarbon R-11. *XVIII Int. Centre for Heat and Mass Transfer*. Edited by Bougard, J., pp 140, Hemisphere, New York.
- YOUNG, S.W. (1911). Mechanical stimulus to crystallization in supercooled liquids. *Journal of the American Chemical Society*, **33**, 148-162.
- ZAKY, A.A. and HAWLEY, R. (1970). *Dielectric Solids*, London: Routledge and Kegan Paul Lit; New York: Dover Publications Inc.

- ZHELTUKHIN, V.A., SOLOMATNIKOV, Y.K., MIKHAYLOV, D.M. and USMANOV, A.G. (1978). Effect of electric field frequency on heat transfer. *Heat Transfer – Soviet Research*, **10**, 10-13.
- ZHORZHOLIANI, A.G. and SHEKRILADZE, I.G. (1972). Study of the effect of an electrostatic field on heat transfer with boiling dielectric fluids. *Heat Transfer – Soviet Research*, **4**, 81-98.
- ZUBER, N. (1958). On the stability of boiling heat transfer. *Trans. ASME*, **80**, 711-720.
- CHERNOV, A.A. (1980). *Modern Crystallography III: Crystal Growth*. Springer – Verlag, Berlin.
- CHERNOV, A.A. (1989). Formation of crystals in solution. *Contemporary Physics*, **30**, 251-276.
- LEWIS, B. (1980). Nucleation and growth theory. In *Crystal Growth, 2nd edn.*, B.R. Pamplin (ed.), Pergamon Press, Oxford, 23-63.
- TAMMAN, G. (1925). *States of Aggregation*. (Translated by R.F. Mehl), Van Nostrand, New York.
- TURNBULL, D. (1950). Kinetics of heterogeneous nucleation. *J. of Chemical Physics*, **18**, 198-203.
- WELLS, A.F. (1946). *Crystal Growth*. Annual Reports on the Progress of Chemistry. The Chemical Society, London, **43**, 62-87.

# Appendix A

## Experimental Data for EHD Nucleate Boiling

### A – A: Data for the Thermoexcel-HE tube

#### A – A.1.1 Applying 0 kV (increasing superheat, +)

$\Delta T$ (K)	$Q(+)$ (W)	$q(+)$ (W/m <sup>2</sup> )	$h(+)$ (W/m <sup>2</sup> K)	$r_m(+)$
3.08	401.70	13299.88	4318.14	793.87
3.20	326.20	10800.15	3375.05	644.66
3.32	308.07	10199.88	3072.26	608.83
3.32	422.85	14000.13	4216.91	835.67
3.35	534.60	17700.06	5283.60	1056.52
3.40	353.38	11700.05	3441.19	698.38
3.40	534.60	17700.06	5205.90	1056.552
3.47	395.66	13099.90	3775.19	781.94

#### A – A.1.2 Applying 0 kV (decreasing superheat, -)

$\Delta T$ (K)	$Q(-)$ (W)	$q(-)$ (W/m <sup>2</sup> )	$h(-)$ (W/m <sup>2</sup> K)	$r_m(-)$
3.35	527.88	17477.57	5217.19	1043.24
3.30	482.54	15876.41	4841.34	953.64
3.12	442.49	14650.39	4695.64	874.49
2.82	362.44	12000.02	4255.33	716.28
2.63	326.14	10798.16	4105.77	644.55
2.51	295.99	9799.93	3904.36	584.96
2.35	276.96	9169.87	3902.07	547.35
2.29	239.21	7920.00	3458.52	472.75
2.12	238.25	7888.22	3720.86	470.85
2.05	205.99	6820.12	3326.89	407.09

A – A.2.1 Applying 10 kV d.c. (increasing superheat, +)

$\Delta T$ (K)	Q(+) (W)	q(+) (W/m <sup>2</sup> )	h(+) (W/m <sup>2</sup> K)	$r_m$ (+)
1.98	229.24	7589.91	3833.29	453.04
2.14	259.75	8600.06	4018.72	513.04
2.26	289.95	9599.95	4247.77	573.02
2.50	362.50	12002.01	4800.80	716.40
2.90	398.68	13199.89	4551.69	787.91
3.05	462.17	15301.98	5017.04	913.38
3.28	507.41	16799.83	5121.90	1002.79

A – A.2.2 Applying 10 kV d.c. (decreasing superheat, -)

$\Delta T$ (K)	Q(-) (W)	q(-) (W/m <sup>2</sup> )	h(-) (W/m <sup>2</sup> K)	$r_m$ (-)
3.15	443.99	14700.06	4666.69	877.45
2.82	401.70	13299.88	4716.27	793.87
2.50	320.15	10599.84	4239.94	632.71
2.27	259.75	8600.06	3788.57	513.34
1.80	247.67	8200.11	4555.61	489.47
1.80	205.38	6799.93	3777.74	405.89
1.48	187.26	6199.99	4189.18	370.08

A – A.3.1 Applying 20 kV d.c. (increasing superheat, +)

$\Delta T$ (K)	Q(+) (W)	q(+) (W/m <sup>2</sup> )	h(+) (W/m <sup>2</sup> K)	$r_m$ (+)
1.13	199.95	6620.14	5858.53	395.16
1.52	250.69	8300.09	5460.59	495.43
1.68	303.51	10048.91	5981.49	599.82
1.78	303.54	10049.90	5646.01	599.88
2.24	431.91	14300.10	6383.98	853.58
2.95	622.19	20600.08	6983.08	1229.62

A – A.3.2 Applying 20 kV d.c. (decreasing superheat, –)

$\Delta T$ (K)	$Q(-)$ (W)	$q(-)$ (W/m <sup>2</sup> )	$h(-)$ (W/m <sup>2</sup> K)	$r_m(-)$
2.58	537.62	17800.05	6899.25	1062.49
2.37	437.95	14500.08	6188.18	865.51
1.96	341.30	11300.10	5765.36	674.51
1.72	265.79	8800.04	5116.30	525.28
1.34	199.95	6620.14	4940.41	395.16
1.05	165.51	5479.87	5218.92	327.09

A – A.4 Applying 30 kV d.c. (increasing superheat, +)

$\Delta T$ (K)	$Q(+)$ (W)	$q(+)$ (W/m <sup>2</sup> )	$h(+)$ (W/m <sup>2</sup> K)	$r_m(+)$
1.07	169.14	5600.06	5233.70	334.27
1.00	211.42	6999.90	6999.90	417.83
1.09	238.61	7900.14	7247.83	471.56
1.18	217.46	7199.88	6101.60	429.76
1.25	259.75	8600.06	6800.05	513.34

A – A.5 Dada for the Thermoexcel-HE ( $h_{e,m}/h_{o,m}^+ - E$ )

$q$ (W/m <sup>2</sup> )	heat transfer coefficient, $h_m$ , (W/m <sup>2</sup> )			
	0 kV (+)	10 kV (+,-)	20 kV (+,-)	30 kV (+)
7000	2213.26	3541.22	5356.10	6639.79
10000	3069.44	4082.35	5463.60	6998.31
13000	3945.61	4475.194	5692.13	7380.14

## A – B: Data for the Gewa-T tube

### A – B.1.1 Applying 0 kV (increasing superheat, +)

$\Delta T$ (K)	Q(+) (W)	q(+) (W/m <sup>2</sup> )	h(+) (W/m <sup>2</sup> K)	r <sub>m</sub> (+)
2.81	106.17	3515.18	1250.95	209.82
2.89	160.02	5298.10	1833.25	316.25
3.25	365.62	12105.31	3724.71	722.57
3.76	547.89	18140.08	4824.49	1082.79
4.09	642.98	21288.42	5204.99	1270.71

### A – B.1.2 Applying 0 kV (decreasing superheat, -)

$\Delta T$ (K)	Q(-) (W)	q(-) (W/m <sup>2</sup> )	h(-) (W/m <sup>2</sup> K)	r <sub>m</sub> (-)
4.06	611.98	20262.04	4990.65	1209.45
3.74	560.31	18551.30	4960.24	1107.33
3.26	511.86	16947.17	5198.52	1011.58
2.84	442.34	14645.43	5156.84	874.19
2.88	403.02	13343.58	4633.19	796.4822
2.58	353.26	11696.08	4533.37	698.14
2.33	301.23	9973.42	4280.44	595.32
1.80	201.79	6681.06	3711.70	398.79

### A – B.2.1 Applying 10 kV (increasing superheat, +)

$\Delta T$ (K)	Q(+) (W)	q(+) (W/m <sup>2</sup> )	h(+) (W/m <sup>2</sup> K)	r <sub>m</sub> (+)
1.21	66.69	2208.04	1824.83	131.80
1.77	137.43	4550.17	2570.72	271.60
1.93	235.06	7782.60	4032.44	464.55
2.81	415.45	13755.13	4895.06	821.05
3.38	485.82	16085.01	4758.88	960.12
3.57	549.87	18205.64	5099.62	1086.70
4.14	659.40	21832.07	5273.45	1303.16

A – B.2.2 Applying 10 kV (decreasing superheat, –)

$\Delta T$ (K)	$Q(-)$ (W)	$q(-)$ (W/m <sup>2</sup> )	$h(-)$ (W/m <sup>2</sup> K)	$r_m(-)$
3.80	618.16	20466.65	5385.96	1221.66
3.41	552.03	18277.15	5359.87	1090.97
3.19	477.52	15810.20	4956.18	943.72
2.65	378.04	12516.52	4723.22	747.11
2.36	293.10	9704.25	4111.97	579.25
1.80	212.15	7024.07	3902.26	419.27
1.60	158.16	5236.52	3272.82	312.57

A – B.3.1 Applying 20 kV (increasing superheat, +)

$\Delta T$ (K)	$Q(+)$ (W)	$q(+)$ (W/m <sup>2</sup> )	$h(+)$ (W/m <sup>2</sup> K)	$r_m(+)$
0.69	70.87	2346.43	3400.63	140.06
0.94	105.28	3485.72	3708.21	208.06
1.62	213.49	7068.44	4363.23	421.92
1.85	245.43	8125.94	4392.40	485.04
2.52	392.77	13004.22	5160.40	776.23
3.02	481.75	15950.25	5281.54	952.08
3.67	617.96	20460.03	5574.94	1221.26

A – B.3.2 Applying 10 kV (decreasing superheat, –)

$\Delta T$ (K)	$Q(-)$ (W)	$q(-)$ (W/m <sup>2</sup> )	$h(-)$ (W/m <sup>2</sup> K)	$r_m(-)$
2.25	325.00	10760.42	4782.41	642.29
1.25	147.29	4876.62	3901.30	291.09
0.85	92.33	3056.95	3596.42	182.47
0.76	86.87	2876.18	3784.45	171.68

**A – B.4** Dada for the Thermoexcel-HE ( $h_{e,m}/h_{o,m}^+ - E$ )

q (W/m <sup>2</sup> )	heat transfer coefficient, $h_m$ , (W/m <sup>2</sup> )			
	0 kV (+)	10 kV (+,-)	20 kV (+,-)	30 kV (+)
3000	1323.40	3070.28	3679.05	4486.32
4000	1548.75	2927.15	3453.72	4197.12
6000	1999.47	3139.16	3559.05	4138.89
8000	2450.18	3332.24	3675.27	4214.31
10000	2900.89	3684.13	3829.17	4351.34

# Appendix B

## Error Analysis for EHD Nucleate Boiling Experiments

The thermocouples were calibrated in a water bath against a British Standard calibrated mercury thermometer. The instantaneous temperature read is accurate to better than 0.1 K. Assuming the mercury-in-glass scale ( $0 \sim 70^\circ\text{C}$ ) to be linear, a quadratic function of thermocouple voltage versus temperature was fitted and the standard deviation was estimated as 0.03 K. The Voltmeter readings were to the nearest  $\mu\text{V}$  ( $\approx 0.025$  K) so the experimental accuracy is

$$\delta_T = \sqrt{0.03^2 + 0.025^2} = 0.039 \text{ K}$$

The magnitude of the fluctuation for  $(T_{in} - T_{out})$  over a 5 min. interval for data reading at a steady state was less than 0.05 K ( $\pm 0.025$  K). So the standard deviation for  $(T_{in} - T_{out})$  is estimated as

$$\begin{aligned} \delta_{\Delta T_{in-out}} &= \sqrt{(\delta_{T_{in}})^2 + (\delta_{T_{out}})^2} \\ &= \sqrt{(0.039)^2 + (0.025)^2} = 0.046 \text{ K} \end{aligned}$$

The fluctuation of thermocouple readings for tube wall temperature,  $T_{wm}$ , varied and had a maximum of 0.08 K ( $\pm 0.04$  K) for the Thermoexcel-HE tube and 0.06 K ( $\pm 0.03$  K) for the Gewa-T tube over a 5 min time interval for data reading at a steady state. So the standard deviation for  $T_{wm}$  and  $T_{wm} - T_{sat}$  were estimated respectively as

For the Thermoexcel-HE tube:

$$\begin{aligned} \delta_{T_{wm}} &= \sqrt{0.039^2 + 0.04^2} = 0.056 \text{ K} \\ \delta_{\Delta T_{wm-sat}} &= \sqrt{(\delta_{T_{wm}})^2 + (\delta_{T_{sat}})^2} \\ &= \sqrt{(0.056)^2 + (0.04)^2} = 0.0688 \text{ K} \end{aligned}$$

For the Gewa-T tube:

$$\begin{aligned} \delta_{T_{wm}} &= \sqrt{0.039^2 + 0.03^2} = 0.049 \text{ K} \\ \delta_{\Delta T_{wm-sat}} &= \sqrt{(\delta_{T_{wm}})^2 + (\delta_{T_{sat}})^2} \\ &= \sqrt{(0.049)^2 + (0.04)^2} = 0.0633 \text{ K} \end{aligned}$$

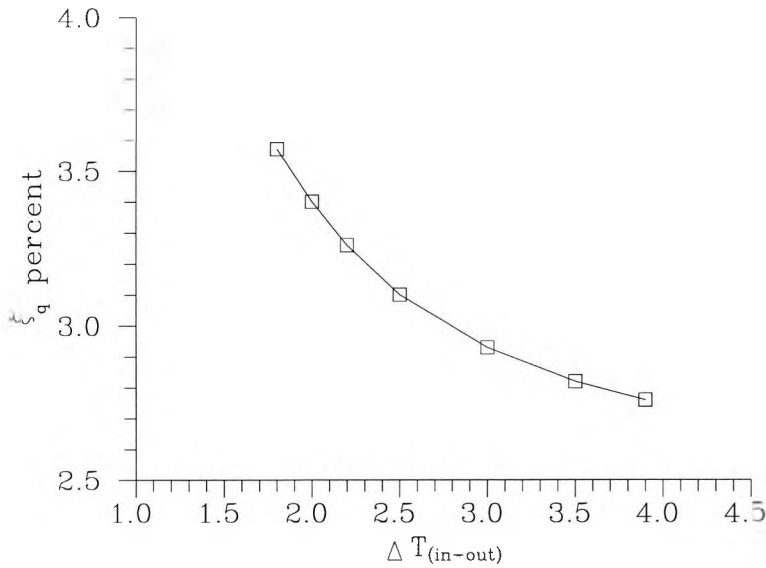
The heat flux was obtained as

$$q = \dot{m}(T_{in} - T_{out})$$

the relative error was estimated as

$$\begin{aligned}\xi_q &= \frac{\delta_q}{q} = \sqrt{\left(\frac{\dot{m}}{q}\right)^2 \left(\frac{\partial q}{\partial \dot{m}}\right)^2 \xi_{\dot{m}}^2 + \left(\frac{\Delta T_{in-out}}{q}\right)^2 \left(\frac{\partial q}{\partial \Delta T_{in-out}}\right)^2 \xi_{\Delta T_{in-out}}^2} \\ &= \sqrt{\xi_{\dot{m}}^2 + \xi_{\Delta T_{in-out}}^2} = \sqrt{\xi_{\dot{m}}^2 + \left(\delta_{\Delta T_{in-out}} / \Delta T_{in-out}\right)^2} \\ &= \sqrt{0.025^2 + (0.046 / \Delta T_{in-out})^2}\end{aligned}$$

In the experiments,  $\Delta T_{in-out}$  was mostly ranged between 1.8 K and 3.9 K; accordingly, the relative errors for heat flux were estimated to be 2.76 – 3.57 %, as shown in App-fig. 1.



App-fig. 1: Error for heat flux,  $\xi_q$ , versus temperature differences,  $\Delta T_{in-out}$ .

On the above basis, the nominal uncertainty in heat flux was estimated to be less than 3.5 %.

Similarly, the relative error for heat transfer coefficient was estimated as

$$\begin{aligned}\xi_h &= \frac{\delta_h}{h} = \sqrt{\xi_q^2 + \left(\delta_{\Delta T_{wm-sat}} / \Delta T_{wm-sat}\right)^2} \\ &= \sqrt{\xi_q^2 + (0.0633 \sim 0.0688 / \Delta T_{wm-sat})^2}\end{aligned}$$

Considering the superheat range in the experiments (0.9 ~ 4.0 K), the relative errors for heat transfer coefficient were estimated to be 3.5 ~ 8.4 % for the Thermoexcel-HE and 3.19 ~ 7.56 %, for the Gewa-T. These results indicated that the errors for heat transfer coefficient were larger than 5 % when the experimental superheat was lower than 1.5 K. However, in experiments, only a few data were

obtained for  $\Delta T < 1.5$  K, for example, for the Gewa-T, one data for 10 kV and two data for 20 kV; for the Thermoexcel-HE, one data for 20 kV and 5 data for 30 kV. Therefore, the nominal errors of the experiments for heat transfer coefficient may be estimated as

App-table: nominal errors for heat transfer coefficient

with EHD (kV)	nominal error (Thermoexcel-HE)	nominal error (Gewa-T)
0 kV	less than 4 %	less than 4 %
10 kV	3.5 ~ 4.5 %	3.2 ~ 5 %
20 kV	3.5 ~ 5 %	3.3 % ~ 5 %
30 kV	5 % ~ 8.4 %	—